Energy

SOLAR

DOE/JPL-1060-66
(DE85000337)

NASA-CR-173896
19840024844

WIND LOADING ON SOLAR CONCENTRATORS: SOME GENERAL CONSIDERATIONS

By
E. J. Roschke

May 1, 1984

Work Performed Under Contract No. AM04-80AL13137

Jet Propulsion Laboratory
Pasadena, California

Technical Information Center
Office of Scientific and Technical Information
United States Department of Energy

DISCLAIMER

Available from the National Technical Information Service, U. S. Department of Commerce, Springfield, Virginia 22161.

Price: Printed Copy A08
Microfiche A01

Codes are used for pricing all publications. The code is determined by the number of pages in the publication. Information pertaining to the pricing codes can be found in the current issues of the following publications, which are generally available in most libraries: *Energy Research Abstracts (ERA); Government Reports Announcements* and Index *(GRA* and I); *Scientific and Technical Abstract Reports (STAR);* and publication NTIS-PR-360 available from NTIS at the above address.

25 1 1 UTP/WIND *+1 LOADING *+2 SOLAR *+1 CONCENTRAT
DISPLAY 25/2/1
84N32915** ISSUE 22 PAGE 3616 CATEGORY 44 RPT#: NASA-CR-173896
JPL-PUB-83-101 DOE/JPL-1060/66 NAS 1.26:173896 CNT#: NAS7-918
DE-AM04-80AL-13137 84/05/01 151 PAGES UNCLASSIFIED DOCUMENT
UTTL: Wind loading on solar concentrators: Some general considerations
AUTH: A/ROSCHKE, E. J.
CORP: Jet Propulsion Lab., California Inst. of Tech., Pasadena. AVAIL.NTIS
SAP: HC A08/MF A01
COI: UNITED STATES
MAJS: /*FLUID MECHANICS/*HEAT TRANSFER/*LOADS (FORCES)/*SOLAR COLLECTORS/*WIND (METEOROLOGY)
MINS: / AEROELASTICITY/ COST ANALYSIS/ PERFORMANCE PREDICTION/ STRUCTURAL DESIGN CRITERIA/ WIND TUNNEL TESTS/ WIND VELOCITY
ABA: Author
ABS: A survey was completed to examine the problems and complications arising from wind loading on solar concentrators. Wind loading is site specific and has an important bearing on the design, cost, performance, operation and maintenance, safety, survival, and replacement of solar collecting systems. Emphasis herein is on paraboloidal, two-axis tracking systems. Thermal receiver problems also are discussed. Wind characteristics are discussed from a general point of view. Current methods for determining design wind speed are reviewed. Aerodynamic coefficients are defined and illustrative examples are presented. Wind tunnel testing is discussed, and
ENTER:

5105-130
Solar Thermal Power Systems Project
Parabolic Dish Systems Development

DOE/JPL-1060-66
(JPL-Pub-83-101)
(DE85000337)
Distribution Category UC-62b

Wind Loading on Solar Concentrators: Some General Considerations

E.J. Roschke

May 1, 1984

Prepared for
U.S. Department of Energy
Through an Agreement with
National Aeronautics and Space Administration
by
Jet Propulsion Laboratory
California Institute of Technology
Pasadena, California

JPL Publication 83-101

ABSTRACT

A survey has been completed to examine the problems and complications arising from wind loading on solar concentrators. Wind loading is site specific and has an important bearing on the design, cost, performance, operation and maintenance, safety, survival, and replacement of solar collecting systems. Emphasis herein is on paraboloidal, two-axis tracking systems. Thermal receiver problems also are discussed.

Wind characteristics are discussed from a general point of view; current methods for determining design wind speed are reviewed. Aerodynamic coefficients are defined and illustrative examples are presented. Wind tunnel testing is discussed, and environmental wind tunnels are reviewed; recent results on heliostat arrays are reviewed as well. Aeroelasticity in relation to structural design is discussed briefly.

Wind loads, i.e., forces and moments, are proportional to the square of the mean wind velocity. Forces are proportional to the square of concentrator diameter, and moments are proportional to the cube of diameter. Thus, wind loads have an important bearing on size selection from both cost and performance standpoints. It is concluded that sufficient information exists so that reasonably accurate predictions of wind loading are possible for a given paraboloidal concentrator configuration, provided that reliable and relevant wind conditions are specified. Such predictions will be useful to the design engineer and to the systems engineer as well. Information is lacking, however, on wind effects in field arrays of paraboloidal concentrators. Wind tunnel tests have been performed on model heliostat arrays, but there are important aerodynamic differences between heliostats and paraboloidal dishes.

PREFACE

This report is based on work that was completed at the Jet Propulsion Laboratory (JPL) in July 1980. Subsequently, portions of the unpublished memorandum were reviewed internally by M. Alper, L. Jaffe, E. Laumann, R. Levy, W. Menard, J. Patzold, R. Turner, and L. Wen. This report has been updated to include revisions, corrections, and additional references, tables, and figures.

Liberal use has been made of charts, graphs, and tables obtained (or adapted) from other literature, which results in a mixture of English and metric units. These differences in units arise from historical usage that has become conventional in the diverse fields of aeronautics and aerodynamics, meteorology, atmospheric physics, and various fields of engineering and science.

ACKNOWLEDGMENTS

Many JPL people provided the author with reference sources, the references themselves, useful data and information, and otherwise provided support and encouragement: F. Livingston provided information sources relating to past wind tunnel testing of JPL paraboloidal dish models (Goldstone antenna). B. Dayman kindly provided access to unpublished internal reports (Refs. 13, 70, 71, and 92). S. Holian provided Edwards Air Force Base wind data (Ref. 45). H. Bank, L. Wen, J. Patzold, and H. Steele provided useful information of various types. R. Wallace provided Ref. 80, and T. Fujita provided Refs. 63 and 64.

Special thanks are due to S. Peglow, Sandia National Laboratories - Livermore, for providing Ref. 62; and to D. Elliott, U.S. Department of Energy (DOE) San Francisco Operations Office, for providing Refs. 58, 59, and 60.

This report was published by JPL through the National Aeronautics and Space Administration (NASA) Task Order RE-152, Amendment 327 and was sponsored by DOE under Interagency Agreement DE-AM04-80AL13137 with NASA.

CONTENTS

APPENDIXES

SECTION I

INTRODUCTION

Many fields of engineering and the physical sciences come to bear in the successful design, construction and operation of paraboloidal reflectors, whether they are solar concentrators, radio antennas, or astronomical radio/optical telescopes. They are, to varying degrees, large precision instruments that must perform well even in often hostile environments.

Performance of reflecting surfaces depends essentially on two types of factors: (1) manufacturing and assembly tolerances, and (2) changes brought about by environmental conditions. There is no single universally accepted definition of surface accuracy, partly because of a disparity between applied, theoretical statistical methods and practical, low-cost measurement techniques. The problem is to relate measurable and quantifiable surface irregularities to overall optical performance. Surface slope error frequently has been used for characterizing the optical performance of solar paraboloidal surfaces, e.g., see Appendix A of Reference 1.

Environmental factors may stem from climate/weather effects or geological effects. Among the former are hail, snow/ice loads, sand/dirt erosion, thermal differentials caused by variable heating effects such as partial shading, and wind loads varying from "normal" to those caused by severe local storms such as thunderstorms and tornados; wind loading tends to exacerbate other environmental effects. Included in the latter (geological factors) are Earth settling and slippage, and earthquakes. Additionally, there are static gravitational loads that must be addressed during design. Clearly, all of these factors must be considered in a cost and performance tradeoff for design, fabrication, and long-term operation. The utility or degree of expected usage of a solar plant will singularly affect the tradeoffs.

The present survey is confined mostly to wind loading, which itself is extremely complicated and has far-reaching consequences. Wind loads have a direct influence on the design, cost, optical performance, operation and maintenance, safety, survival, and replacement of solar concentrators. These will affect:

- Dimensional stability of structural reflecting surfaces and support structures
- Pointing and tracking accuracy
- Loads on drive mechanisms
- Safety/survival (in high winds)
- Base/foundation design
- Potential structural vibrations that depend on wind conditions, aerodynamic shape, natural frequency, and structural damping

Wind loads, i.e., forces, and moments or torques, depend on a large number of variables that include:

- Dish configuration, e.g., focal length to diameter ratio (f/D), and porosity of reflecting surfaces
- Dish diameter (concentrator size)
- Wind velocity (speed and direction)
- Wind velocity profile
- Gust (turbulence) magnitude and frequency
- Ground clearance (dish to ground)
- Steering axis position/location
- Design of base, reflecting surface support, and multipod structures
- Field layout (multiple dish systems)

The main purposes of this survey were to review wind loading considerations for paraboloidal solar concentrators and to document useful sources of information that are pertinent to the various aspects of wind loading. Information is presented on general wind characteristics, design wind speed, aerodynamic coefficients, wind tunnel testing of models, and aeroelasticity problems. Results on heliostat field arrays will be discussed as well. Some wind data for Edwards Air Force Base is presented in the Appendixes. The material is not intended to be directly applicable for design purposes but, rather, to illustrate descriptive examples. Liberal use has been made of charts, graphs, and tables taken (or adapted) from other literature; therefore, an unavoidable mixture of English and metric units is seen.

SECTION II

BACKGROUND

Rudimentary wind engineering has historic roots dating at least as early as the design of windmills, to develop mechanical power, and wind shelters. The development of large urban and industrial centers containing many large and complex structures required more sophisticated approaches for wind loading design. An early application of modern wind engineering was to suspension bridges (Ref. 2). Building codes have evolved and are steadily being improved as the local safety and comfort needs dictate. A large and growing literature on wind engineering exists; a new periodical, The Journal of Industrial Aerodynamics, is devoted to such diverse applications as wind turbines, smoke stacks and cooling towers, high-rise buildings, ground transportation, air pollution problems, and atmospheric physics. Within the last decade special wind tunnels have been developed and used in model studies for numerous industrial, environmental, and meteorological applications.

The starting point for this review was the literature relating to terrestrial radio antennas for deep-space communications. Work on large, steerable radio antennas began in the late 1950s and continued throughout the 1960's; a wealth of information is furnished in Ref. 3. The Jet Propulsion Laboratory (JPL) began wind tunnel testing of paraboloidal reflectors during the early 1960's; the immediate application of that work was to the large Goldstone radio antenna at the Goldstone Deep-Space Communication Complex (GDSCC); see Ref. 4. It is interesting that the total cost of the model wind tunnel testing for the Goldstone antenna was less than 1% of the total estimated project cost (Ref. 5). It is likely that wind tunnel testing costs for model paraboloidal solar concentrators and field arrays would be an even smaller fraction of the total cost of a solar plant.

There are several recurring themes in the radio antenna wind engineering literature. Wind conditions are highly site specific and, therefore, reliable wind measurements as close to the selected site as possible are highly desirable, and records should include as many years of observation as possible. Both "steady" and gust velocities should be known to help determine the design wind velocity as well as various safety factors for design. The cost/performance tradeoff will be strongly influenced by this input information. Clearly, a too-high design wind velocity will result in an over-designed, costly reflector; but the probability of reduced performance, reduced operating time, and susceptibility to damage will increase with decreasing design velocity. Good wind tunnel data should be available for design. Wind tunnel tests on scale models should be performed because they may provide crucial information, and will incur an insignificant relative investment.

Very little wind tunnel information on solar dish concentrators exists for single models, and none exists for field-array models. Radio antenna data probably are sufficient for preliminary design purposes, but may not be adequate for final design or field deployment. Radio antennas differ from solar concentrators in many respects. Large radio antennas are larger than solar concentrators are ever likely to be. They are custom, one-of-a-kind designs that are not intended for mass production. They are relatively deeper (shorter

f/D), and have different operating modes; long-term reliability must be higher than solar concentrators. Finally, they are not used in close-packed arrays.

Although radio antennas are moving (tracking) structures, paraboloidal radio reflectors generally are designed by methods similar to those used for buildings, i.e., a static design wind velocity is used. However, there are different wind velocity values associated with different performance and safety levels. Some preliminary wind requirements for the Goldstone antenna are shown in Table 1 as they were set forth in Ref. 5.

A scenario for probability of wind damage is shown in Figure 1 (from Ref. 6), where wind pressure is proportional to the square of wind velocity. Failure modes are converted to the probability of wind damage occurrence in the lower part of Figure 1. Repair costs mount with increasing wind velocity. Failure (Ref. 6) is defined as structural collapse or permanent deformations that affect pointing/tracking accuracy and/or performance. Structural deformations have been widely discussed in the literature (e.g., Refs. 6, 7, and 8). Complete damage or failure necessitates module replacement. In the case of a large field array, it might be possible to develop different strategies for repair/replacement using statistical models for local wind conditions and reliability statistics developed for components, modules, and groups of modules. Such studies might affect initial capital costs as well as operation and maintenance costs.

SECTION III

WIND CHARACTERISTICS

Wind is caused by atmospheric pressure differences that arise from unequal heating of the Earth's surface. Atmospheric disturbances may vary in size from very small (several meters) to almost global proportions. Important factors that influence the wind include the Earth's rotation, cloud cover, precipitation, nonuniform surface temperature and roughness, and topographic relief (Ref. 9). It is very difficult to characterize wind mathematically because of its extreme variability and randomness. Useful descriptions can be formulated by statistical approaches, expecially when high-quality, long-term wind measurements exist for a specific site of interest. Such work has been in progress for the solar thermal plant planned for the Barstow, California site (Ref. 10). In that case, 10 years of data at the Daggett, China Lake, and Edwards Air Force Base weather stations have been utilized. Parameters in common use include time-average of wind speed and temperature, recurrence periods for maximum wind speeds, probabilities coupling wind direction at a specified speed, and variations in velocity components (turbulence). All of these parameters may vary with height above the Earth's surface. Height variations are discussed subsequently.

A. THE ATMOSPHERIC SURFACE LAYER

The planetary, or atmospheric, boundary layer is loosely described as a layer that has a thickness of roughly 1000 ft, i.e., it extends to an altitude, which varies with many conditions such as surface roughness, of several thousand feet. In approximately the upper 90% of this layer, the Earth's rotation and thermal stratification play dominant roles. There may be strong vertical mixing; wind direction varies with altitude and need not be parallel (locally) to the Earth's surface. It is at the upper regions of the planetary boundary layer that the geostrophic or "free-stream" wind speed is achieved unencumbered by surface friction. This velocity is sometimes called the gradient velocity, and has been expressed (Ref. 11) as:

$$V_G = rw \sin \lambda \left[\left(\frac{dP/dN}{\rho\, rw^2 \sin^2 \lambda} + 1 \right)^{1/2} - 1 \right] \qquad (1)$$

where r is the radius of curvature of isobars, w is the Earth's rotational speed, λ is angle of latitude, dP/dN represents the pressure gradient, and ρ is the density of air. For example, Equation (1) is useful when precise weather data exists.

Figure 2 (from Ref. 9) shows a typical planetary boundary layer model. Conditions for the model are that the atmosphere is horizontally homogeneous, dry, with adiabatic lapse rate, no vertical motions, invariant velocity fluctuations, and negligible effects of turbulence. The lower portion of the planetary boundary layer is often called the atmospheric surface layer (Figure 2). Its thickness may vary from 100 ft (Ref. 12) to perhaps 500 ft and, for neutrally stable atmospheres, it often is a region of constant stress, momentum, and heat fluxes for moderate to strong winds. The atmospheric surface

layer may be very thin at night (Ref. 12), when thermal stratification is strong. Because most man-made structures will be immersed in the atmospheric surface layer, it is the region of main interest. The Earth's rotation and thermal stratification are not dominant effects for strong wind conditions in the atmospheric surface layer. Moderate to strong wind conditions are important for structure design; conversely, weak wind conditions may be more critical for air-pollution problems.

B. VELOCITY PROFILES AND MODELS

An awareness of wind velocity variation with height above ground is important to the wind and design engineers for two reasons: (1) wind loads vary as the square of time-mean velocity and, therefore, the effects of varying forces and moments become increasingly important as the size of a structure increases, and (2) wind tunnel testing of model structures should be conducted using a boundary layer that closely models an expected atmospheric surface layer. The latter point becomes apparent for dish antennas in Figure 3 (from Ref. 13). Note the variation of dynamic pressure across the antenna surface for various elevation angles. Note, also, that the unmodified wind tunnel boundary layer would lead to essentially constant (vertically invariant) velocity across the antenna surface.

Various empirical and semi-empirical forms have been developed to express the variation of wind velocity with height. These include the spiral, exponential and logarithmic forms. Various logarithmic forms have been developed (e.g., Refs. 12, 14, and 15). Exponential, or power law, forms are more commonly used for design purposes because of their simplicity and relatively good accuracy (e.g., Refs. 9,11, and 15). The general power-law expression is:

$$V_z/V_G = (z/z_G)^{1/n} \qquad (2)$$

where z is height above ground, V_G is the gradient wind velocity at the gradient height z_G, and n is the power-law index. Equation (2) is similar to common boundary layer profiles that occur in fluid dynamics, e.g., n has the value of 2 and 7, respectively, for fully developed laminar and turbulent flat-plate boundary layers. A test of the power-law expression for the wind velocity profile shown in Figure 2 is presented in Figure 4, where individual points have been taken from Figure 2. The inverse slope in log-log coordinates is 0.35 so that n = 2.86; the fit is good up to a height of approximately 300 m, or about 1000 ft. Equation (2) was found to fit six different sets of airport weather data (measured at either 10 m or 100 m) using a value of n = 6 (Ref. 16).

Both n and z_G vary with surface roughness, and z_G may vary at the same site between day and night and the seasons of the year. Surface roughness does not refer to the height of individual structures or obstacles (trees, rocks, etc.) but rather to the statistical average that gives rise to the local surface friction. Davenport (Ref. 11) was able to correlate a large amount of wind data to arrive at a relationship between surface roughness and values of n and z_G. His results are reproduced here in Table 2 and Figure 5. Cermak (Ref. 9) replotted Davenport's data in a form shown here in Figure 6, where 1/n and z_G are plotted as functions of the statistical surface roughness length z_o. The lower curve for 1/n (Figure 6) is based on an empirical expression proposed in Ref. 17.

The reference velocity V_G (gradient wind velocity) used in Equation (2), and displayed in Figure 5, is based on relatively few high-altitude measurements and is difficult to establish. Wind measurements in this country and Europe are becoming standardized at 30 ft and 10 m off the ground, respectively. Airport weather data abounds. Thus, it is convenient to convert Equation (2) to a reference velocity at 30 ft for flat, open country (i.e., n = 7, z_G = 900 ft):

$$(V_z/V_{30}) = (900/30)^{1/7}(z/z_G)^{1/n}$$

or (3)

$$(V_z/V_{30}) = 1.63(z/z_G)^{1/n}$$

where V_z is wind speed at height z, V_{30} is the reference velocity at 30 ft above ground, and z_G is the gradient wind height (Table 2 or Figure 6).

Power-law and logarithmic velocity profile models are valid only for neutral or near-neutral atmospheric conditions in flat terrain far removed from large topographic features. They apply for relatively slow-changing weather conditions (near-steady state) when changes in the horizontal plane are small. The simplest case of neutral stability occurs when the vertical temperature distribution follows the adiabatic lapse rate. Thus, these models apply for moderate to strong winds and to large-scale mature storms where turbulence causes thorough mixing without violent thermal interchange; the dominating influence is surface roughness. They do not apply to storms with strong vertical interchanges that destroy the boundary layer structure and are therefore unstable. Examples of unstable storms are severe local thunderstorms, frontal squalls, tornados, and hurricanes. In such storms vertical heat and momentum exhanges are dominant factors, not the surface roughness; in fact, the power-law exponent 1/n may approach zero for such storms. In recent years much progress has been made in modeling the planetary boundary layer, for both stable and unstable atmospheric conditions (Ref. 18).

Stable atmospheric conditions occur when the temperature increases with height, i.e., the inversion case. Temperature inversions most often occur at night when the atmospheric surface layer tends to be the thinnest and the surface wind speeds are the smallest. However, they may occur during the day as well. In Figure 7 (from Ref. 19), a low-level jet is revealed by three smoke plumes issuing from a weather tower at Brookhaven, New York. A hypothetical velocity profile (artist's rendition), divided into three zones, has been superimposed on the photograph. The location of zero velocity, but maximum wind shear, appears to be about 75 ft above ground. Low-level jets can be dangerous to landing aircraft (Ref. 14). Rather large (mesoscale) nocturnal jet winds may occur between inversion layers and are common in flat, open country (Ref. 20).

For additional information the reader may consult Refs. 9, 11, 12, 14, 15, 17, and 18.

C. GUST CHARACTERISTICS

Gust and turbulence characteristics are important for solar concentrators insofar as they contribute to additional wind loads above those based on mean wind speed, cause aerodynamic vibration and amplification, and affect pointing and tracking. Of interest are the magnitude of fluctuating components of velocity, their duration or period, the frequency and probability of their occurrence, relations or correlations among the various components, and the spatial size of eddies. This is a specialized and extremely complex field that cannot be treated in depth in this report; the reader may consult Refs. 9, 15, 19, 21, and 22 for more detailed information. Short wind fluctuations that appear over a period of 1 hour are generally termed gusts (Ref. 22); turbulent fluctuations seem to be associated with even shorter time durations, and usually refer to rapid, random departures from the mean wind speed.

A typical record of horizontal wind speed is shown at three heights above ground in Figure 8 (from Ref. 22). Note that the wind speed seems to have a steady component with superimposed irregular fluctuations. The steady component increases with height but the fluctuating component seems to be relatively independent of height, in agreement with one of the conclusions of Ref. 19. Long-duration fluctuations seem similar at the different heights, but this is not true of short-duration fluctuations. Mean wind speed calculated over periods of 20 min to 1 hour probably will differ little over various randomly selected periods, but mean wind speeds for short periods, such as 1/2 min, will vary considerably. Hence, wind speeds averaged over a 1-hour duration are best adapted to determining wind loads except for conditions when weather is changing rapidly.

It is well known that fluctuating fluid components can markedly increase the forces on a submerged body. Figure 9, for example, shows the increase in drag coefficient in air of a flat plate in fluctuating flow. In Figure 9 (from Ref. 22), the abscissa is the dimensionless reduced frequency. In fluid mechanics this is the Strouhal number commonly associated with periodic, or vortex, flows; the symbol n is the frequency of the "periodic" fluctuations superimposed on a mean speed of V. The Strouhal number is, essentially, a dimensionless frequency of vortex shedding or wake periodicity. In the example shown here, the effective drag coefficient may increase by a factor of 1.5 to 1.8 because of fluctuating flow. See Ref. 16 for further examples and discussion.

The magnitude of gusts relative to the mean wind speed is of interest for design purposes. A typical example of the maximum 3-s gust speed in a given hour, and the mean speed at a height of 10 m, is shown to be dependent on surface roughness in Figure 10a (from Ref. 23). The surface roughnesses indicated in Figure 10a are similar to those shown in Figure 6. Figure 10b (from Ref. 23) shows how the power-law index [Equations (2) and (3)] varies with the same surface roughness coefficient K_R used in Figure 10a.

The anomolies of wind at specific sites are illustrated by the experimental observations of Ref. 24. At a site in Bedford, England, the occurrence of large, rapid wind fluctuations under otherwise light wind conditions is a relatively frequent event. These squall-like fluctuations did not correspond to the usual relationship between the physical size of the fluctuations and the mean wind speed, and were attributed to atmospheric convection.

Figure 11 (from Ref. 22) characterizes the energy spectrum of wind fluctuations (mean square) as a function of fluctuation wavelength. The significance of the energy spectrum is related to the vibrational response times of structural elements exposed to the wind. Figure 11 shows the spectrum of combined horizontal components of wind velocity. The dimensionless spectral density contains a factor K, which is the surface drag coefficient; K depends on surface roughness and has suggested values that correspond to the four terrain types indicated in Figure 6. The energy spectrum peaks at a wavelength of about 2000 ft in Figure 11. Thus, the period would be about 20 s for a wind speed of 100 ft/s (68 mph), which is much longer than vibrational structural periods of even large antennas. For smaller periods (fractions of a second), the energy drops off significantly. At heights lower than 10 m the energy spectrum retains a similar shape, but shifts to the right.

Horizontal gustiness generates force and moment fluctuations. Vertical gustiness may be important too, and may contribute to problems related to stow conditions in paraboloidal concentrators (face-up, or face-down). Vertical gustiness has a spectrum similar to that shown in Figure 11, but the energy is less. Frequency distributions for the longitudinal, transverse (cross-wind), and vertical wind velocity components are shown in Figure 12 (from Ref. 19); they can be approximated by Gaussian distributions. The horizontal components generally are much larger than the vertical component for near-neutral stability conditions. Fluctuation intensities tend to remain constant with increasing height. Standard deviations of the three wind fluctuation components vary linearly with mean wind speed and bear fixed relations to one another (Ref. 19).

D. SOME IMPLICATIONS FOR SOLAR MODULES AND PLANTS

There are many existing studies that characterize the energy cost and performance of candidate concepts for solar production of electric power (e.g., Refs. 1, 25, and 26). Insolation differences among representative sites have been studied as well (e.g., Ref. 27). In all of these studies, the annual production of energy is calculated assuming various site-specific models of insolation. Assuming that local wind characteristics contribute significantly to concentrator and module design, cost, and performance, it is clear that local wind models should be incorporated into annual energy production estimates.

Annual energy production depends on viable operating time as well as insolation. Operating time will, in turn, depend on wind conditions, i.e., statistical measures of daily, seasonal, and yearly wind speed and direction properties that affect operational modes (Table 1). There will be site-specific intersections of solar insolation models and wind models that modify operating time. For some sites, including perhaps the high desert, there may occur higher order, wind-condition models that relate probability of ice formation (which contributes to static loads) with high-wind conditions. Finally, the probability of intense and damage-producing storms, such as tornados and hurricanes, needs to be included as a tradeoff with earthquake damage. In the longer range, probability and risk studies associated with wind damage to field arrays may merit investigation. In large field arrays, the damage or destruction probability of individual modules will influence plant operations and maintenance. As a supporting example, it has been observed (Ref. 1) that the occurrence of local wind direction not parallel to the ground is not

uncommon in Southern California locations. Thus, operational conditions near and at the stow position of paraboloidal concentrators could be affected significantly.

Hybrid operation of solar modules, i.e., the use of fossil fuel combustion to supplement solar energy input, presents yet different problems when considering wind environments. The potential for fouling of reflecting surfaces by exhaust products would seem to be high for fossil fuel operation during nighttime hours when the paraboloidal dish is stowed facing to the ground. Additionally, the dissipation of pollutants might be a problem under very stable atmospheric conditions that generate inversions or low-level jets (e.g., Figure 7). Although the latter problem might be minimal for solar plants in cities and large suburbs, the effect in remote sites and small communities could be more serious.

The JPL Parabolic Dish Test Site (PDTS) is located at Edwards Air Force Base, California (Ref. 28). It is appropriate herein to include some wind measurement data for that site (see Appendix A for some results and discussion). An interesting problem concerns the design wind speed that is appropriate for the PDTS: Only minimal test data can be obtained on hardware that is designed and rated for a much lower, annual average wind speed than is indigenous to the PDTS. However, the problem is mitigated by the relatively short hardware test times (a few months to a year or two) in comparison to statistical design wind speeds obtained from many years of weather data.

Finally, there is concern that there may be a disparity between design wind speed, for specific sites, and actual values used for general design purposes. Suppose, for example, that only one, or a few, generic concentrator designs are to be developed as limited by the availability of development funds, and that the intended sites for applications experiments are unknown during the development period. Then, the designs must be developed to meet the highest expected design wind speed. This would lead to over-designed, high-cost systems if the actual applications sites turned out to have much more benign wind environments. That is, it is unlikely that a few designs can be develped to match the needs for all expected sites unless a penalty for over-design is deemed acceptable. To illuminate this problem, it would be useful to select a specific concentrator concept, and to estimate how its mass production cost would vary with design wind speed and concentrator size.

E. SITE SELECTION AND COMPLEX TERRAIN

The site selection for large solar thermal plants obviously depends on many requirements and factors. Good annual average insolation is a leading requirement and has been dealt with in detail, e.g., Ref. 27. Of interest herein is the consideration of wind effects, which have received little attention. Desirable would be a site having high insolation and moderate-to-low mean wind speeds, with a minimum number of large, peak-wind events. Useful information correlating insolation and wind speeds has become available recently (Ref. 29). Results for 26 SOLMET stations distributed throughout the United States, which utilized wind speed data for more than 12 years, were analyzed. The correlations indicated that more than 97% of the available direct insolation occurred at wind speeds of 15 m/s (approximately 34 mph) or less, for all 26 stations. As will be shown later, these results are encouraging with respect to routine dish operation, albeit at degraded accuracy. Methodology developed for wind energy conversion systems (Ref. 30) well might be useful for solar thermal plants as

well. This three-dimensional model interpolates values of wind from measurements at irregularly spaced stations (weather stations) and accounts for terrain features.

The influence of complex terrain features on local wind conditions has received considerable attention in recent years, e.g., Refs. 31 through 34. In Ref. 31, theoretical statistical models involving the key turbulence parameters were developed for uniform and rolling terrain, as well as for complex terrain including hills and escarpments. Table 3 (from Ref. 31) shows a qualitative relationship that was conjectured for turbulence and atmospheric weather conditions. Note that moderately and extremely unstable conditions tend to occur together with light, daytime winds. Wind tunnel model tests and measurements for a variety of complex terrain configurations are reported in Refs. 32 and 33. A classification of the effects of terrain on atmospheric motions is shown in Table 4 (from Ref. 32). Note use of the terms: microscale, mesoscale, and macroscale, and the regimes for which physical models have been studied.

Field measurements over complex terrain are reported in Ref. 34. It was found that fluctuations in vertical velocity were governed alone by the surface roughness length. However, larger-scale terrain features themselves were found to increase fluctuation of the horizontal wind components.

At a selected site, the placement of both insolation and wind measurement instrumentation is important for determining accurate, long-term plant performance and, in the case of wind, for determining when the concentrators (or heliostats) are to be driven to stow position for safety and survival during plant shutdown.

Insolation measurements made at Barstow, California, (Ref. 35) over a field area approximating the Solar 10-MWe Pilot Plant size indicated both spatial and temporal changes due to irregular cloud cover. These phenomena have practical applications for selecting the number and location of insolation measurement instruments that determine plant performance and control transient operation. It is interesting that the wind energy conversion developers (Ref. 36) have made a similar study with respect to wind measurements from wind turbine field arrays. Errors in establishing reference wind velocity can occur according to the placement of the measurement instruments (anemometers) with respect to the field array.

SECTION IV

DESIGN WIND SPEED

At one time the building and structures industry used peak velocities from maximum gust records for design wind speed; the inadequacy of this approach has been discussed (Ref. 11). It is now common practice in the United States to use the annual extreme wind velocity averaged over 1 mile, or 1 min, as the basic design wind speed for steady wind loads. The approach has been developed by Davenport (Refs. 11 and 37), Thom (Ref. 38), and others. The "extreme fastest mile" (or minute) has a sound physical basis, is well suited to natural wind phenomena, adapts well to existing wind instrumentation and, therefore, permits maximum uitilization of the numerous weather station recording facilities at airports. It seems to be the best approach for solar field applications as well.

Sets of wind/weather records may be related numerically by extreme value theory to account for the number of years of record, the quality and consistency of records, the location of instrument height above ground, and the relative ground surface roughness. The standard height for quoting basic design wind speeds is 30 ft, in the United States. These data easily can be converted to any desired height by applying the power-law velocity profile; for many airport sites the weather data correspond well to a 1/7 power law (Figure 6). As will be shown, data that are adequate for preliminary design purposes exist, and may be used if specific site data is lacking.

A. STATISTICAL APPROACHES

Wind risk models are useful for generating design approaches. The probability for the occurrence of wind velocity near Barstow, California, is illustrated in Figure 13 (from Ref. 10); the annual probability for winds to exceed 50 mph is 35 to 40%. Note that the probability of occurrence of tornados (an extreme, unstable, local storm) is orders of magnitude less than "straight" winds associated with large, mature storms (Figure 13). This is in agreement with other estimates for tornados (Ref. 38).

Essentially equivalent approaches are outlined in Refs. 11, 37, 38, and 39. Annual extreme wind data series are fitted with an empirical distribution function which can be expressed as:

$$F = \exp[-(V/\beta)^{-\delta}] \qquad (4)$$

where V is a threshold wind velocity, β and δ are parameters that are estimated from actual wind data, and F is the probability that the annual extreme fastest mile will be less than V. An example of such a fit is illustrated in Figure 14. The parameter $(1 - F)$ is related to the risk probability of Figure 13. However, it seems that different distribution functions were employed to obtain Figures 13 and 14 (note that the ordinates of Figure 14 are not logarithmic scales). Information such as shown in Figure 14 can be applied for design purposes.

A more useful and practical approach introduces the concept of structure (plant) lifetime. Lifetime is defined as the number of years of usefulness, T, as determined by obsolescence or deterioration. Introducing a risk q that the basic design wind velocity V will be exceeded in T years, the mean return (or recurrence) period R of the basic wind speed is given by:

$$R = -T/\ln(1 - q), \text{ or } \sim T/q \text{ for small } q \tag{5}$$

Building codes (e.g., Ref. 40) specify that R should be: (1) 100 years for permanent structures that present a high sensitivity to wind and an unusually high degree of hazard to life and property, (2) 50 years for ordinary permanent structures, and (3) 25 years for negligible risk structures that are not intended for human application. Until contrary evidence is presented, it seems that R = 100 years should be adopted for solar plants. Equation (5) is plotted in Figure 15 for three different values of T. Clearly, large values of R are required to achieve a low risk, q. For T = 10 and q = 0.10, R = 100 years. Structure designs become increasingly robust as the risk q diminishes, or as the recurrence period R increases.

The required gradient wind velocity (see Section III.1 and Figure 2) to satisfy the basic design speed is obtained by extreme value theory (see Refs. 11, 37, and 38):

$$V_G = \frac{1}{a}\left\{-\ln\left[\ln\left(1 - \frac{1}{R}\right)\right]\right\} + u \tag{6}$$

where a and u are determined from local wind data. Values of V_G can then be transformed to basic design speed at a reference height (e.g., 30 ft) by applying the appropriate terrain roughness factor and the power-law velocity profile (Equation 2).

This process has been done for the entire United States (e.g., see Ref. 40), and the results are suitable for very rough design purposes. Contour maps for three different recurrence intervals are given in Appendix B; the annual extreme fastest mile is referenced to a height of 30 ft above ground. The average extreme fastest mile governs the annual maximum, steady wind loads; it does not account for gust loading. Values of the basic wind speed from the figures given in Appendix B can be converted to any height desired by using Equation(3).

B. EFFECTS OF WIND GUSTINESS

For structures that are anticipated to be sensitive to gust loading, there are standard procedures for dealing with gustiness (Ref. 40). This is done by assigning gust response factors that account for an increase in loading over that derived from the basic design speed. A general expression for the gust response factor is:

$$G_F = c_1 + c_2\,(\sigma\sqrt{P}) \tag{7}$$

where $\sigma\sqrt{P}$ is the ratio of the standard deviation of the wind loading to the mean wind loading, and c_1 and c_2 are constants. A value of $G_F = 1.0$ corresponds to the fastest-mile wind speed. Gust response factors do not account for vortex shedding or instabilities because of galloping or flutter. Vortex shedding, a precursor of galloping, can generate aeolian vibrations (like

violin strings); galloping is a high-amplitude, low-frequency vibration such as may occur in ice-coated electric transmission lines, towers, and tall, slender buildings. Gust reponse factors are best determined from wind tunnel model tests. Detailed information on gust response factors can be found in Refs. 41, 42, 43, and 44. It is interesting that some wind data shows that there is a linear relationship between peak wind gusts and the annual fastest mile (Ref. 38). However, in Ref. 44 it is shown that the annual mean wind speed and the annual peak gust speed correlate very poorly.

For specific design purposes, more sophisticated approaches have been developed (Ref. 22) The velocity of gust responses is examined with respect to the mean response, the probability of the response, and its spectrum (Figure 16). Using conventional assumptions, a linear differential equation can be developed for the response of an elastic structure to fluctuating pressure forces (Ref. 22). If the velocity fluctuations are small compared to the mean wind speed and are sinusoidal, analysis indicates that pressure fluctuations are four times as great as the velocity fluctuations. Corresponding forces and moments arising from gusts then may be calculated. In Figure 16, the aerodynamic admittance relates the fluctuating aerodynamic forces with the fluctuating velocities arising from wind gusts.

Short duration gusts can be an important concern to the antenna or concentrator designer. Dynamic load response depends on the history of the load as well as the structure. Structure behavior can be assessed in terms of the natural period of vibration of elastic systems. Peak loads and time history have no significance for gust durations that are small compared with the natural period. The opposite is true for gust durations of the same order as the natural period. Critical components smaller than the reflector structure may have much shorter natural vibration periods; thus, information on very short duration gusts may be necessary to establish safety factors for all the individual structural components.

C. HEIGHT SELECTION FOR DESIGN WIND SPEED

Because wind forces are proportional to the dynamic pressure ($\rho V^2/2$), and the wind velocity varies with height above ground, a natural question arises as to how the height above ground should be selected for a given structure. If the maximum height of the structure is selected, then it is likely that a very conservative structural design will result, i.e., an over-design. In the final stages of design, large and very tall structures (or structures that are highly sensitive to wind) will require specific and detailed analyses using the best site-specific wind data that are available. For preliminary design, more convenient and simpler approaches are appropriate.

To assess this problem for solar concentrators, an elementary analysis has been performed (Appendix C). As an approximation, a square plate with basic dimension L and a ground clearance g is placed vertical and normal to an approaching wind with speed V. A power-law wind velocity profile is assumed but ground interference effects are ignored. Force is obtained by integration of the wind pressure over the area of the square plate; for this purpose force coefficients are assumed to be unity. The result is compared with the force calculated using the velocity at the height of the plate centerline. A second case is considered by comparing the force calculated using the wind speed at

the top of the plate and the force calculated using the centerline speed. When the force ratios are formed for the two cases, the results can be expressed in terms of two parameters, the dimensionless ground spacing b = g/L, and the denominator n of the power-law exponent, see Equation (2).

The results are shown in Figure 17. Figure 17a is a plot of the ratio of the "actual" (integrated) force to the force derived from using the centerline velocity. For n = 2, i.e., parabolic wind velocity profile, the ratio is unity for all b, indicating that zero error is incurred by using the plate centerline velocity. Use of the centerline velocity will underestimate the actual force by approximately 3% or less for $b > 0.1$. The force ratio using wind velocities at the top and centerline of the plate, respectively, is shown in Figure 17b. This ratio may be viewed as a safety factor. For n = 7, the ratio is between 1.2 and 1.1 for $b > 0.1$.

These results clearly are illustrative only; they will not be accurate for paraboloidal concentrators over widely varying azimuth and elevation angles. They do show, however, that the design wind speed corresponding to the concentrator centerline probably is adequate for first-order estimates of wind forces.

D. RECOMMENDED DESIGN SPEEDS FOR EDWARDS AIR FORCE BASE

The JPL Parabolic Dish Test Site (PDTS) is located at Edwards Air Force Base, California (Ref. 28). The approach used in Table 1 was adopted; the center point of the Goldstone antenna was assumed to be 115 ft above ground. All values were scaled down to a standard 30-ft height using a 1/7 power-law wind-speed profile applicable to flat, open country. An exception was made for the survival of the reflector in any position; for this case the design speed was retained as 70 mph, which agrees with Figure B-1 (Appendix B) for R = 100 years. Further adjustments were made taking into account the data given in Ref. 45. The base values for standard 30-ft height then were scaled with height above ground using a 1/7 power-law profile. The results are shown in Figure 18. Design speeds for any size concentrator may be obtained for the five selected operating conditions by selecting a height above ground corresponding to the reflector centerline, or pivot point.

E. STANDARDS AND CODES

Although the annual extreme fastest mile is used as the basis for design wind speed in the United States (Ref. 40), this is not the case in Australia, Britain, and Canada (Refs. 44 and 46). Tables 5, 6, and 7 (from Ref. 46) show comparisons of these four standards for wind loading. Tables 5 and 6 show the differences in the reference wind speed; the differences are significant, considering that wind forces and moments depend on the square of wind speed. Table 7 indicates that the Australian and Canadian standards are more flexible than the British and United States standards. Consult Ref. 46 for the cited references to the foreign standards.

SECTION V

REVIEW OF PREVIOUS STUDIES

Although emphasis is placed herein on paraboloidal, two-axis tracking solar concentrators, it is of interest to review, briefly, previous work done on other types of collectors and concentrators.

Experimental and theoretical wind loading and heat transfer work on flat-plate collectors is reported in Refs. 47, 48, and 49. References 48 and 49 also give results on air flow over buildings for the application of roof-top collectors, a subject that is not widely discussed in the solar literature. Single collectors, or arrays, mounted on the roofs of industrial, commercial, or residential buildings will experience greatly different approaching wind conditions than are discussed in Sections III and IV. The power-law index 1/n (Table 2 and Figures 5 and 6) is very large for urban centers and may not be applicable in specific cases because of the complex configuration of local buildings and structures. One effect, the lateral spacing of buildings, is treated in Ref. 50.

Work on flat-plate photovoltaic arrays is reported in Refs. 51 through 53, and work on parabolic troughs and trough field arrays is reported in Refs. 54 through 57. Considerable work has been accomplished on heliostats (Refs. 58 through 65), varying from wind tunnel tests on a full-scale heliostat to models of field arrays including the effects of perimeter fences. Further discussion on heliostats is given in Section IX. Sachs (Ref. 44) provides much information on the aerodynamic coefficients of paraboloidal radio antennas. A detailed review of paraboloidal reflectors and concentrators is given next in Section VI. Murphy (Refs. 66 and 67) provides some interesting wind-loading comparisons among various types of collectors and concentrators; his work will be discussed in Section VI. I.

SECTION VI

AERODYNAMICS OF PARABOLOIDAL DISHES

A paraboloidal concentrator essentially is a circular, parabolic-arc airfoil which, depending on design, may or may not have a sharp leading edge. In general, it will behave aerodynamically like an airfoil, or airplane wing, located near the ground. Ground interference effects may be more important at some combinations of azimuth and elevation than at others (the corresponding terms in aerodynamics are yaw, and pitch, or angle of attack), just as airfoils experience an "added" lift at angle of attack near the ground. The resultant force on the concentrator acts through the center of pressure and, for convenience, may be resolved into three components, e.g., lift, drag, and lateral force. Moments arising from these forces will depend on the structural pivot-point location with respect to the paraboloidal surface. The power required for actuating drive components will be determined by the moments, or torques.

Even when the wind is parallel to the ground, the relative wind vector may differ in attitude because of upwash and downwash effects induced by the concentrator acting as an airfoil. Just as an aircraft has wing-fuselage interference effects, so a solar concentrator will have varying aerodynamic interference effects arising from the base structure, the supporting structure, alidade, multipod structure supporting the receiver/engine, etc. In addition to static wind loads, dynamic wind loads arising from turbulence or gusts may be important for pointing/tracking considerations. Finally, in a field array, mutual flow blockage of adjacent concentrators and wind-channeling effects between rows cannot be ignored. In a field array, the field layout for "best" aerodynamic behavior may not coincide with optimal layouts determined from solar concentrator shadowing considerations. It is not difficult to see that wind aerodynamic effects are very complex and that wind loads must be thoroughly understood to arrive at viable designs.

Flat plates, at angle of attack, behave somewhat differently than airfoils; an analogy is the difference in wind loads between heliostats and paraboloidal concentrators. A dish facing into the wind will have a higher drag than a flat, circular plate of equivalent diameter. Figure 19 indicates this clearly, and shows the drag coefficient of hollow sheet metal caps facing directly into the wind as a function of depth-to-diameter ratio h/D. Radio antenna literature more frequently uses h/D than f/D; the latter is more familiar to solar concentrator investigators. Because wind load samples from radio antenna literature will be presented later, it will be convenient to the reader to have a ready reference conversion. The relationship between h/D and f/D is shown in Figure 20. An extensive theoretical treatment of paraboloidal dish aerodynamics is presented in Ref. 68. Some wind tunnel data on models of large radio antennas are given in Ref. 69, and are compared with theory developed therein. JPL wind tunnel test results on paraboloidal reflector models, including the Goldstone antenna, are given in Refs. 13, 70, and 71, which are summarized in Ref. 5. Extensive bibliographies are available in Refs. 68 and 70.

A. AXES SYSTEMS FOR FORCES AND MOMENTS

In using the wind tunnel literature on paraboloidal reflectors, the reader is cautioned to determine which coordinate system is being used in a specific reference. Additionally, the sign conventions for positive and negative directions of forces and moments vary among different authors and need to be understood by the user. A starting assumption is that the ground surface is always flat and level, which is automatically satisfied in most wind tunnel testing. Field conditions, however, may vary.

Forces and moments arising from wind loads, which are caused by pressure variations across the reflector surfaces, may be expressed in several orthogonal Cartesian coordinate systems with varying angular orientation (Ref. 70):

(1) Wind Axis: An axis system that is always parallel to the ground surface, the wind direction, and the direction of gravity.

(2) Body Axis: An axis system that is always parallel and perpendicular to the axis of symmetry of the model body (paraboloidal generating centerline). In this particular case, the side force is also parallel to the ground surface as there is no roll angle.

(3) Stability Axis: An axis system that is parallel to the ground surface and the direction of gravity but is perpendicular to the model axis of symmetry (and, therefore, not necessarily parallel to the wind direction).

These three axes systems coincide when the yaw and pitch angles (azimuth and elevation angles) are zero. The wind-axis system is used commonly in aeronautics. For azimuth-elevation mounted paraboloidal reflectors, Ref. 70 recommends use of the stability-axis system; however, the body-axis system is used in Ref. 72. References 68 and 69 use the wind-axis and the stability-axis systems, respectively. The position of the center of moments for the stability-axis system, Refs. 13 and 70, is the paraboloidal surface-generating centerline measured from the vertex of the paraboloidal reflecting surface.

The stability-axis system is shown in Figure 21; the sign conventions for the various forces and moments are those used in Ref. 13. In the body-axis system (Ref. 72), the lateral force is called the side force; the normal and axial forces are perpendicular and parallel to the surface-generating centerline, respectively, and the axial force is parallel to the ground only when the elevation angle is zero.

B. DEFINITIONS OF AERODYNAMIC COEFFICIENTS

Conventional dimensionless aerodynamic coefficients are used. The force coefficients are defined as:

$$\frac{\text{(force)}}{\text{(dynamic pressure) x (reflector frontal area)}}$$

and the moment coefficients as:

$$\frac{\text{(moment)}}{\text{(dynamic pressure) x (reflector frontal area) x (reflector diameter)}}$$

and the pressure coefficients as:

$$\frac{\text{(local surface pressure) - (ambient static barometric pressure)}}{\text{(dynamic pressure)}}$$

Reflector frontal area is the same as aperture area. Sometimes (Ref. 70) the pressure coefficients are plotted in the form ΔC_p, where the delta refers to the difference in pressure coefficients between the front and rear surfaces of the reflector at corresponding coordinate positions. The dynamic pressure is defined as:

$$(1/2)(\text{ambient static air density}) \times (\text{air velocity})^2$$

For example, when standard sea-level density is used with a wind speed of 50 mph, the dynamic pressure exceeds six pounds per square foot.

Having determined the aerodynamic coefficients from wind tunnel model tests, wherein the forces, moments, and pressures are measured experimentally or from theory, then the forces and moments for any size structure or wind speed can be determined from the known coefficients. This presumes, of course, that the conditions of dynamic similarity between model and full-scale structure have been preserved.

For convenience, the ratios of force-to-force coefficient, and moment-to-moment coefficient, are plotted in Figures 22 and 23 as a function of mean wind speed $\overline{V}$ for concentrators of varying diameter. These plots correspond to the product of dynamic pressure and aperture area, and to the product of dynamic pressure, aperture area, and dish diameter, respectively. Absolute values of force and moment may be obtained from Figures 22 and 23 by multiplying graphical values by appropriate force and moment coefficients determined experimentally or obtained from the literature.

C. ASPECTS OF WIND TUNNEL TESTING

Full-scale and model testing in wind tunnels has become an indispensable and cost-effective research and development tool in aeronautics and astronautics. Many specialized wind tunnels have been developed to address specific requirements. In recent years environmental wind tunnels have been developed to study wind characteristics of all types of man-made structures, e.g., model cities, smokestacks, etc., and to carry out research on topographic land surface models. When compared with full-scale field tests, wind tunnel tests using models are convenient, low-cost, and have the advantage of superior and systematic controllability. However, the drawbacks and limitations should be recognized as well.

Careful attention should be given to preserve geometrical similarity between model and full scale; there are instances where this must be violated because of practical constraints. For example, surface finish cannot always

be modeled accurately. In the case of paraboloidal dishes, the expected ground surface roughness should be modeled; fortunately this is not difficult for terrain that consists of flat, open country (Figure 6).

Flow similarity must be maintained, and this has two aspects: (1) mean, or quasi-steady flow, and (2) fluctuating flow. The latter aspect is much more difficult to simulate. For paraboloidal dish modeling there are at least three key simulation factors to be preserved: (1) dynamic (quasi-steady) flow, (2) velocity profile of wind (Figure 3), and (3) turbulence properties (intensity, eddy size, and the frequency of turbulent fluctuations). The turbulent properties of wind can be modeled, but the very random gustiness characteristics are more difficult.

The usual flow similarity parameter is the Reynolds number, which can be perceived as a ratio of inertia to viscous fluid forces, and is dimensionless. Reynolds number characterizes distinctive flow regimes. Compressibility effects (Mach number) will not be important for paraboloidal dishes; however, very high-speed wind tunnel tests using tiny models should be avoided. Thermal modeling of wind flows cannot be ignored completely, but thermal effects are thought to be of second order.

Flow-scaling laws for paraboloidal dishes (or heliostats) have not been firmly established. A reasonable approach is given in Ref. 5. The drag coefficient of common bluff objects as a function of Reynolds number is given in Figure 24. Circular and square flat plates are relatively insensitive to Reynolds number. Bodies that have curvature in the direction of flow (cylinders, spheres) are very sensitive to Reynolds number, especially in the range $10^5 < Re < 10^6$. The onset of the critical Reynolds number, which may depend on free-stream turbulence level and relative surface finish, portends transition to fully turbulent boundary layer and wake structure. Figure 24 suggests that Reynolds numbers greater than 10^6 should be maintained. Full-scale dishes in moderate winds easily will exceed that value.

Further insight is obtained from Figure 25, which is a general plot of Reynolds number as it varies with mean wind speed and characteristic geometric dimension. A dish with diameter of 30 m will have $Re > 10^6$ for almost all, but zero, wind speeds. A 1/100 scale model, i.e., diameter equal to 0.3 m, would require wind tunnel speeds in excess of 100 mph to achieve $Re > 10^6$. The picture for smaller structures, i.e., quadripod supports, is different. The possibility exists that small, full-scale structures in high winds will be subject to a different flow regime when modeled to small scale. The consequences probably are not significant except for aerodynamic amplification arising from vortex shedding that could cause differing vibrational characteristics in the different flow regimes.

Figure 24 suggests that curved surfaces should be avoided because of inherent flow instability problems, e.g., see Ref. 73. As a matter of fact, most large radio antennas employ box-like supports in the quadripod structure rather than pipes or cylinders to alleviate this problem (see Refs. 5 and 68). See also Ref. 2 relative to bridge structures. The vortex shedding and wake structure of cylinders are extremely complex (Ref. 73).

A final concern is wind tunnel blockage. Obviously, if models are relatively large compared to the wind tunnel cross-sectional area, then the

flow field experienced by the models will become modified and will not represent undisturbed "free-stream" conditions. Ways to offset this problem are discussed commonly in the wind tunnel literature. Further, accepted methods of correcting for wind tunnel blockage are available (Ref. 74). Basically, the treatment of bluff bodies in wind tunnels cannot be treated with independent contributions of body blockage and wake blockage, as is the case for slender bodies.

Despite all caveats, meaningful wind tunnel testing of paraboloidal concentrators is feasible and has relevant practical application. Historically, the successful design and application of large radio antennas would have been severely hampered without guidance provided by wind tunnel testing of models.

D. GENERAL FLOW FIELD CONSIDERATIONS

Some interesting features of wind flow over single concentrator modules are suggested by Figure 26, which shows the concentrator at an elevation angle of approximately 45 deg (zero azimuth angle), but with the wind approaching the front surface (upper figure) and the rear surface (lower figure), respectively.

If the approaching wind velocity was uniform, ground effects were negligible, and the effects of base and concentrator support structure and receiver support structure were negligible, then symmetry would prevail in the wind-axis system. That is, equivalent azimuth or elevation angles (expressed as a single angle-of-attack) would yield identical wind loading. Departures from symmetry will depend on all of the above factors. An illustration is shown in Figure 27; the side force and the lift force are symmetric and equivalent except for angles of about plus and minus 30 deg from the zenith position.

A turbulent wake will prevail behind the dish and, beyond the stall point of the dish, separated flow with reversed velocity will occur. Experimental data for the flow field behind a circular, flat plate normal to a uniform wind are shown in Figure 28 (from Ref. 68). It is evident that the region of separated flow extends about three plate diameters downstream. A receiver placed behind the plate would experience a reversed flow region. The size and shape of the separated flow region obviously will depend on angle of attack with respect to the wind.

Shielding effects are evident in Figure 26. For front-facing wind (upper part of figure), the receiver wake would influence a portion of the top surface of the dish. This effect diminishes at higher elevation angles near zenith. Conversely, for rear-facing wind (lower part of figure), the receiver is influenced by the wake of the dish. Similar comments apply to the base structure.

For front-facing wind (upper part of Figure 26), the lift force is negative and the elevation moment tends to rotate the dish towards the wind. For rear-facing wind, the elevation moment tends to rotate the dish to the opposite direction. However, at elevation angles below the stall point, the moment is in fact opposite to that shown in the lower part of Figure 26.

Ground effects will depend mainly on the size of a concentrator and the relative ground spacing. An insight into ground plane effects is shown in

Figure 29 (from Ref. 68). Plotted is the additional contribution to local free-stream velocity because of ground presence; the result shown is based on theory. Ground effects become negligible when the gap-to-diameter spacing g/d exceeds 0.3. The case shown (Figure 29) is for a solid reflector with a value of g/d = 0.0167 for zero elevation angle. Basically, the presence of the ground changes the pressure distribution over the reflector surface; ground pressure will tend to influence lift forces more than drag forces. Ground effects should be essentially negligible for dishes in the stow (horizontal) position.

An example of velocity profile effects is shown in Figure 30 (from Ref. 5). Wind tunnel results for a particular reflector model are given for elevation moment at two angles of elevation for varying azimuth angle. Contrasted are results for an essentially flat boundary-layer profile and an approximate 1/7 power-law profile (see also Figure 3). Considerable effects are evident. The other two moments and the three forces are not as much affected by velocity profile when the reference velocity is taken at the dish centerline (Appendix C). Detailed results for the Goldstone antenna model are given in Ref. 5, which contrasts the same two velocity profiles. Other information on wind profile effects is given in Ref. 69.

The smoothest flow field around a dish concentrator might be expected when the dish is edge-on to the wind (stow position). Damage results of an intense hail storm at Sandia, Albuquerque, are described in Ref. 75. During the storm the Raytheon dish was stowed facing vertically upwards and sustained no hail damage. Speculation may be employed to associate lack of damage to dish aerodynamics, i.e., hail impact could have been minimized because of the flow field induced by the wind.

In a field array, the wakes of dish concentrators will have some influence on downstream concentrators. Also, adjacent concentrators will be influenced by one another.

E. REVIEW OF WIND TUNNEL TEST RESULTS

All known wind tunnel test results for paraboloidal reflectors were obtained from model studies on radio antennas; comparable results for solar concentrators apparently are not available. Most of the earlier theoretical and experimental studies for paraboloidal reflectors were performed with uniform velocity profiles using single reflectors (no field-array results). Sample results given herein derive from Refs. 5, 13, 68, and 72.

Figures 31, 32, and 33 (From Ref. 68) show wind tunnel test results for the drag, lift, and yawing (azimuth) moment coefficients, respectively, of a solid reflector (porosity $\phi = 0$) as a function of angle of attack in the wind-axis system. Curves for various depth-to-diameter ratio values are shown (see Figure 20 for conversion to f/D). The angle of attack α in the wind-axis system easily can be expressed in terms of both the elevation and azimuth angles (Refs. 68 and 69). Note that the relative wind vector V may differ from the actual wind vector (with respect to ground) because of upwash effects created by the dish acting as an airfoil (see Ref. 68).

As expected, the minimum drag (Figure 31) occurs at zero angle of attack; the deeper dish has the higher drag. Maximum lift (Figure 32) occurs at a positive angle of attack of 30 deg, which corresponds to an elevation angle of 60 deg for zero azimuth angle, and is directed towards the ground; thereafter the dish becomes aerodynamically stalled. The lift is low, and directed upwards for negative angles of attack (see Figure 26). The yawing moment is negative (as defined in Figure 33) for positive angles of attack greater than 20 deg to 30 deg; peak moments occur at a negative angle of attack of about 30 deg. Note that the deeper dishes are subject to the highest yawing moments, as might be expected. The data in Figure 33 came originally from Ref. 70.

A composite graph (from Ref. 68) is shown in Figure 34. The results were calculated from empirical considerations. A purely theoretical lift result is also shown for comparison as based on potential flow theory; it is high because it does not account for real flow effects.

A wide variety of data illustrating the effects of various parameters on the wind tunnel results of model paraboloidal reflectors are given in Ref. 5; most of the results presented were for the azimuth or yawing moment because of its design importance. Selected graphs are shown in Figures 35 through 38. The test Reynolds number based on dish diameter was 2.7×10^6. Results were for a single model with an essentially uniform and steady wind velocity profile. The stability-axis system (Figure 21) was used to reduce data. Data were used to help design the 210-ft Goldstone radio antenna; see also Refs. 13 and 44.

Figure 35 shows the azimuth moment coefficient (about the reflector surface vertex) as a function of azimuth and elevation angles. When the azimuth angle is zero, the dish faces directly into the wind; when it is 90 deg the dish "sees" the wind approaching edge-on; and when it is 180 deg the dish faces directly downstream. For high-elevation angles (approaching zenith), the azimuth moment is small and varies little with the azimuth angle.

The effect of depth-to-diameter ratio is shown in Figure 36; note that $h/D = 0$ corresponds to a flat, circular plate. The curves for $h/D = 0.189$ in Figures 33 and 36 are identical. In Figure 36, the arrows indicate azimuth angles at which the edge of the reflector is parallel with the direction of the approaching wind. For a flat plate, this angle is 90 deg; for other h/D, this is not true because the flow field is three-dimensional because of the dish curvature, as explained previously. Side (or lateral forces) are a stronger function of h/D than are the axial, or drag, forces (Ref. 5).

The effect of moving the azimuth moment center forward or aft of the vertex, but along the paraboloid centerline, is shown in Figure 37. Both positive and negative peak moments can be reduced considerably by moving the moment center forward of the vertex. However, depending on the particular design, a penalty might be incurred by increased structural weight and changes in stiffness.

A final example is shown in Figure 38, where some effects of reflector surface support structure are illustrated. Extended counterweights, using fairings, for example, can reduce azimuth moments. According to Ref. 5, support structures generally have a tendency to reduce peak loads, but in certain cases they may increase the loads.

Complete wind tunnel results for the model Goldstone radio antenna (from Ref. 13) are presented in Appendix D for reference. These results depict the three force and the three moment coefficients as they vary with azimuth angle from zero to 180 deg and elevation angle from zero to 90 deg, all in the stability-axis system (Figure 21). Reference 72 contains extensive tables of suggested aerodynamic force and moment coefficients for four specific paraboloidal reflector configurations. Basic parameters are h/D, or f/D, and reflector porosity P. Combination No. 1 pertains to a solid reflector with f/D = 0.313. All results are referred to the body-axis system. Recall that this axis system utilizes the surface-generating centerline of the reflector. Trigonometric relations are readily employed to convert forces and moments from one axis system to another. A set of summary curves is shown in Figure 39 (from Ref. 72) for the four configurations at zero azimuth angle, i.e., only elevation angle is varied. The relative magnitude of the various coefficients can be interpreted for the body-axis system from Figure 39: the predominant force and moment is the axial force (parallel to the generating centerline) and the pitch, or elevation, moment. Because the aximuth angle is zero, the other four aerodynamic coefficients are small or negligible, as would be expected.

Another convenient and illuminating comparison is found in results for (flat-plate) heliostats. Wind tunnel test results of a single, full-scale heliostat are available (Ref. 61). Heliostat investigators tend to use yet another axis system: forces and moments are measured with respect to the intersection of the ground and the central, post support. Some typical measurement results are presented in Appendix E; this experimental data may be compared with the analytical results (Ref. 65) presented in Appendix F. Heliostat results would be expected to approximate flat-plate results, and this turns out to be the case.

Reynolds number effects were found to be negligible in Ref. 5 provided that the values exceeded 10^6 based on dish diameter. Some data available for heliostats (Ref. 62) permit an assessment of scale factor. Results are shown in Figure 40, where base moment coefficients are plotted against Reynolds number. The moment coefficients have been normalized to the value obtained for a full-scale heliostat (see also Ref. 61); the cross-hatched region has been estimated by the present author. It is encouraging that results for models will tend to overestimate the values appropriate for larger, full-scale configurations. Errors on the order of 10% to 20% maximum might be anticipated for models where the test Reynolds number exceeds 10^6. Comparable data are not available for paraboloidal dishes.

An interesting R&D program was begun in 1970 by LTV Electrosystems, Inc. (Ref. 79). The objectives were: (1) to compare all available wind tunnel test data for paraboloidal antennas to produce computer plots of wind load coefficients, (2) to use the plots to quantitatively establish the effects of changes in the antenna structure on wind load coefficients, and (3) to develop empirical formulas for the coefficients to be used for design purposes. LTV obtained six sets of test data for nine different wind tunnel models (including JPL results given in Ref. 13 and 70) and one set of data for a full-scale 60-ft dia antenna. First, all data had to be converted to one set of coordinates, axes, and sign conventions; a computer program was developed for the body-axis system. Only limited results were given. Two succeeding quarterly reports

following Ref. 79 have not been located. "Universal" coefficients for wind loads would be very useful to a high degree of confidence.

Another interesting study is seen in Ref. 80. Three diameters of paraboloidal reflectors (15 m, 26 m, and 40 m) were examined theoretically; backup structures were designed to accommodate combinations of gravity, seismic, wind, and snow loads. Changes in structure weight were determined as a function of wind speed. Survival wind speed was assumed to be twice the maximum value for drive to stow. Percent weight increases (and, presumably increasing structure costs) were not found to be strongly influenced by wind speeds less than about 80 mph. Rather, the slenderness ratio of structural elements, i.e., the ratio of length to radius of gyration of the cross section, was found to be the controlling factor for backup structure weight. The 15-m dish was examined for applicability as a solar collector and found to be satisfactory. If cost is proportional to weight, the results given in Ref. 80 would seem to suggest that wind loads are not of major concern.

However, the assumptions described in Ref. 80 need to be examined. First, the backup structure consisted of the traditional microwave antenna ring and rib construction that is not likely to be cost effective for solar concentrators. Second, performance degradation because of potential reflector panel deformation was not investigated. Third, only wind loads in varying elevation angle, and not in azimuth, were examined. Finally, only static wind loads were considered, and no allowance was made for gust loading or safety factors. Solar concentrators may have a wide variety of structural design concepts (see Appendix A of Ref. 1), some of them very flimsy indeed. Hence, this author remains convinced that wind loads on solar paraboloidal concentrators are and will be important to their design, performance, operation, and cost.

F. METHODS OF REDUCING AERODYNAMIC LOADS

The parameter that had the single greatest effect on reducing aerodynamic loads in Ref. 5 was reflector porosity. The pressure relief gained from uniformly distributed porosity can be construed as a "spoiler" effect. Peak moments (positive and negative), especially the azimuth moment, can be reduced substantially by porosity. Nor is porosity required over the entire reflector surface; reductions in loads can be achieved by incorporating porosity over the outer portion of the rim only. A value of 25% porosity over the outer 25% of the reflector radius is reasonably effective. The implications for solar concentrators is less clear. Whereas the optical contributions to focal plane flux are least at the rim, the contributing area at the rim is nevertheless the largest. The introduction of rim porosity would require a relatively larger concentrator aperture area. Because wind loads are the largest single contributor to concentrator costs, the tradeoff in increased size against potential wind load reductions would have to be examined carefully for each specific design. Many concentrator designs, e.g., those employing gore segments, individual mirrors, or petals, will provide some natural wind relief.

An unusual Fresnel-type parabolic concentrator has been designed and tested successfully to provide a large amount of wind relief (Ref. 81). The concentrator consists of annular conical frustums arranged on a parabolic substructure. Two designs were investigated: (1) a front-focus design, and (2) a rear-focus design, to correspond to frontal and rear-ward winds,

respectively. Whereas large reductions in wind drag were measured, the optical performance of these concentrators was greatly reduced compared to more conventional types.

For frontal winds, little can be done to decrease force coefficients on solid concentrators. Enclosure of concentrator support structure, by shrouds or fairings, is probably not worth the effort for rearward winds. Base and alidade structures could be provided with fairings, but they would need to be rotationally symmetric to afford gains considering wind from all directions. Small gains can be achieved by installing "spoilers" (short trip-ribs protruding from the rear of reflector surface, see Refs. 5 and 13). Moment coefficients can be reduced by shifting the pivot center of rotation forward of the reflector vertex (Figure 37), and by providing aerodynamic fairings to the counterweights (Figure 38). Methods of reducing aerodynamic loads on paraboloidal reflectors are reviewed by Sachs (Ref. 44, Chapter 9, Special Structures).

Because wind forces vary with the square of concentrator diameter, and moments vary respectively as diameter cubed, size alone will have important effects. A "wind engineering" viewpoint to keep concentrator sizes small, and close to the ground, is understandable but cannot be justified a priori.

In field arrays, perimeter wind fences, hedges, or other wind breaks can reduce loads on the outermost concentrators (the field interior is affected little). This will be discussed later.

G. AEROELASTICITY AND STRUCTURAL BUFFETING EFFECTS

An early and catastrophic failure of a major engineering structure occurred 40 years ago when the Tacoma Narrows Bridge (Puget Sound, Washington) collapsed because of wind interactions suffered in a mild gale (Ref. 2). This bridge had been designed for dead loads, live loads, and temperature effects, but only for static wind loads. An early pioneer who recognized aerodynamic instabilities as potentially dangerous was Steinman (Ref. 2). His definition of aerodynamic instability is still timely: "The effect of a steady wind, acting on a flexible structure of conventional cross section, is to produce a fluctuating resultant force automatically synchronizing in timing and direction with the harmonic motions of the structure so as to cause a progressive amplification of those motions to dangerous or destructive amplitudes." Much has been learned since that time. Today, for example, aerodynamic analysis for flutter of aircraft wings and structures is routine; hydrodynamic analysis is applied to underwater structures. Large buildings and structures are designed to account for wind gust loading (Refs. 22, 37, and 41 through 44).

The design of large radio antennas has not neglected aerodynamic considerations either (Ref. 3); general discussions are available (Refs. 82 and 83). Aside from wind conditions, the compatibility between the dynamic structural response of a paraboloidal dish and its control system, when operating in an automatic tracking mode, needs to be determined (Ref. 83). It is important to recognize that aerodynamic instabilities can occur in steady winds because of aeroelastic, self-excited vibrations which derive their

energy from the airstream. Additionally, there are the effects of unsteady airstream contributions arising from turbulence and gusts to consider.

Scruton (Ref. 82) has defined three classes of dynamic wind effects for paraboloidal reflectors: (1) oscillations of the reflector bowl as a rigid body on a flexible mounting, (2) oscillatory deformations of the flexible reflector bowl, and (3) the vibration of individual structural members (these may, or may not, be coupled). The various aerodynamic instabilities that may occur in paraboloidal dishes are complex and, even today, are not amenable to rigorous analysis in the design phase. Experimental wind tunnel investigations therefore are a useful adjunct to analysis.

To gain a better understanding of aerodynamic instability effects, it is instructive first to consider simple structural elements, e.g., cylinders, prisms, and other bluff bodies, in the light of vortex shedding phenomena (Refs. 73 and 84). As mentioned earlier, vortex shedding at low Reynolds number can lead to aeolian, or "singing," small-amplitude vibrations; these, in turn, can lead to large-amplitude, or galloping, vibrations that can become destructive. Typically, the latter occur when there exists a resonant condition between periodic wake structure and one of the natural, structural vibrational modes, e.g., transverse or torsional. Amplification of aerodynamic loads can result in such circumstances. Nonuniform free-stream conditions can affect the results (Refs. 85 and 86).

Significant vibrational motion itself may further enhance the wake structure and modify the flow field and resulting loads (Refs. 84 and 87). The effect of the upstream turbulence scale too is an important consideration; in general, drag forces reach a peak when the eddy size of turbulent fluctuations is about the same size as the bluff-body dimension measured in the direction of flow (Ref. 88). This has consequences for model wind tunnel experiments. The vortex shedding parameter, or Strouhal number, cannot always be held fixed for constant Reynolds number modeling. However, there are similarities between two-dimensional and axisymmetric wakes that have useful applications (Ref. 89).

Tubular elements frequently are used as members in reflector support structures. Slender cylindrical elements, which are especially susceptible to flow instabilities, have been studied experimentally (Refs. 82 and 90); helical strakes, or spirally-wound spoilers, have been found effective for suppressing aeroelastically-generated lift forces. Weaver (Ref. 91) has developed design charts for lateral vibrations of reflector support frames consisting of tubular aluminum members.

Dish reflector vibrations might be expected to occur when separated flow conditions or stalling phenomena occur at high angles of attack. An analogy is stalling flutter that can occur in aircraft wings. Under accelerating wind gusts, neutral stability may occur as the critical wind speed is achieved. Above the critical speed, called the critical flutter speed in Ref. 83, divergent oscillations may occur with sufficient intensity to cause structural damage or destruction.

A variety of reflector system vibrational instabilities are described in Ref. 83, which presents a simplified (but not elementary) analysis of dish reflector flutter. It is concluded that flutter-type aerodynamic instabilities are potentially significant and should be checked for specific reflector

designs. Some results of Hull's analysis for a particular reflector design are reproduced here in Figure 41; ω_α is the natural pitch frequency and ω_h is the natural plunge frequency (perpendicular to the generating axis of the reflector). The flutter speed (Figure 41a) has a minimum at $\omega_\alpha/\omega_h \sim 1.0$, but is sufficiently high that the system is stable for usual wind speeds. Corresponding structural damping factors for bending and pitch modes are shown in Figure 41b; aircraft criteria call for specifying flutter speeds at wind speeds for which a damping factor of +0.02 exists.

Aeroelastic wind tunnel investigations using models of larger structures may be questionable because it is difficult to reproduce dynamic model scaling parameters such as stiffness, mass distribution, and structural/aerodynamic damping (Ref. 92). In general, elasticity modeling is accomplished by providing a flexible mounting/support arrangement. Large radio antennas are relatively stiff and solid, and vibrations of the entire dish have been observed only rarely. Large reflector vibrations have been observed in models, however (Refs. 82 and 92). For example, Fox (Ref. 92) observed vibration amplitudes of the order of 1 in. at the edge of an 18-in.-dia model reflector.

Some model experimental results are given here in Figures 42 and 43 (from Ref. 92). Figure 42 shows oscillograph traces of relatively high-frequency oscillations in the three moment coefficients. In Figure 43, pitch-moment amplitudes are shown versus azimuth angle at zero elevation angle; they are compared to time averages (dashed curve).

Davenport (Ref. 22) has developed an approach for analyzing the response of paraboloidal reflectors to wind gusts. An illustrative calculation was given for a specific design of a 140-ft-dia radio antenna. The results were interesting: 14% of the total, dynamic thrust load was attributed to gusts, and 59% of the total moment was attributed to gust action.

H. STRUCTURAL DEFORMATIONS

Early work on structural deflections/deformations was cited previously (Refs. 6, 7, and 8). Static wind loads and gust loads affect the design and performance of paraboloidal concentrators in at least three ways. First, the increased stresses, which may be random and variable, affect the design of the reflecting surfaces and backup structure. Second, the distortion of optical surfaces will affect optical performance by reducing solar collecting efficiency and increasing the size of the receiver aperture. Finally, the control system must be designed to compensate so that pointing and tracking design requirements are met.

JPL performed a preliminary analysis of structural deformation effects at the receiver focal plane for an advanced solar concentrator conceptual design (Ref. 93). The structural deformation effect on the concentration of rays reflected by a representative concentrator with aperture diameter of 12 m was evaluated by determining the displacement of ray intercepts associated with 100 equal area regions of the dish relative to the displaced focus. The impinging rays were parallel with the undistorted optical axis (Figure 44a). For an undistorted dish, the rays would all intercept exactly at the focus. The effects of displacements and rotations of the reflective surface support structure (other than the mirrored glass gores), the feed support quadripod,

the azimuth axis pedestal, the structure between the azimuth and elevation axis, including the elevation drive linear actuator, were included. While the mirrored glass gores were treated as rigid, the effect of their distortion is expected to be small. The resulting distorted ray intercepts are shown in Figures 44b, 44c, and 44d for three separate loading conditions for all the 100 points.

The envelope of intercepts for the cases considered was no larger than a 9.0-cm-dia circle. It can be located within the aperture for static and slowly changing conditions such as wind loads, but not gust loads. The dispersion of intercepts (e.g., circular envelope diameter of 9.0 cm) due to structural deformation under the operational design loads at the focal point would contribute no more than 6% growth of receiver aperture (e.g., 1.6 cm above the baseline aperture diameter of 25 cm). This work was extended in Ref. 94 by treating the mirrored glass gores and their associated support struts as elastic rather than rigid bodies. The effect of this assumption, for the case considered, was to increase the diameter of the circular envelope of intercepts by 25% compared with the rigid-body case.

In their tradeoff studies on the low-cost concentrator design (Ref. 95), Acurex considered the effect of wind speed on the thermal power collected by the concentrator/receiver as affected by optical surface distortion. The result is shown in Figure 45. As expected, the decrease in relative thermal performance is significant when the relative receiver aperture diameter is small and the wind speed is high. However, at the baseline value of $d/D = 0.022$, the loss in performance for a 30-mph wind is only about 6% compared to the zero wind case.

An interesting study performed on heliostats was reported in Ref. 65. The total surface slope error was calculated for various combinations of gravity and wind loads as a function of heliostat elevation angle. The combined slope error was taken as the vector sum of the beam (ray) deflection error, the torque-tube (mounting post) torsional deflection error, and the torque-tube bending deflection error. Results are shown in Figure 46, where the rms slope error is expressed in milliradians. The contribution due to wind is relatively less than for gravity. For the combined case, wind plus gravity, the maximum slope error occurs when the heliostat is at an angle of 20 deg with respect to the wind direction. (See also Appendix F.)

To offset wind-induced deflections, there is a tradeoff between increasing the concentrator structural rigidity and utilizing compensation provided by the guidance (pointing and tracking) controller. This problem is studied in Ref. 96. Use of a compensating controller allows a large reduction in concentrator rigidity. However, an array of wind sensors within a field array of concentrators is required to provide the information necessary to calculate compensating corrections and actuator positions.

I. COMPARISON TO OTHER COLLECTOR/CONCENTRATOR TYPES

Murphy (Refs. 66 and 67) has compiled information and tabulated comparisons of different collectors/concentrators for wind speed requirements and representative wind load coefficients. Table 8 (from Ref. 67) shows wind speed requirements for various concentrator operating conditions. Values for

parabolic dishes may be compared with values given in Table 1. Drag, lift, and moment coefficients are compared in Table 9 (from Ref. 67); geometry and coordinates are defined in Figure 47. The aerodynamic coefficients among the various concentrators are of roughly comparable value (Table 9) but the parabolic dish drag and lift coefficients tend to be the highest, in agreement with previous observations. Maximum drag per unit area and dynamic pressure versus wind speed are shown in Figure 48; values were taken from Table 9.

SECTION VII

FIELD OBSERVATIONS OF THE OMNIUM-G CONCENTRATOR

An Omnium-G (OG) unit (OG-7500) purchased by JPL was installed and tested for several years at the PDTS located at Edwards Air Force Base, California. Generally, it was operated in the manual override mode because of early faults in the tracking electronics and the ephemeris clock. Subsequently, it was tested in the automatic operation mode.

A weakness in the early Omnium-G design was the elevation drive, which had considerable play, i.e., was "loose." This was evidenced by motion that could be introduced into the system when the concentrator was statically balanced, the tracker electronics was turned off, and there was no power being supplied to the drive motors. For this situation, an operator could grasp the concentrator support structure and, by applying physical force, could induce a considerable motion at the focal plane. In its "as delivered" state, this plane motion was approximately ±6 to ±7 inches. Several hardware changes were made by the Omnium-G Company: addition of an outboard bearing and an additional 10-to-1 gear reduction to the elevation drive assembly. This alleviated the problem somewhat so that the focal plane motion was reduced to approximately half of its original value, but some motion still persisted. This motion was no doubt intimately related to some of the observed behavior of the concentrator in winds.

Focal plane oscillations were observed for winds as low as 5 mph. Apparently, the tracker command signal and the mechanical drive motion became unsynchronized leading to an oscillation in the elevation plane which has been termed a "hobby horse" motion. The amplitude of the oscillation was sufficiently large so that, at maximum deflection, the solar image at the focal plane moved entirely out of the field of intercept for a 4-in. aperture diameter. Under some wind conditions that motion stabilized, and then damped out.

In high winds, with gusts exceeding 40 to 45 mph, the OG concentrator "weather vaned" on at least two occasions, i.e., the concentrator suddenly spun on its track, due to loss of frictional contact. Partly for this reason, the concentrator later was stowed facing zenith when not in use, and tie-down ropes were employed. High wind gusts caused several mechanical failures in the elevation drive. On one occasion, the OG system was hit broadside by a "dust devil" (whirlwind). This occurred in early afternoon when the concentrator was pointing 20 deg to 30 deg from zenith. Immediately, the concentrator was driven to the zenith position, but returned to its original position after the dust devil passed. It was an unsettling experience for on-site personnel.

Qualitative observations were made concerning the quadripod legs. These legs were tubular members to which had been welded fairings to approximate a sharp, "streamlined" trailing edge (see Figure 49); the trailing edges all point towards the concentrator centerline. The quadripod legs were observed to vibrate because of buffeting in winds exceeding 40 to 45 mph. Judged visually, amplitudes of approximately 0.25 in. occurred in a torsional mode. Moreover, under some conditions, these vibrations generated audible sounds. For reasons mentioned earlier, the cross-sectional shape of the quadripod legs

was not optimal from a fluid dynamic point of view. This shape is stable only when the leading edge faces the wind and the cross section is at zero angle of attack. Thus, when the quadripod legs are arranged as shown in Figure 49, almost any wind direction will render at least two of the legs susceptible to aerodynamic instability. See Ref. 2 for a discussion of stable and unstable structural sections.

Motion pictures of the OG concentrator operating in the "hobby horse" mode were analyzed frame by frame. The motion pictures were made during the late spring of 1979 when the wind was gusting to 40 to 45 mph. The cold-water calorimeter with aperture plate was installed at the focal point. Some sequences were shot of the image motion as it appeared through intensity-reducing filters. Motion of the image, primarily in the elevation plane, was probably due to a relative motion of the quadripod structure with respect to the dish as well as to the gross motion of the dish. The results of the film analysis were qualitative and incomplete, but revealed some interesting behavior. Image motion, at times, was approximately periodic (sinusoidal) and at other times was not. The period and amplitude of the oscillation was approximately 4 s, and ±6 to ±7 in.

SECTION VIII

THERMAL RECEIVER AERODYNAMIC ENVIRONMENTS

The point-focusing distributed receiver concept employs a thermal receiver and, for electric power production, a power conversion unit at the focal point of the paraboloidal dish. Means for mounting and locating this hardware usually is afforded by a multipod (multilegged) structure. Currently, internal cavity-type receivers are most commonly used. The presence of winds will affect the multipod and focal plane structures in three ways: (1) wind loading, which will affect the concentrator design and may affect performance because of pointing and tracking errors; (2) convection heat transfer losses, which will contribute to receiver performance degradation; and (3) noise generation from open cavity receivers, which may merely be a nuisance factor but might be related to cavity heat convection losses.

A. WIND LOADING EFFECTS

The multipod structure itself is not likely to contribute significantly to dish wind loading (Ref. 5); however, it must be sufficiently rigid to prevent large focal plane motions in moderate winds. Wind tunnel test results on solar dish models with installed receiver and power conversion unit models have not been performed so that the wind loading effects of focal plane structures can only be conjectured. Radio antennas probably have a lesser problem because they have a relatively shorter focal length and less weight and bulk at the focal point.

The receiver and engine/generator package is a bluff body that may have a roughly cylindrical shape and an aspect ratio (length-to-diameter ratio) on the order of two to three. There is not much experimental information known about the flow over such a body shape, especially for a wide range of wind directions and high Reynolds numbers. Reference to Figure 26 will bring the reminder that in many instances the receiver/engine will perturb the flow over the concentrator. In other instances the concentrator will block/shield flow over the receiver/engine, so that the latter may be in the concentrator wake (Figure 28). It would appear that wind loading effects on the concentrator caused by the receiver/engine would become maximum for grazing wind flow, i.e., when the angle of attack of the wind (the angle α in Figures 31, 32, and 33) is zero with respect to the concentrator. In this case, a substantial moment could be exerted on the concentrator structure due to drag of the focal point structure.

The flow over long circular cylinders (and other cross-sectional shapes) has been studied extensively over a wide range of Reynolds numbers, and the vortex shedding and wake structures are well understood. Practical application is very wide, e.g., flow over cables, bridge structures, posts, smokestacks, submarine cables, etc. There is little information, however, available for short cylinders where the flow is highly three-dimensional due to end effects. More information is needed for application to solar concentrators.

B. CONVECTION HEAT TRANSFER LOSSES

Receiver wind convection losses will occur from the external surface (shell) of the receiver as well as from the aperture. When quiescent ambient conditions prevail, the loss mode is free convection caused by buoyancy forces. Forced convection occurs with the blowing wind. When the transition occurs, i.e., when forced convection dominates free convection, is not wholly clear, especially for large surfaces. It is standard practice to calculate the free and forced convection heat transfer coefficients (Ref. 103), and to use the larger of the two for engineering heat transfer calculations. Attempts to analyze combined free and forced convection have not been notably successful (Ref. 104).

Shell convection losses can be minimized by providing ample insulation thereby reducing the exterior surface temperature. Aperture convection losses can be minimized by reducing the aperture area to the minimum possible, or by providing an aperture window. All convection losses will depend on the direction and magnitude of the wind with respect to both the concentrator and the receiver. It is likely that the greatest free convection loss from the receiver aperture would occur when the aperture is facing vertically upwards (concentrator nadir position), but this would occur only during the night and is, therefore, an insignificant case when an aperture cover is provided.

Estimates of shell free and forced convection losses are hampered by the same basic difficulty mentioned in the previous section, i.e., lack of definitive knowledge concerning the flow over short, circular cylinders. Of all the thermal receiver losses, including thermal radiation from the shell (relatively insignificant) and aperture radiation, the most difficult to assess is forced convection loss from the aperture. This is due to the complex interactive effects of fluid flow and heat transfer. Aperture forced convection losses will be explored in subsequent paragraphs.

The present author has compared standard heat transfer coefficient expressions for horizontal and vertical cylinders in free and forced convection, and for axial flow (wind parallel to the cylinder axis) and normal flow (wind normal to the cylinder axis). Sources for heat transfer coefficients are Refs. 103, 105, and 106. A relative, composite prediction for receiver convection losses is suggested in Figure 50, based on these comparisons. Approximate assumptions for aperture convection were employed. The decreases in aperture convection when the concentrator elevation angle reaches about 135 deg are due to wind blocking (shielding) by the concentrator (Figure 26). For example, for $f/D = 0.6$ (rim angle equal to 45 deg), the geometric focal point lies directly behind the upper rim of the concentrator when the concentrator elevation angle is 135 deg. Much more experimental and theoretical work will be required before these convective losses can be assessed quantitatively.

The previous discussion for forced convection relates to steady wind speeds. Heat transfer for cylinders in unsteady crossflow, e.g., because of the influence of turbulence and gusts, is poorly understood. Most of the existing experimental work applies to long, slender cylinders at very low Reynolds numbers, e.g., Ref. 107. However, some limited information for short cylinders at high Reynolds numbers is available (Ref. 108); there is a strong effect on heat transfer for aspect ratios less than 3. Time-dependent heat transfer in combined free and forced convection, even with steady upstream

flow, occurs in connection with periodic vortex shedding, e.g., Ref. 109. The complexity of flow and the convective heat transfer from circular cylinders, which is applicable to thermal receivers, is easily established; the consequences for thermal receiver performance are not yet fully determined. Further information on cylinder flow and vortex formation can be found in Refs. 110, 111, and 112.

Forced convection losses from the aperture are likely to be unsteady for near-grazing flow because of flow instabilities that are common in cavities. Under some conditions, it is clear that mass flow of air into, and out of, the cavity will occur on an unsteady basis. Cavities may behave like classic Helmholtz resonators (often designed and used to suppress, or muffle, flow pulsations in duct flows). Thermo-acoustic effects must be explored more fully with reference to internal cavity solar receivers.

Clausing has performed considerable analytical and experimental work on large, solar central cavity receivers (Refs. 113, 114, and 115). There are special problems associated with such large receivers because the dimensionless parameters associated with the cavity flow and heat transfer are beyond the range of conventional engineering experience. Conversely, there is relatively little information available for small cavity receivers designed for paraboloidal concentrators. Some experimental data for receiver apertures facing an oncoming wind at varying angles of attack has recently become available (Ref. 116).

This author believes that the design of high-temperature receivers will be difficult, not only from the standpoint of excessive thermal radiation losses, but also because convective wind losses from the aperture will be difficult to ascertain. There may be a non-linear effect of absolute aperture size, i.e., aperture convective losses might become relatively larger as aperture size increases. Very large dishes will require proportionately larger receivers, which could suffer serious convective losses in moderate winds. Prospects for improving the efficiency of thermal cavity receivers has been explored by Owen (Ref. 117).

C. NOISE GENERATION ASPECTS

The ability of a cavity to produce sound, and even discrete tones, is familiar to nearly everyone. At an early age children discover that sounds can be made to emanate from various bottles by blowing across their openings (mouths) at just the right speed. Indeed, the pitch can be changed by adding varying amounts of water to the bottle. An elegant treatment of this seemingly simple problem (it is not simple) was given by Cummings (Ref. 118). The sound field within the bottle can be predicted by simple plane-wave theory neglecting friction.

There are two aspects of wind-generated cavity noise as it relates to cavity thermal receivers: (1) noise generation may prove to be no more than a nuisance factor, but the potential problem of dozens, or hundreds, of separate noise sources in combination may be greater than anticipated; perhaps the problem can be eliminated by employing receiver aperture designs using shrouds and/or wind screens; and (2) periodic in-flow and out-flow across the aperture plane, which may occur with or without noise generation, may be a dominant

factor in aperture convection heat transfer losses. Flow-disturbance waves may not be infinitesimal in amplitude, as are mere acoustic waves.

There is extensive literature for unsteady flow and acoustics of cavities, e.g., Ref. 119. Self-sustained oscillations arise from three sources: (1) fluid dynamic oscillations caused by wave instabilities across the cavity opening, (2) fluid resonant oscillations caused by standing waves within the cavity, and (3) fluid elastic oscillations caused by solid boundary vibrations. For cavity-type receivers, the dominant mode, and probably the only mode of importance, is due to fluid resonant oscillations. Flow oscillations and acoustic waves in cavities depend on the volume and shape of the cavity, the size, length and configuration of the neck, or opening, dynamic flow conditions at the mouth or opening, and the gas properties. In the case of relatively shallow rectangular cavities, it was found that existing theories generally were adequate to correlate experimental data (Ref. 120). The studies in Ref. 120 were motivated partly by airframe noise in aircraft landing-gear wheel wells. One interesting result could have application to cavity receivers that have a thin, sharp lip forming the aperture entrance: tonal intensities, perhaps edge-tones, could become amplified in such a geometry. Unsteady flow past cavities has been studied experimentally (Ref. 121). In Ref. 122, an analytical study was performed to investigate the heat transfer from a square cavity as influenced by varying-angle crossflow.

It is appropriate to discuss Helmholtz resonators briefly because they are not unlike cavity-type thermal receivers. Helmholtz resonators can be tuned to absorb or cancel periodic, upstream flow oscillations (grazing flow), and thereby act as muffling devices, or they can be excited to generate noise of their own. Steady or oscillating grazing flow produces pulsating flow conditions across the opening that are highly three-dimensional. A complete cycle of operation consists of an in-flow phase and an out-flow phase that have roughly equivalent time periods (Ref. 123).

Based on one-dimensional wave propagation, the fundamental frequency of a Helmholtz resonator can be expressed as (Ref. 124):

$$f_o = \frac{\pi}{2a}\left(\frac{S}{\ell' V}\right)^{1/2} \tag{8}$$

where a is the velocity of sound, S is the area of the neck or opening, ℓ' is the effective neck length, and V is the cavity volume. If the geometric length of the neck is ℓ, the effective neck length is estimated from $\ell' = 1 + 0.75\ d$, where d is the neck diameter. There will also be higher harmonics than expressed by Equation (8), and these may not necessarily be integer multiples of f_o. Equation (8), applicable only to short necks, is plotted in Figure 51. Estimates are included for the first-generation air and steam receivers in Figure 51; whereas the fundamental frequencies are low (61 Hz and 75 Hz, respectively, for the air and steam receivers), they are well above the hearing threshold for normal human ears (approximately 15 to 20 Hz).

Again, for ideal flow, the sound pressure level gain expressed in decibels is given for Helmholtz resonators (Ref. 124) as:

$$n_o = 10 \log\ (4\pi\ell'^3 V/S^3) \tag{9}$$

Recall, however that sound intensity is proportional to the square of sound pressure.

When the resonator is excited by an external, turbulent boundary layer, strong excitation has been noted to occur for a Strouhal number range $35 < St_o < 40$ (Ref. 125), where the Strouhal number based on the fundamental frequency is $St_o = 2f_o d/u^*$ and u^* is the wall-friction velocity.

The previous discussion applies mainly to idealized flow conditions (grazing flow) and infinitesimal disturbances without the presence of high gas temperatures and significant heat transfer and wall friction. Conditions in real thermal receivers may be significantly different than ideal. It is well known that deep cavities (e.g., like an organ pipe) driven by a perpendicular high-speed jet (stagnation entrance flow) can generate intense gas heating effects within the cavity (Refs. 126 and 127). Disturbances are not infinitesimal and take the form of standing or moving shock waves. This author does not believe that resonance-tube modes would be important for receivers facing directly into a high wind; however, if these gas heating modes did occur, they probably would cause receiver burnout, and very quickly (fractions of a second). Fortunately, thermal receivers in point-focusing concepts can never face directly into the wind because of concentrator blocking. Clearly, however, thermo-acoustic effects in thermal receivers merit further investigation.

Thermo-acoustic effects in heat and mass transfer were recognized years ago (Ref. 128) as an important new field. The emphasis has been on promoting increased heat transfer in engineering applications. In the present context the emphasis is, rather, to recognize augmented heat transfer conditions and then to take appropriate steps to minimize or eliminate these conditions through judicious design methods.

SECTION IX

FIELD ARRAYS

Field arrays consisting of groupings of individual collectors or modules will be required if significant amounts of electricity or thermal energy are to be generated by solar collectors. Examples include flat-plate collectors, photovoltaic panels, parabolic troughs, heliostats in the central receiver concept (power tower), and paraboloidal dish modules. Arrays are characterized by: (1) field layout, i.e., the geometric distribution of individual modules, which may be uniform or non-uniform; and (2) land packing factor, i.e., the ratio of total concentrator aperture area to total land area. Additional consideration includes perimeter wind protection by natural or man-made barriers.

Of interest here are the characteristics of field arrays subject to wind of varying speed and direction, with and without protective wind fences at the perimeter. It is important to determine the wind loads on individual modules within an array because the aggregate flow field is influenced by adjacent modules. This is especially true if mutual interactions between modules were such as to augment wind loads compared to those that would occur on a single concentrator at equivalent wind free-stream conditions. Some information is available for photovoltaic and parabolic-trough arrays, e.g., Refs. 51 through 57, but such concentrators differ considerably from paraboloidal dishes from an aerodynamic point of view.

Some interesting wind loading considerations for paraboloidal dish arrays are suggested by reference to Figure 52. Shown (Figure 52) is a portion of a typical rectangular field array. North-to-south spacing is 1.25D between dish centerlines, where D is the dish diameter; east-to-west centerline spacing is 2.0D. Thus, the land packing factor is 0.314. The dishes are shown facing west at an elevation angle of 45 deg. A range of wind directions are indicated; some are symmetrical and some are not. Direction a and a' are symmetrical and would yield equivalent wind loading results. Directions b and b', and c and c' are symmetrical, but directions b and c', and d and e are not symmetrical.

The land requirements for solar thermal/electric power systems are easy to demonstrate in relation to the land packing factor (PF). If all the solar energy incident on a portion of land could be converted to electric power without losses, then approximately 0.25 acre of land would generate 1 MWe of power for PF = 1.0 and an insolation of 1.0 kW/m^2. Figure 53 shows land requirements per MWe of power plotted against overall system conversion efficiency for various values of packing factor. Dish concentrators would have a maximum packing factor, if all concentrators when facing zenith were touching each other physically, of 0.907 for a diamond-packed square array (Figure 53). Practical values of packing factor might be in the range $0.3 < PF < 0.4$ for dish-concentrator field arrays. The current limit of system efficiency for non-solar power conversion is about 0.5 (advanced combined-cycle power plants). Hence, the range of application is to the left of the vertical limit line indicated in Figure 53.

It is not difficult to see that some differences in mutual blockage, wake interference effects, and wind channeling between dish rows and columns, might occur in field arrays, depending on wind velocity and direction. Such effects

also will depend on field layout. In addition to rectangular arrays, other dish-array types include diamond, hexagonal, radial, etc. Except for radial arrays, however, they all tend to use uniform packing distribution. An optimal field layout must consider: (1) mutual dish shading, (2) composite wind loading effects and, in the case of storage or thermal transport, (3) transport layout. Least is known about wind loading.

Because there are no wind tunnel test results available for model arrays of paraboloidal dishes, emphasis was placed herein on reviewing the information available for heliostat arrays. It is likely that the general results for heliostat arrays, with and without perimeter wind fences, will be valid for paraboloidal dish arrays.

A. WIND FENCES AND BREAKS

Some early work on wind barriers and breaks was due to Woodruff and Zingg (Ref. 129). An extensive literature review and new wind tunnel results were presented by Raine and Stevenson (Ref. 130). The latter reference discusses reasons for significant differences between results obtained for full-scale and wind-tunnel model tests of wind breaks. Reference 131 presents extensive wind tunnel results for a wide variety of wind fences; parameters that were varied included permeability (porosity), shape, and size relative to the boundary layer thickness. Also included in Ref. 131 are results for two wind breaks in series (and effects of corner fence junctions), as well as natural fences composed of vegetation such as hedges. Natural and man-made wind breaks also are discussed in Ref. 44 (Appendix 4, "Shelter Effects").

The aerodynamic effects of wind breaks, or shelters, are not difficult to understand. Drag on the barrier modifies the upstream velocity field and causes a loss of momentum in the airflow, thus producing a "sheltering effect." A solid barrier will displace the maximum wind velocities upwards, and create a flow separation bubble. The flow reattachment point will vary with the height of the fence, or barrier (relative to surface boundary layer thickness), and the permeability or porosity of the barrier. Permeability will introduce a modifying "bleed flow" that will soften the effects of a solid barrier.

These effects are indicated schematically in Figure 54 (from Ref. 130). The wind sheltering effect becomes a tradeoff between mean wind velocity reduction in the lee of the barrier and turbulence in the separation bubble as determined by barrier permeability. Of course, the location of flow reattachment is important because there will be nearby regions of high wind shear, which has implications for location and spacing of protective wind perimeter fences.

Appropriately designed perimeter fences (or, hedges, trees, etc.) could serve a multiple function for field arrays of paraboloidal dishes:
(1) alleviation of wind loads on, at least, the outer fringe of concentrators;
(2) security barrier; and (3) esthetic appearance of the array.

B. HELIOSTAT WIND TUNNEL TEST PROGRAMS

As seen from Table 10, furnished by S. Peglow (Ref. 62), a wide variety of heliostat wind tunnel tests were conducted in the late 1970's. Tests have been conducted on models varying from 1/60 to full scale (see also Figure 40), and partial arrays with and without fences. Wind forces and moments have been measured, vortex shedding has been studied, and turbulence measurements and flow visualization have been performed. There are no parallel efforts to date for paraboloidal dish concentrators or field arrays.

It is true that some of the heliostat wind tunnel data tends to be somewhat conflicting and nonreproducible. This may be due partly to early inexperience; nevertheless, a great deal has been learned and has been utilized for design purposes. Table 10 indicates that a variety of wind tunnel test facilities have been employed. Perhaps the most versatile overall facility is the one located at Colorado State University. This will be discussed in a subsequent section.

C. SAMPLE WIND TUNNEL RESULTS

Table 10 indicates that there have been several field array studies, with and without perimeter fences, sponsored by DOE for central receiver/heliostat systems. References 58 through 60 differ in numerical and technical detail, and in model scale size, but tend to agree in qualitative results with respect to perimeter fences. That is, perimeter wind fences or breaks tend to markedly decrease the heliostat base bending moments in the extreme periphery of a heliostat array. However, wind loads in the first few rows of peripheral heliostats can actually be increased in regions downstream of sharp corners of peripheral fences. In addition, in the central portions of field arrays, far removed from peripheral wind breaks, wind fences provide little protection from wind loads but mutual flow blockage alleviates the problem. Results described herein will be limited to Ref. 60, because it is the most complete study, and includes the accumulated experience of earlier studies.

In Ref. 60, 1/60 scale model heliostats were tested for Reynolds numbers varying from 10^4 to 10^5. The central receiver, or power tower, was not simulated. Two zones of the heliostat array (Figure 55) were investigated. Zone A had a land packing factor of 0.36, and Zone B (mixed field array) had an average packing factor of 0.13; Zone B is far removed from the power tower. Variables in these tests included wind speed, heliostat elevation angle and stow configurations, and fence size and spacing relative to the field array. However, in most cases, the fence permeability (porosity) was 0.32. Effects of fences internal to the perimeter fence also were studied. Flow visualization studies were performed to provide qualitative flow-field information. A 1/7 power-law velocity profile [see Equation (2)] was used, typical of flat, open country (see Figure 6).

Results from Ref. 60 are shown in Figure 56 for Zones A and B (Figure 55) with and without fences. The effect of the perimeter fence is evident especially at the outer edge of the array. Base bending moments were lower and persisted further into the field in the more densely packed Zone A, indicating the greater mutual blocking protection in that zone. In Zone A, with or without a fence, the base bending moment was roughly constant from 25 m

into the field and inwards. Zone B, however, shows increases in base bending moment at a point of 75 to 100 m into the field.

Some of the more interesting conclusions of Ref. 60 were: (1) sharp corners in fences are to be avoided, (2) fences need to be relatively high and close to the field or their benefit is compromised, (3) fence porosity ranging from 0.32 to 0.57 had little effect on heliostat loads, (4) little difference in loads was seen for the stowed conditions of alternate rows at 87-deg and 93-deg pitch angle, and all rows at 90-deg pitch angle, and (5) row alignments caused noticeable flow channeling, especially for winds out of the west (Figure 55). Whereas various individual heliostat models were instrumented in Ref. 60, none of the cases studied involved two adjacent models in series (to the wind direction) so that downstream flow blockage could be studied directly. Flow blockage has interesting practical implications for aerodynamic loads because of vortex shedding, turbulence generation, etc. Realizing that a very large number of parameters and variables are involved, it would be interesting to know under what conditions, if any, wake interference effects might augment wind loading effects.

A variety of wind tunnel tests were performed in Ref. 64: static tests on a 1/20 scale model heliostat, dynamic tests on a 1/3 scale model, tests on single models in comparison with an array, and tests of a full-scale model. An interesting difference between results for a single model and an array was that downstream models in an array were subject to reduced loading (compared to a single model), but had much higher oscillation amplitudes because of wake buffeting. Reference 64 is of interest because it is one of the few studies available that addresses dynamic response of a reflector (heliostat) to wind loading.

D. VORTEX SHEDDING AND BLOCKAGE INTERFERENCE

It is well known from wind tunnel studies of model buildings, obstacles, and bluff bodies, e.g., Refs. 132 and 133, that objects in the lee of one another can experience significant effects in forces and moments.

An interesting study, with application to heliostats, has been performed to study vortex shedding from a square plate with variable ground spacing, set normal to the ground and the parallel wind direction (Ref. 134). Because the boundary layer was very thin in this wind tunnel study, the plate was subject to an essentially uniform velocity profile. Wake oscillation frequencies were determined by hot wire anemometer and then cast into the dimensionless shedding frequency, or Strouhal number. Empirical data correlations successfully accounted for ground spacing and Reynolds number. Above Re $\sim 10^5$ the Strouhal number approached a constant value (consistent with Ref. 16). Ground spacing effects became negligible for plates placed at heights greater than half their breadth from the ground. For this case St ~ 0.12.

Using the latter result, the wake oscillation frequency is plotted in Figure 57 versus wind speed for various sizes of square plates. The vortex shedding frequency increases with wind speed and decreases with plate size. Shedding frequencies are of interest when they approach natural vibrational frequencies of a plate, for then aerodynamic coupling leading to excited vibrational amplitudes can occur.

The results of Figure 57 probably can be applied to paraboloidal dishes with fair approximation. In Ref. 16, it is shown that the drag coefficient of a variety of body shapes is directly related to the Strouhal number for high Reynolds numbers. Because the drag of dishes (facing into the wind) is somewhat higher than flat plates (see Figure 19), the corresponding Strouhal number is somewhat lower (also see Figure 28). In Ref. 16, it is suggested that a universal Strouhal number exists at high Reynolds numbers regardless of the body shape. Vortex shedding was discussed previously in Section VI.G.

SECTION X

ENVIRONMENTAL WIND TUNNELS

A brief discussion will be given of simulation requirements and criteria for testing model man-made structures in laboratory simulation of the atmospheric boundary layer, and of existing wind tunnel facilities.

A. SIMULATION REQUIREMENTS AND CRITERIA

Rigorous modeling of the atmospheric boundary layer, and testing of models therein, require modeling the flow field according to: (1) dynamic similarity as obtained from the fluid dynamic conservation equations of mass, momentum and energy, (2) surface boundary-condition similarity, and (3) approach-flow similarity (Refs. 9 and 135). Some of the dimensionless parameters involve the Earth's rotation, atmospheric density stratification, and other (probably) second-order effects. A listing of requirements from Ref. 9 is:

(1) Dynamic Flow Similarity

- (a) Undistorted geometry scaling
- (b) Equal Rossby number (Earth's rotation)
- (c) Equal gross Richardson number (mixing)
- (d) Equal Reynolds number (flow)
- (e) Equal Prandtl number (gas properties)
- (f) Equal Eckert number (heat transfer)

(2) Surface Boundary Condition

- (a) Equivalent surface roughness distribution similarity
- (b) Preservation of topographic relief
- (c) Surface temperature distribution

(3) Approach-Flow Similarity

- (a) Distributions of mean and turbulent velocity
- (b) Distributions of mean and fluctuating temperatures
- (c) Zero longitudinal pressure gradient
- (d) Equality of length scales for atmospheric stratification

In addition, there are relative properties of the models that need to be considered. For example, for tall buildings and towers in dynamic motion, Refs. 136 and 137 recommend that equality between model and prototype be preserved in the following dimensionless parameters: (1) frequency ratio: ratio of natural frequencies about horizontal and vertical axes; (2) ratio of energy dissipation per cycle to total energy of oscillation; (3) density ratio: structure to air; and (4) ratio of mean wind velocity to reference oscillation velocity. The difficulty of elastic modeling of paraboloidal dishes was discussed previously in Section VI.G.

Finally, there are conditions imposed by the wind tunnel itself that can affect the model flow field. Blockage results when the model is not small

compared to the wind tunnel cross-sectional area (Section VI.C); the presence of the wind tunnel walls can produce three-dimensional disturbances in the flow field that affect the force and moment measurements.

Not all of the requirements and criteria discussed above can be satisfied simultaneously in existing laboratory facilities. For steady-state testing of paraboloidal dish modules in wind tunnels, it probably is sufficient to: (1) utilize geometric similarity between model and prototype; (2) maintain Reynolds numbers above $Re > 10^5$ based on dish diameter; (3) model a "typical" time-mean boundary layer, e.g., for flat, open country, 4) preserve the turbulence scale, or fluctuation intensity; and (5) minimize wind tunnel blockage, or determine the corrections necessary for application to experimental data. For field arrays, the topographic relief should be preserved with zero longitudinal pressure gradient and, of course, the field packing factor should be simulated geometrically. Thermal and heat transfer effects probably are insignificant for most design purposes.

B. EXAMPLES OF EXISTING FACILITIES

The JPL results for paraboloidal dishes (Refs. 5, 13, 70, 71, and 92) were obtained in an ordinary subsonic wind tunnel located at Northrup Aircraft Company. This tunnel has a 20-ft-long test section which is rectangular in cross section, i.e., 7 ft high and 10 ft wide. Tunnel air speeds up to 250 mph are possible. The JPL dish model (see also Appendix D) had an 18-in. diameter.

Wind tunnel results for the Honeywell tests on heliostat arrays (Ref. 58) were obtained in the Georgia Institute of Technology (GIT) wind tunnel (Figure 58). The GIT tunnel is a closed-circuit, single-return subsonic tunnel capable of test section speeds of up to 160 mph. It has a circular test section 9 ft in diameter and 12 ft long. Boundary layer profiles are adjusted by using various mesh configurations at the test section inlet.

The Fluid Dynamics and Diffusion Laboratory, at Colorado State University (CSU), has three wind tunnels used for environmental testing. They are the meteorological wind tunnel (Figure 59), the environmental wind tunnel (Figure 60), and the industrial aerodynamics wind tunnel. All of these are described briefly in Ref. 136. The most sophisticated of these is the meteorological wind tunnel, which has a very long test section (27 m), adjustable ceiling for pressure gradient control, test section walls that can be heated or cooled, and provision for heating or cooling return air. The test section is 1.8 m x 1.8 m square; maximum air speeds up to 30 m/s are attainable.

The CSU environmental wind tunnel (Figure 60) is an induction tunnel (single pass) with a test section 17.4 m long by 3.7 m wide by 2.4 m high. It is the simplest of the CSU tunnels and is versatile; there are three turntables in the floor. The industrial aerodynamics tunnel, not shown here, is less expensive to operate; it is a conventional closed-loop subsonic tunnel with an 18.3-m-length test section.

Many other appropriate wind tunnels exist; however, almost none can be rotated, so that earth rotation cannot be simulated. Rossby number cannot be simulated; this, however, is not critical. Other facilities exist at the

University of Toronto, Canada, in Great Britain, in France (Ref. 17), and in New Zealand (Ref. 138).

Cryogenic wind tunnels have been developed (Refs. 104, 139, and 140) to exploit the large gains that can be obtained in Reynolds and Grashof numbers for heat transfer experiments in forced, free, and combined heat convection. Such tunnels are compact and have low operating costs because of reduced compression requirements. The University of Illinois tunnel (Figure 61) has a rectangular test section measuring 0.6 m by 1.2 m. It can achieve Reynolds numbers greater than 10^6 and Grashof numbers greater than 10^{11}, values typical for a central receiver (power tower concept). Some early heat transfer measurements for vertical cylinders in crossflow are presented in Ref. 140. It is shown in Ref. 141 that turbulent boundary-layer simulation in cryogenic wind tunnels is not significantly affected by real gas effects. This is comforting because real gas effects can be difficult to deal with.

SECTION XI

CONCLUSIONS

A. MAJOR CONCLUSIONS

The major conclusions reached as a result of this study are given below:

(1) Wind loads have a direct influence on the design, cost, performance, operating and maintenance, safety, survival, and replacement of solar dish concentrators.

(2) Force and moment wind loads are functions of a large number of variables that depend on wind conditions as well as the design and configuration of the concentrator.

(3) Forces and moments depend on the square of the mean wind speed. Forces are proportional to the dish diameter squared and moments are proportional to the dish diameter cubed.

(4) Wind characteristics are highly nonuniform and random, and are handled best by statistical approaches; further, wind conditions are highly site specific. Thus, the selection of the basic design wind speed is very important for concentrator design. Reliable wind measurements close to a selected site are highly desirable, and records should include as many years observation as possible.

(5) The effects of gusts on concentrator wind loads, especially moments, can be considerable. Wind speeds that are averaged over periods of 1 hour are satisfactory for design purposes, except for rapidly changing weather conditions. Empirical gust reponse factors derived from the literature can be utilized to assess the effects of gusts on wind loading.

(6) Reduction of aerodynamic wind loads is possible by applying various means, e.g., the introduction of porosity into the reflecting surface, the use of spoilers and fairings, and by shifting the pivot center of rotation forward of the dish vertex (especially effective for reducing moment loads). Porosity is most effective near the rim of the concentrator. Faceted concentrators provide natural wind relief if air gaps are permitted between adjacent facets. Gap spacing should be increased with increasing distance from the dish axis.

(7) There are no wind tunnel data available for paraboloidal solar concentrators. However, sufficient data are available from model radio antenna tests to assist in preliminary design. Also, there are no data available for field arrays of paraboloidal reflectors. Wind tunnel data for heliostat arrays are available and should be generally applicable for dish field arrays.

(8) Considerable reductions in wind loads are evidenced in the outer periphery of concentrators in a field array enclosed by a suitably designed perimeter fence, or wind break. However, the fence

influences mainly the outer rows of concentrators and does not persist far into the field interior.

(9) The selection of basic design wind speed, and the level of wind speed chosen to permit concentrator performance at acceptable degradation, will influence the annual operating time at specific sites. Thus, the annual energy production may depend on wind conditions as well as annual variations in insolation.

(10) Optical field layout designs for solar concentrators, based on trade-offs between land packing factors and mutual concentrator shading, may not be optimal for local, annual wind conditions.

B. ADDITIONAL CONCLUSIONS

Additional conclusions reached are given below:

(1) The atmospheric surface layer is the region of interest for man-made structures. For neutrally stable atmospheric conditions, this region extends to a height above ground of approximately 100 ft to 500 ft during the daytime and is thinner at night. The atmospheric surface layer is governed mainly by surface roughness and not by thermal stratification or the Earth's rotation.

(2) In general, wind speed varies (increases) with height above ground in the absence of significant vertical motion that might occur in violent storms.

(3) Power-law models for wind profiles generally are satisfactory for engineering design purposes. They are valid, however, only for specific conditions, e.g., no violent, vertical mixing. They are applicable even for mature storms.

(4) Most of the available wind tunnel data for model paraboloidal reflectors (radio antennas) was obtained for steady flow conditions with a uniform velocity profile of the approaching wind.

(5) Paraboloidal dishes essentially are circular, parabolic-arc airfoils, and their aerodynamic behavior is interpreted in this light accounting for ground effects. The larger the f/D, the more they behave like flat plates. Heliostats behave essentially like flat plates.

(6) Aerodynamic force and moment coefficients vary considerably with wind angle of attack (elevation and azimuth), and may have positive or negative values.

(7) The dimensionless aerodynamic coefficients can be determined from wind tunnel testing and then used to predict forces and moments for dishes of arbitrary size provided that proper flow modeling is observed.

(8) To avoid scale effects (Reynolds number), as indicated by experience with model heliostat testing in wind tunnels, Reynolds numbers greater

than 10^5, and preferably 10^6, should be preserved in wind tunnel testing as based on dish diameter. However, testing very small models at very high wind tunnel speeds is not advisable.

(9) The reader/user of radio antenna wind tunnel testing literature is cautioned to exercise care to determine exactly which coordinate systems and sign conventions have been employed in a given reference. Three different axis systems commonly are utilized: (1) wind-axis, (2) body-axis, and (3) stability-axis. They are equivalent only when the elevation and azimuth angles of the dish concentrator are zero relative to the approaching wind.

(10) Field arrays of dish concentrators may be subject to varying wind effects depending on wind direction and velocity, field layout pattern, and land packing factor. If perimeter fences are used for wind protection, the fences should not have sharp corner junctions, which can augment wind loads on nearby concentrators.

(11) Little is known about aerodynamics effects for receivers mounted at the focal plane. Wind loads on the receiver/power conversion unit structure could augment dish wind loads, especially for small dish angles of attack relative to the approaching wind vector, or for grazing flow when the wind approaches the dish edge-on. Wind-flow patterns over the receiver could have significant effects on aperture convective heat losses. Because of concentrator blocking, direct stagnation flow into the receiver cavity cannot occur physically.

(12) A variety of wind tunnel facilities suitable for testing models of concentrators and field arrays are available at modest test cost.

SECTION XII

RECOMMENDATIONS

As a result of this study, the following recommendations have been made:

(1) The appropriate basic design wind speed for solar concentrators is the "annual extreme fastest mile" (see Section IV), a statistical concept based on actual wind measurements and extreme value theory. Design wind speed should not be based on maximum gust records, which will lead to over-design.

(2) Basic design wind speeds usually are quoted for a height that is 30 ft above ground. Such values easily may be converted to any desired height by using an appropriate wind profile model, e.g., the power-law model. The basic design wind speed may be applied to survival of the reflector in any position (conservative), or to survival at stow position (optimistic).

(3) For design purposes of a specific concentrator, the basic design wind speed should be specified at the concentrator centerline when the elevation angle is zero.

(4) Unless future studies determine otherwise, building code practice (Section IV.A) should be employed and the return, or recurrence, period of the basic design speed should be R = 100 years for a plant lifetime of 30 years.

(5) As soon as reasonably fixed designs for first-generation dish concentrators are developed, wind tunnel testing of models is encouraged and should be supported. Single and field array models should be tested, and structures at the focal point (receivers/engines) should be simulated in the model. Such wind tunnel test programs probably will cost only a small fraction of the concentrator development. For potential urban sites utilizing roof-top concentrators, model concentrators should be mounted on model buildings (industrial, commercial, etc.) to model the selected locale in wind tunnel testing.

(6) Thermal receivers should be studied to determine their contributions to concentrator wind loads at varying elevation and azimuth angles. Aperture wind convection losses should be studied theoretically and experimentally. Aperture convection losses are poorly understood.

(7) Wind conditions, in addition to annual insolation, should be considered to determine if plant operation time at specific locations might be affected significantly by winds. At a particular site, for example, suppose that the frequency of incidence of high winds was "substantial" during hours of peak insolation. Such a site would not be the best choice for a solar thermal plant. That is, site-specific studies should be performed to determine if annual energy production is impacted significantly by annual, statistical wind conditions.

(8) Field layout designs and studies should include prevailing wind conditions (magnitude, direction, frequency spectrum statistics) in addition to mutual dish shading and thermal transport (in the case of process heat). However, to accomplish this, wind tunnel field array test results first would be required. That is, optimal field layouts for land utilization from an insolation point of view may not be optimal for performance and survival in winds.

SECTION XIII

CITED TABLES AND FIGURES

A. TABLES

1. Preliminary Wind Requirements for the 210-ft-dia Goldstone Antenna
2. Types of Terrain Grouped According to Their Aerodynamic Roughness
3. Relation of Atmospheric Stability Conditions to Weather Conditions
4. Classification of Terrain Effects on Atmospheric Motions
5. Factors Considered in American and Foreign National Standards
6. Comparison of Reference Wind Speeds in National Standards
7. Levels of Approaches Permitted in National Standards
8. Criteria in Use (Circa 1980) for the Design of Solar Concentrators/Collectors
9. Typical Maximum Force and Moment Coefficients Determined Experimentally for Various Solar Collectors Subjected to Wind Loading
10. Chronology of Heliostat Wind Tunnel Tests

B. FIGURES

1. Probability Scenario of Antenna Wind Damage
2. Typical Planetary Boundary Layer for Rough Surfaces
3. Velocity Profile Related to Paraboloidal Antennas
4. Test of the Power-Law Velocity Profile for the Planetary Boundary Layer Model Shown in Figure 2
5. Change of Velocity with Height Over Level Ground for Three Different Types of Surface Roughness According to Power Law
6. Power-Law Wind Profile Parameters for Strong Winds Over Surfaces of Different Roughness
7. Smoke Emission from Three Heights of a Weather Tower During a Temperature Inversion
8. Typical Record of Horizontal Wind Speed at Three Heights
9. Coefficient of Drag for a Flat Plate in Fluctuating Flow

10. Gust Ratios and Power-Law Index for Various Terrain Categories

11. Spectrum of Horizontal Gustiness in High Winds

12. Frequency Distribution of Wind Components

13. Risk Model for Extreme Winds at Daggett Airport

14. Distribution of Fastest Mile Speed at 30-ft Elevation, Elkins Airport

15. Mean Recurrence Period for Different Structure Lifetimes

16. Elements of a Statistical Approach to Gust Loading

17. Calculated Horizontal Force Ratios on a Square Plate

18. Recommended Design Wind Speed for the Parabolic Dish Test Site

19. Drag of Sheet Metal Caps Facing Directly into Wind

20. Relationship Between L/D, X, and f/D for Paraboloidal Reflectors

21. Stability-Axes System for Paraboloidal Reflectors

22. Ratio of Force-to-Force Coefficient

23. Ratio of Moment-to-Moment Coefficient

24. Drag Coefficient versus Reynolds Number for Common Shapes

25. Reynolds Number Variation with Wind Speed and Characteristic Dimension

26. Conceptual Flow Patterns Around a Paraboloidal Concentrator at Zero Azimuth Angle

27. Departure from Symmetry (Wind-Axes System) Caused by Ground-Plane Interface

28. Experimental Flow Field Behind a Circular Flat Plate Normal to the Airstream

29. Theoretical Effect of Ground Plane on the Local Velocity Near a Paraboloidal Reflector

30. Effects of Nonuniform Velocity Profile on Elevation Moment (Stability Axis System)

31. Drag Coefficients for Solid Paraboloidal Reflectors

32. Lift Coefficients for Solid Paraboloidal Reflectors

33. Yawing Moment Coefficients for Solid Reflectors

34. Empirical Aerodynamics Coefficients for Solid Paraboloidal Reflectors

Table 1. Preliminary Wind Requirements for the 210-ft-dia Goldstone Antenna (Reproduced from Ref. 5)

	Precision I operation full accuracy	Precision II operation degraded accuracy	Limit operation drive to stow (worst position)	Survival reflector, any position	Survival reflector in stow position (Zenith)
Wind velocity, mph., average velocity across antenna	30	45	50	70	120
Associated axis torque from steady-state wind, reflector in worst position, pound-feet†	AZ–2.3 × 10^6 EL–1.9 × 10^6	AZ–5.0 × 10^6 EL–4.3 × 10^6	AZ–6.4 × 10^6 EL–5.2 × 10^6	AZ–12.5 × 10^6 EL–10.3 × 10^6	AZ–2.7 × 10^6 EL–18.8 × 10^6‡
Tracking accuracy at 0.0015°/sec. deg.	0.01	0.02	—	—	—
Surface accuracy, RMS, in., worst position including wind, gravity, and thermals	0.25	0.375	—	—	—
Required axis velocity, at max. wind torque, deg./sec.	0.5	0.2	0.1	0.0	0.0

† Torques based on a solid surface for the inner 105-ft. diameter and a perforated surface over the outer 52½-ft. radius.

‡ Stow locks may be used in elevation.

Table 2. Types of Terrain Grouped According to Their Aerodynamic Roughness (Adapted from Ref. 11)

Category	Description	$\frac{1}{n}$	z_G
1	Very smooth surfaces: e.g. large expanses of open water; low unsheltered islands; tidal flats; lowlands verging on the sea	$\frac{1}{8.5}$	800
2	Level surfaces with only low, surface obstructions: e.g. prairie grassland; desert; arctic tundra	$\frac{1}{7.5}$	900
3	Level, or slightly rolling surfaces, with slightly larger surface obstructions: e.g. farmland with very scattered trees and buildings, without hedgerows or other barriers; wasteland with low brush or surface vegetation; moorland	$\frac{1}{6.5}$	1,000
4	Gently rolling, or level country with low obstructions and barriers: e.g. open fields with walls and hedges scattered trees and buildings	$\frac{1}{5.5}$	1,100
5	Rolling or level surface broken by more numerous obstructions of various sizes: e.g. farmland, with small fields and dense hedges or barriers; scattered windbreaks of trees, scattered two-story buildings	$\frac{1}{4.5}$	1,200
6	Rolling or level surface, uniformly covered with numerous large obstructions: e.g. forest, scrub trees, parkland	$\frac{1}{3.5}$	1,350
7	Very broken surface with large obstructions: e.g. towns; suburbs; outskirts of large cities; farmland with numerous woods and copses and large windbreaks of tall trees	$\frac{1}{3}$	1,500
8	Surface broken by extremely large obstructions: e.g. center of large city	$\frac{1}{2.5} - \frac{1}{1.5}$	1,800

Table 3. Relation of Atmospheric Stability Conditions to Weather Conditions (From Ref. 31)

A - Extremely unstable conditions
B - Moderately unstable conditions
C - Slightly unstable conditions
D - Neutral conditions*
E - Slightly stable conditions
F - Moderately stable conditions

Surface wind speed, m/sec	Daytime insolation			Nighttime conditions	
	Strong	Moderate	Slight	Thin overcast or ≥ 4/8 cloudiness+	≤ 3/8 cloudiness
<2	A	A-B	B		
2	A-B	B	C	E	F
4	B	B-C	C	D	E
6	C	C-D	D	D	D
>6	C	D	D	D	D

* Applicable to heavy overcast, day or night.

+ The degree of cloudiness is defined as that fraction of the sky above the local apparent horizon which is covered by clouds.

Table 4. Classification of Terrain Effects on Atmospheric Motions (From Ref. 32)

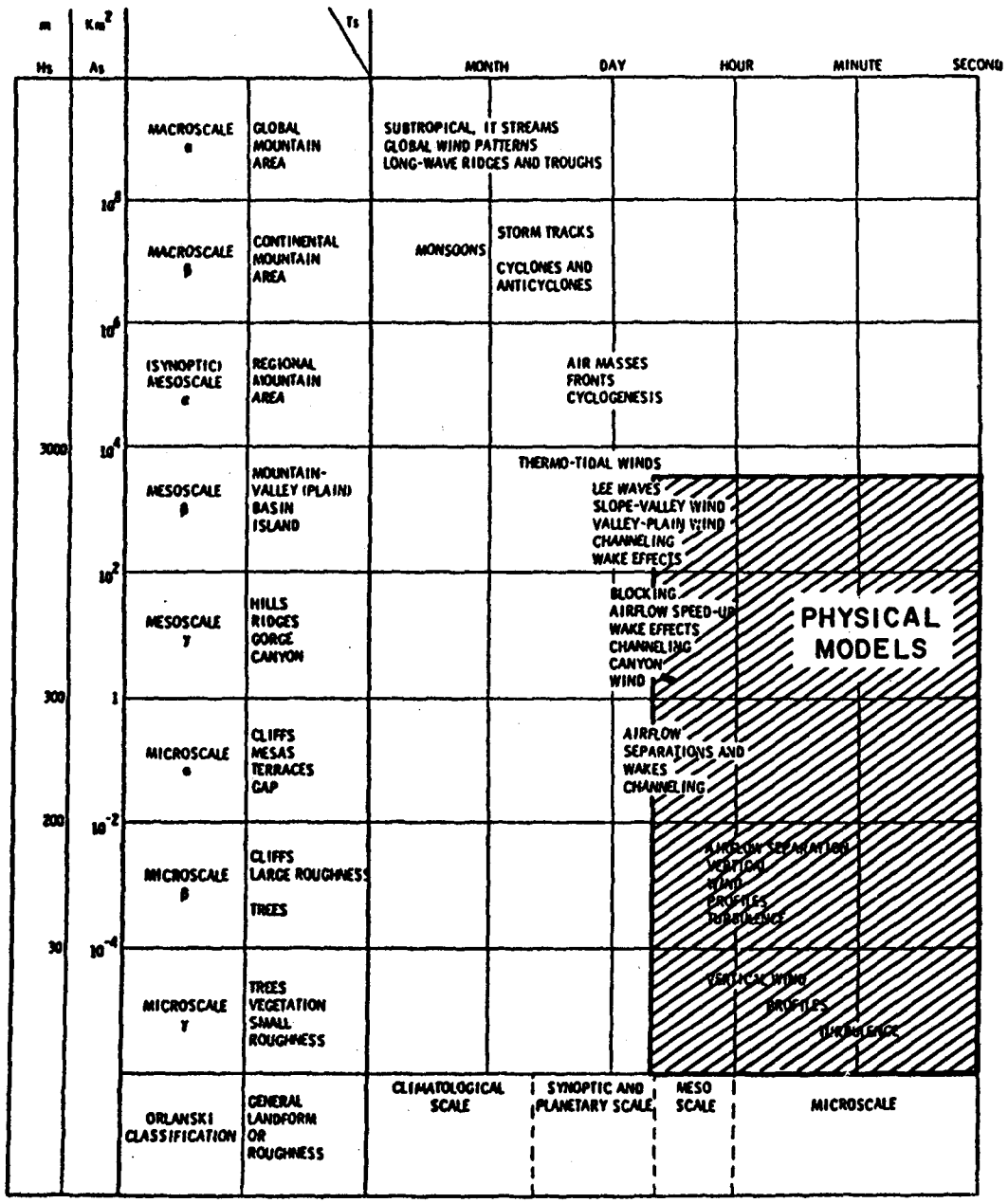

Table 5. Factors Considered in American and Foreign National Standards[a]

Factors Considered	ANSI A58.1-1972	Australian	British	Canadian
WINDSPEED				
Reference speed	Fastest mile	Two-second gust	Two-second gust	Mean hourly
Variation with height	Yes	Yes	Yes	Yes
Terrain roughness	Three	Four	Four	Three
Local terrain	None	Yes	Yes	None
GUSTS				
Magnitude	Gust response factor	Gust Speed	Gust Speed	Gust effect factor
Spatial Correlation	Parts and portions	Reduction for large area	None	Gust effect factor
Gust frequency	Dynamic consideration for h/b > 5	Dynamic consideration for h/b > 5	Dynamic consideration not included	Dynamic consideration for h/b > 4 or for h > 400 ft
WIND PRESSURE				
Pressure coefficients	Tables, text	Tables in Appendix, includes sketches	Tables, includes sketches	Figures and tables in commentaries

[a]Adapted from Ref. 46

Table 6. Comparison of Reference Wind Speeds in National Standards[a]

Reference Windspeed	ANSI A58.1-1972	Australian	British	Canadian
Averaging time	Fastest mile	2-3-sec. gust	2-sec. gust	Mean hourly average
Equivalent reference windspeed to fastest mile 100 mph (161 km/h)	100 mph (161 km/h)	118 mph (190 km/h)	118 mph (190 km/h)	78 mph (126 km/h)

Table 7. Levels of Approaches Permitted in National Standards[a]

Levels of Approaches	ANSI A58.1-1972	Australian	British	Canadian
Tables or simple procedures	Yes	Yes	Yes	Yes
Detailed procedures	Yes	No	No	Yes
Wind tunnel	No	Yes	Yes	Yes
References	No	Yes	No	No

[a]Adapted from Ref. 46

Table 8. Criteria in Use (Circa 1980) for the Design of Solar Concentrators/Collectors (Adapted from Ref. 67)

Collector Technology	Heliostats[a]	Troughs[b]	Dishes[c]	Photovoltaic[d] Arrays (Nontracking)
Maximum survival wind speed, m/s(mph)	(stowed) 40 (90)	(stowed) 35 (80)	(stowed) 44 (100)	Based on 100-yr mean recurrence at site
Design wind speed for normal operation, m/s (mph)	12 (27)	11 (25)	16 (36)	Based on 25-yr mean recurrence at site
Maximum wind speed during which collector must track, m/s(mph)	22 (50)	22 (50)	16 (36)	Not applicable
Stated or implied mean recurrence internal, yr	100 (extreme)	25 ground mounted 50 roof mounted (extreme)	100 (extreme)	25 (operating) 100 (extreme)

[a]Reference 97.
[b]Reference 98.
[c]Reference 99.
[d]Recommendation in Reference 100.

Table 9. Typical Maximum Force and Moment Coefficients Determined Experimentally for Various Solar Collectors Subjected to Wind Loading [a,b] (Adapted from Ref. 67)

Coefficient	Flat Plate [101]	Heliostat [61]	Trough [54][c]	Dish [72][d]
Lateral Load C_D (β = 0°)	1.2	1.18	1.44	1.5
C_D (β = 180°)	1.2	1.0	1.05	1.0
Lift Load C_L (β = 0°)	0.90 (α = 155°)	0.90 (α = 155°)	2.0 (α = 150°)	0.25-0.30[f]
	-0.90 (α = 35°)	-0.90 (α = 35°)	-1.2 (α = 30°)	-1.4 (α = 35°)
Moment Coefficient C_{M_z} (β = 0°)	-0.12 (α = 30°)	-0.21 (α = 30°)	-0.30 (α = 45°,180°)[e]	-0.05 (α = 40°)
C_M (β = 180°)	0.12 (α = -30°)	0.13 (α = 30°)	0.175 (α = 30°)[e]	+0.12 (α = 0°)

[a]See Fig. 47 for definitions of geometry and force directions.

[b]Moments are taken with respect to the attachment or pivot point, which for simplicity is assumed coincident with the center (in the heliostat case) or the surface apex (in the dish and trough cases). In real hardware cases, there will be some amount of offset, which must be carefully considered. Further, data very often is given for moments at the base of the structure. In this case, the resulting moments from the lift and lateral loads must also be considered. For example, see Ref. 61.

[c]90° rim angle length/aperture = 3.75.

[d]75° rim angle, dish depth/diameter = 0.20.

[e]These relatively high values for the pitching moment appear to be caused primarily by combination of boundary layer and ground effects.

[f]See Refs. 44 (pp. 294-295) and 102 (pp. 3-48).

Table 10. Chronology of Heliostat Wind Tunnel Tests (Adapted from Ref. 62)

DATE	CONTRACTOR	FACILITY	SCALE	COMMENTS
Nov 1975	Martin Marietta EY-77-C-03-1110	CSU Industrial	1/10	PDR Work
June 1976	McDonnell Douglas EY-76-C-03-1108	Douglas	1/10	PDR Work
June 1977	Honeywell EY-76-C-03-1109	GIT 9-ft Subsonic	1/10	Test of SRE Model
August 1977	Boeing EY-76-C-03-1111	U of Washington	1/30	PDR Work
Jan 1978	Honeywell EY-76-C-03-1109(14)	GIT 9-ft Subsonic	1/30	PDR Work Fence Study (Ref. 58)
July 1978	MDAC EY-76-C-03-1108(20)	CSU Meteorological	1/22	Fence Study $50K (Ref. 59)
Dec 1978	Sandia Livermore	NASA 40 x 80 ft	Full	MDAC Prototype $12K (Ref. 61)
Feb 1979	Martin Marietta DE-AC03-76ET20422	CSU Environmental	1/60	Array Study $62K (Ref. 60)
Ongoing	Texas Tech EG-77-C-01-3974 Task VII	Texas Tech M.E. Blower	1/22	Vortex Shedding $31K
Proposed	McDonnell Douglas	CSU Environmental	1/22	Profile Effects $21K

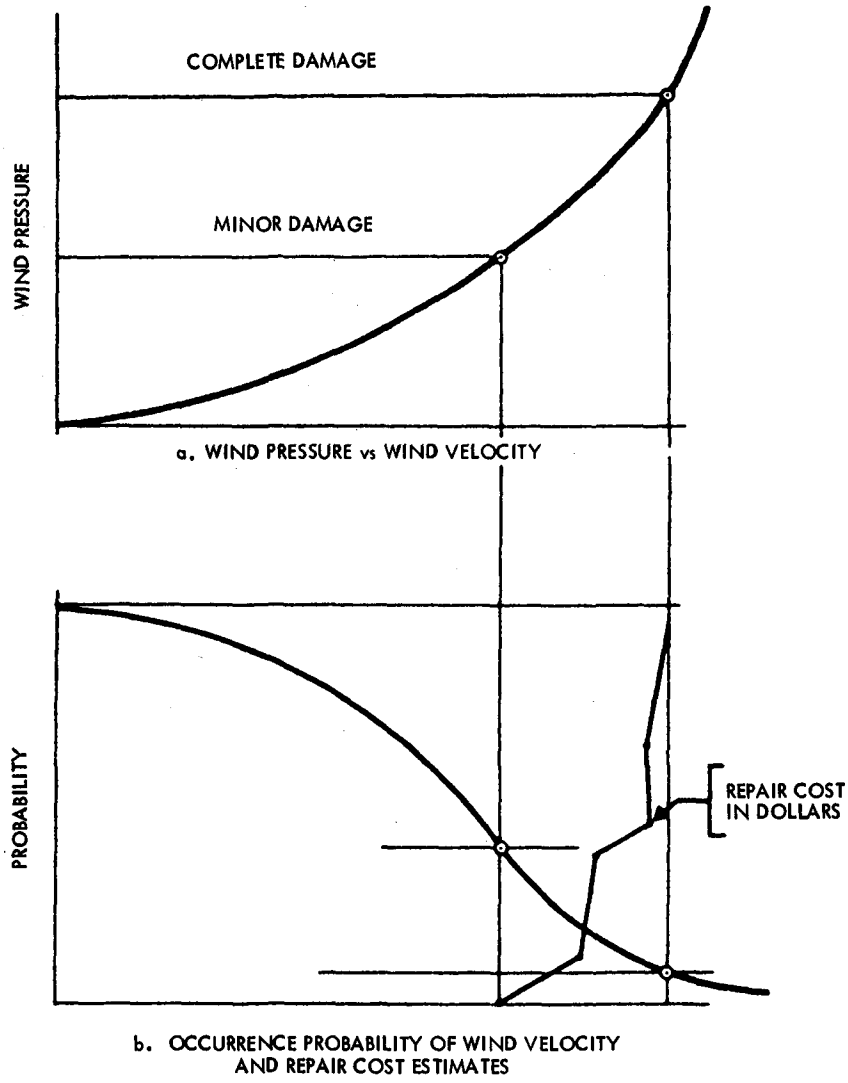

Figure 1. Probability Scenario of Antenna Wind Damage (Adapted from Ref. 6)

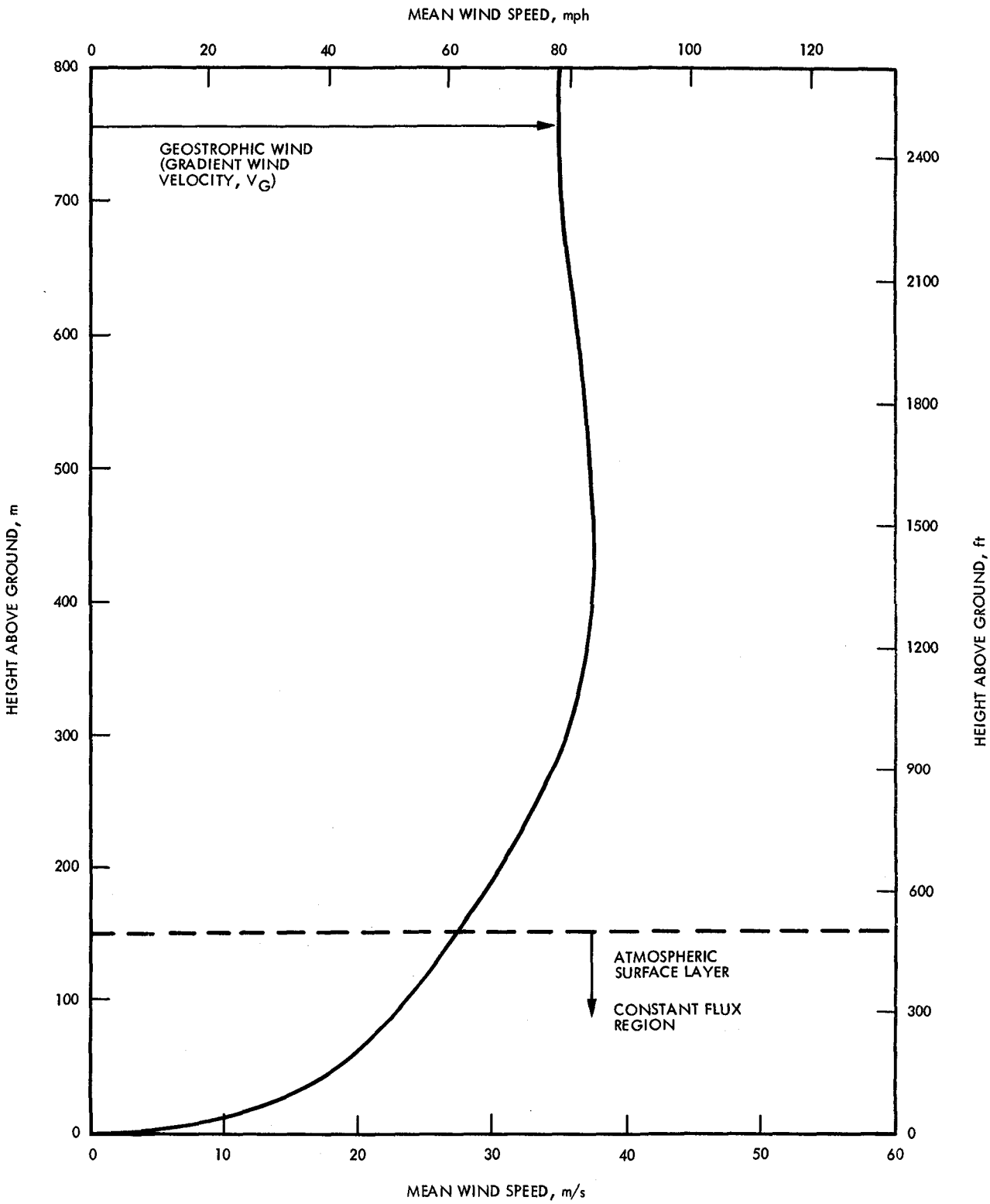

Figure 2. Typical Planetary Boundary Layer for Rough Surfaces (Based on Data in Ref. 9)

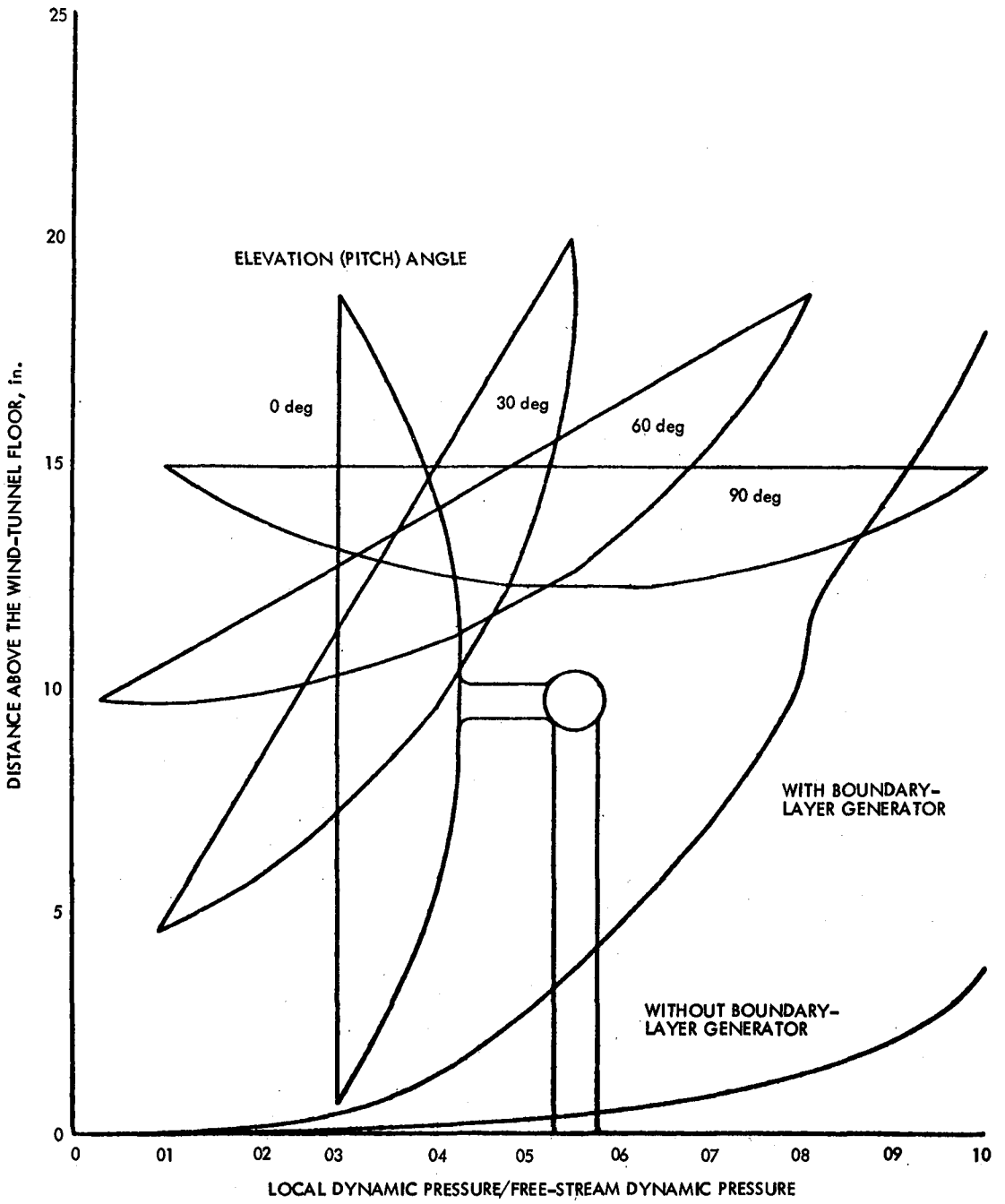

Figure 3. Velocity Profile Related to Paraboloidal Antennas (From Ref. 13)

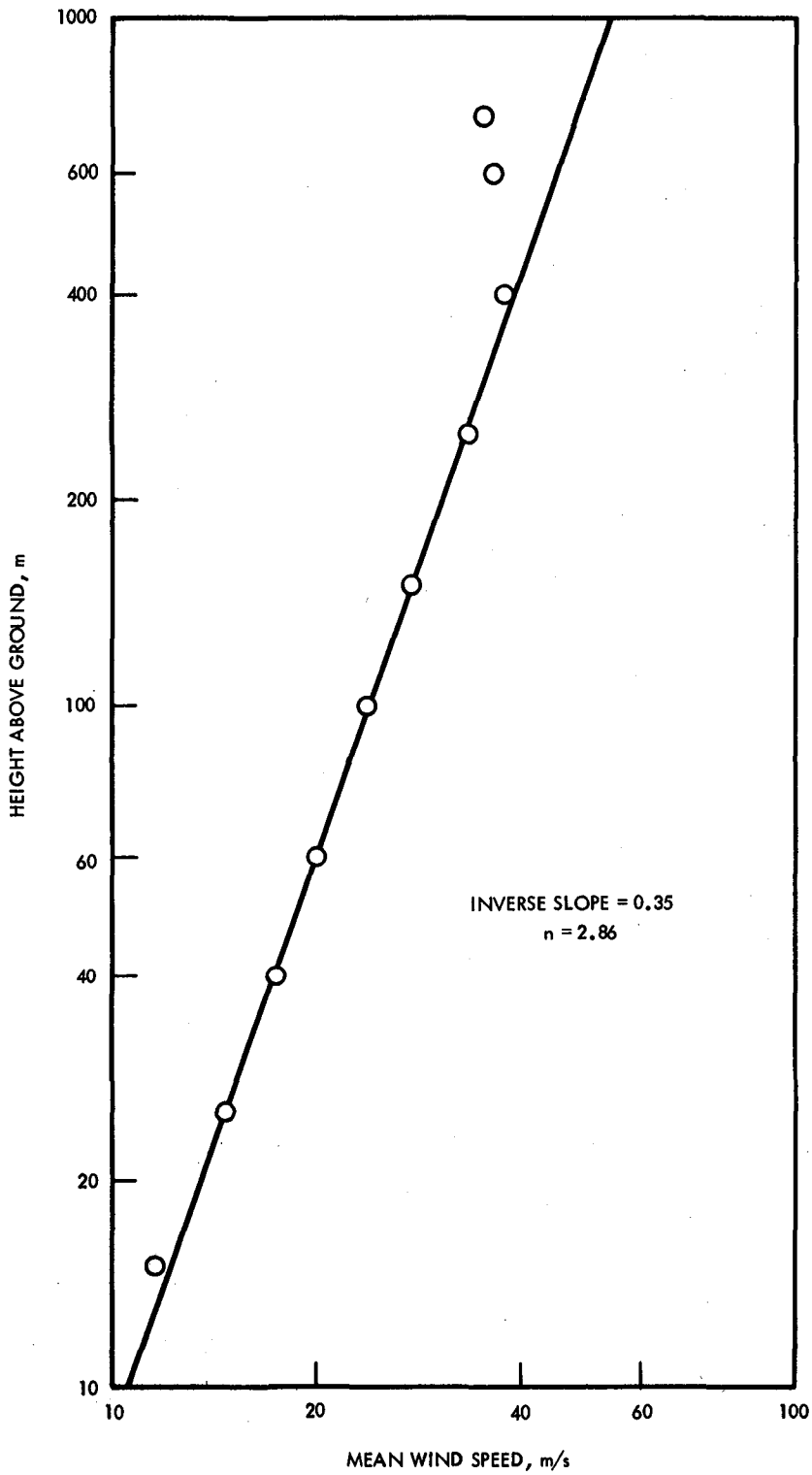

Figure 4. Test of the Power-Law Velocity Profile for the Planetary Boundary Layer Model Shown in Figure 2

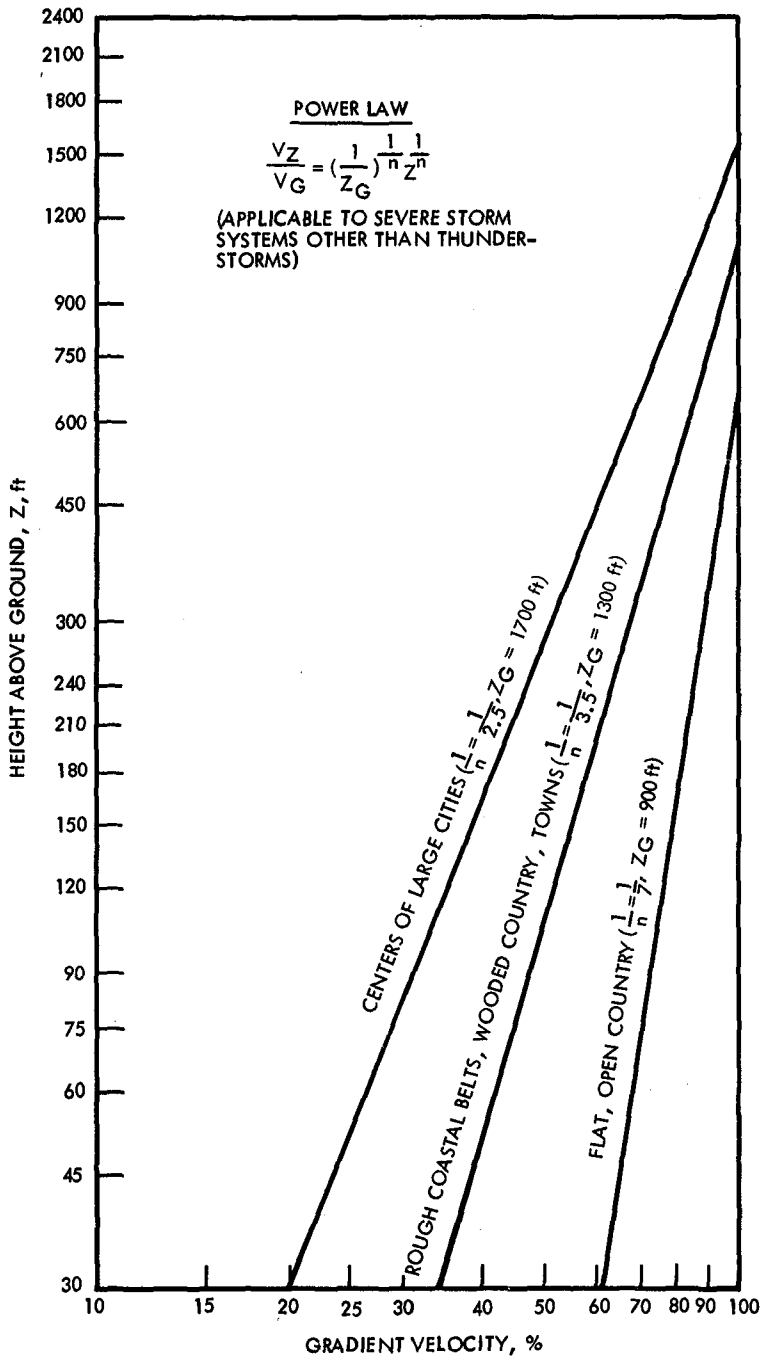

Figure 5. Change of Velocity with Height Over Level Ground for Three Different Types of Surface Roughness According to the Power Law (Adapted from Ref. 11)

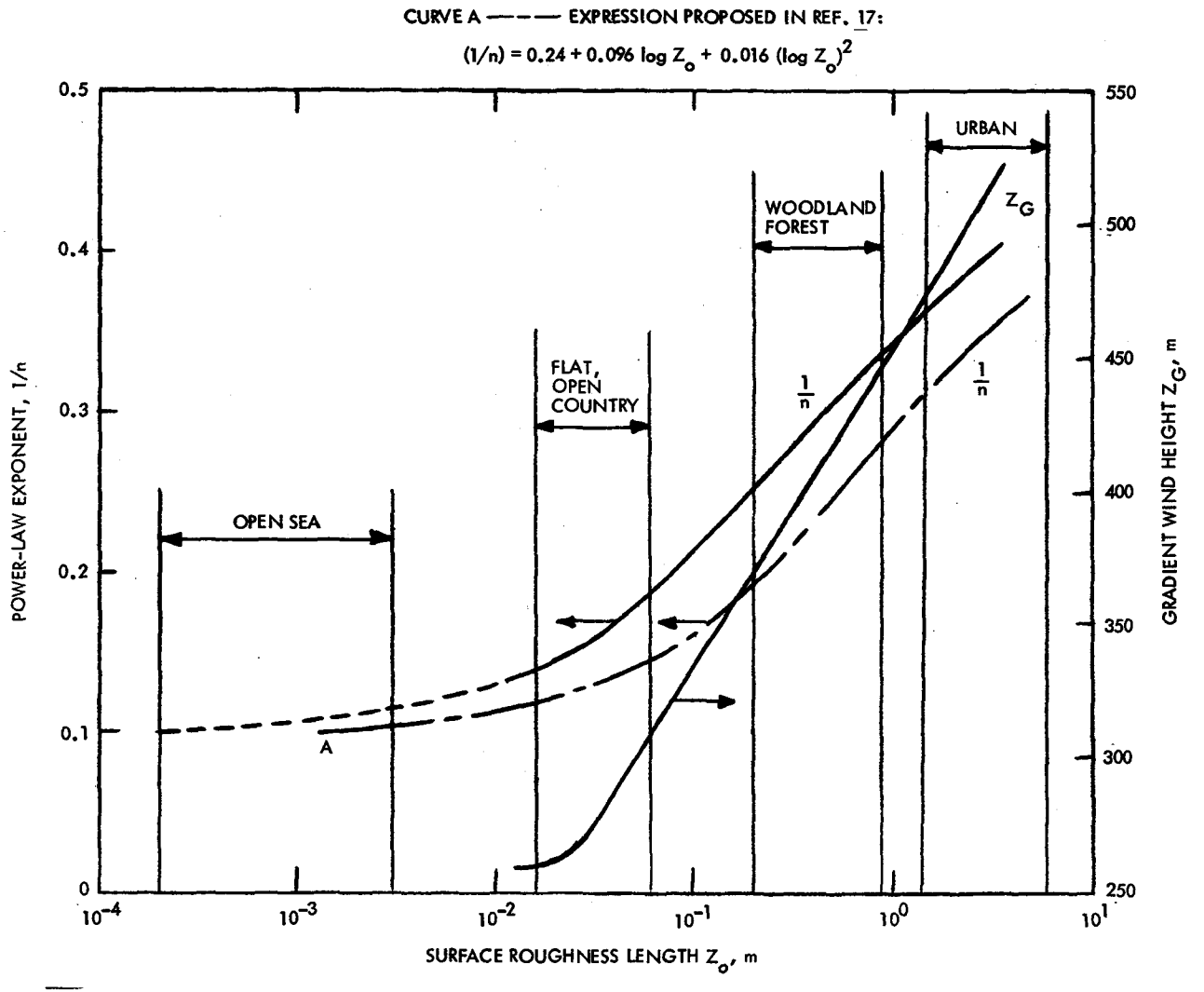

Figure 6. Power-Law Wind Profile Parameters for Strong Winds Over Surfaces of Different Roughness (Based on Data in Ref. 9)

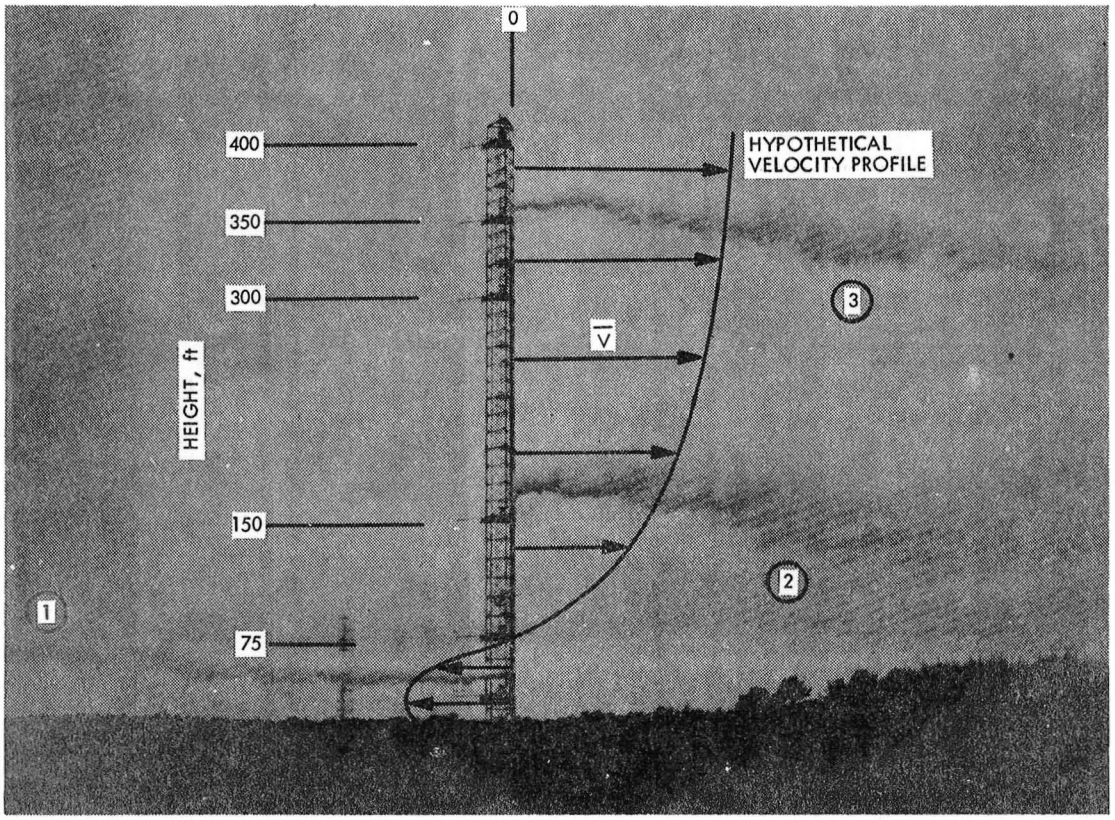

Figure 7. Smoke Emission from Three Heights of a Weather Tower During a Temperature Inversion, Note Differing Wind Directions (Adapted from Ref. 19)

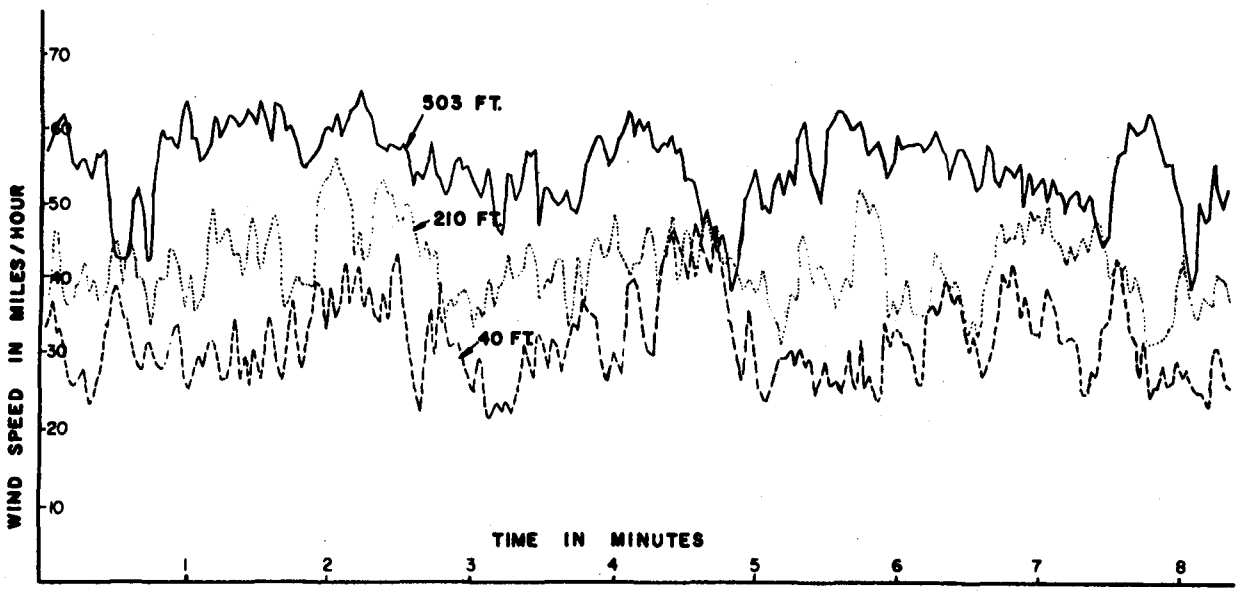

Figure 8. Typical Record of Horizontal Wind Speed at Three Heights (Reproduced from Ref. 22)

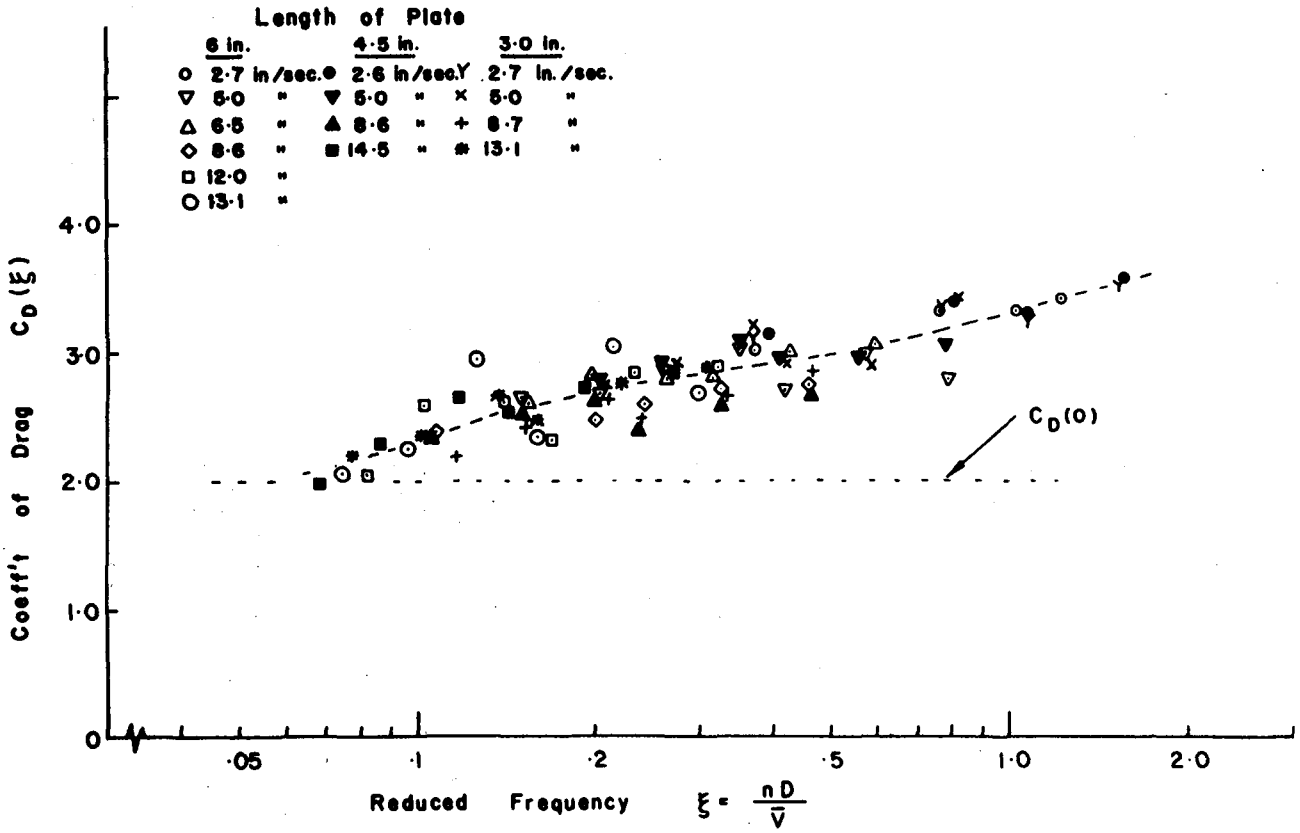

Figure 9. Coefficient of Drag for a Flat Plate in Fluctuating Flow (Reproduced from Ref. 22)

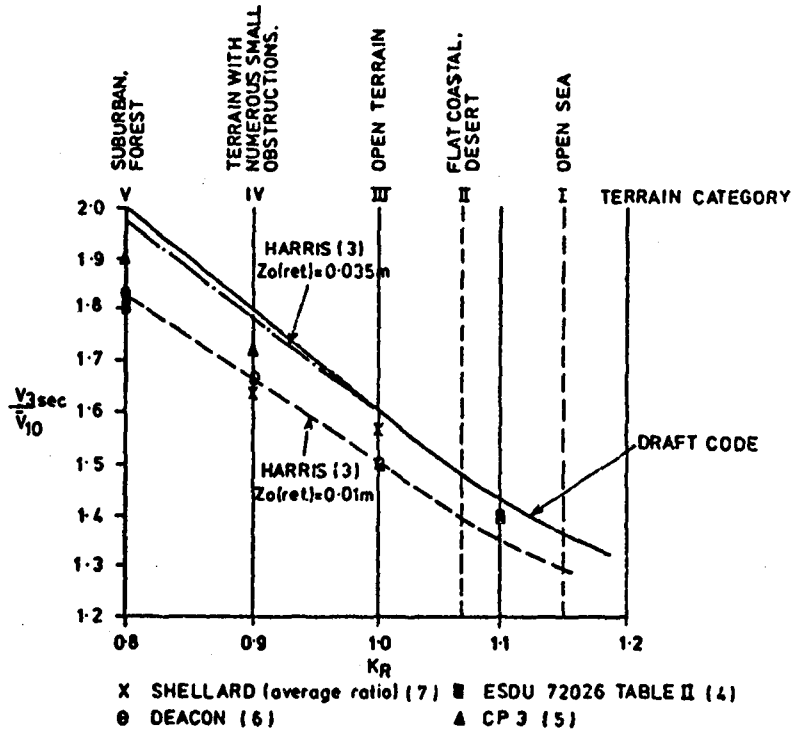

a. RATIO, MAXIMUM 3-second GUST PER HOUR TO MEAN WIND SPEED

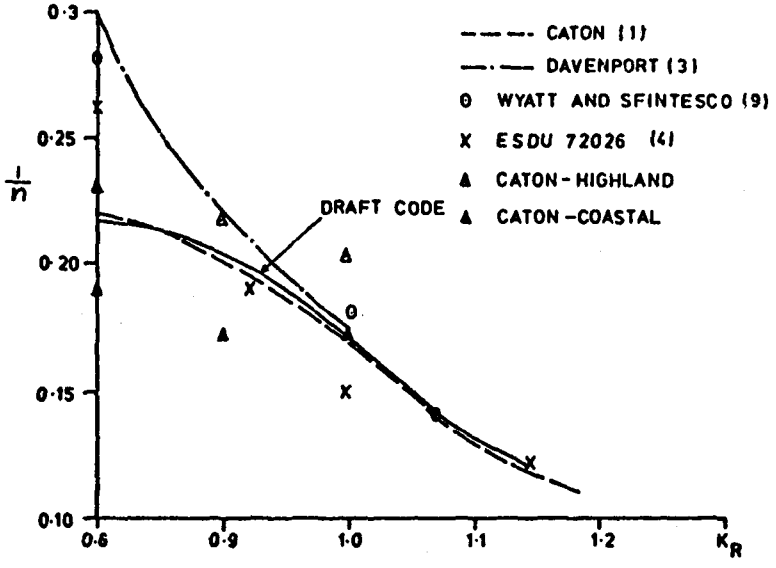

b. POWER-LAW INDEX RELATED TO TERRAIN ROUGHNESS FACTOR

Figure 10. Gust Ratios and Power-Law Index for Various Terrain Categories (Adapted from Ref. 23)

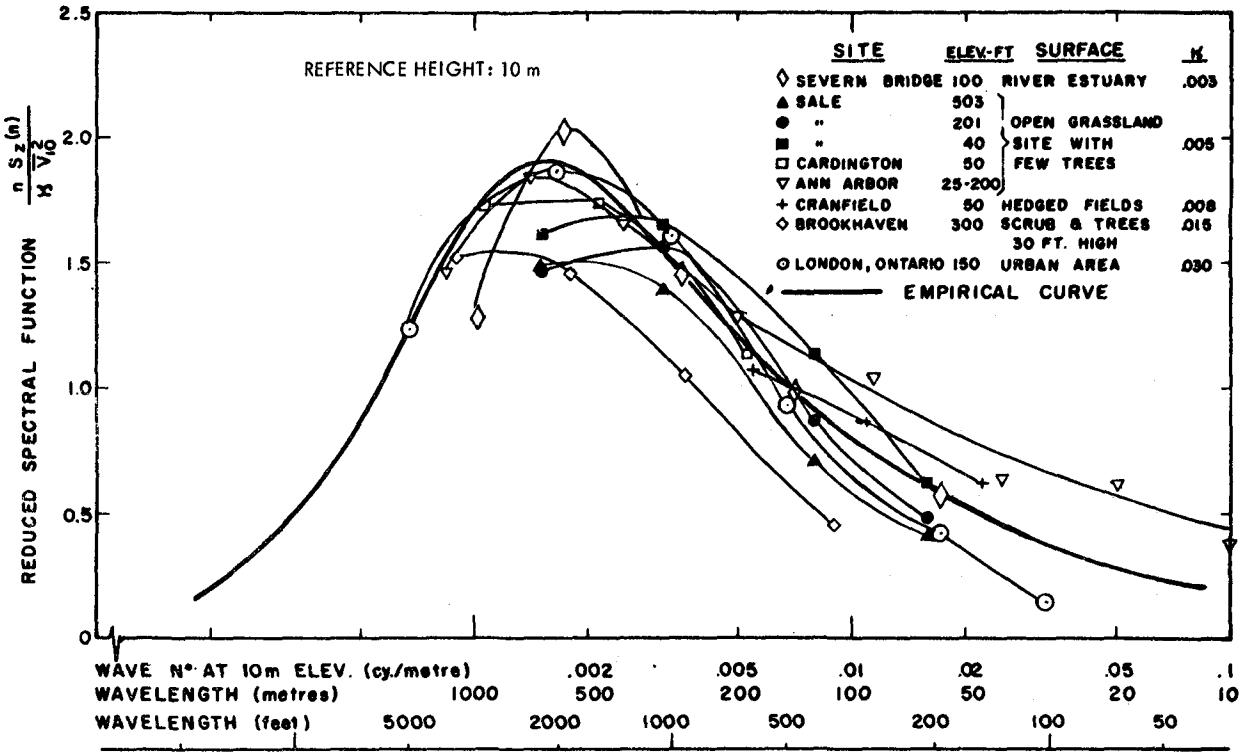

Figure 11. Spectrum of Horizontal Gustiness in High Winds (Adapted from Ref. 22)

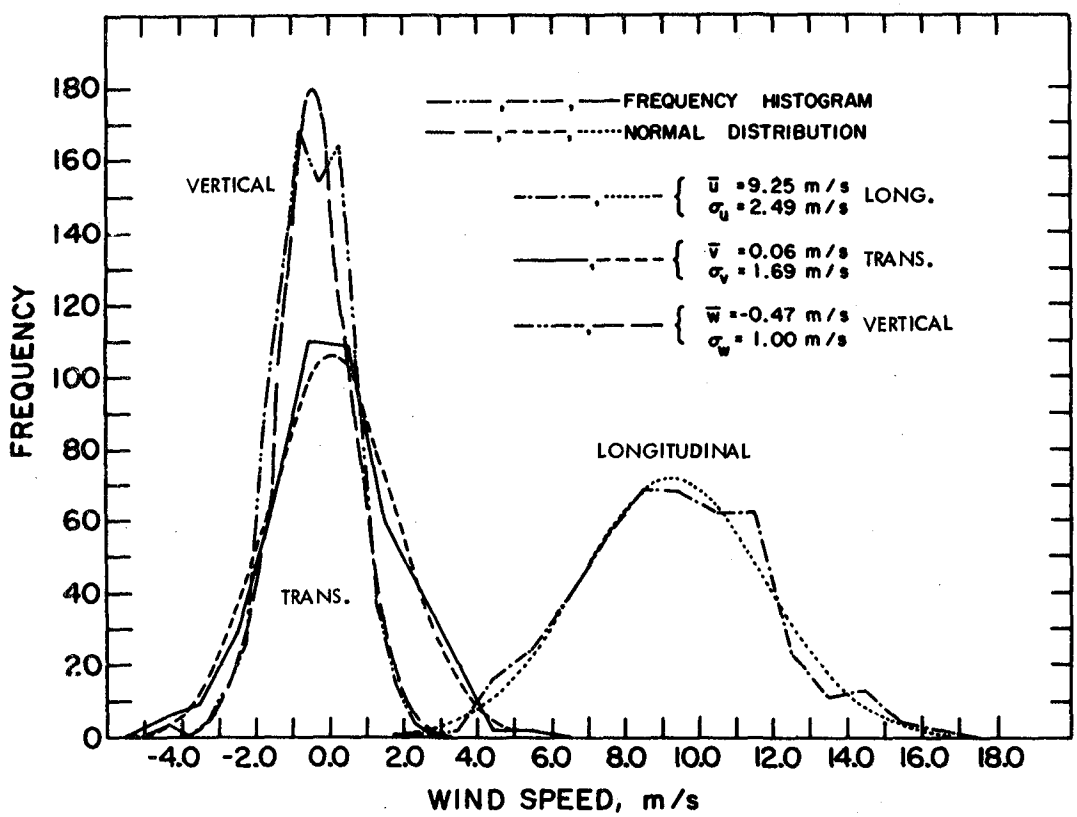

Figure 12. Frequency Distribution of Wind Components (Adapted from Ref. 19)

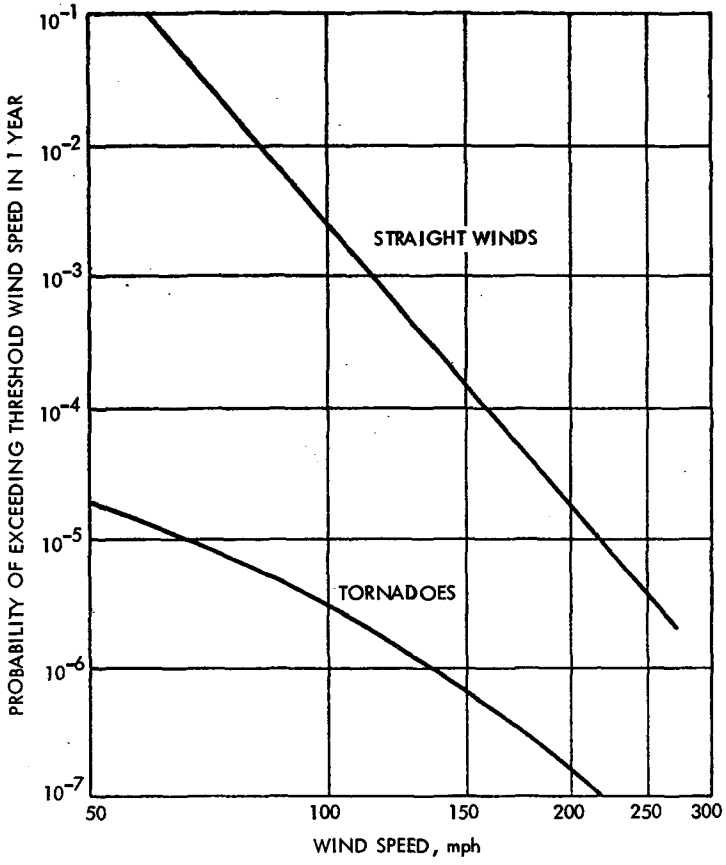

Figure 13. Risk Model for Extreme Winds at Daggett Airport, Located Near Barstow, California (From Ref. 10)

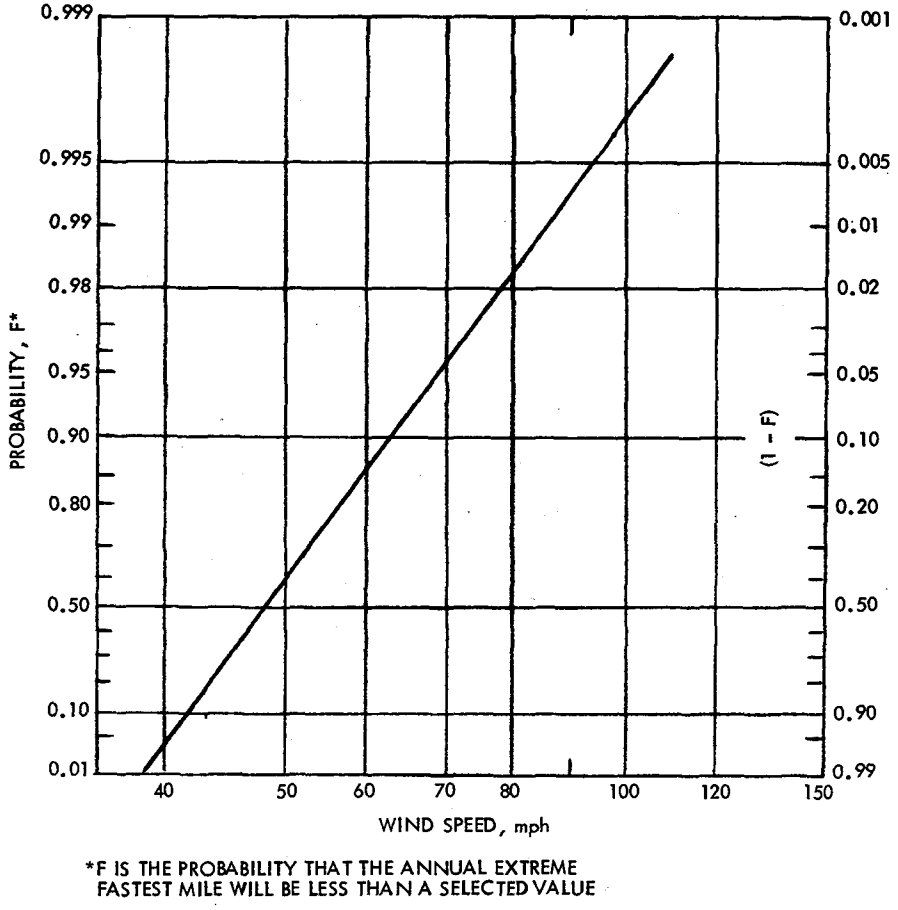

Figure 14. Distribution of Fastest Mile Speed at 30-ft Elevation, Elkins Airport (Approx. 40 miles from Sugar Grove Antenna in West Virginia) (Adapted from Ref. 37)

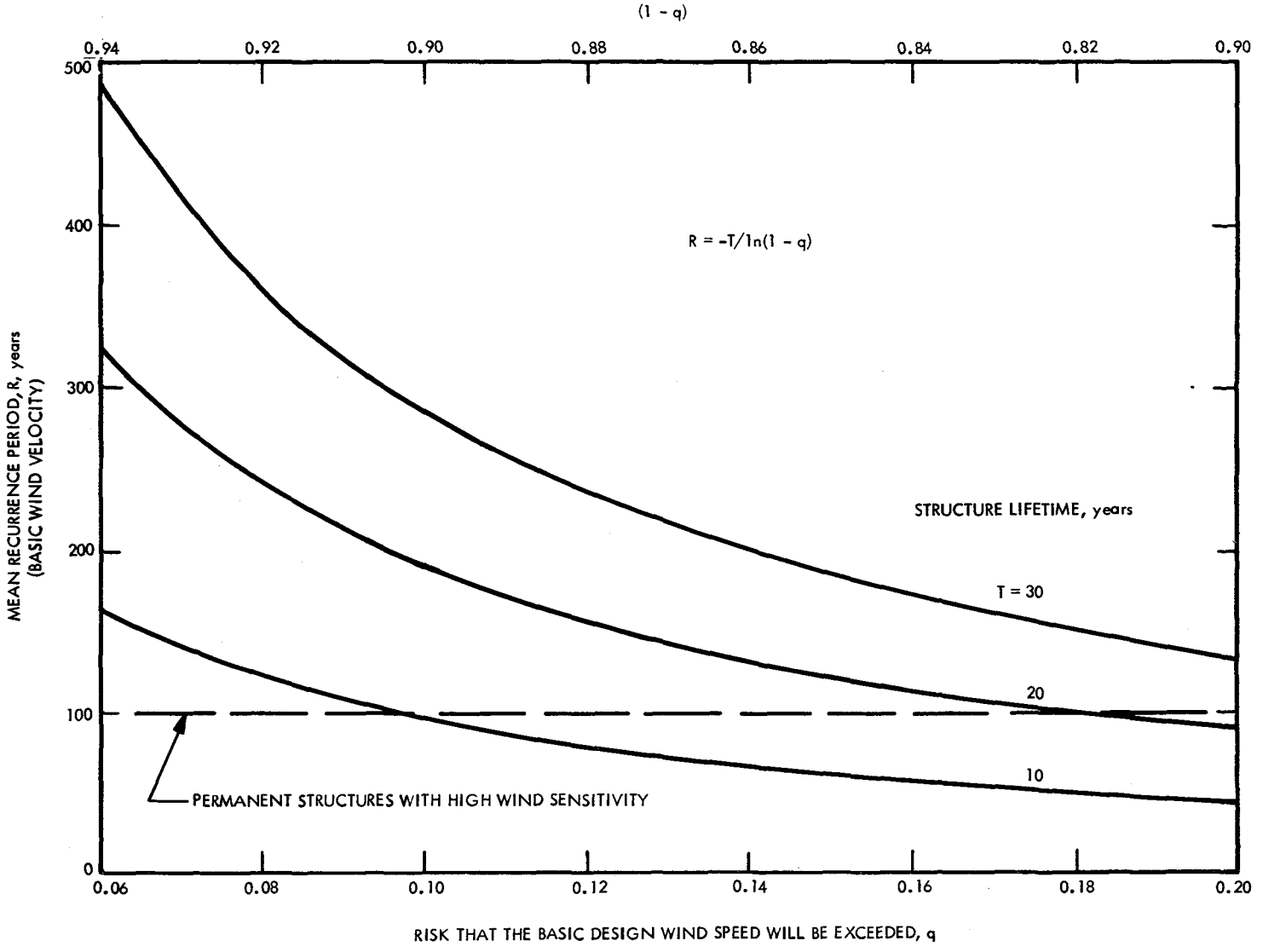

Figure 15. Mean Recurrence Period for Different Structure Lifetimes

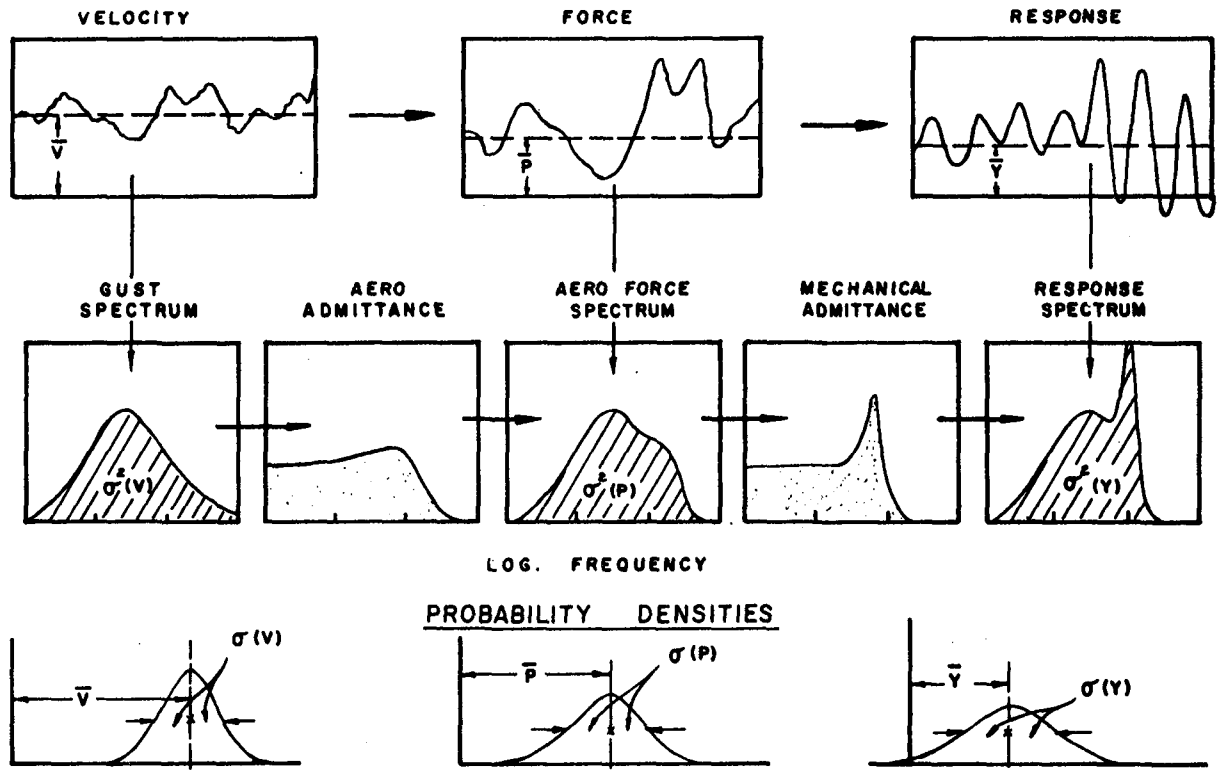

Figure 16. Elements of a Statistical Approach to Gust Loading (Reproduced from Ref. 22)

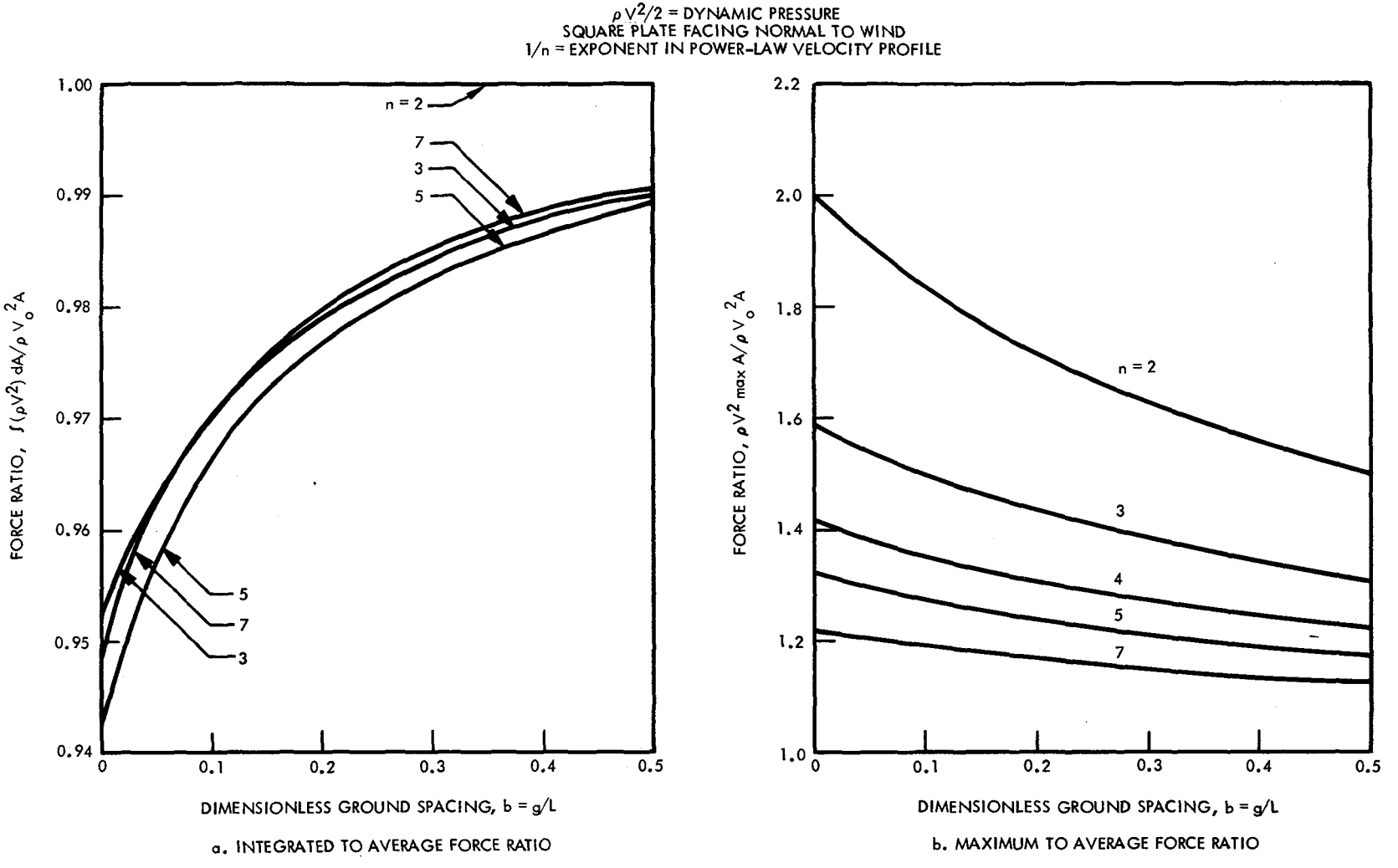

Figure 17. Calculated Horizontal Force Ratios on a Square Plate

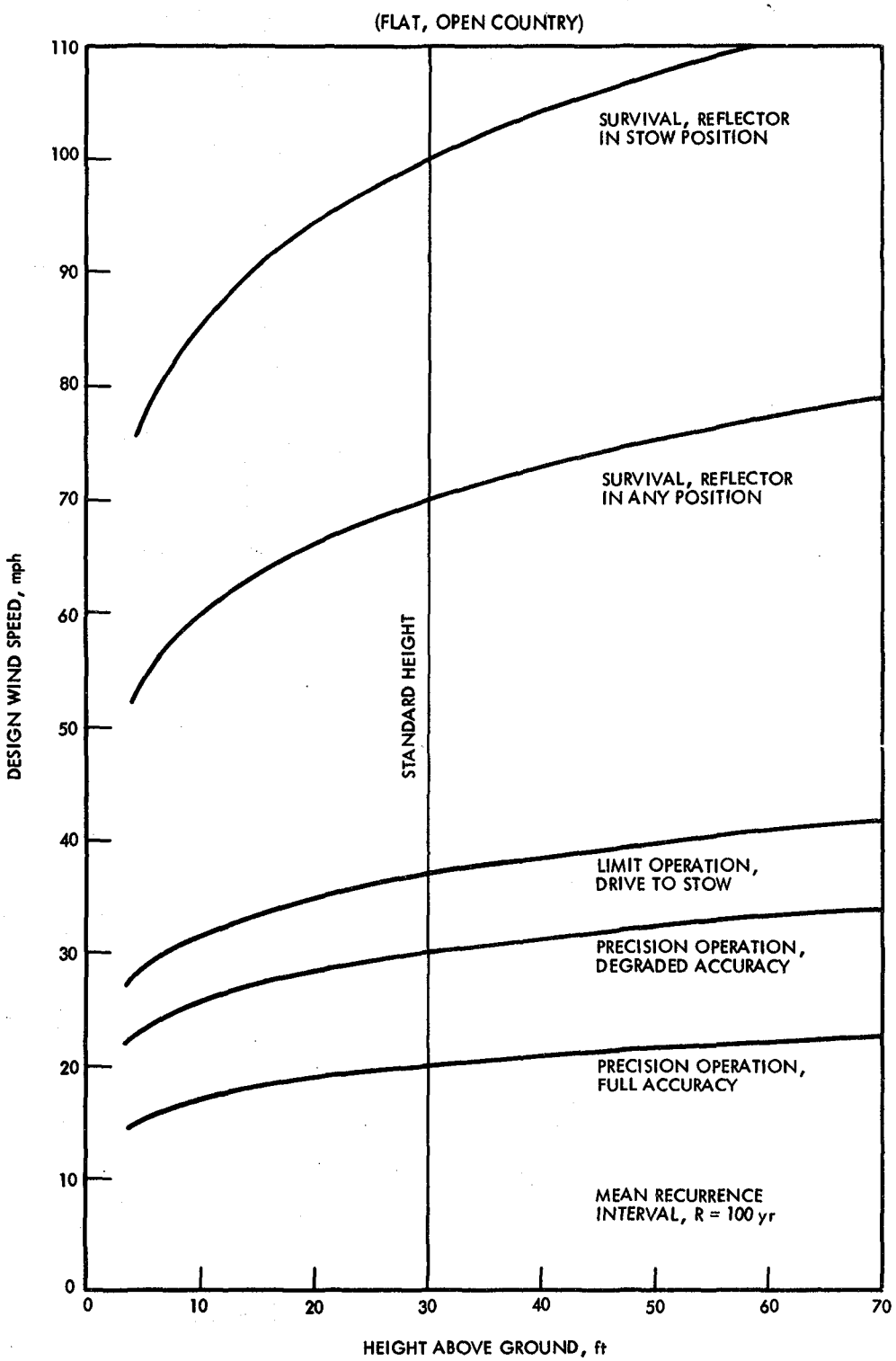

Figure 18. Recommended Design Wind Speed for the Parabolic Dish Test Site at Edwards Air Force Base, California

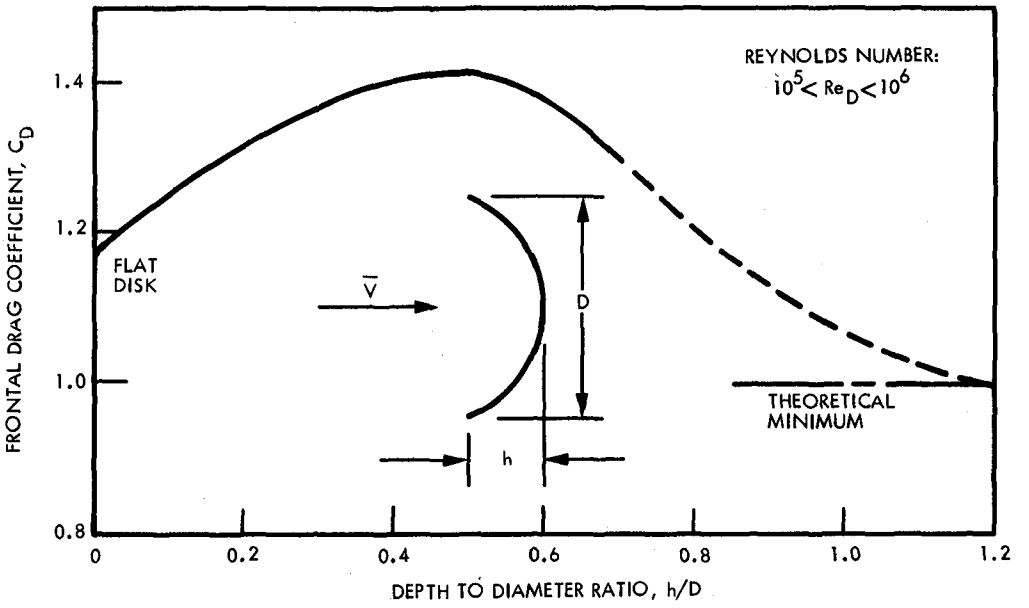

Figure 19. Drag of Sheet Metal Caps Facing Directly Into Wind (Adapted from Ref. 16)

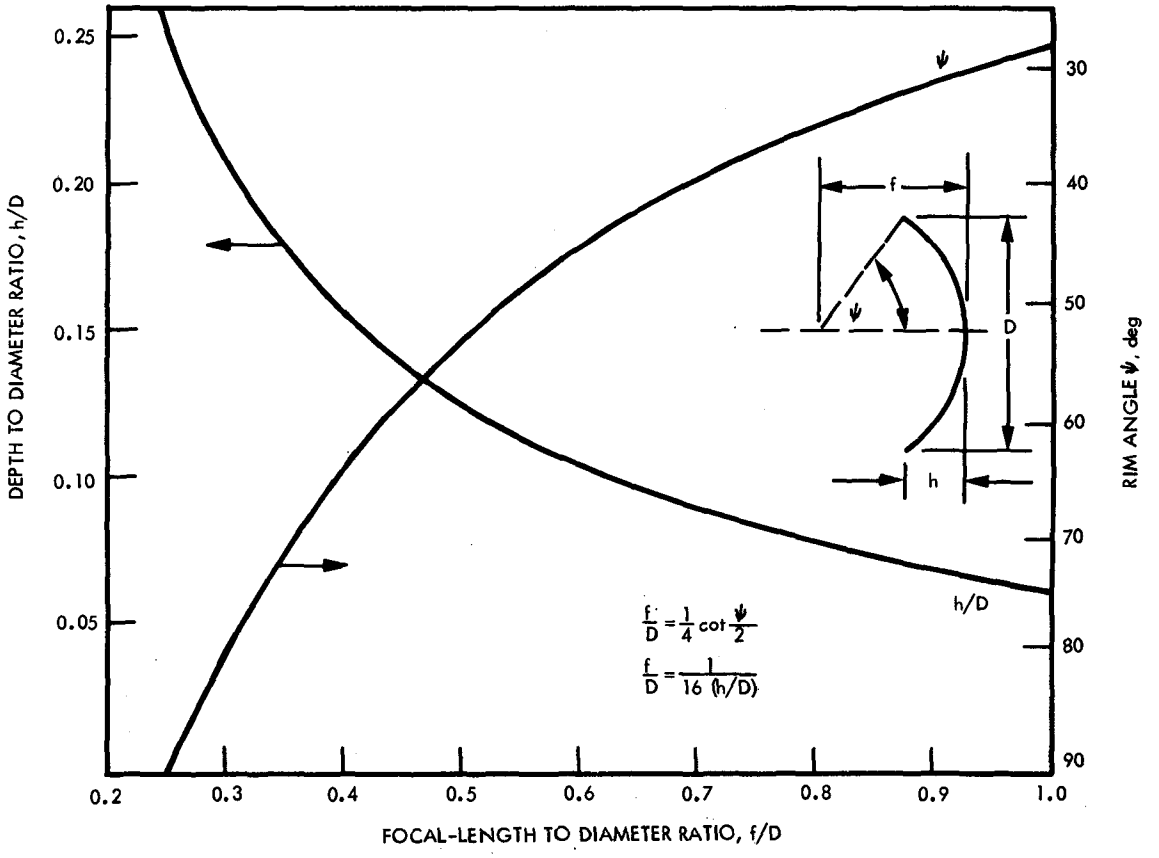

Figure 20. Relationship Between h/D, ψ, and f/D for Paraboloidal Reflectors

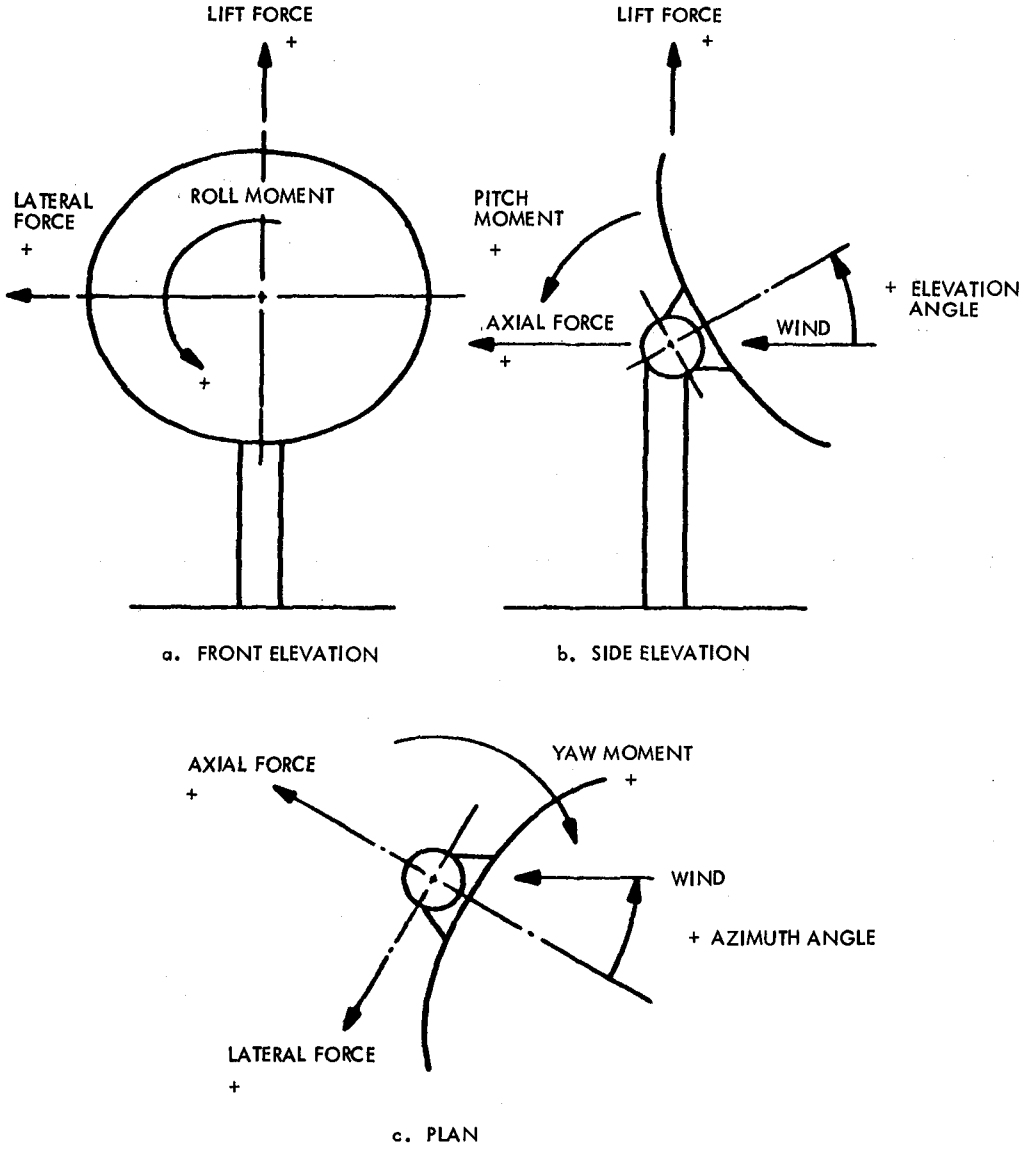

Figure 21. Stability-Axes System for Paraboloidal Reflectors (From Ref. 13)

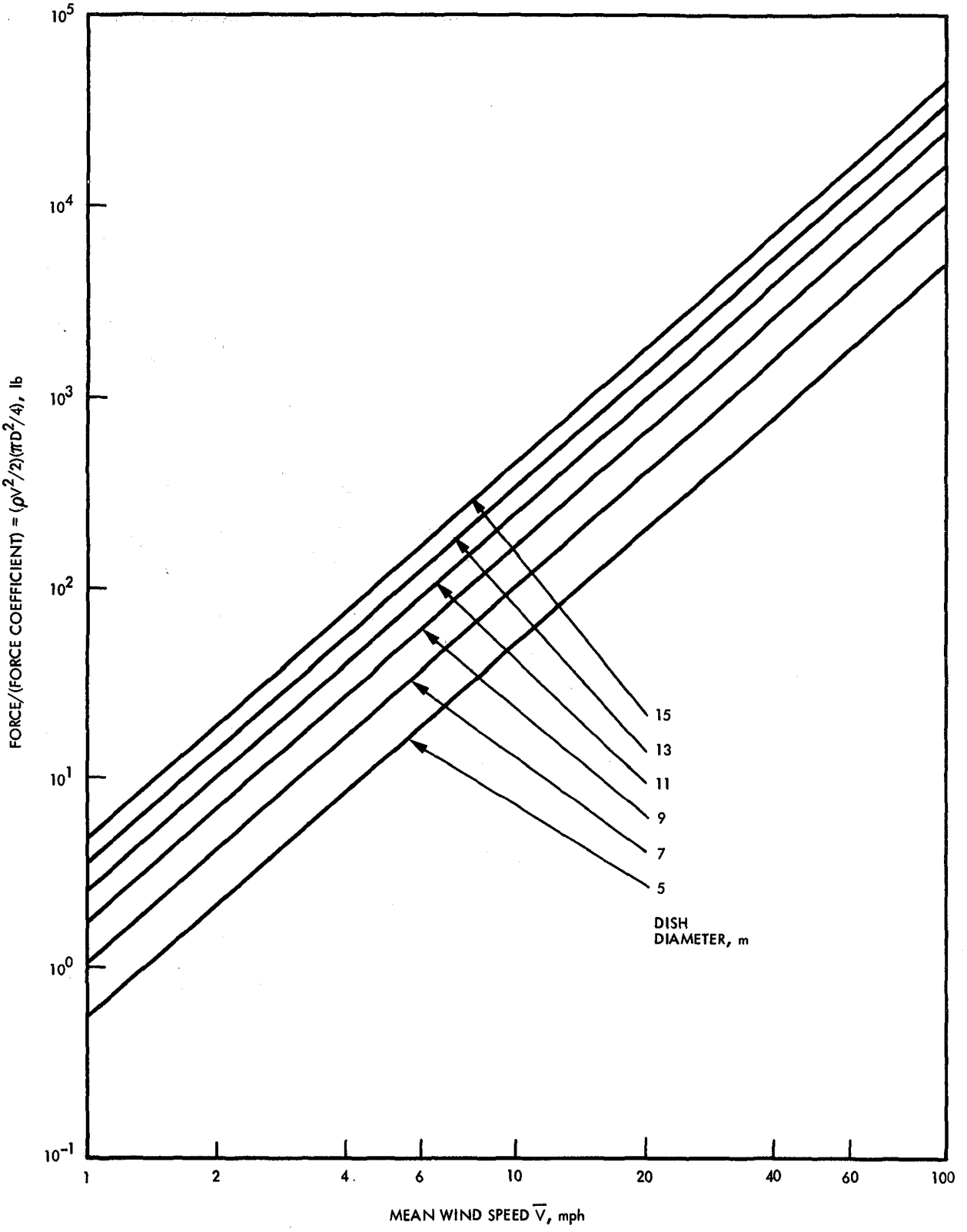

Figure 22. Ratio of Force-to-Force Coefficient

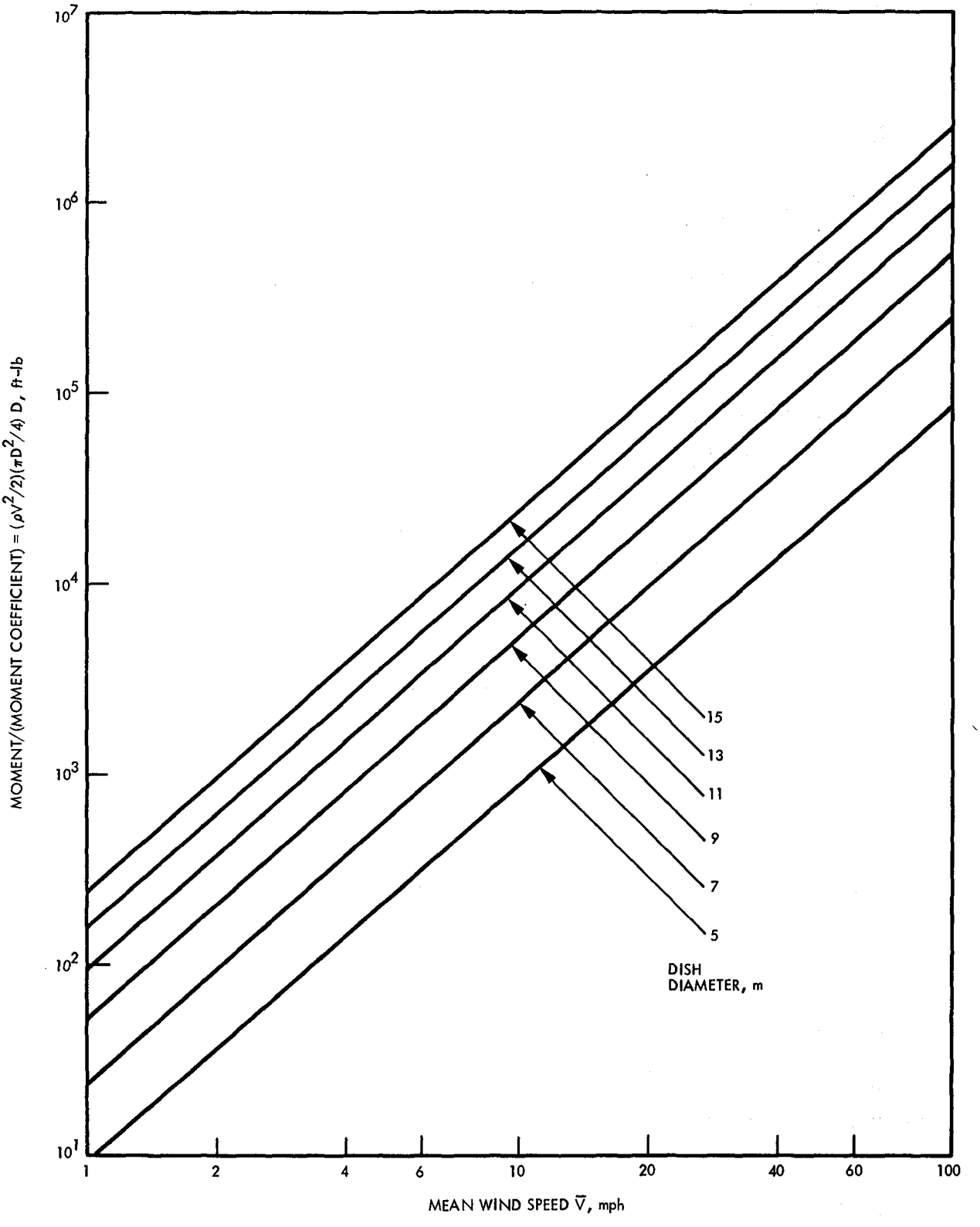

Figure 23. Ratio of Moment-to-Moment Coefficient

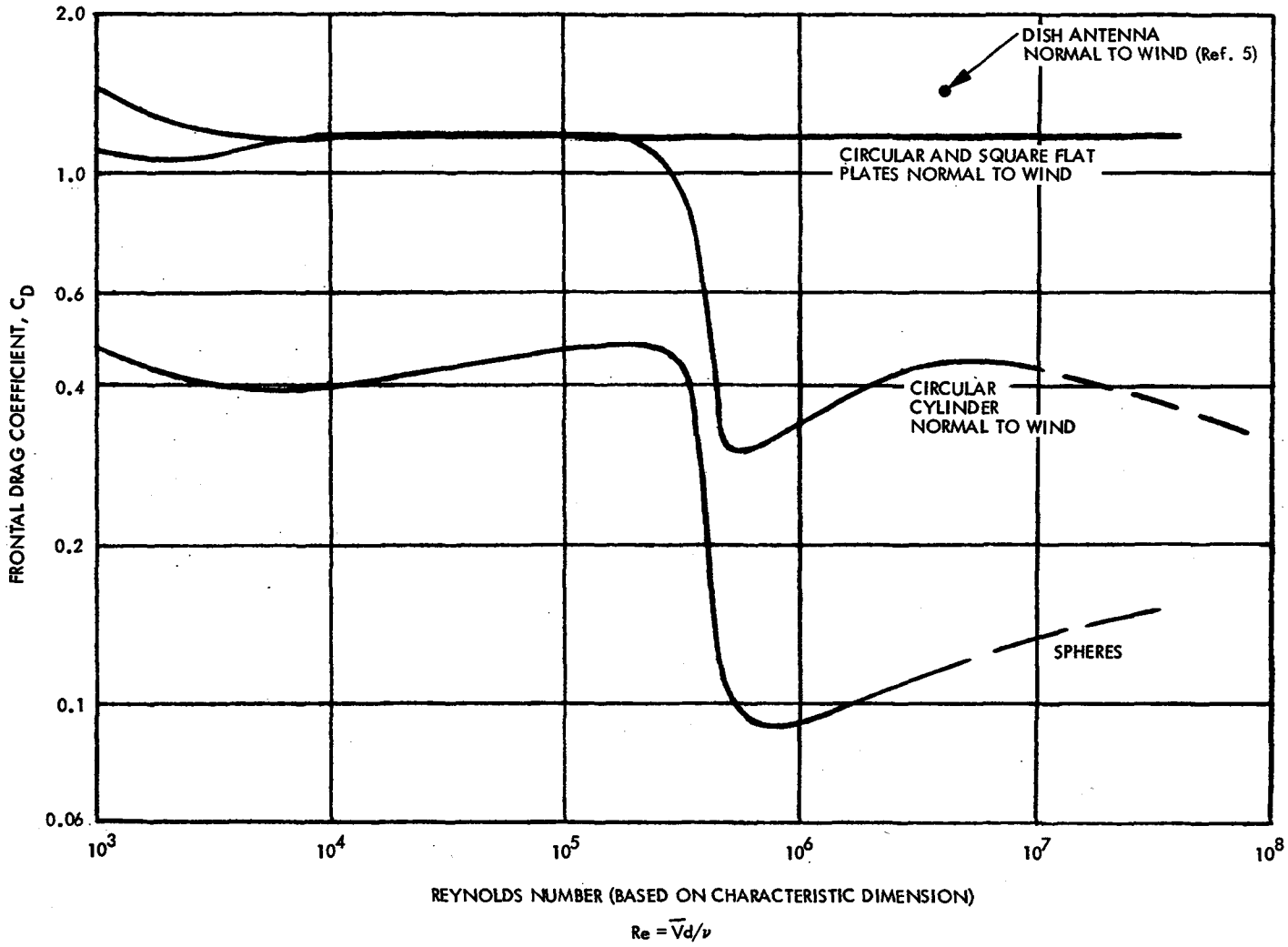

Figure 24. Drag Coefficient Versus Reynolds Number for Common Shapes (Based on Data in Ref. 16)

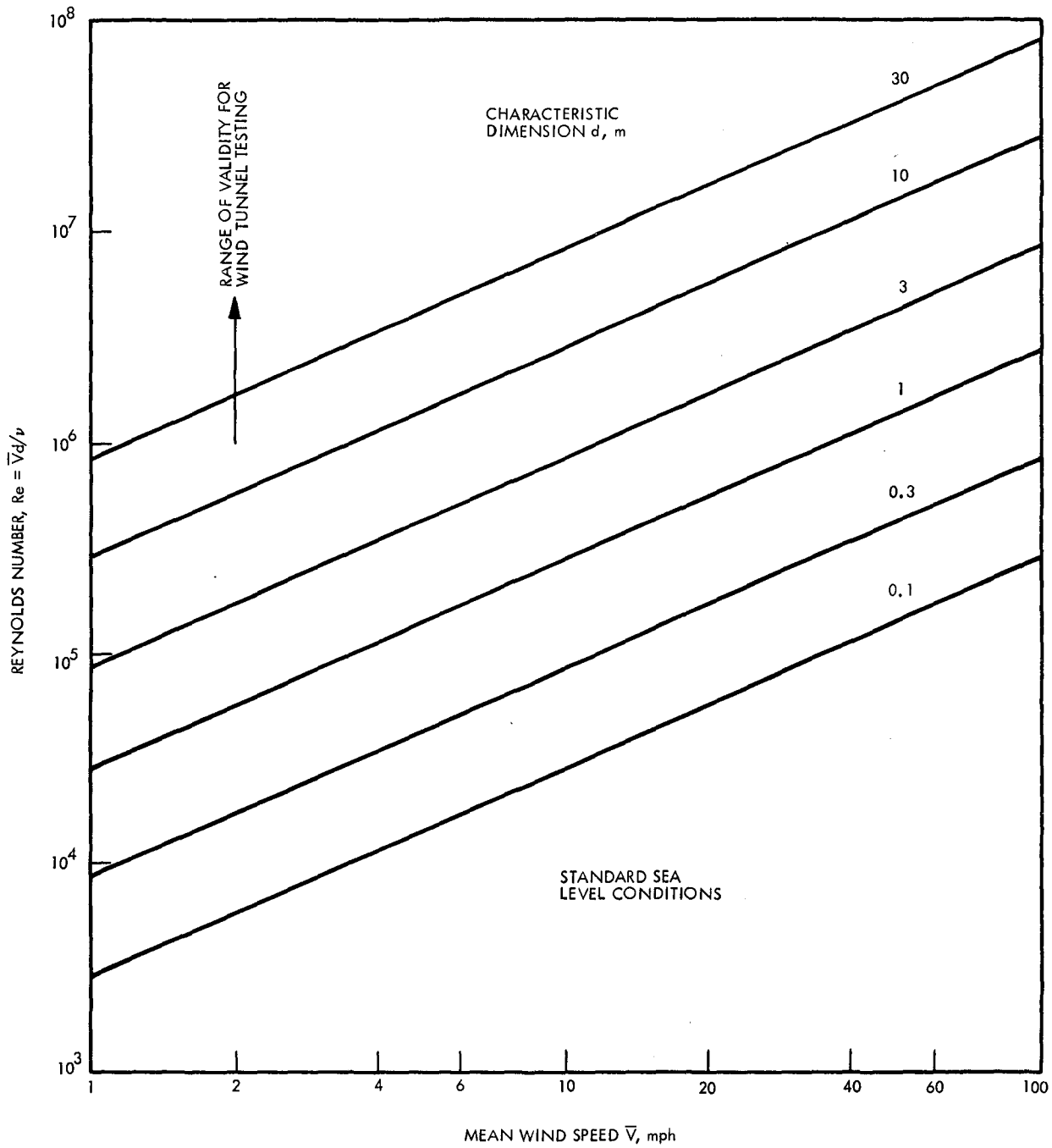

Figure 25. Reynolds Number Variation with Wind Speed and Characteristic Dimension

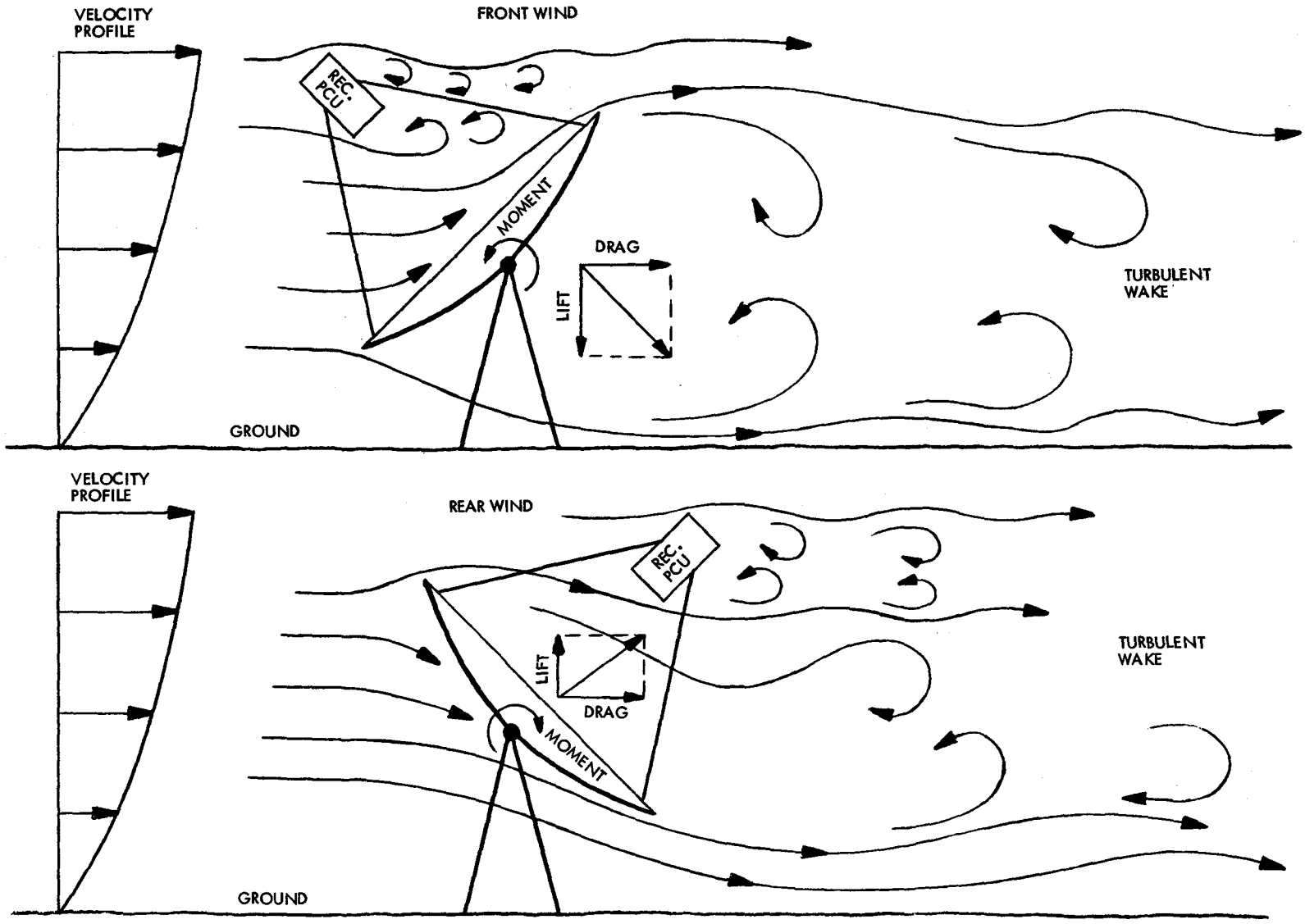

Figure 26. Conceptual Flow Patterns Around a Paraboloidal Concentrator at Zero Azimuth Angle

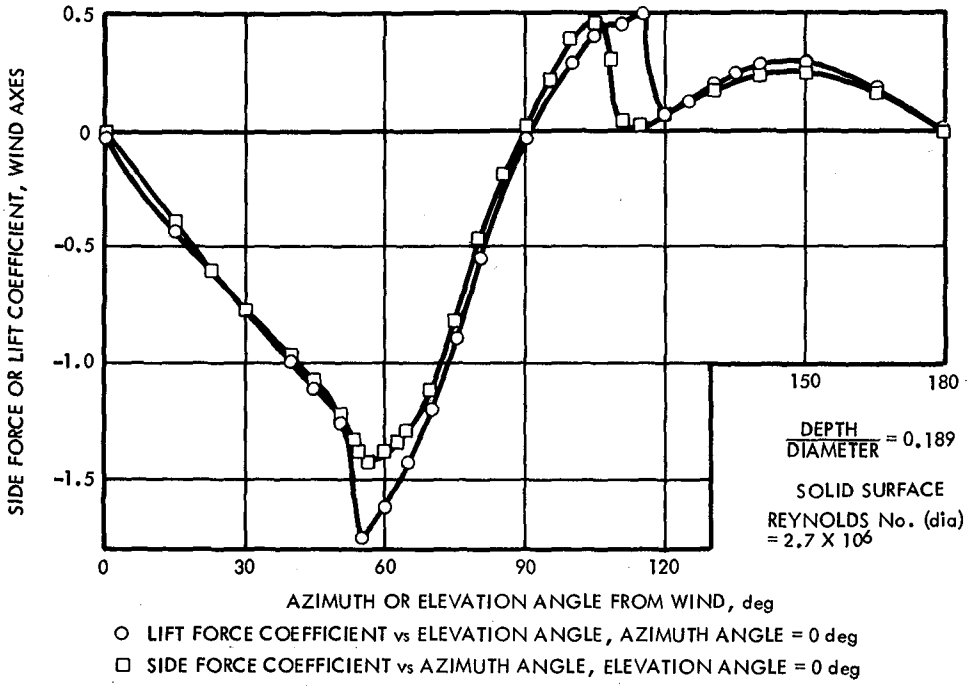

Figure 27. Departure from Symmetry (Wind-Axes System) Caused by Ground-Plane Interface (Adapted from Ref. 5)

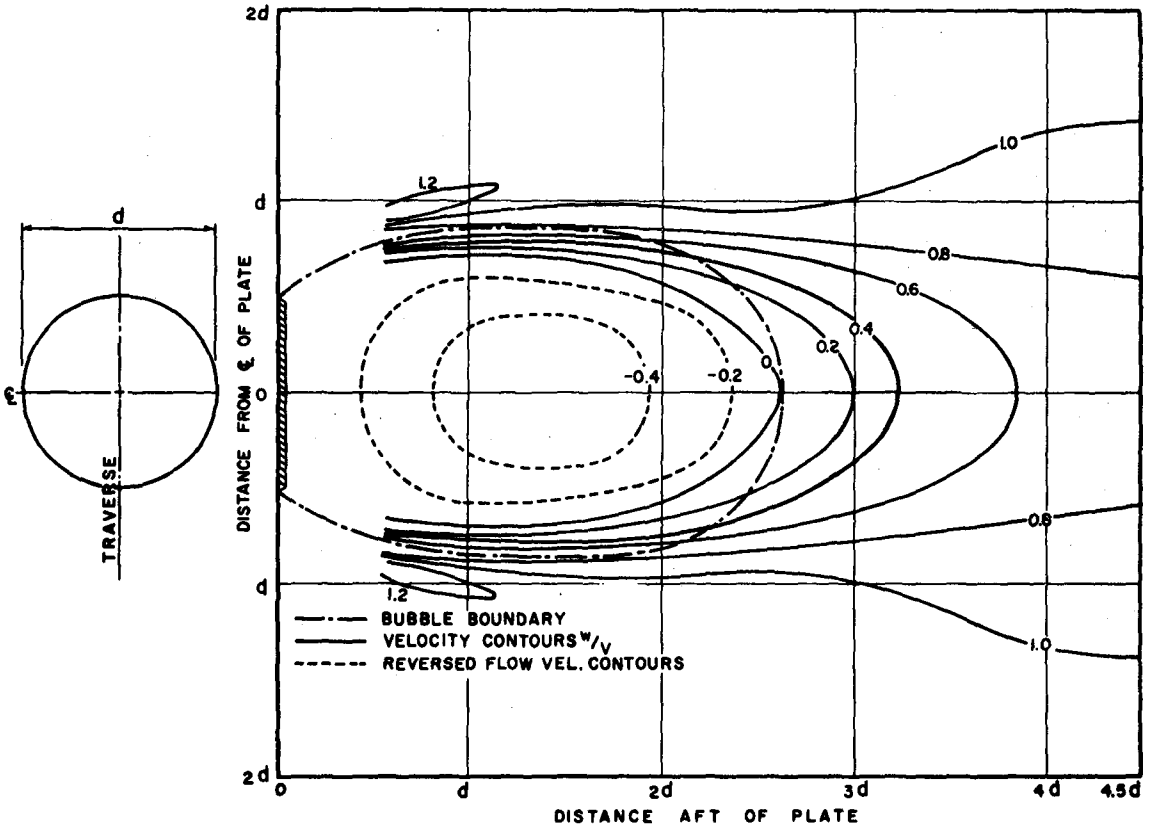

Figure 28. Experimental Flow Field Behind a Circular Flat Plate Normal to the Airstream (Reproduced from Ref. 68)

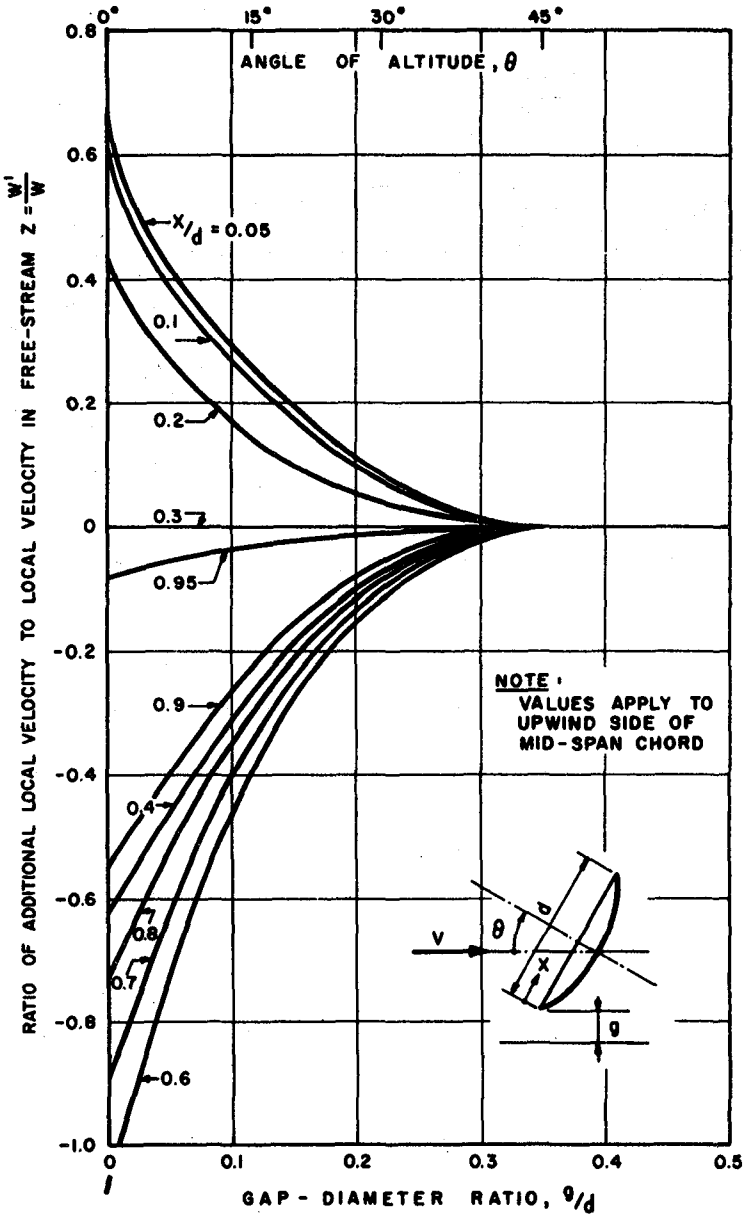

Figure 29. Theoretical Effect of Ground Plane on the Local Velocity Near a Paraboloidal Reflector (Reproduced from Ref. 68)

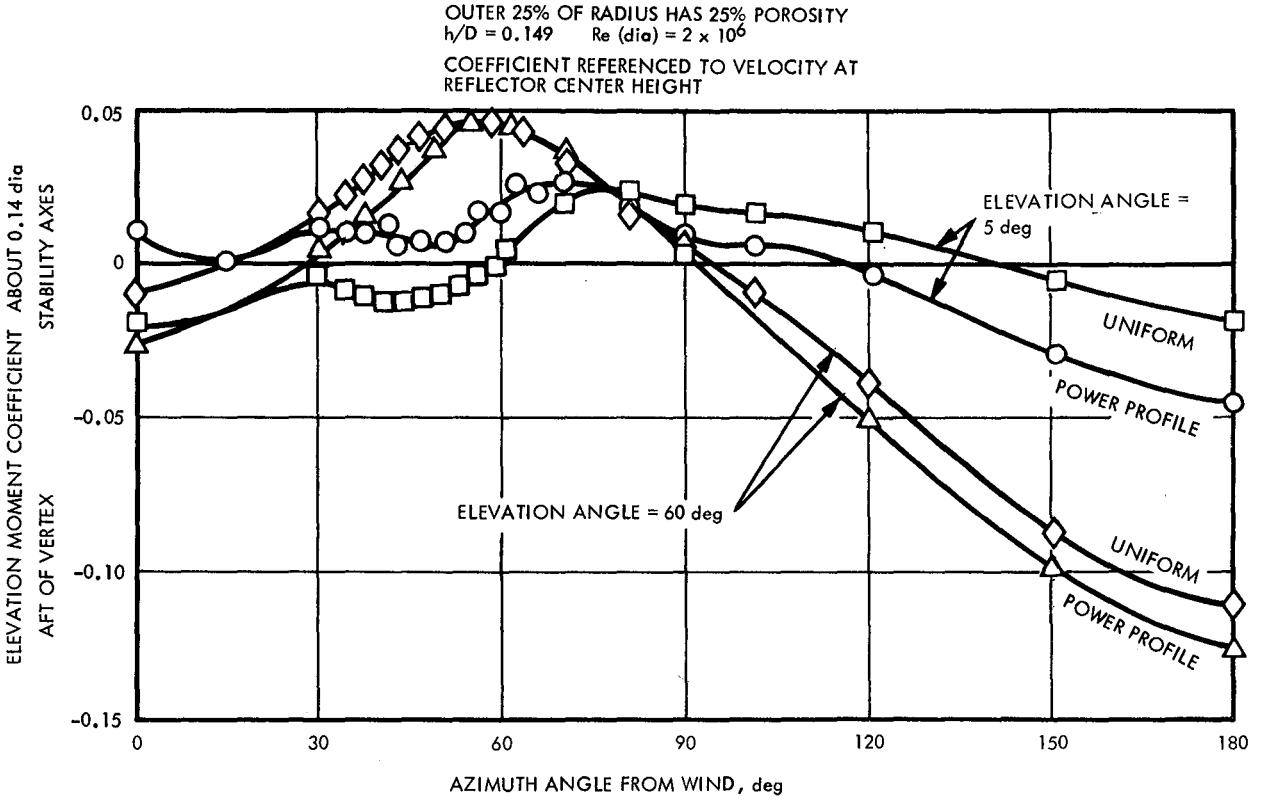

Figure 30. Effects of Nonuniform Velocity Profile on Elevation Moment (Stability Axis System) (Adapted from Ref. 5)

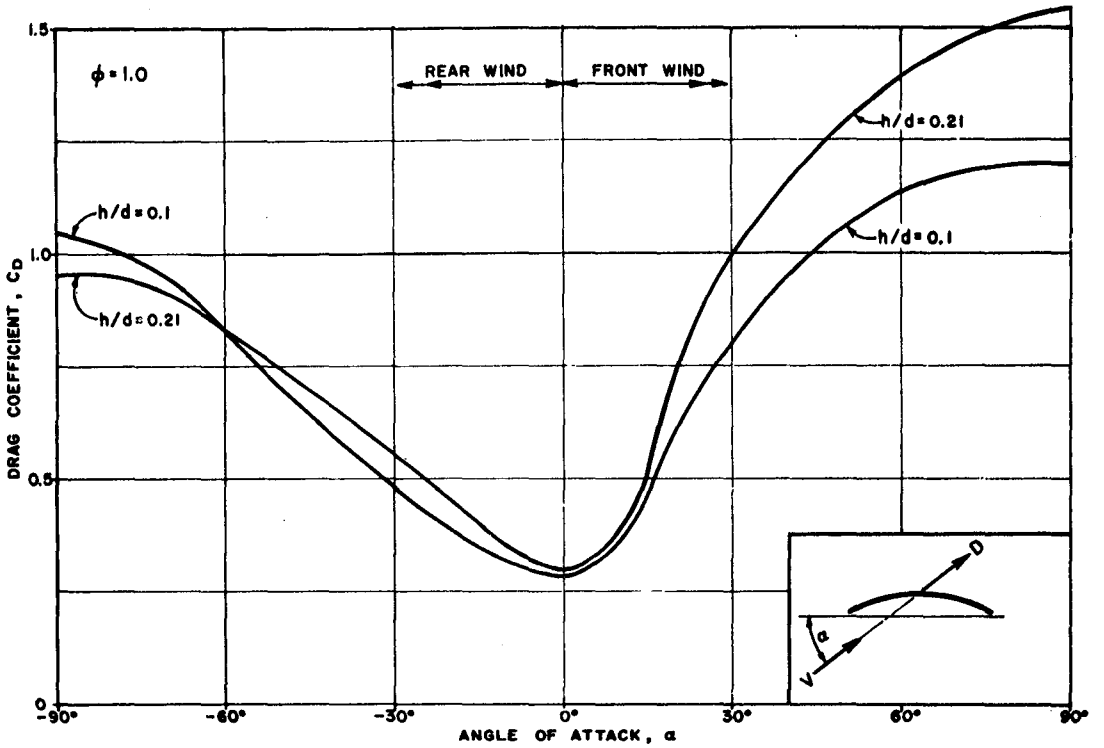

Figure 31. Drag Coefficients for Solid Paraboloidal Reflectors (Adapted from Ref. 68)

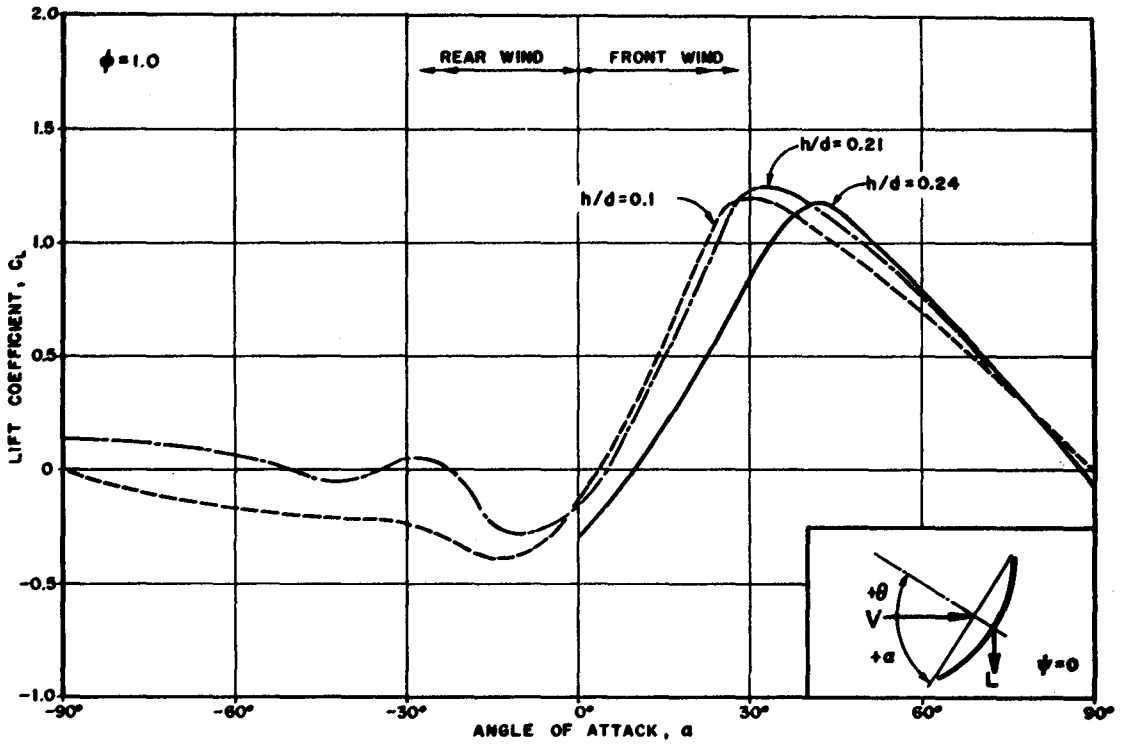

Figure 32. Lift Coefficients for Solid Paraboloidal Reflectors (Adapted from Ref. 68)

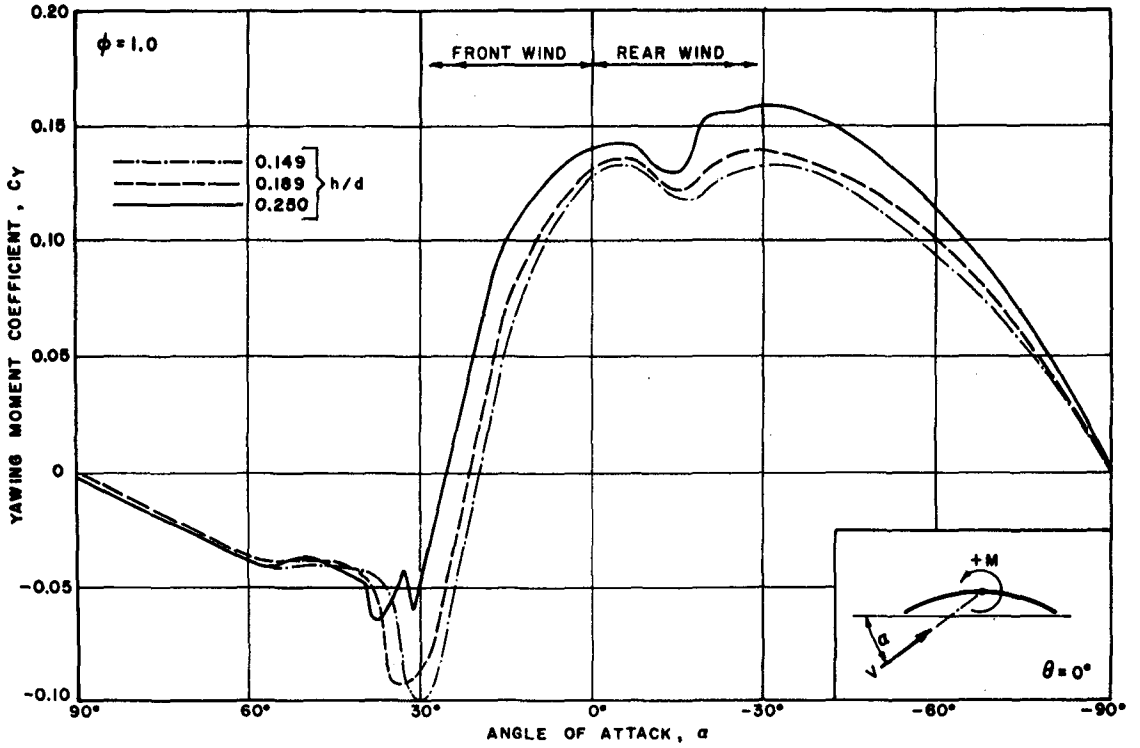

Figure 33. Yawing Moment Coefficients for Solid Reflectors (Reproduced from Ref. 68)

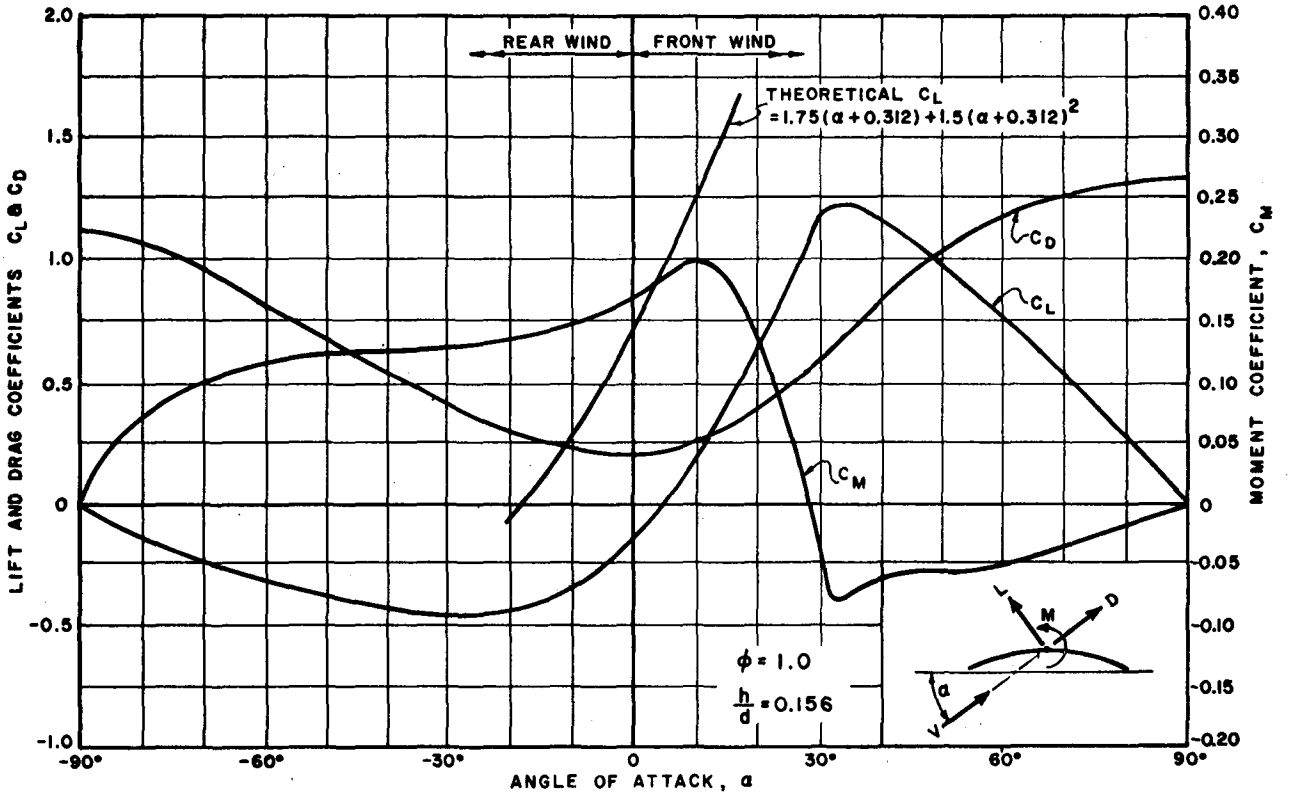

Figure 34. Empirical Aerodynamics Coefficients for Solid Paraboloidal Reflectors, h/D = 0.156 (Reproduced from Ref. 68)

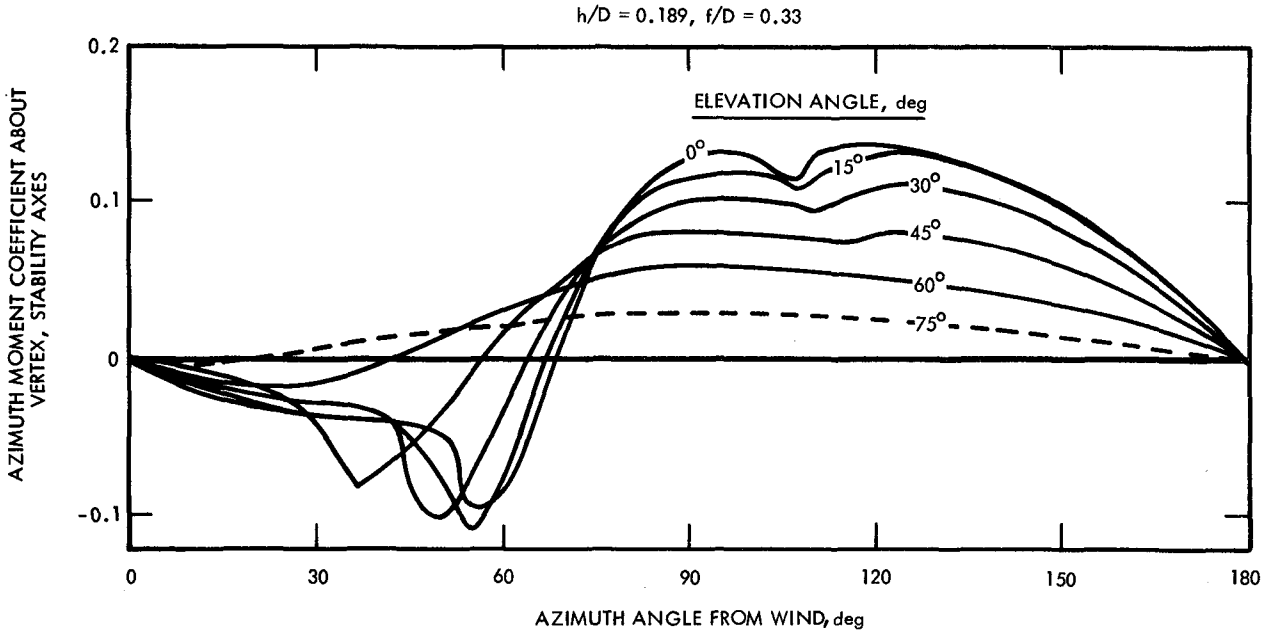

Figure 35. Effect of Elevation Angle on Azimuth (Yawing) Moment of Solid Paraboloidal Reflectors (Adapted from Ref. 5)

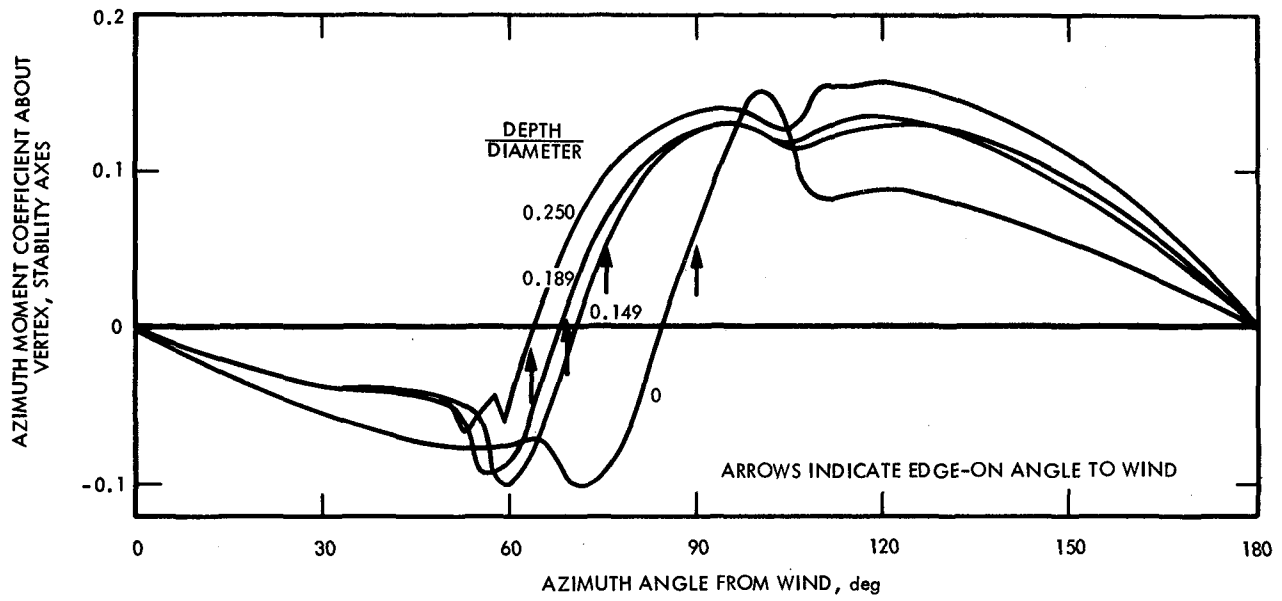

Figure 36. Effect of Depth-to-Diameter Ratio on Azimuth Moment of Solid Paraboloidal Reflectors, Arrows Denote Angles at which Edge of Reflector is Parallel with the Wind Direction (Adapted from Ref. 5)

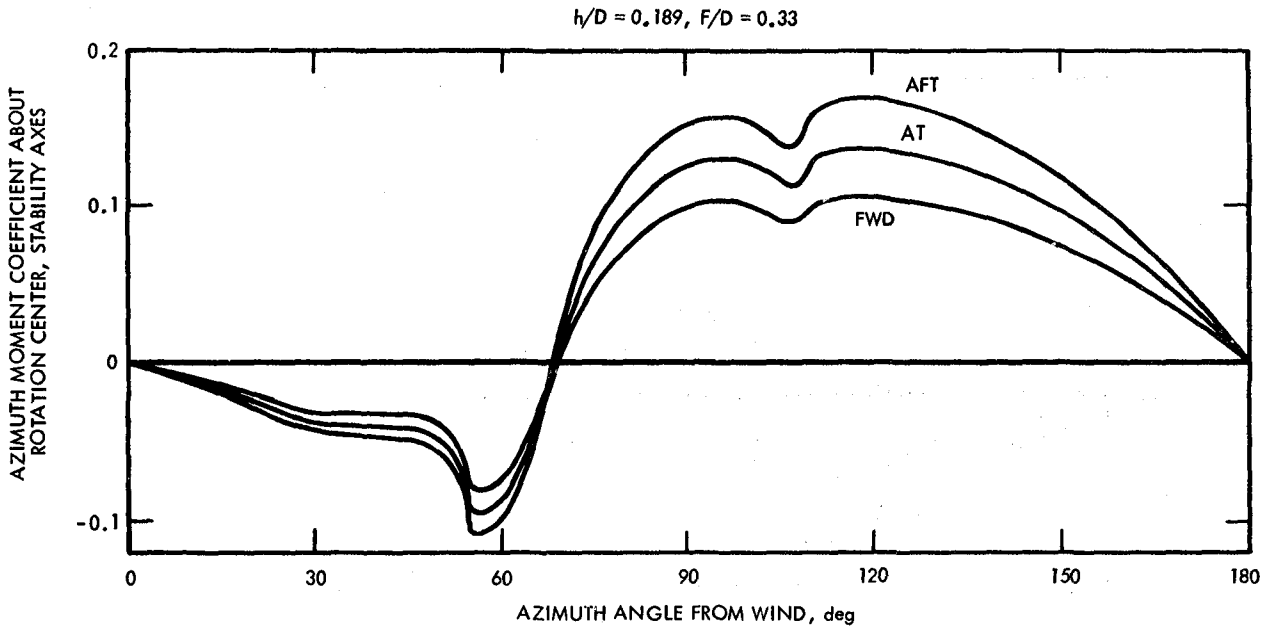

Figure 37. Effect of Rotation Center Position on Azimuth Moment for Zero Elevation Angle (Adapted from Ref. 5)

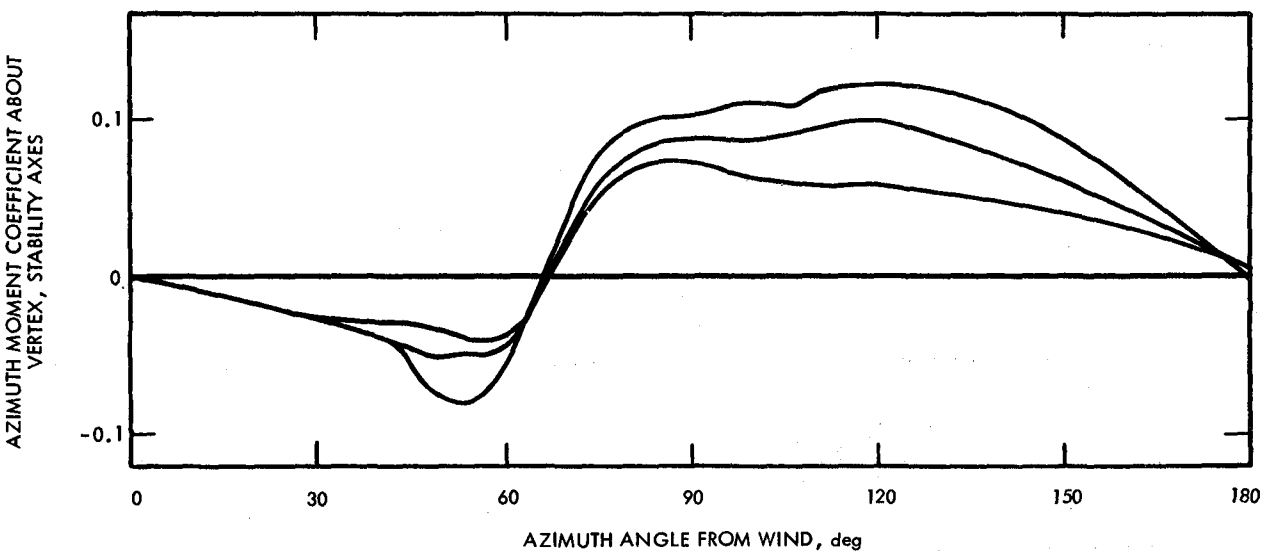

DEPTH / DIAMETER = 0.189

ELEVATION ANGLE = 0 deg

25 % POROUS ON OUTER 25 % RADIUS

Figure 38. Effect of Reflector Surface Support Structure on Azimuth Moment (Adapted from Ref. 5)

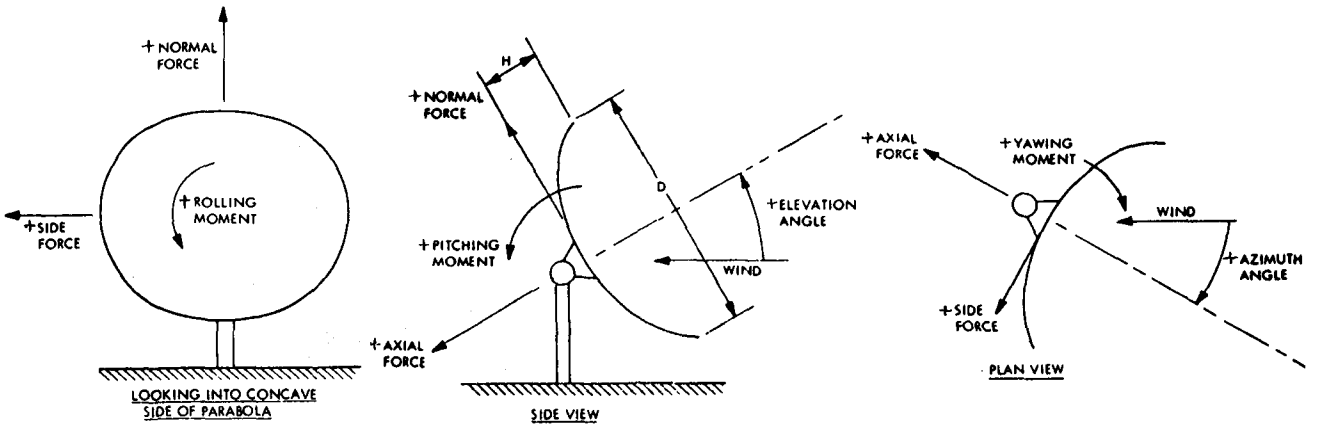

Body-axis orientation

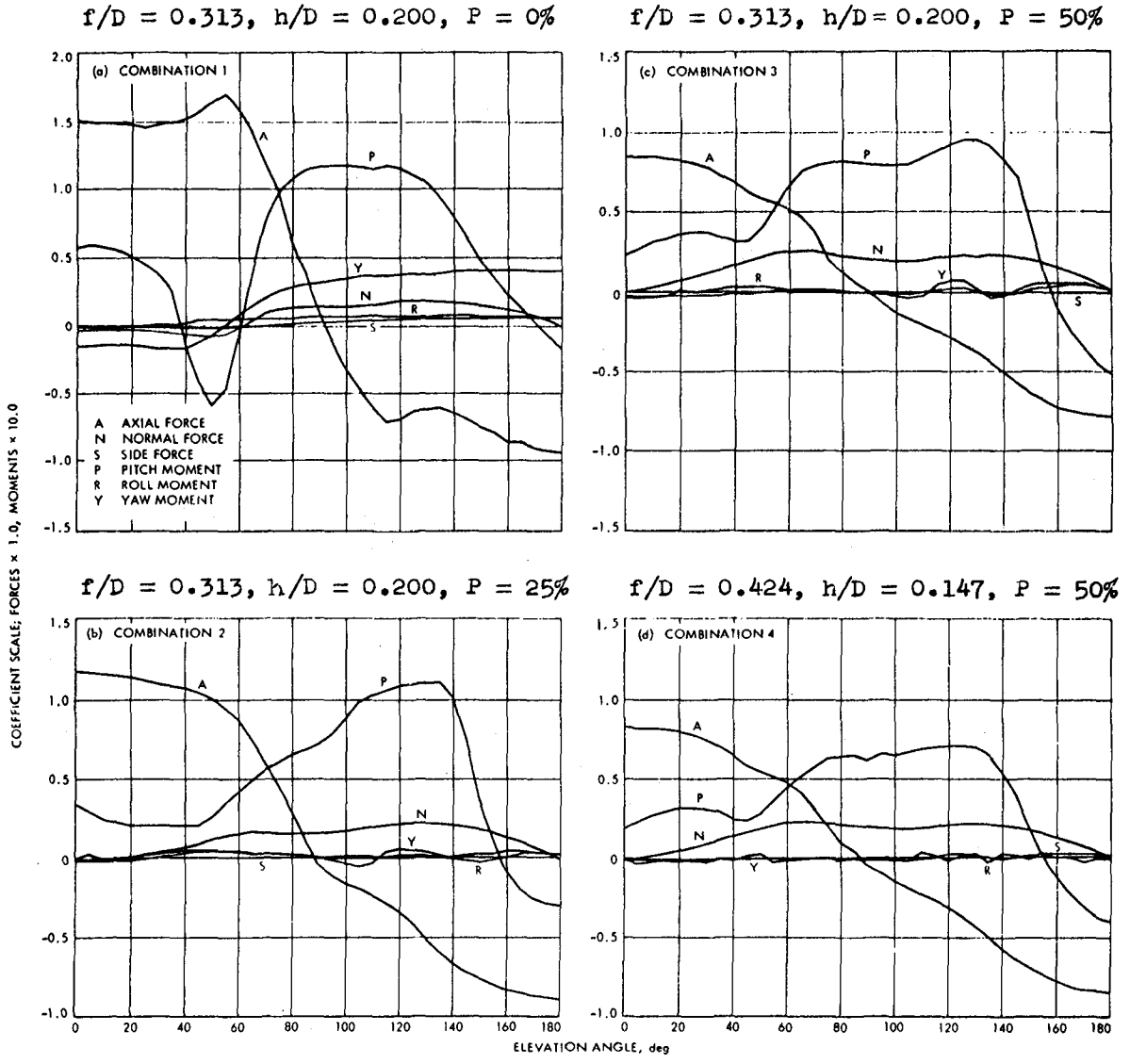

Figure 39. Coefficient Curves for 0-deg Azimuth (From Ref. 72)

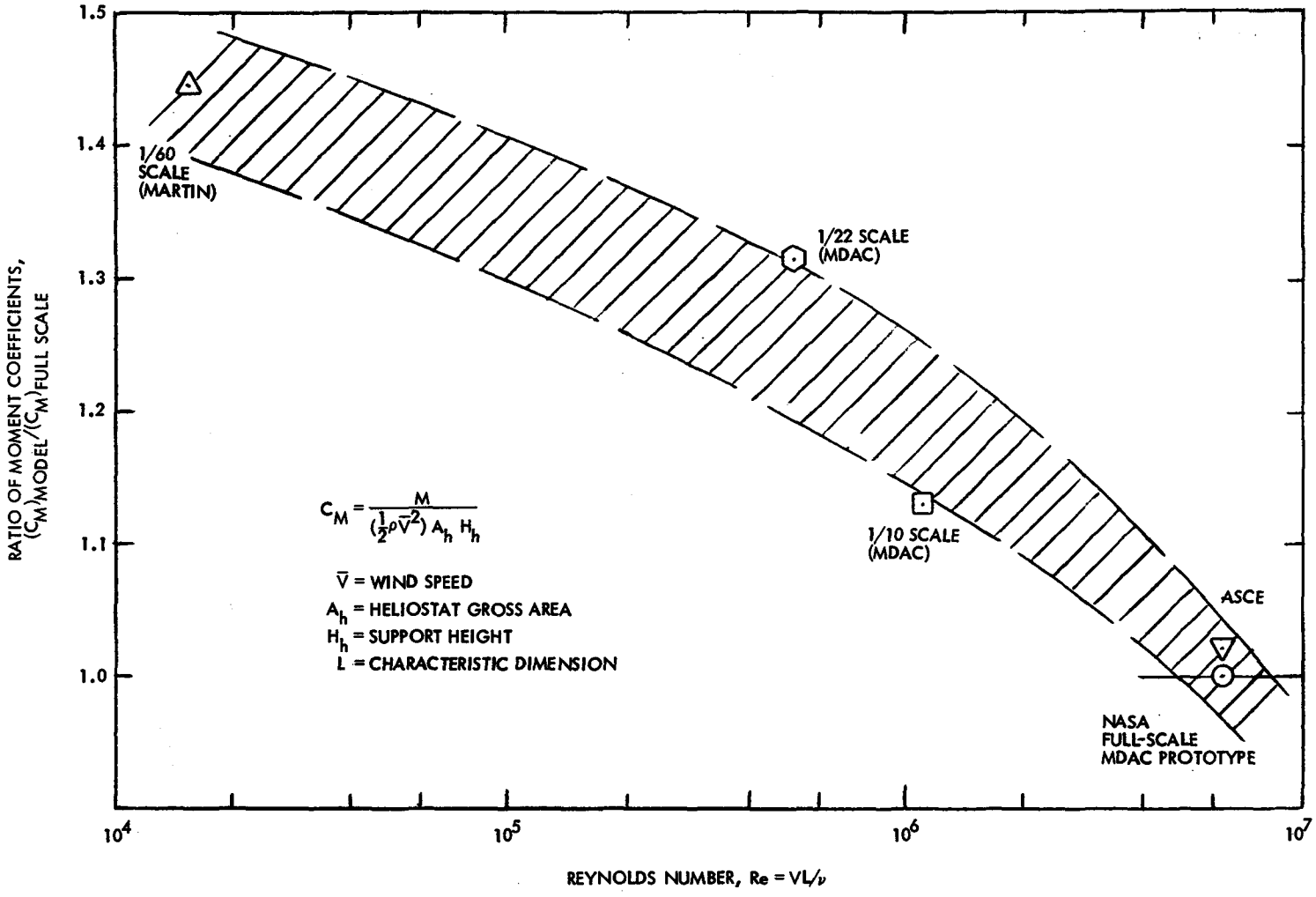

Figure 40. Wind Tunnel Heliostat Tests - Effects of Scale Size
(Based on Data in Ref. 62)

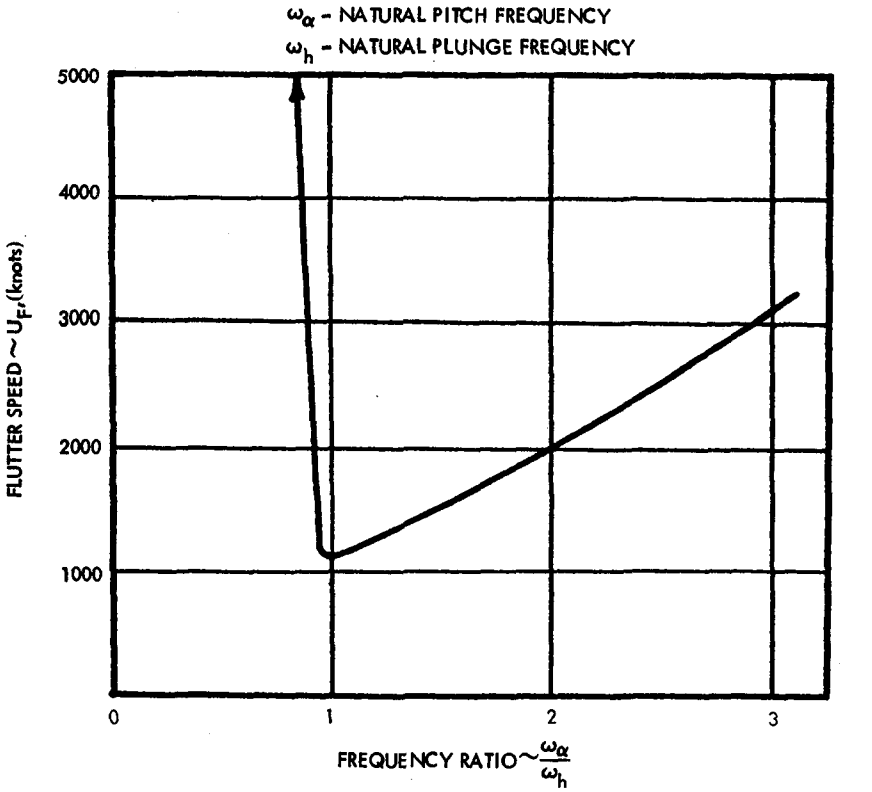

a. FLUTTER SPEED vs FREQUENCY RATIO

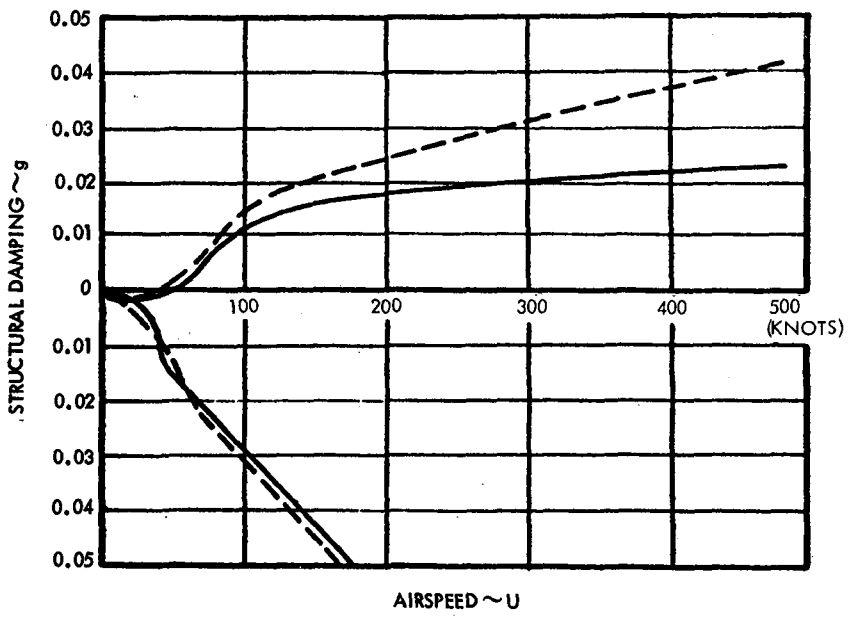

b. STRUCTURAL DAMPING FACTORS FOR BENDING AND PITCH MODES vs AIRSPEED

Figure 41. Example of Theoretical Flutter Analysis for a 30-ft-dia Paraboloidal Antenna (Adapted from Ref. 83)

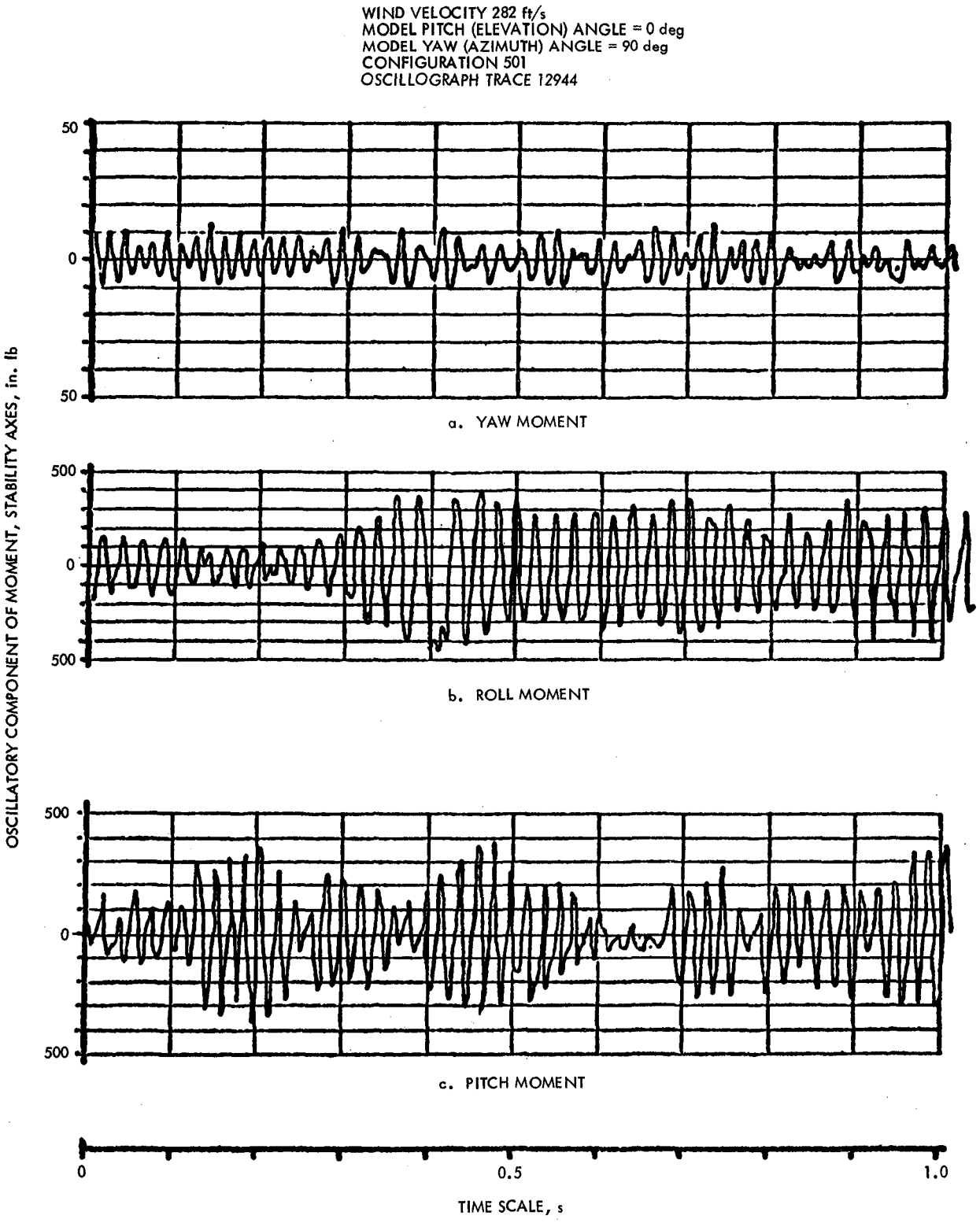

Figure 42. Wind-Induced Vibrations of an Antenna Model: Samples of Time-Dependent Moment Amplitudes (From Ref. 92)

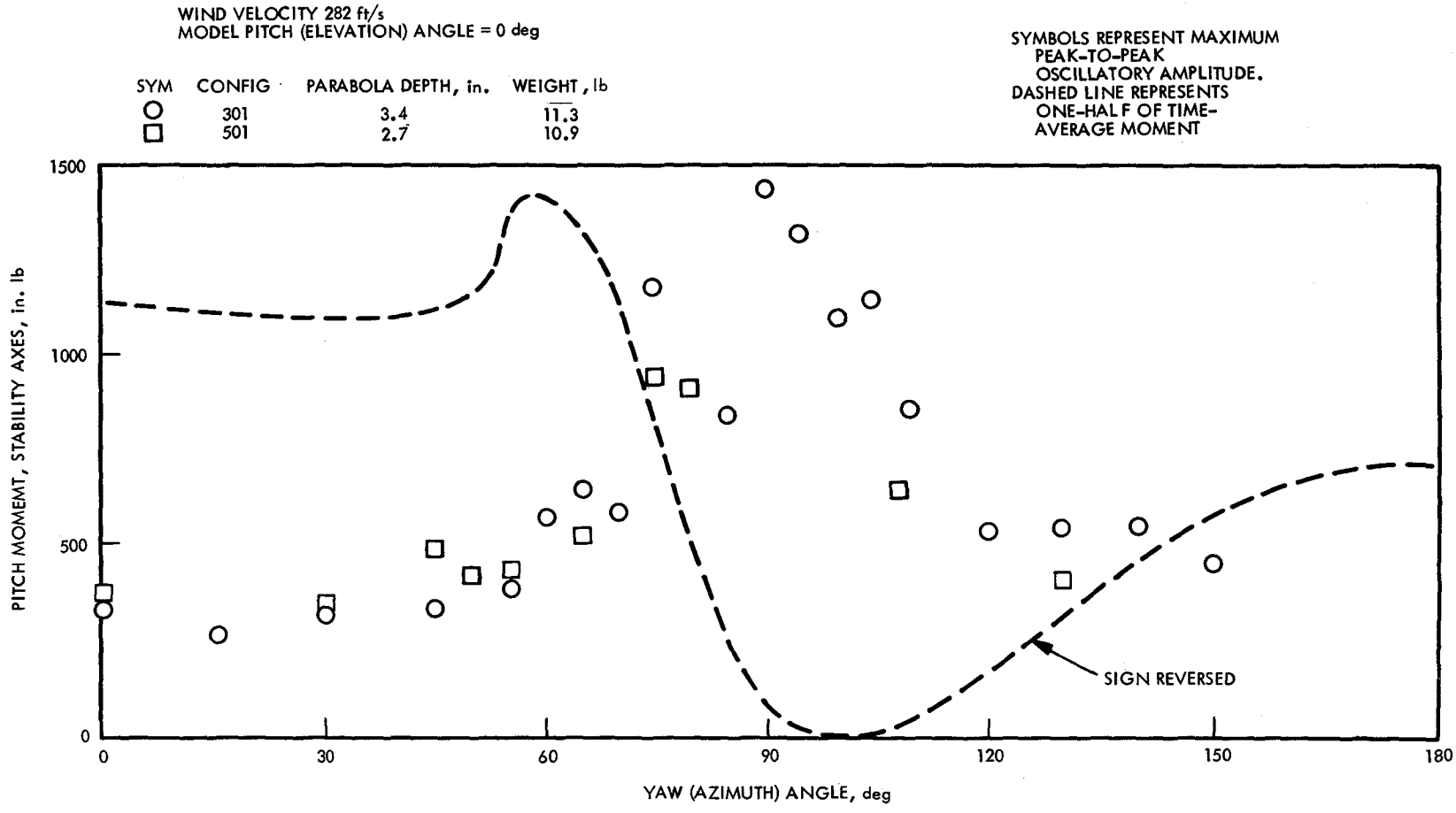

Figure 43. Comparison of Oscillatory to Steady Pitch Moment Amplitude (Adapted from Ref. 92)

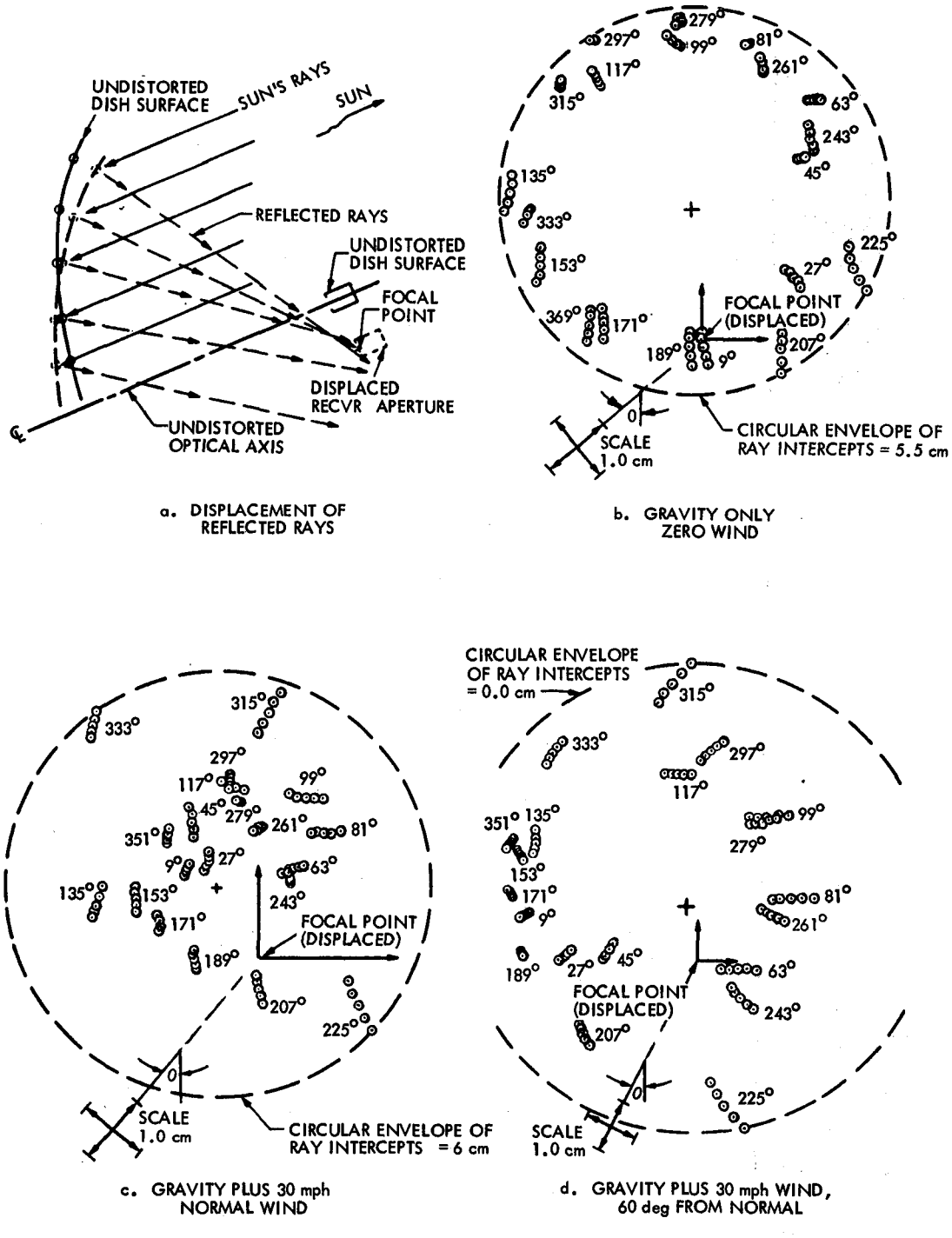

Figure 44. Theoretical Displacement of Ray Intercepts and Focal Points Due to Structural Deformation, Paraboloidal Concentrator Under Gravity and Wind Loads Facing the Horizon (From Ref. 93)

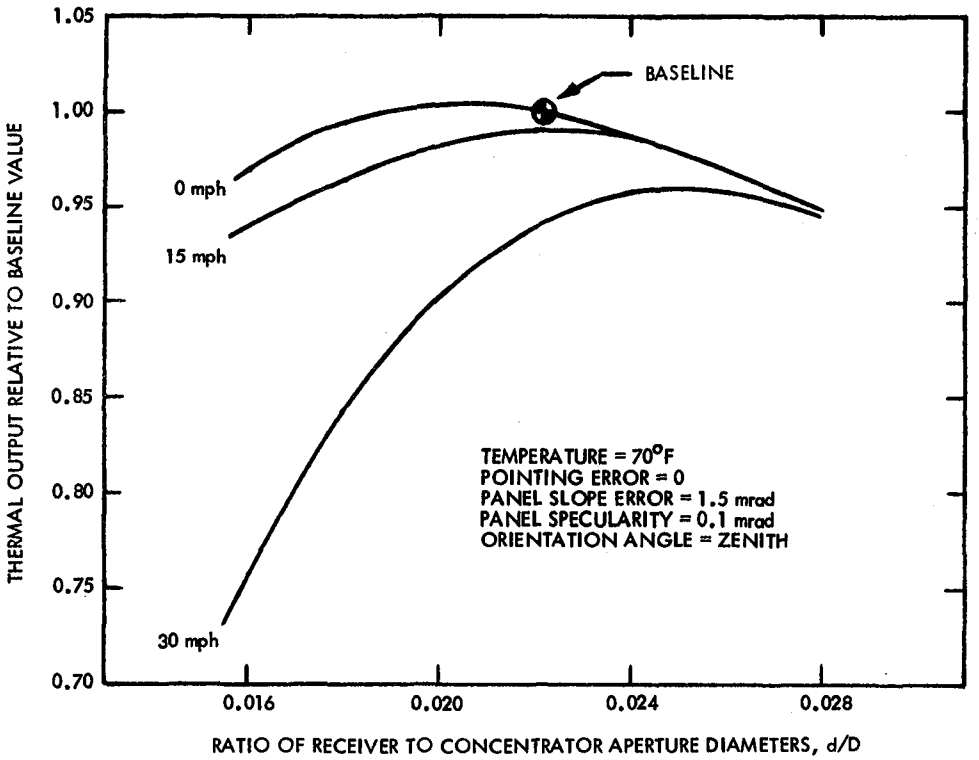

Figure 45. Effect of Wind Speed on Thermal Performance of Acurex Concentrator/Receiver Design (From Ref. 95)

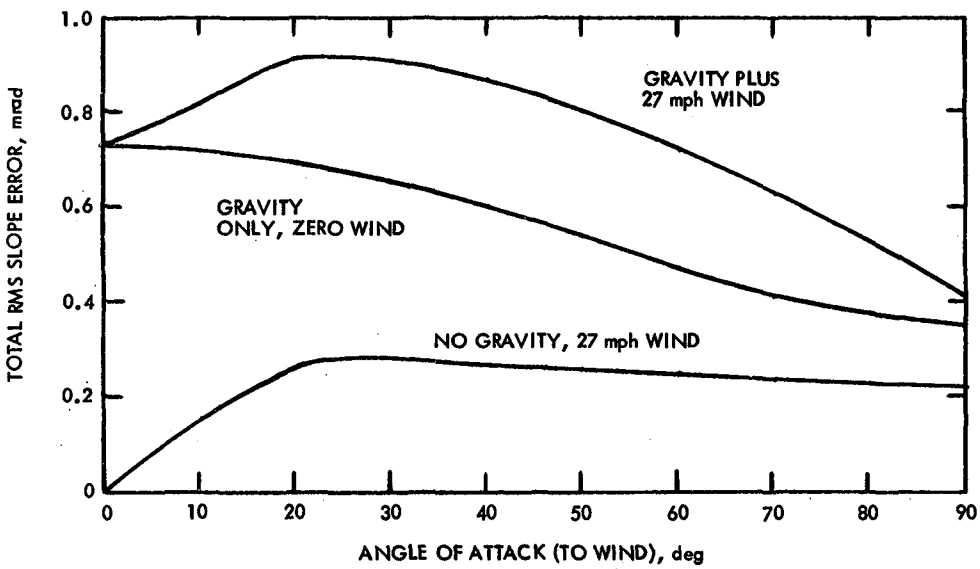

Figure 46. Contribution of Gravity and Wind Loads to Calculated Surface Slope Error for a Second-Generation Heliostat Design (Based on Data in Ref. 65)

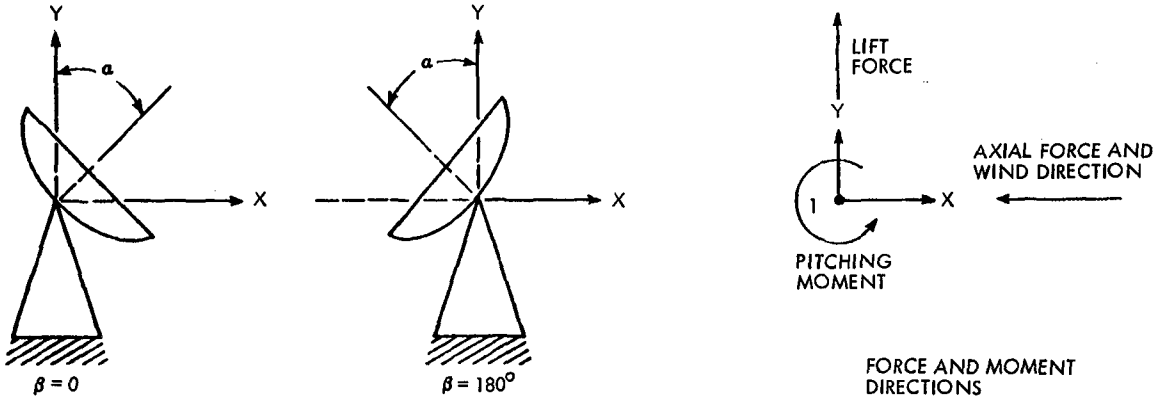

Figure 47. Definition of Geometry and Coordinates Used in Table 9 (From Ref. 66)

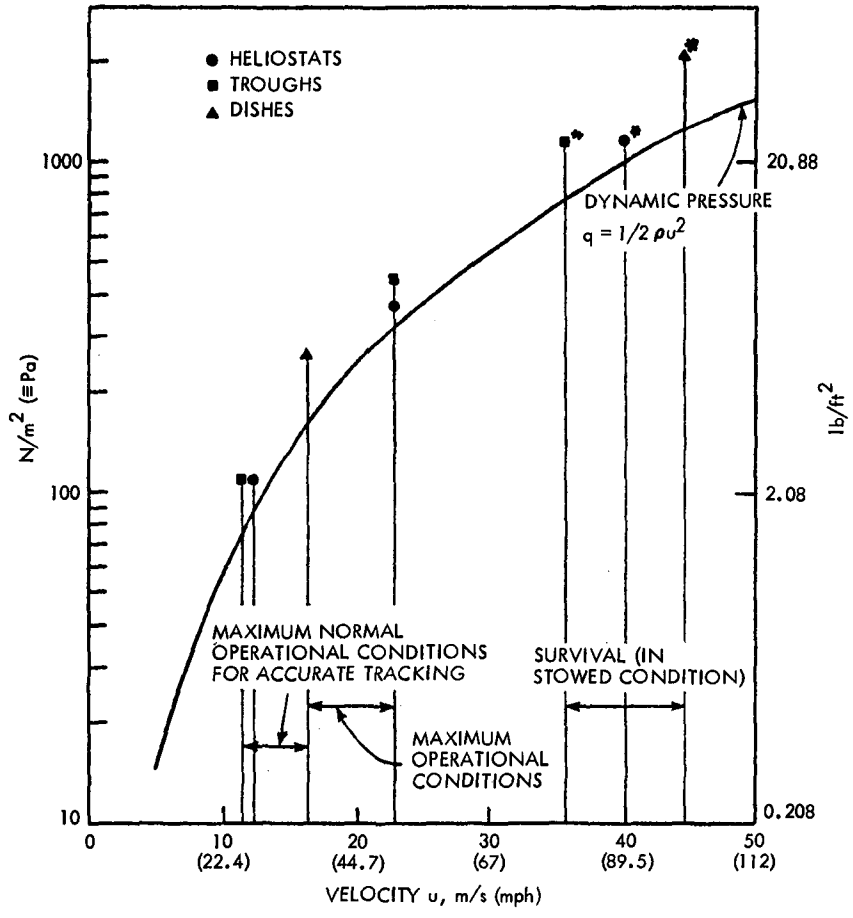

THESE LEVELS ARE SHOWN FOR COMPARATIVE PURPOSES ONLY AND SHOULD NOT BE REACHED IN PRACTICE. IN THE STOWED CONFIGURATION THE LOAD NORMAL TO THE COLLECTOR SURFACE SHOULD BE MUCH LOWER.

Figure 48. Maximum Drag Per Unit Area, qC_D, vs Wind Speed Showing Typical Collector Design Criteria (Drag Coefficients) from Table 9 (From Ref. 66)

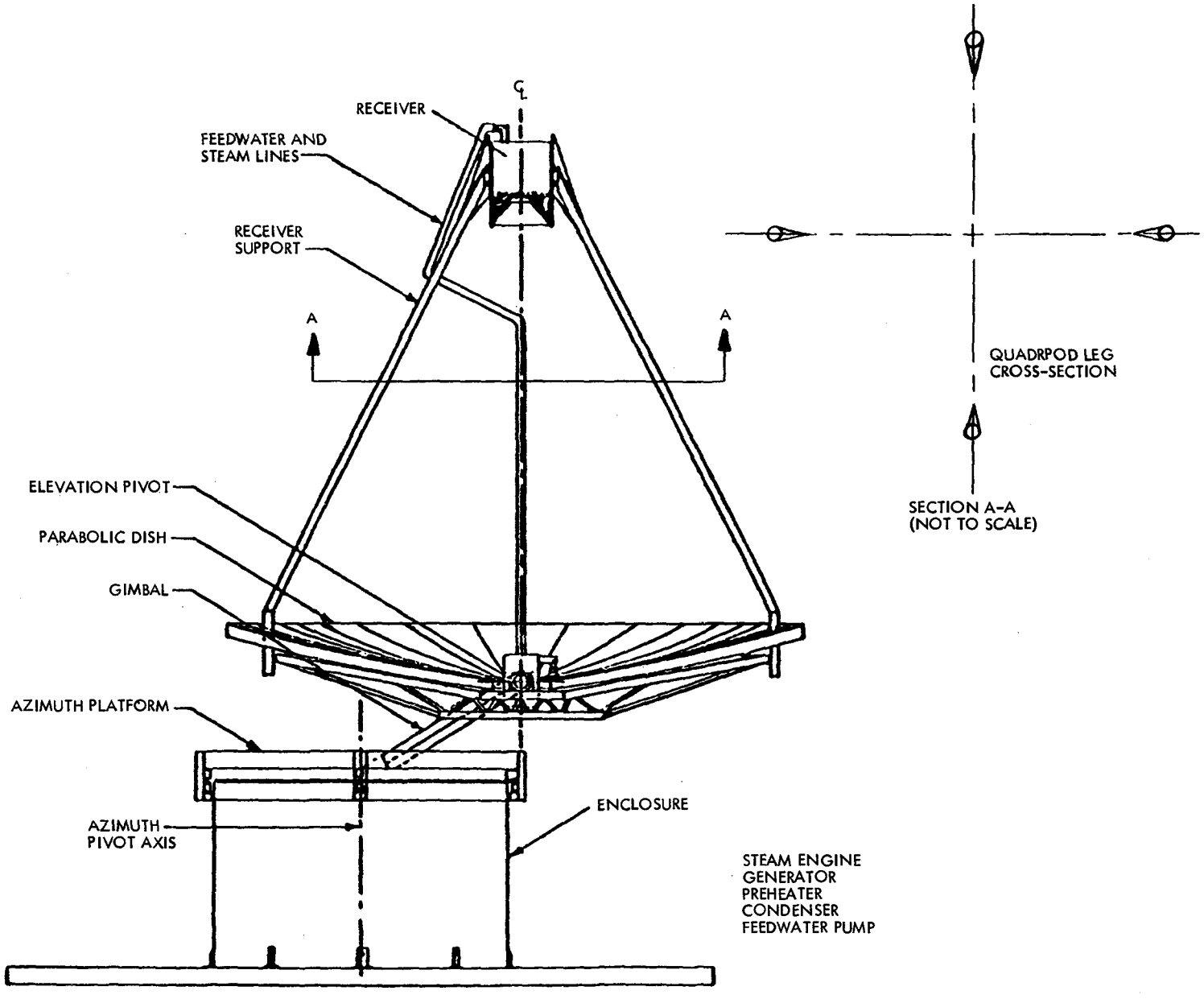

Figure 49. Omnium-G Module, Quadripod Leg Cross-Section Detail

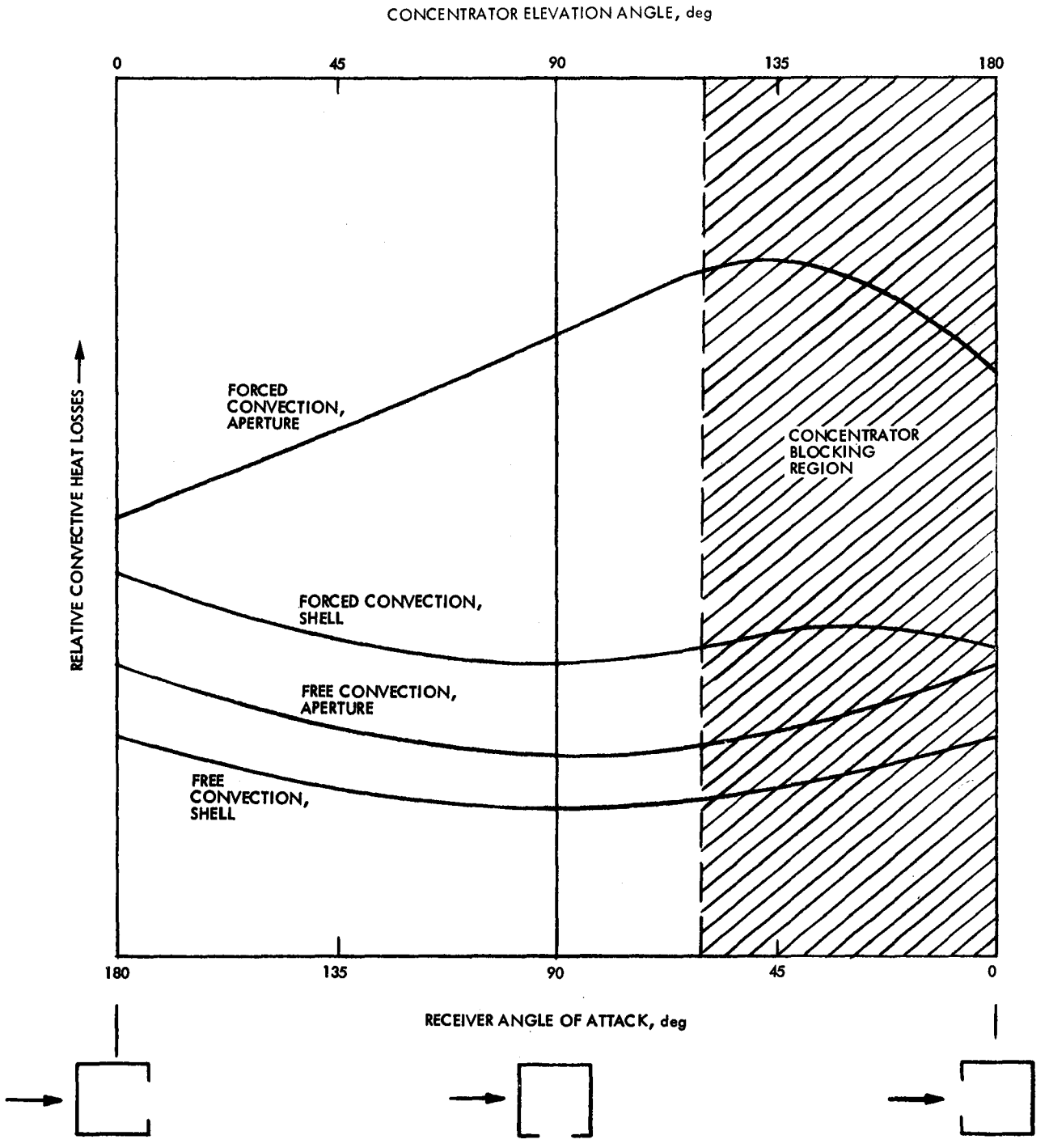

Figure 50. Relative Convective Heat Transfer Losses Conjectured for Cavity Thermal Receivers

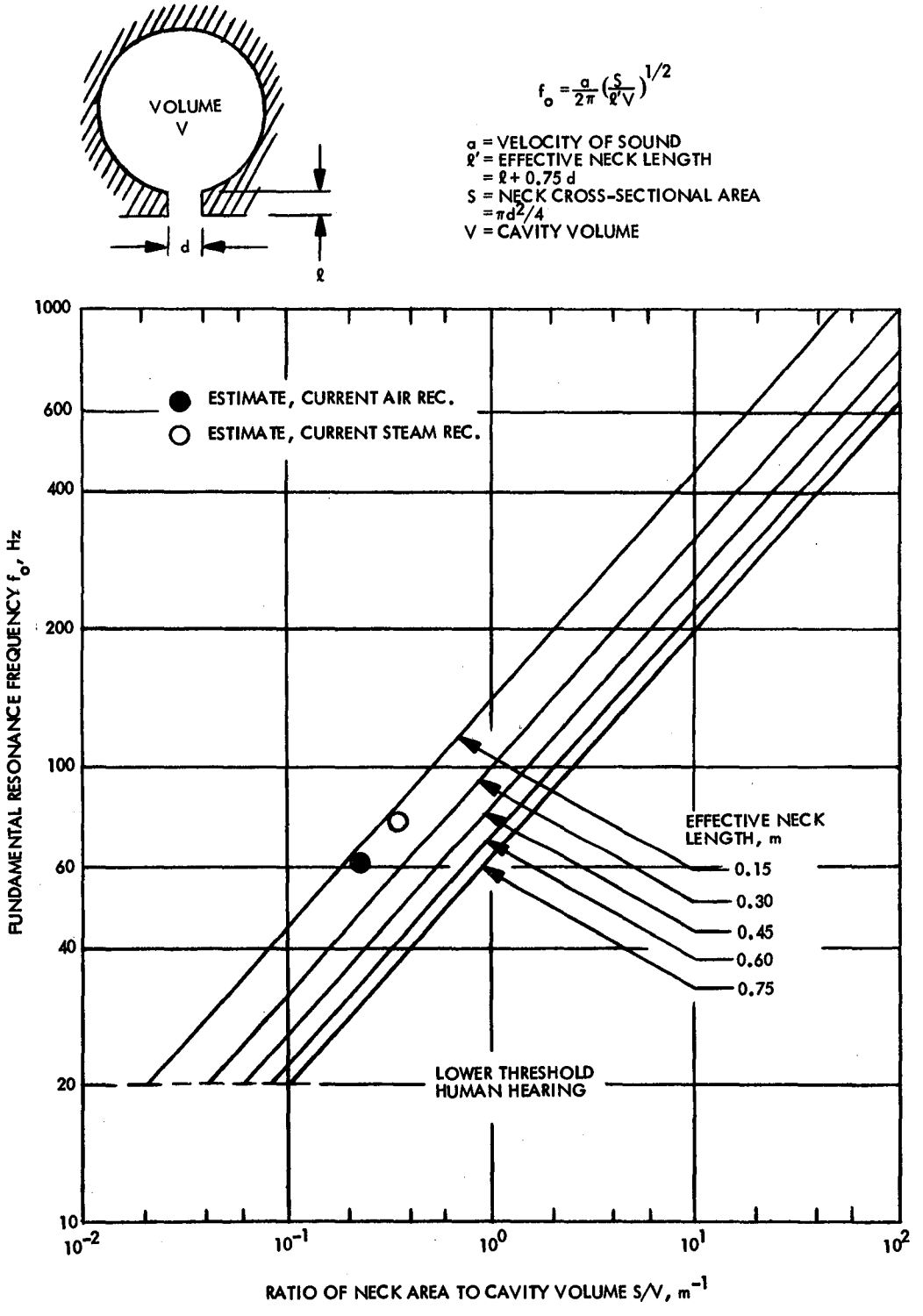

Figure 51. Theoretical Fundamental Frequency of Short-Neck Cavity Helmholtz Resonators

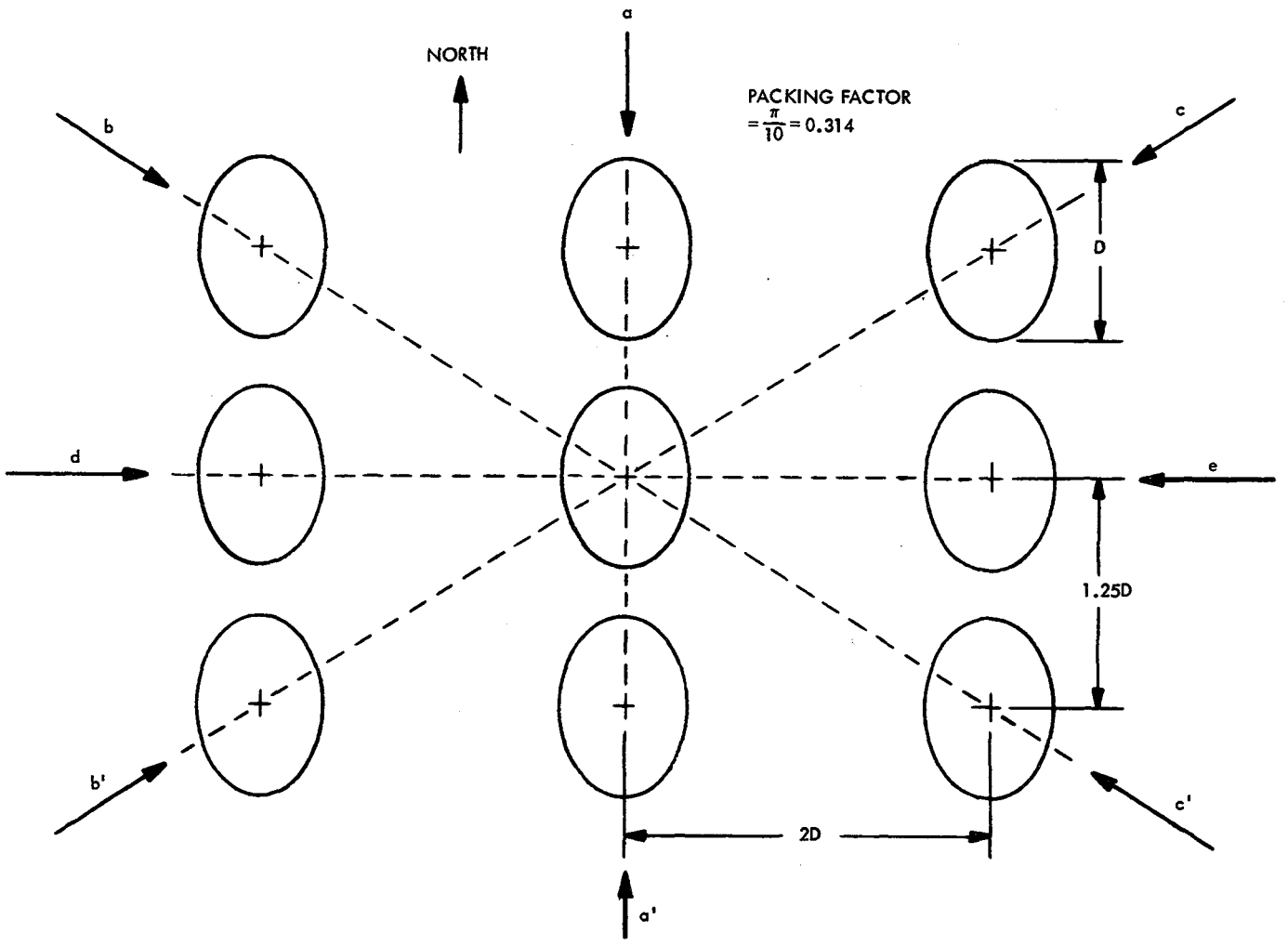

Figure 52. Portion of a Typical Rectangular Array with Dishes Facing West at an Elevation Angle of 45 deg. Varying Wake and Mutual Interactive Effects Depend on Mean Wind Speed and Direction (Labeled Arrows)

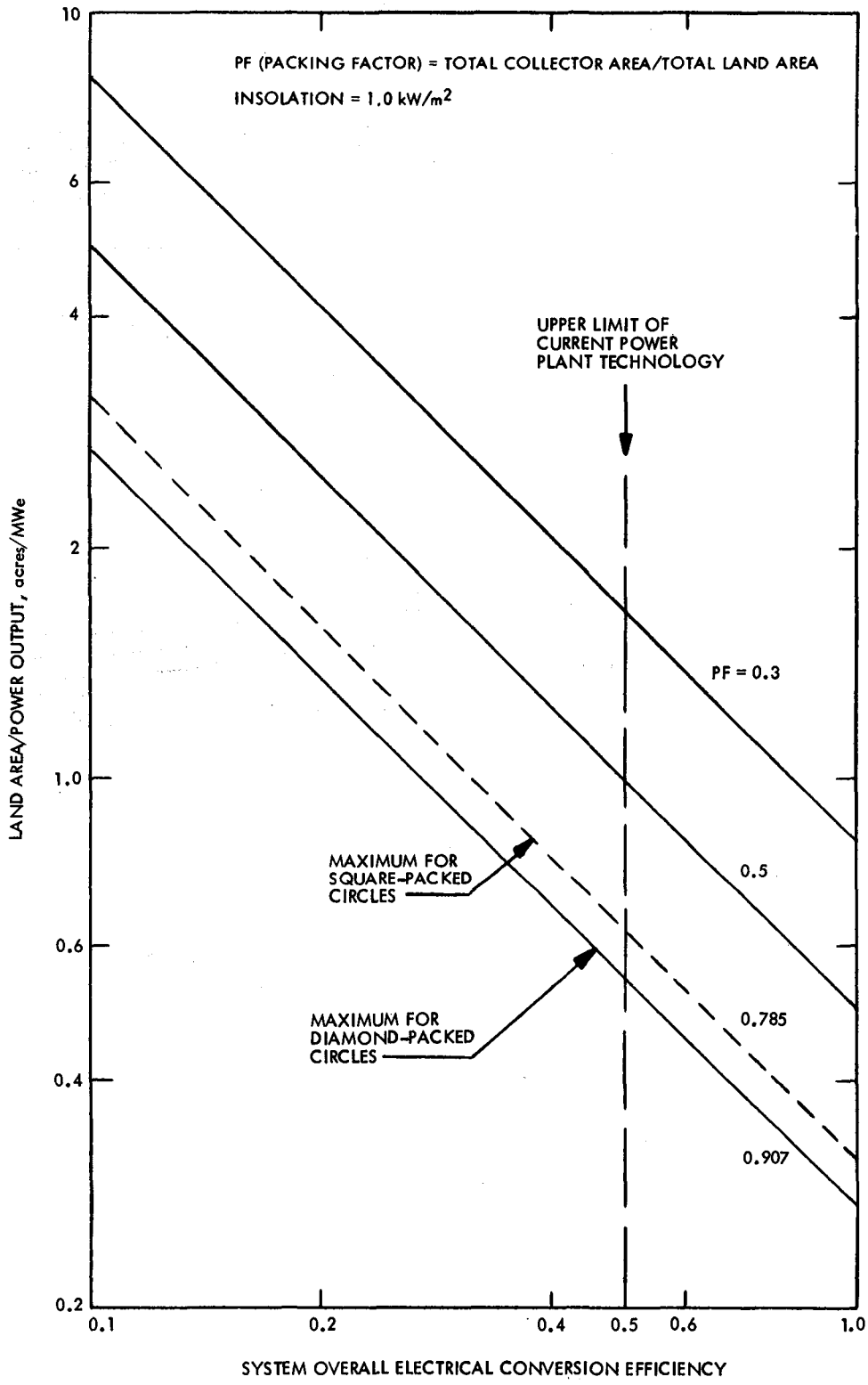

Figure 53. Land/Power Ratio vs System Conversion Efficiency for Various Packing Factors

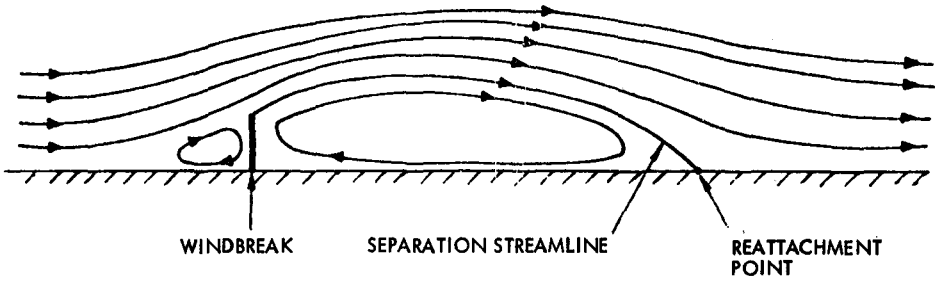

a. SOLID WINDBREAK

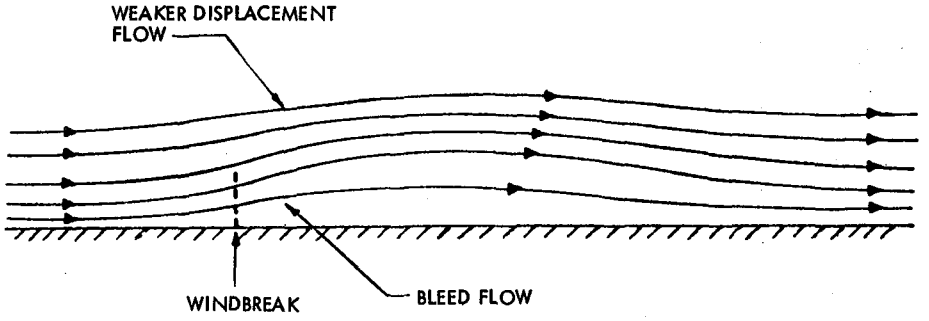

b. MODERATELY PERMEABLE WINDBREAK

Figure 54. Streamline Patterns for Flow Over Solid and Permeable Wind Breaks (Adapted from Ref. 130)

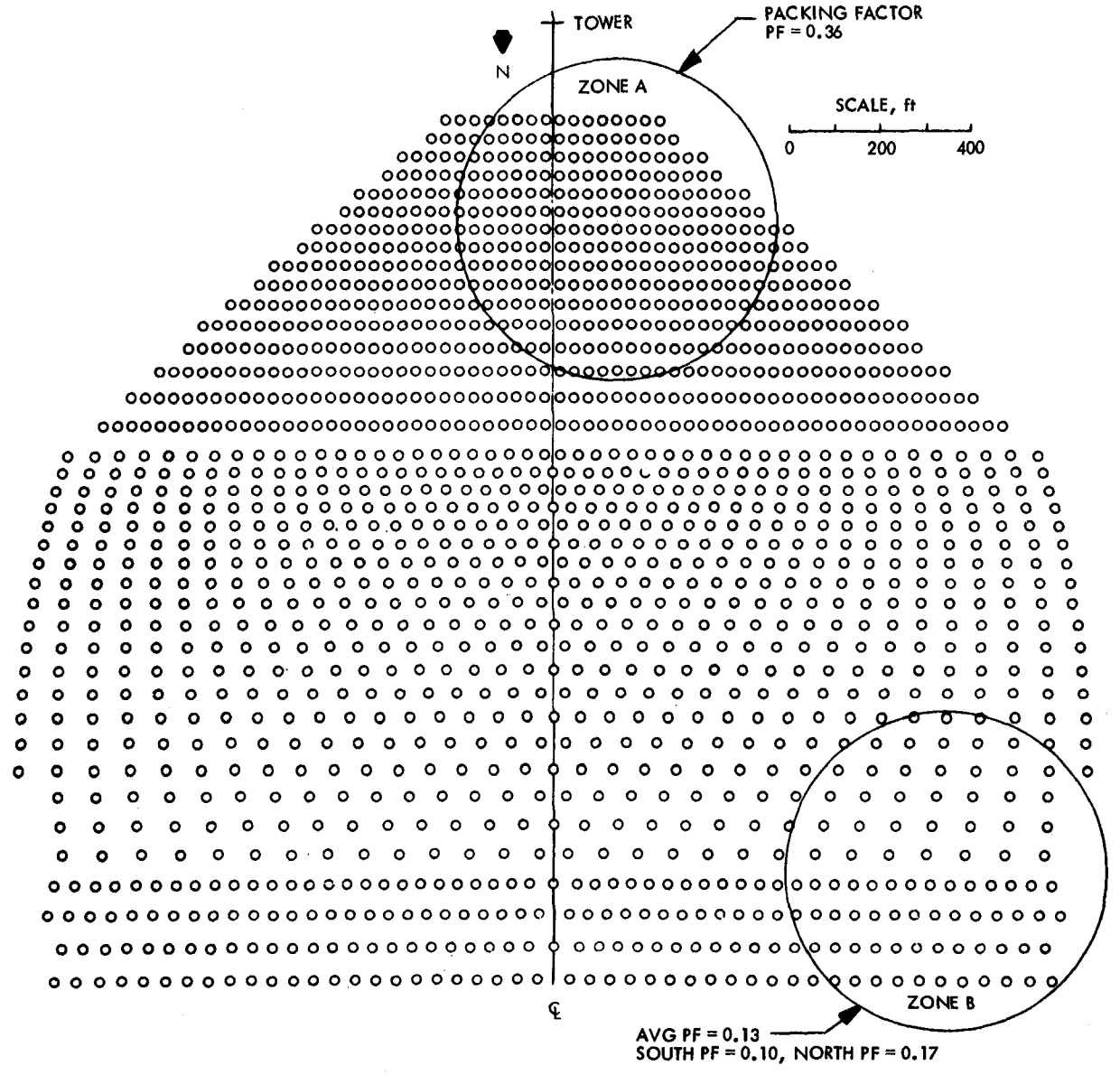

Figure 55. Central Tower Heliostat Field Array Showing Zones Selected for Model Wind Tunnel Testing (From Ref. 60)

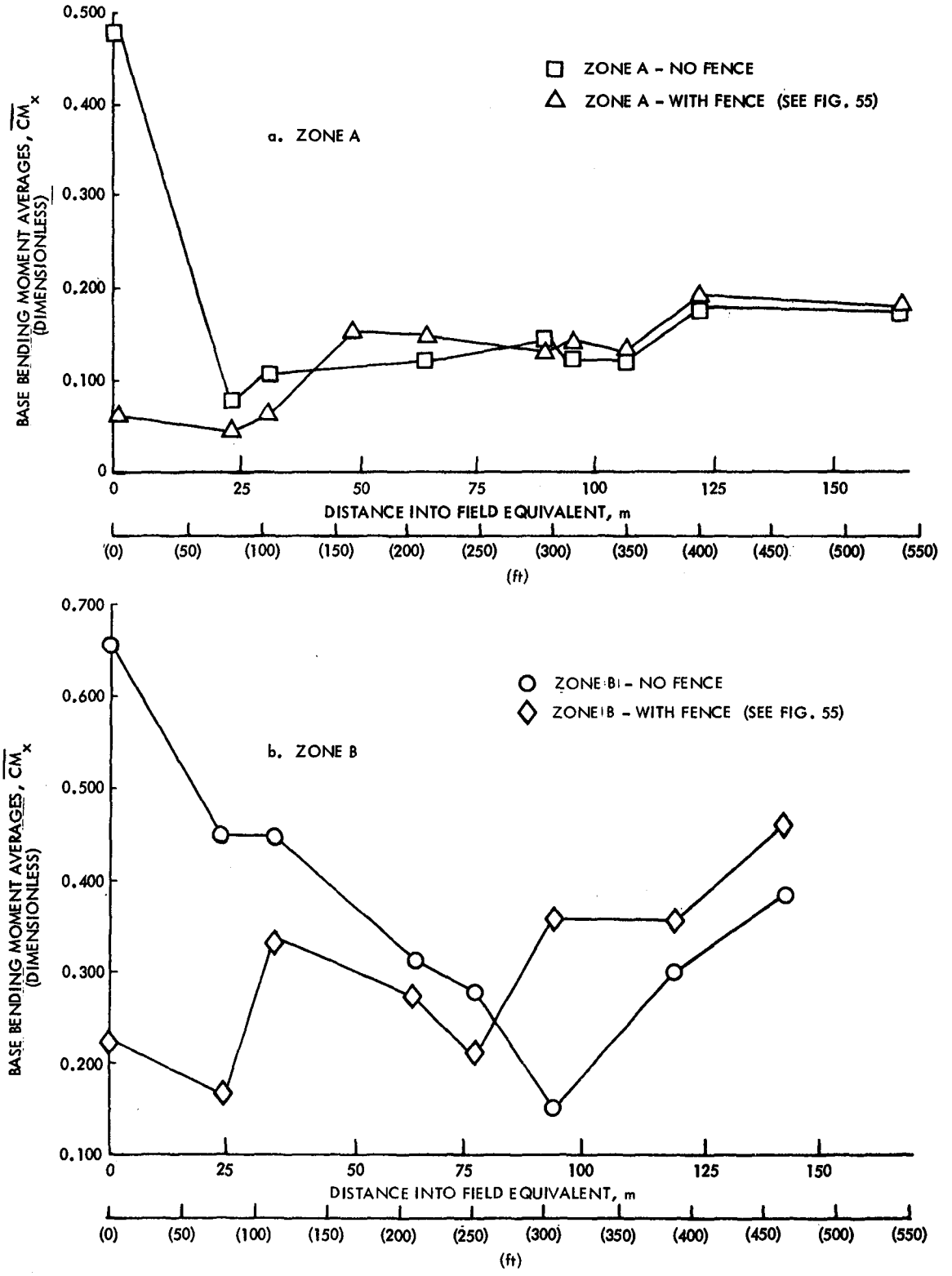

Figure 56. Wind Tunnel Results for Model Heliostat Array. Base Bending Moments (Averaged) vs Distance into the Field, With and Without Perimeter Fences (Wind Breaks) (From Ref. 60)

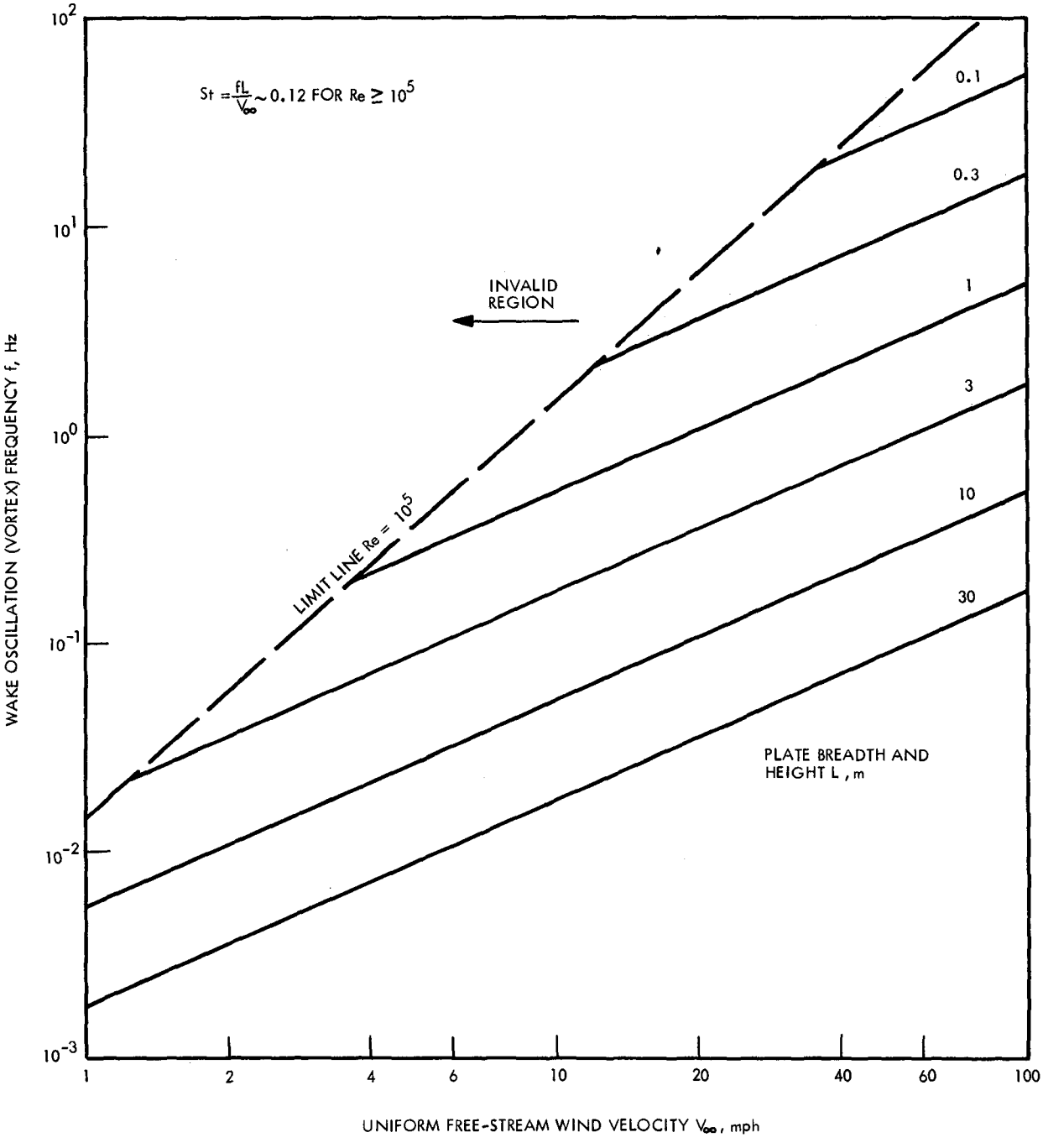

Figure 57. Variation of Wake Oscillation Frequency with Wind Speed and Plate Dimension for a Square Plate Facing Directly into a Uniform Airstream (Based on Data in Ref. 134)

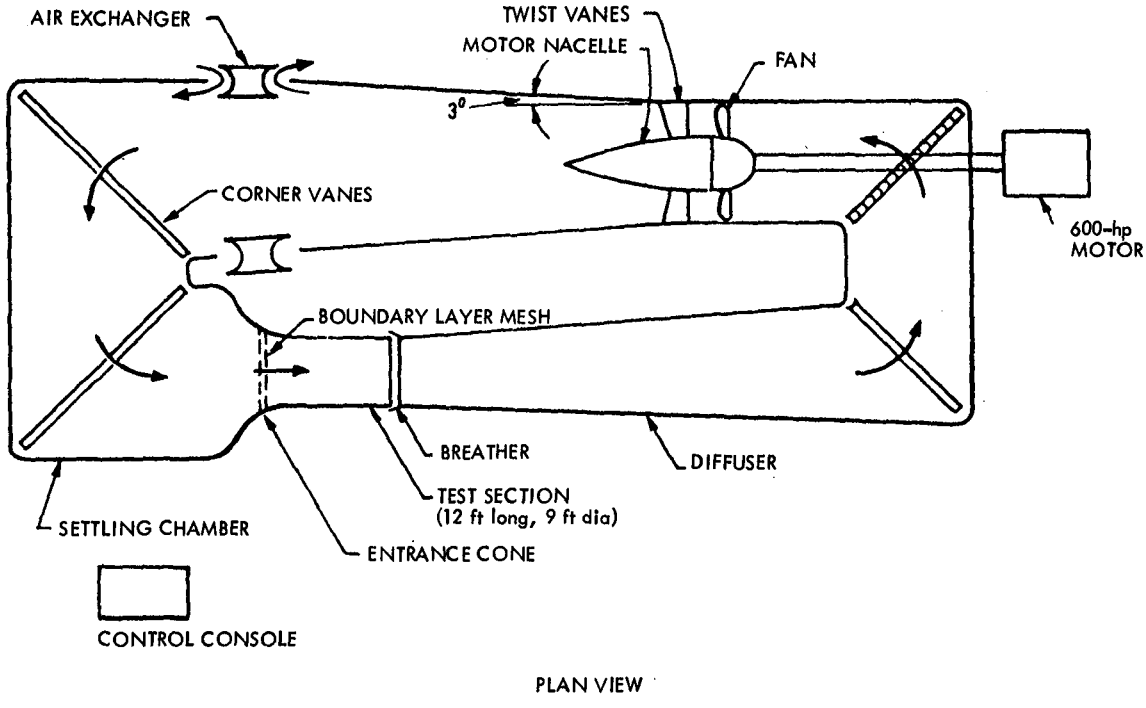

Figure 58. Georgia Institute of Technology Single Return, Subsonic Wind Tunnel, Used for Honeywell Heliostat Array Tests (From Ref. 58)

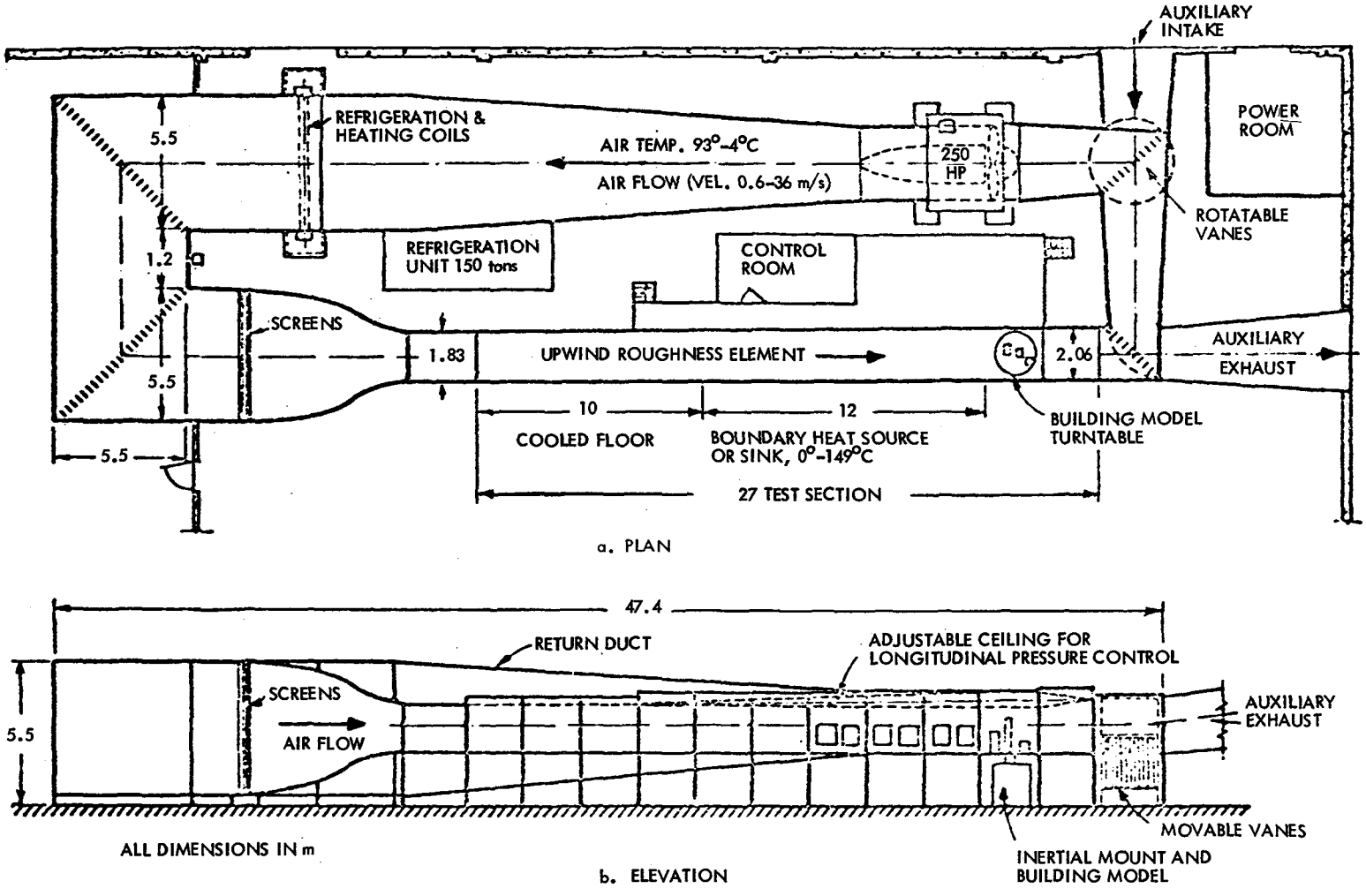

Figure 59. Meteorological Wind Tunnel (Completed in 1963), Fluid Dynamics and Diffusion Laboratory, Colorado State University (Adapted from Ref. 59)

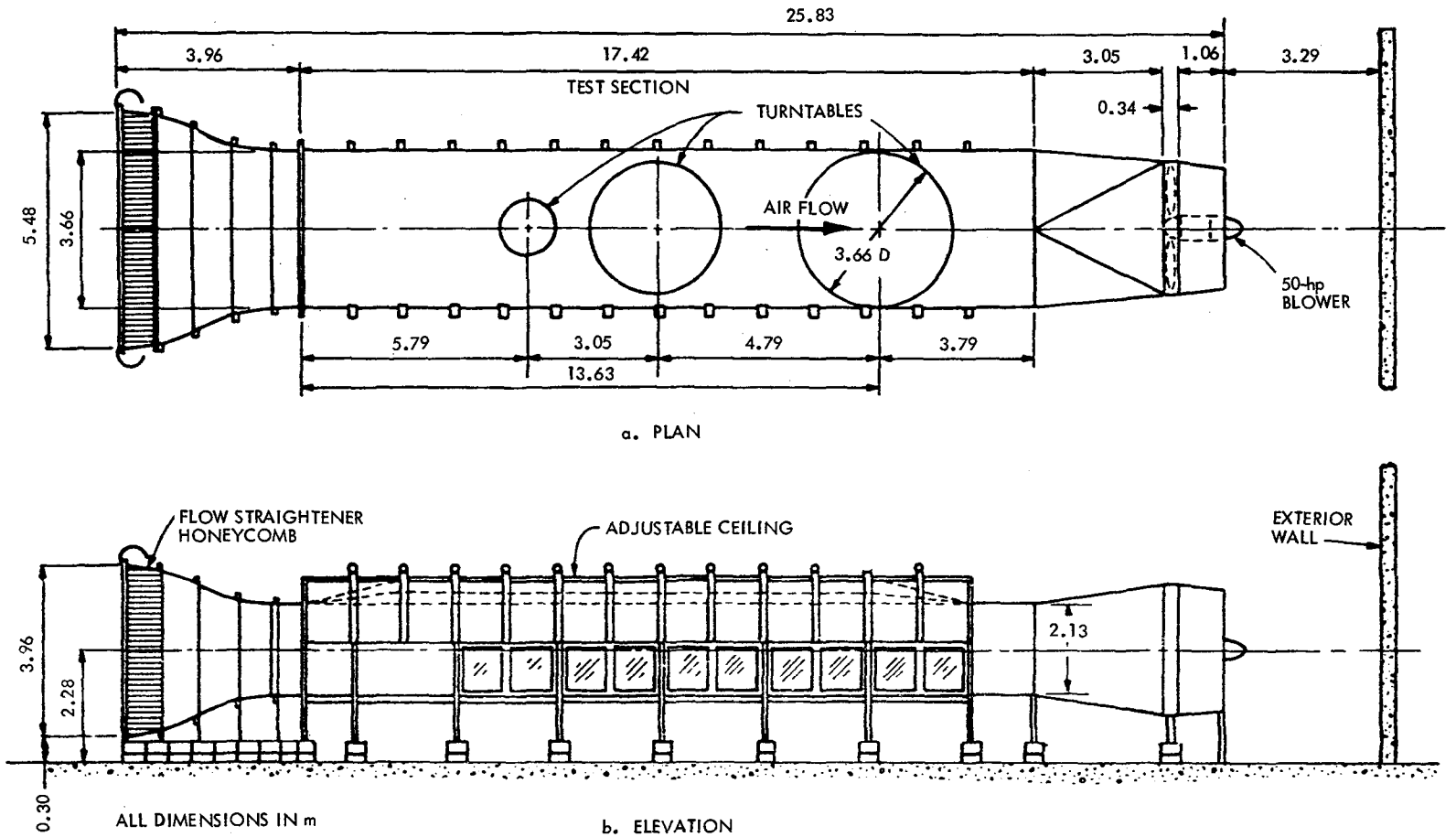

Figure 60. Environmental Wind Tunnel, Colorado State University (From Ref. 60)

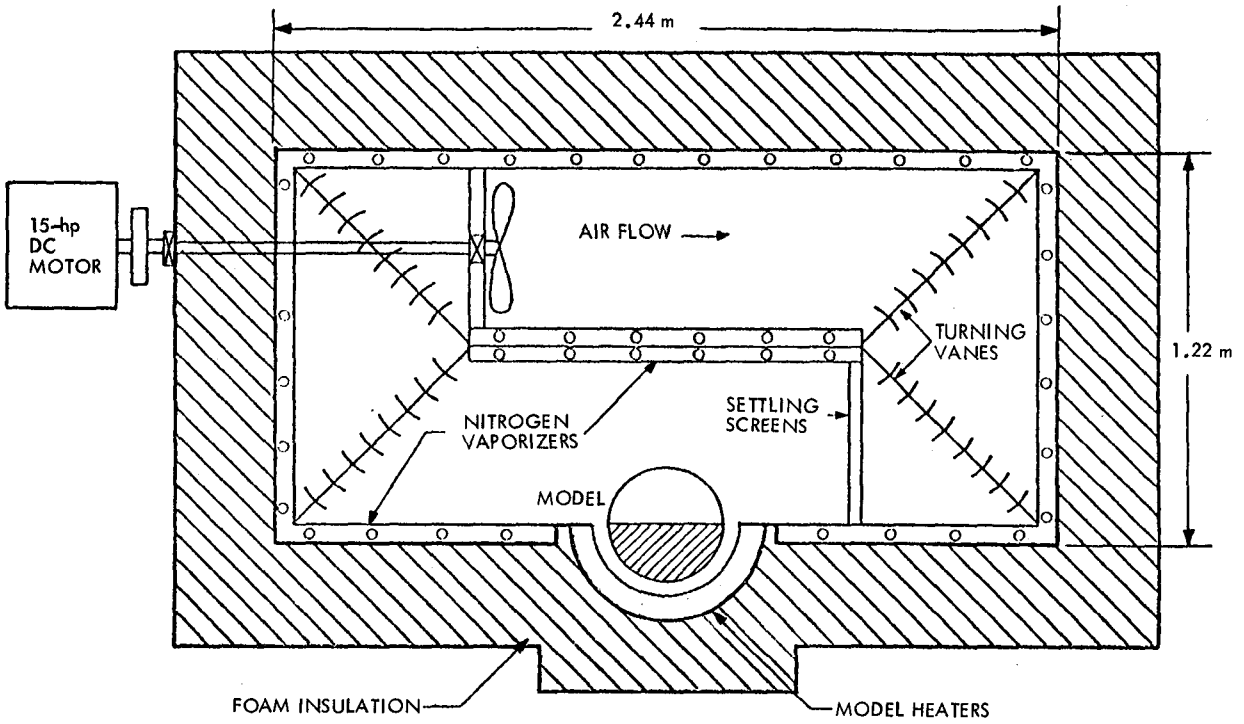

a. PLAN VIEW

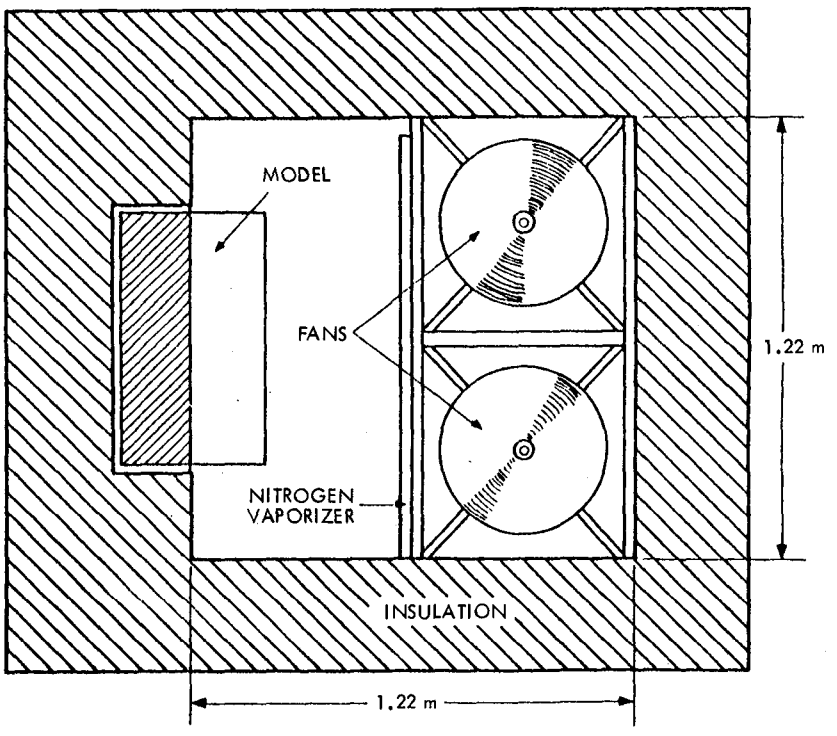

b. END VIEW

Figure 61. University of Illinois Cryogenic Wind Tunnel for Heat Transfer Experiments at High Reynolds and Grashof Numbers (From Ref. 104)

SECTION XIV

REFERENCES

1. Roschke, E.J., Wen, L., Steele, H., El Gabalawi, N., and Wang, J., A Preliminary Assessment of Small Steam Rankine and Brayton Point-Focusing Solar Modules, DOE/JPL-1060-16, JPL Publication 79-21, Jet Propulsion Laboratory, Pasadena, Calif., March 1, 1979.

2. Steinman, D.B., "Suspension Bridges: The Aerodynamic Problem and Its Solution," American Scientist, Vol. 42, pp. 397-429, 1954.

3. Whipple, H.E. (editor), "Large Steerable Radio Antennas - Climatological and Aerodynamic Considerations," Annals, New York Academy of Sciences, Vol. 116, pp. 1-355, 1964.

4. Goldstone DSCC: A Part of the Worldwide Deep Space Network, NASA Brochure, JPL Publication 400-27, Jet Propulsion Laboratory, Pasadena, Calif., September 1979.

5. Blaylock, R.B., Dayman, B., Fox, N.L., "Wind Tunnel Testing of Antenna Models," Annals, New York Academy of Sciences, Vol. 116, pp. 239-272, 1964. (A summary of Refs. 13 and 70.)

6. Rothman, H., "The Impact of Climatological Effects on the Structural Design" (of large antennas), Annals, New York Academy of Sciences, Vol. 116, pp. 324-335, 1964.

7. Humphrey, A.T., and Sunley, V.K., "Analysis of Deflection in Reflecting Surfaces of Communication Aerials," Marconi Review, Vol. 31, pp. 79-96, 1968.

8. Korolev, V.M., et al, "Thermal Deformations of Solar-Energy Concentrators," Geliotekhnika (Applied Solar Energy), Vol. 14, pp. 13-19, 1978.

9. Cermak, J.E., "Applications of Fluid Mechanics to Wind Engineering - A Freeman Scholar Lecture," Trans. ASME, J. of Fluids Engineering, Vol. 97, pp. 9-38, 1975.

10. Department of Energy (DOE) Solar Thermal Central Power Systems Semiannual Review, San Diego, California, March 2-3, 1978. See Report No. SAND 78-8015, pp. 135-136, April 1978.

11. Davenport, A.G., "Rationale for Determining Design Wind Velocities," Proc. ASCE, J. of the Structural Division, Vol. 86, pp. 39-68, 1960.

12. Panofsky, H.A., "The Atmospheric Boundary Layer Below 150 Meters," Annual Review of Fluid Mechanics, Van Dyke, M., Vincenti, W.G., and Wehausen, J.V., (editors), Vol. 6, pp. 147-177, Annual Review, Inc., Palo Alto, California, 1974.

13. Blaylock, R.B., "Aerodynamic Coefficients for a Model of a Paraboloidal-Reflector Directional Antenna Proposed for a JPL Advanced Antenna System," Internal Memorandum CP-6, Jet Propulsion Laboratory, Pasadena, California, May 1964.

14. Blackadar, A.K., "Wind Velocity Profiles," Annals, New York Academy of Sciences, Vol. 116, pp. 101-115, 1974.

15. Levy, R., and McGinness, H., "Wind Power Prediction Models," Technical Memorandum 33-802, Jet Propulsion Laboratory, Pasadena, California, November 1976.

16. Hoerner, S.F., Fluid-Dynamic Drag, book published and copyrighted by the author, Midland Park, New Jersey, 1958. (See Chapter III, Pressure Drag, and Chapter IV, Wind Forces on Structures.)

17. Barnaud, C., and Gandemer, J., "Dynamic Simulation of the Atmospheric Boundary Layer at Model Scale of 1/250," J. of Industrial Aerodynamics, Vol. 4, pp. 35-41, 1979.

18. Smeda, M.S., "A Bulk Model for the Atmospheric Planetary Boundary Layer," Boundary-Layer Meteorology, Vol. 17, pp. 411-427, 1979.

19. Singer, I.A., "Wind Gust Spectra," Annals, New York Academy of Sciences, Vol. 116, pp. 116-133, 1964.

20. Hsu, S.A., "Mesoscale Nocturnal Jetlike Winds within the Planetary Boundary Layer over a Flat, Open Coast," Boundary-Layer Meteorology, Vol. 17, pp. 485-494, 1979.

21. Davenport, A.G., "The Spectrum of Horizontal Gustiness Near the Ground in High Winds," Quart. J. Royal Meteorological Society, Vol. 87, pp. 184-211, 1961.

22. Davenport, A.G., "The Buffeting of Large Superficial Structures by Atmospheric Turbulence," Annals, New York Academy of Sciences, Vol. 116, pp. 135-159, 1964.

23. Flint, A.R., and Smith, B.W., "The Development of the British Draft Code of Practice for the Loading of Lattice Towers," Proc. Fifth International Conference on Wind Engineering, Cermak, J.E., (editor), Vol. II, pp. X-4-1, Pergamon Press, July 1979.

24. Burnham, J., and Colmer, J.J., "On Large and Rapid Wind Fluctuations which occur when the Wind had previously been Relatively Light," Ministry of Aviation Supply, Aeronautical Research Council Paper No. 1158, London, 1971.

25. Fujita, T., El Gabalawi, N., Herrera, G., and Turner, R.H., Projection of Distributed Collector Solar-Thermal Electric Power Plant Economics to Years 1990-2000, DOE/JPL-1060-77/1, JPL Publication 77-79, Jet Propulsion Laboratory, Pasadena, Calif., December 1977.

26. Fujita, T., Manvi, R., Roschke, E.J., El Gabalawi, N., Herrera, G., Kuo, T.J., and Chen, K.H., Techno-Economic Projections for Advanced Small Solar Thermal Electric Power Plants to Years 1990-2000, DOE/JPL-1060-4, JPL Publication 79-25, Jet Propulsion Laboratory, Pasadena, California, November 15, 1978.

27. Latta, A.F., Bowyer, J.M., Fujita, T., and Richter, P.H., The Effects of Regional Insolation Differences Upon Advanced Solar Thermal Electric Power Plant Performance and Energy Cost, DOE/JPL-1060-17, JPL Publication 79-39, Jet Propulsion Laboratory, Pasadena, Calif., March 15, 1979.

28. User's Manual for the U.S. Department of Energy Parabolic Dish Test Site, JPL Publication 5104-59, Jet Propulsion Laboratory, Pasadena, Calif., November 30, 1979. (See also Supplement to the User's Manual for the PDTS, JPL Internal Document, June 4, 1981.)

29. Randall, D.E., and Grandjean, N.R., Correlations of Insolation and Wind Data for SOLMET Stations, SAND 82-0094, Sandia Laboratories, Albuquerque, New Mexico, April 1982.

30. Bhumralkar, C.M., Mancuso, R.L., Ludwig, F.L., and Renne, D.S., "A Practical and Economic Method for Estimating Wind Characteristics at Potential Wind Energy Conversion Sites," Solar Energy, Vol. 25, pp. 55-65, 1980.

31. Dutton, J.A., Panofsky, H.A., Larko, D., Shier, H.N., Stone, G., and Vilardo, M., Statistics of Wind Fluctuations Over Complex Terrain, work performed by Pennsylvania State University for DOE, DOE/ET/20560-1, October 1979.

32. Meroney, R.N., Sandborn, V.A., Bouwmeester, R.J.B., Chien, H.C., and Rider, M., Sites for Wind-Power Installations: Physical Modeling of the Influence of Hills, Ridges, and Complex Terrain on Wind Speed and Turbulence, work performed by Colorado State University for DOE, RLO-243878/1, June 1978.

33. Hunt, J.C.R., and Snyder, W.H., "Experiments on Stably and Neutrally Stratified Flow over a Three-Dimensional Model Hill," J. Fluid Mechanics, Vol. 96, pp. 671-704, 1980.

34. Panofsky, H.A., Vilardo, M., and Lipschutz, R., "Terrain Effects on Wind Fluctuations," Proc. Fifth International Conference on Wind Engineering, Cermak, J.E. (editor), Vol. I, p. II-7-1, Pergamon Press, July 1979.

35. Measurements of Insolation Variation Over a Solar Collector Field, prepared by Aerospace Corp. for DOE under contract ET-78-C-03-2028, DOE Report No. ATR-79-(7747)-2, December 1978.

36. Akins, R.E., Wind Characteristics for Field Testing of Wind Energy Conversion Systems, SAND 78-1563, Sandia Laboratories, Albuquerque, New Mexico, November 1979.

37. Davenport, A.G., "The Application of Statistical Concepts to the Wind Loading of Structures," Proc. Institute of Civil Engineers, Vol. 19, pp. 449-471, 1961.

38. Thom, H.C.S., "Prediction of Design and Operating Wind Velocities for Large Steerable Radio Antennas," Annals, New York Academy of Sciences, Vol. 116, pp. 90-100, 1964.

39. Simiu, E., and Shaver, J.R., "Wind Loading and Reliability - Based Design," Proc. Fifth International Conference on Wind Engineering, Cermak, J.E. (editor), Vol. II, p. X-3-1, Pergamon Press, July 1979.

40. Building Code Requirements for Minimum Design Loads in Buildings and Other Structures, ANSI A58.1-1972, American National Standards Institute, New York, 1972.

41. Vellozi, J.W., and Cohen, E., "Gust Response Factors," Proc. ASCE, J. of the Structural Division, Vol. 94, pp. 1295-1313, 1968.

42. Davenport, A.G., "Gust Loading Factors," Proc. ASCE, J. of the Structural Division, Vol. 93, pp. 11-34, 1967.

43. Vickery, B.J., "On the Reliability of Gust Loading Factors," NBS Building Science Series 30, National Bureau of Standards, U.S. Dept. of Commerce, Washington, D.C., 1970.

44. Sachs, P., Wind Forces in Engineering, Second Edition, Pergamon Press, New York, 1978.

45. Holian, S., "Wind Data for Edwards Air Force Base," private communication, unpublished JPL memorandum, August 1978.

46. Mehta, K.C., "Wind Load Standards and Codes," Proc. Fifth International Conference on Wind Engineering, J. E. Cermak editor, Vol. II, p. X-5-1, Pergamon Press, July 1979.

47. Khatamov, S.O., Avezov, R.R., and Umarov, G.G., "Investigation of Aerodynamic Drag of Solar Air Heaters," Geliotekhnika (Applied Solar Energy), Vol. 15, pp. 48-54, 1979.

48. Hewitt, H.C., and Griggs, E.I., Wind Effects on Collectors, Final Report, DOE/CS/35364-T1, work performed by Tennessee Technological University for DOE, November 1979.

49. Tielman, H.W., Akins, R.E., and Sparks, P.R., An Investigation of Wind Loads on Solar Collectors, VPI-E-80-1, work performed by Virginia Polytechnic Institute and State University for National Bureau of Standards, January 1980.

50. Logan, E., and Barber, E.S., Effect of Lateral Spacing on Wake Characteristics of Buildings, NASA Contractor Report 3337, 1980.

51. Miller, R., and Zimmerman, D., Wind Loads on Flat Plate Photovoltaic Array Fields, DOE/JPL 954833-79/2, Jet Propulsion Laboratory, Pasadena, Calif., September 1979.

52. Weaver, R.W., "Wind Loads on Photovoltaic Arrays," Proc. 1980 Annual Meeting, International Solar Energy Society (American Section), Vol. 3.2, pp. 1114-1117, Phoenix, Arizona, June 1979.

53. Miller, R., "Wind Loads on Flat Plate Photovoltaic Array Fields," presentation to Jet Propulsion Laboratory by Boeing Engineering and Construction Company, September 1980.

54. Randall, D.E., McBride, D.D., and Tate, R.E., Parabolic Trough Solar Collector Wind Loading, SAND 79-8034, Sandia Laboratories, Albuquerque, New Mexico, June 1979.

55. Peterka, J.A., Sinou, J.M., and Cermak, J.E., Mean Wind Forces on Parabolic-Trough Solar Collectors, SAND 80-7023, Sandia Laboratories, Albuquerque, New Mexico, May 1980.

56. Randall, D.E., McBride, D.D., and Tate, R.E., Steady-State Wind Loading on Parabolic-Trough Solar Collectors, SAND 79-2134, Sandia Laboratories, Albuquerque, New Mexico, August 1980.

57. Randall, D.E., Tate, R.E., and Powers, D.A., Experimental Results of Pitching Moment Tests on Parabolic-Trough Solar Collector Array Configurations, SAND 82-1569, Sandia Laboratories, Albuquerque, New Mexico, December 1982.

58. Brown, G.L., "Wind Tunnel Test of 1/30 Scale Heliostat Field Array," Test Report, SAN/1109-79-2, Honeywell Avionics Division, St. Petersburg, Florida, February 22, 1978.

59. Cermak, J. E., Peterka, J.A., and Kareem, A., Heliostat Field Array Wind-Tunnel Test, DOE/ET/20417-3, contract work performed for McDonnell Douglas Astronautics Company, by Fluid Mechanics and Wind Engineering Program, Fluid Dynamics and Diffusion Laboratory, Colorado State University, Fort Collins, July 1978.

60. "Heliostat Field Wind-Effects Test," Final Report, SAN/20422-2, by Martin Marietta Corporation, Denver, Colorado, February 1979. Work done at Colorado State University.

61. Peglow, S.G., Wind Tunnel Tests of a Full-Scale Heliostat, SAND 79-8034, Sandia Laboratories, Albuquerque, New Mexico, June 1979.

62. Peglow, S.G., "Wind Tunnel Testing of Heliostats and Heliostat Arrays," private communication, Sandia Laboratories, Livermore, Calif., May 31, 1979.

63. Xerikos, J., Tang, H.H., Cermak, J.E., and Peterka, J.A., "The Aerodynamics of Heliostats for Solar Power Plant Applications," Proc. Fifth International Conference on Wind Engineering, Cermak, J.E. (editor), Vol. II, p. IX-6-1, Pergamon Press, July 1979. (Essentially the same as Ref. 59.)

64. Taguchi, T., Aeroelastic Model Study of Heliostats, report for Mitsubishi Heavy Industries, Hiroshima, Japan, 1980. (Translated by Hosoya, N., Colorado, State University, May 1980.)

65. Second Generation Heliostat Development for Solar Central Receiver Systems, Detailed Design Report, Vol. II, Appendices, Appendix E-System Studies, Northrup, Inc., SAND 79-8194, Sandia Laboratories, Livermore, Calif., May 1981.

66. Murphy, L.M., An Assessment of Existing Studies of Wind Loading on Solar Collectors, SERI/TR-632-812, Draft Report, Solar Energy Research Institute, Golden, Colorado, September 1980.

67. Murphy, L.M., "Wind Loading on Tracking and Field Mounted Solar Collectors," Proc. ASME Solar Energy Division, Solar Engineering - 1981, edited by Reid, R.L., Murphy, L.M., and Ward, D.S., pp. 719-727, April 1981.

68. Cohen, E., and Vellozzi, J., "Calculation of Wind Forces and Pressures on Antennas," Annals New York Academy of Sciences, Vol. 116, pp. 161-221, 1964.

69. Wyatt, T.A., "The Aerodynamics of Shallow Paraboloidal Antennas," Annals, New York Academy of Sciences, Vol. 116, pp. 222-238, 1964.

70. Fox, N.L., and Dayman, B., "Preliminary Report on Paraboloidal Reflector Antenna Wind Tunnel Test," Internal Memorandum CP-3, Jet Propulsion Laboratory, Pasadena, Calif., February 1962.

71. Fox, N.L., "Load Distributions on the Surface of Paraboloidal Reflector Antennas," Internal Memorandum CP-4, Jet Propulsion Laboratory, Pasadena, Calif., July 1962.

72. Levy, R., and Kurtz, D., Compilation of Wind Tunnel Coefficients for Parabolic Reflectors, JPL Publication 78-16, Jet Propulsion Laboratory, Pasadena, Calif., April 1978.

73. Morkovin, M.V., "Flow Around Circular Cylinder - A Kaleidoscope of Challenging Fluid Phenomena," Symposium on Fully Separated Flows, ASME, New York, 1964.

74. Maskell, E.C., "Bluff Bodies and High-Lift Systems," in Subsonic Wind Tunnel Wall Corrections, edited by Garner, H.C., et al., AGARDograph No. 109, NATO, October 1966.

75. Harrison, T.D., Midtemperature Solar Systems Test Facility Test Results: Effects of Severe Hailstorm on August 9, 1978, SAND 78-2182, Sandia Laboratories, Albuquerque, New Mexico, March 1979.

76. Riekert, P., and Barth, R., "Wind Tunnel Measurements with a Reflector 1.4 m in Diameter," Research Institute of Vehicles and Engines, Technical Univ. of Stuttgart, Stuttgart, Germany, 1961.

77. Wind Tunnel Test: 1/24 Scale Needle Reflector Model, Report No. 196, Brewer Engineering Laboratories, Marion, Mass., 1960.

78. Anderson, W.W., "Aerodynamic Tests - Radio Telescope," Naval Air Station, Moffett Field, Calif., (London), Vol. 9, pp. 65-86, 1957.

79. Winters, J.L., and Sheard, W.B., Wind Loading of Parabolic Antenna, Report No. G3705.18.04., Ling-Temco-Vought, Inc., LTV Electrosystems, Inc., Greenville Division, Quarterly R&D Report Ending March 1970.

80. Levy, R. and Strain, D., Sensitivity of Reflector Backup Structure Weight to Variable Wind Speed Loadings, Deep Space Network Progress Report 42-56, Jet Propulsion Laboratory, Pasadena, Calif., January/February 1980.

81. Vermeulen, P.J., Bader, A., and Elfner, P., "Reduced Drag, Paraboloidal Type, Solar Energy Collectors," Joint Conference, American Section, International Solar Energy Society, and Solar Energy Society of Canada, Vol. 2, Solar Collectors, pp. 264-274, August 1976.

82. Scruton, C., "A Brief Review of Wind Effects on Radio Paraboloidal Reflector Installations with Special Reference to the Wind - Excited Vibrations of the Members of the Supporting Structure," Annals, New York Academy of Sciences, Vol. 116, pp. 275-286, 1964.

83. Hull, F.H., "Dynamic Stability and Aeroelastic Considerations in the Design of Large Steerable Antennas," Annals, New York Academy of Sciences, Vol. 116, pp. 311-323, 1964.

84. Marris, A.W., "A Review on Vortex Streets, Periodic Wakes, and Induced Vibration Phenomena," Trans. ASME, J. of Basic Engineering, Vol. 86, pp. 185-196, 1964.

85. Chen, C.F., and Mangione, B.J., "Vortex Shedding from Circular Cylinders in Sheared Flow," AIAA J., Vol. 7, pp. 1211-1212, 1969.

86. Maull, D.G., and Young, R.A., "Vortex Shedding from Bluff Bodies in Shear Flow," J. Fluid Mechanics, Vol. 60, pp. 401-409, 1973.

87. Griffin, O.M., "Instability in the Vortex Street Wakes of Bluff Bodies," Trans. ASME, J. of Fluids Engineering, Vol. 95, pp. 579-581, 1973.

88. Lee, B.E., "Some Effects of Turbulence Scale on the Mean Forces on a Bluff Body," J. of Industrial Aerodynamics, Vol. 1, pp. 361-370, 1975/1976.

89. Simmons, J.E.L., "Similarities Between Two-Dimensional and Axisymmetric Wakes," Aeronautical Quarterly, Vol. 28, pp. 15-20, 1977.

90. Weaver, W., "Wind-Induced Vibrations in Antenna Members," Proc. ASCE, J. of the Engineering Mechanics Division, Vol. 87, pp. 141-165, 1961.

91. Weaver, W., "Criteria for Design Against Wind-Induced Vibrations in Antenna Members," Annals, New York Academy of Sciences, Vol. 116, pp. 287-310, 1964.

92. Fox, N.L., "Experimental Data on Wind-Induced Vibrations of a Paraboloidal Reflector Antenna Model," Internal Memorandum CP-5, Jet Propulsion Laboratory, Pasadena, Calif., January 1963.

93. Focus on Solar Technology: A Review of Advanced Solar Thermal Power Systems, DOE/JPL-1060-78/5, Conference No. 781103, Golden, Colorado, November 1978. (See Structural Deformation Analysis, p. 26.)

94. Advanced Subsystems Development: Third Semiannual Progress Report, DOE/JPL-1060-20, JPL Publication 79-107, Jet Propulsion Laboratory, Pasadena, Calif., August 15, 1979. (See Structrual Deformation Analysis, p. 3-23.)

95. Detail Design Review, Low Cost Concentrator, Vol. 1, p. 65, presented to Jet Propulsion Laboratory by Acurex Corporation, July 30, 1981.

96. Edwards, B., "Collector Deflections due to Wind Gusts and Control Scheme Design," Solar Energy, Vol. 25, p. 231-234, 1980.

97. Collector Subsystem Requirements, Issue C, Sandia Laboratories, Livermore, Calif., October 10, 1979.

98. Line-Focus Solar Thermal Energy Technology Development, A Seminar for Industry, Proceedings, Sandia Laboratories, Albuquerque, New Mexico, September 1980.

99. Design Requirement Specification: Point-Focus Solar Concentrator, Revision D, Jet Propulsion Laboratory, Pasadena, Calif., March 1980.

100. Wind-Design of Flat Panel Photovoltaic Array Structures, SAND 79-7057, work performed for DOE by Bechtel National, Inc., Sandia Laboratories, San Francisco, Calif., 1980.

101. Task Committee on Wind Forces, "Wind Forces on Structures," Transactions, Amer. Soc. of Civil Engineers, (ASCE), Vol. 126, pp. 1124-1198, 1961.

102. Solar Total Energy - Large Scale Equipment at Shenandoah, Georgia - Phase III, Preliminary Design, ALO/3985-1, work performed for DOE by General Electric Company, Space Division, Philadelphia, September 1978.

103. Eckert, E.R.G., and Drake, R.M., Heat and Mass Transfer, Second Edition, McGraw Hill Book Company, Inc., New York, 1959. (See Chapter 11.)

104. Clausing, A.M., "Experimental Investigation of Convective Losses from Solar Receivers," Project Description, University of Illinois, Dept. Mechanical Engineering, Circa 1978/1979. (DOE Project sponsored by Sandia Livermore Laboratories for central receiver/power towers.)

105. Giedt, W.H., Principles of Engineering Heat Transfer, D. van Nostrand Company, Inc., Princeton, New Jersey, 1957. (See Chapter 10.)

106. Aero-Space Applied Thermodynamics Manual, Society of Automotive Engineers, Committee A-9, Aerospace Environmental Systems Publication, February 1960, revised January 1962.

107. Apelt, C.J., and Ledwich, M.A., "Heat Transfer and Unsteady Flows Past a Heated Circular Cylinder in the Range $1<R<40$, "J. Fluid Mechanics, Vol. 95, pp. 761-777, 1979.

108. Quarmby, A., and Al-Fakhri, A.A.M., "Effect of Finite Length on Forced Convection Heat Transfer from Cylinders," Int. J. of Heat and Mass Transfer, Vol. 23, pp. 463-469, 1980.

109. Sandborn, P.A., and Sandborn, V.A., "Periodic Vortex Formation in Combined Free and Forced Convection," Trans. ASME, J. of Heat Transfer, Vol. 102, pp. 174-177, 1980.

110. Ericsson, L.E., and Reding, J.P., "Criterion for Vortex Periodicity in Cylinder Wakes," AIAA J., Vol. 17, pp. 1012-1013, 1979.

111. Guven, O., Farell, C., and Patel, V.C., "Surface-Roughness Effects on the Mean Flow past Circular Cylinders," J. Fluid Mechanics, Vol. 98, pp. 673-701, 1980.

112. Bearman, P.W., and Graham, J.M.R., "Vortex Shedding from Bluff Bodies in Oscillatory Flow: A Report on Euromech 119," J. Fluid Mechanics, Vol. 99, pp. 225-245, 1980.

113. Clausing, A.M., "An Analysis of Convective Losses from Cavity Solar Central Receivers," Solar Energy, Vol. 27, pp. 295-300, 1981.

114. Clausing, A.M., "Modeling Requirements for Determinations of Convective Losses from Solar Receivers," Proc. 1981 Annual Meeting, International Solar Energy Society (American Section), Vol. 4.1, pp. 371-375, Philadelphia, Penn., May 1981.

115. Clausing, M., "Convective Losses from Cavity Solar Receivers - Comparisons between Analytical Predictions and Experimental Results," draft paper, to be published.

116. Koenig, A.A., and Marvin, M., "Convection Heat Loss Sensitivity in Open Cavity Solar Receivers," draft paper, to be published.

117. Owen, W.A., "Prospects for Enhanced Receiver Efficiency," Proc. Fourth Parabolic Dish Solar Thermal Power Program Review, DOE/JPL-1060-58, JPL Publication 83-2, Jet Propulsion Laboratory, Pasadena, Calif., pp. 155-159, February 1, 1983.

118. Cummings, A., "Acoustics of a Wine Bottle," J. Sound and Vibration, Vol. 31, pp. 331-343, 1973.

119. Rockwell, D., and Naudascher, E., "Review: Self-Sustaining Oscillations of Flow Past Cavities," Trans. ASME, J. of Fluids Engineering, Vol. 100, pp. 152-165, 1978.

120. Scheiman, J., "Acoustic Measurements of a Large Cavity in a Wind Tunnel," NASA Technical Memorandum 78658, Langely Research Center, Hampton, Virginia, May 1978.

121. Rockwell, D., and Knisely, C., "Observations of the Three-Dimensional Nature of Unstable Flow Past a Cavity," Physics Fluids, Vol. 23, pp. 425-431, 1980.

122. Humphrey, J.A.C., and Jacobs, E.W., "Free-Forced Laminar Flow Convective Heat Transfer from a Square Cavity in a Channel with Variable Inclination," Int. J. of Heat and Mass Transfer, Vol. 24, pp. 1589-1597, 1981.

123. Baumeister, K.J., and Rice, E.J., "Flow Visualization in Long-Neck Helmholtz Resonators with Grazing Flow," AIAA J., Vol. 16, pp. 233-236, 1978.

124. Kinsler, L.E., and Frey, A.R., Fundamentals of Acoustics, 2nd Edition, John Wiley and Sons, New York, 1962. (See Chapter 8.)

125. Panton, R.L., and Miller, J.M., "Excitation of a Helmholtz Resonator by a Turbulent Boundary Layer," J. Acoustical Soc. of America, Vol. 58, pp. 800-806, 1975.

126. Sarohia, V., Back, L.H., Roschke, E.J., and Parthasarathy, S.P., "An Experimental Investigation of Fluid Flow and Heating in Various Resonance Tube Modes," JPL Technical Memorandum 33-780, Jet Propulsion Laboratory, Pasadena, Calif., September, 1976.

127. Sarohia, V., and Back, L.H., "Experimental Investigation of Flow and Heating in a Resonance Tube," J. Fluid Mechanics, Vol. 94, pp. 649-672, 1979.

128. Richardson, P.D., "Effects of Sound and Vibration on Heat Transfer," Applied Mechanics Reviews, Vol. 20, pp. 201-217, 1967.

129. Woodruff, N.P., and Zingg, A.W., "A Comparative Analysis of Wind Tunnel and Atmospheric Air Flow Patterns about Single and Successive Barriers," Trans. of the American Geophysical Union, Vol. 36, No. 2, 1955.

130. Raine, J.K., and Stevenson, D.C., "Wind Protection by Model Fences in Simulated Atmospheric Boundary Layer," J. of Industrial Aerodynamics, Vol. 2, pp. 159-180, 1977.

131. Gandemer, J., "Wind Shelters," J. of Industrial Aerodynamics, Vol. 4, pp. 371-389, 1979.

132. Kelnhofer, W.J., "Neighboring Body Effects on Bluff Body Form Drag," Developments in Mechanics, Vol. 7, Proc. 13th Midwestern Mechanics Conference, J. I. Abrams and T. C. Woo, co-chairmen, pp. 111-214, Pittsburg, PA, 1973.

133. Kelnhofer, W.J., "Neighboring Body Effects on Bluff Body Tipping Moment," Developments in Mechanics, Vol. 7, Proc. 13th Midwestern Mechanics Conference, J. I. Abrams and T. C. Woo, co-chairmen, pp. 125-137, Pittsburg, PA, 1973.

134. Strickland, J.H., Matty, R.R., and Barton, G.H., "Vortex Shedding from Square Plates Perpendicular to a Ground Plane," AIAA J., Vol. 18, pp. 715-716, 1980.

135. Cermak, J.E., "Laboratory Simulation of the Atmospheric Boundary Layer," AIAA J., Vol. 9, pp. 1746-1754, 1971.

136. Cermak, J.E., "Applications of Wind Tunnels to Investigation of Wind-Engineering Problems," AIAA J., Vol. 17, pp. 679-690, 1979.

137. Cermak, J.E., "Fluid-Mechanics Applications to Problems of Wind Forces on Structures and Air-Pollution" Developments in Mechanics, Vol. 7, Proc. 13th Midwestern Mechanics Conference, J. I. Abrams and T. C. Woo, co-chairmen, pp. 37-53, Pittsburg, PA, 1973.

138. Meroney, R.N., "Wind-Tunnel Simulation of Flow Over Hills and Complex Terrain," J. of Industrial Aerodynamics, Vol. 5, pp. 297-321, 1980.

139. Clausing, A.M., Clark, G.L., Jr., and Mueller, M.H., "The Cryogenic Heat Transfer Tunnel--A New Tool for Convective Research," Modeling, Simulation, Testing and Measurements for Solar Energy Systems, ASME Winter Annual Meeting, San Francisco, Calif., December 1978.

140. Clark, G.L., Jr., Clausing, A.M., Mueller, M.H., Weiner, J.G., and Kempka, S.N., "The Cryogenic Heat Transfer Tunnel-First Experimental Data," Proc. 1980 Annual Meeting, International Solar Energy Society (American Section), Vol. 3.1, pp. 481-484, Phoenix, Arizona, June 1980.

141. Adcock, J., "Simulation of Flat-Plate Turbulent Boundary Layers in Cryogenic Tunnels," J. of Aircraft (AIAA), Vol. 17, pp. 284-285, 1980.

APPENDIX A

WIND DATA FOR EDWARDS AIR FORCE BASE AND OTHER SOUTHERN CALIFORNIA SITES

Air Weather Service data for Edwards Air Force Base (EAFB) for the years 1961 through 1972 has been examined (Ref. 45) and some results are presented in Figure A-1. Measurements were made at 13 ft above ground. Figure A-1a shows that the mean wind speed is most likely to achieve maximum values in late afternoon (about 4 pm) during the late Spring months. This is evident again in Figure A-1b, which shows that winds in the 17- to 21-knot range tend to occur in late afternoon. A gust record is shown in Figure A-1c, which indicates a peak gust of 56 knots (64.5 mph) out of the NNE during the year 1971. As mentioned in the text, peak gusts should not be used for basic wind speed, or design speed. Figure A-1d shows operation time as function of design speed. (It was unclear to this author whether "operation time" referred to 24-hour periods or to sunny, daylight hours only.) A system would be operational about 90% of the time for design speeds between 10.8 knots and 15.4 knots (12.4 to 17.7 mph). Figure A-1d is comparable in magnitudes and shape with the SOLMET correlations of insolation and wind speed (Ref. 29). For all 26 SOLMET stations surveyed, 97% of the available direct insolation occurred at wind speeds of 34 mph or less (approx. 29 knots). Figure A-1d indicates better than 99% operation for this wind speed.

The data for EAFB shown in Figure A-2 (from Ref. 60) is presented differently but, in general, tends to corroborate the previous data. Note that the percent of time of all wind velocities, in various months, is dominated by winds from the SSW to SW (Figure A-2d); however, peak gusts tend to come from the NNE (Figure A-1c). The EAFB data of Figure A-2 refers also to measurements at 13 ft above ground and could be the same data examined in Ref. 45; however, this is by no means certain.

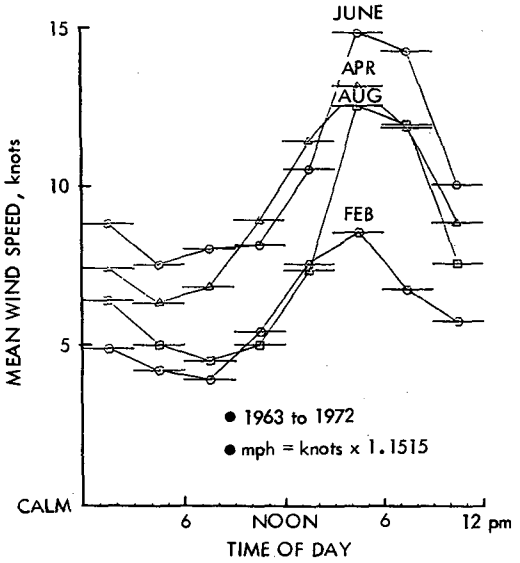

a. DAILY MEAN WIND SPEEDS

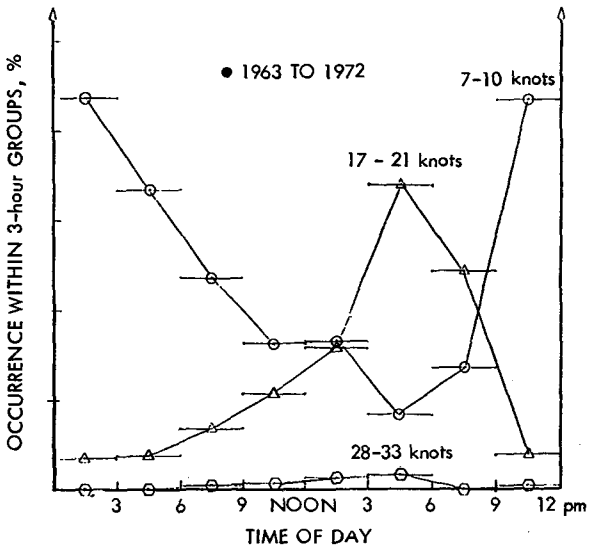

b. DAILY OCCURRENCE OF SELECTED SPEED INTERVALS

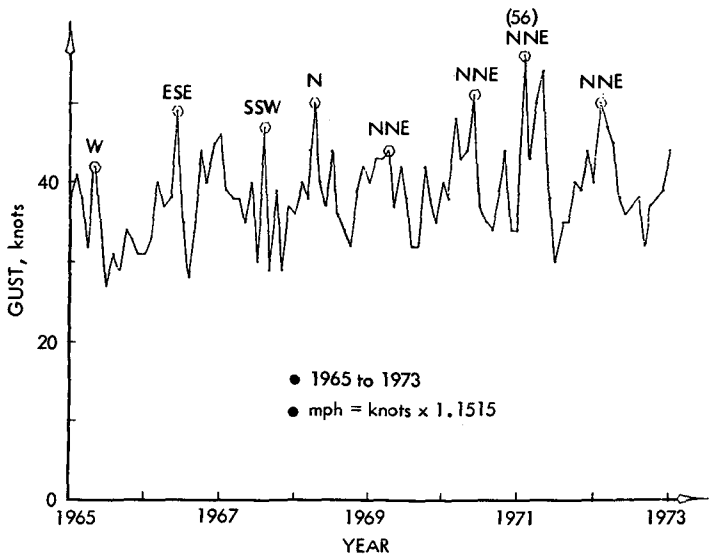

c. GUST RECORD

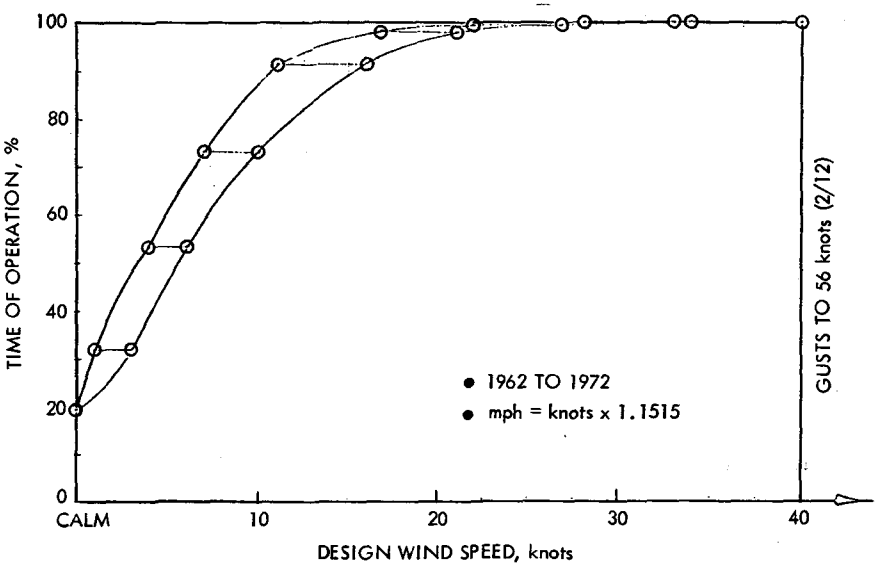

d. DESIGN SPEED VARIATION WITH OPERATIONAL TIME

Figure A-1. Wind Data for Edwards Air Force Base, California (From Ref. 45)

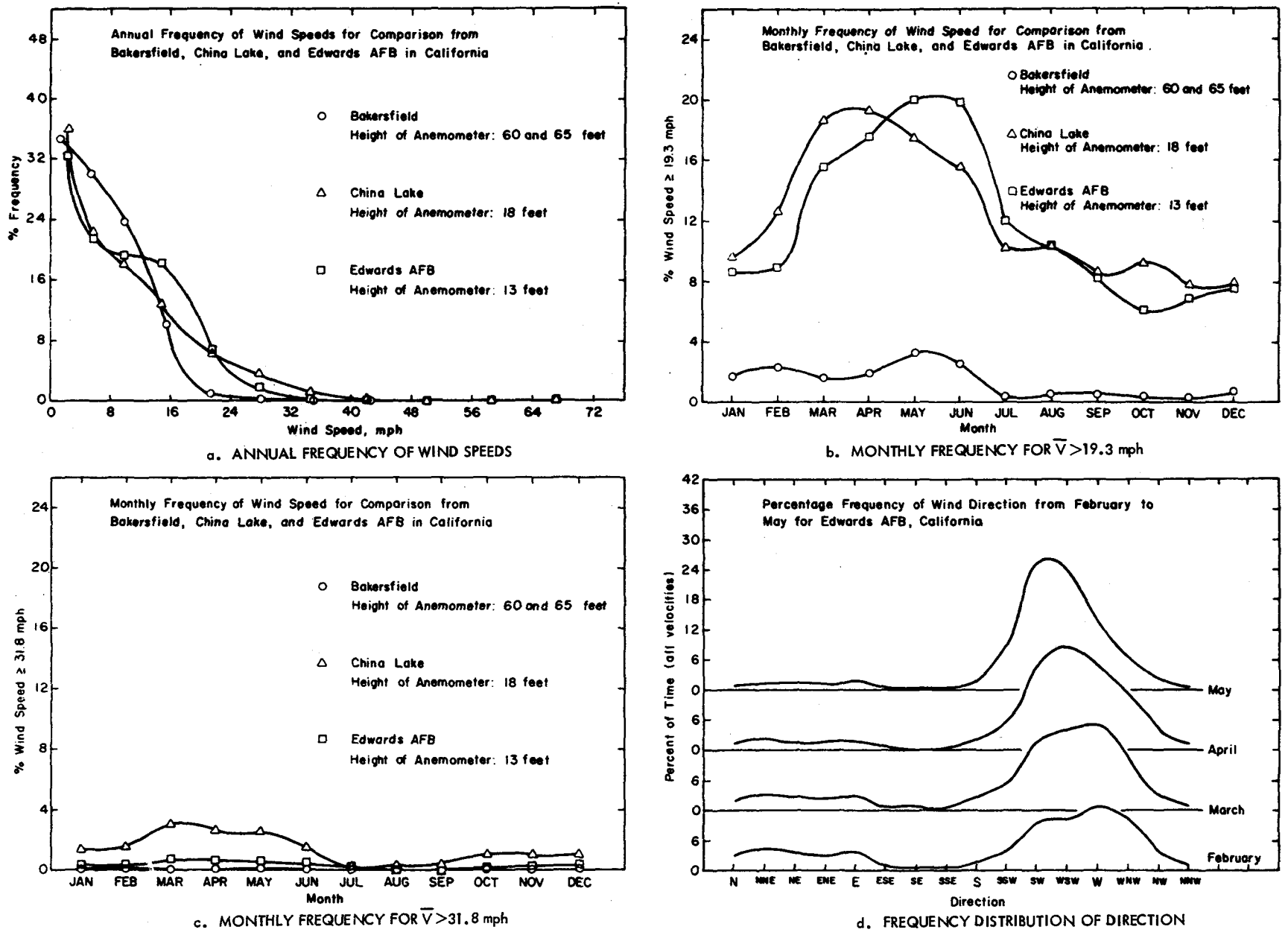

Figure A-2. Wind Data for Three Southern California Sites (From Ref. 60)

APPENDIX B

BASIC WIND SPEEDS FOR THE UNITED STATES

Airport wind measurements observed over many years have been analyzed to determine basic wind speed (design speeds) derived from the annual extreme fastest-mile speed. In general, a 1/7 power-law velocity profile is appropriate for airports which, usually, are located in flat, open country (Figure 5, of text). Some results (reproduced from Ref. 40) are shown in Figures B-1, B-2, and B-3 for mean recurrence periods of 100, 50, and 25 years, respectively. All data have been standardized to a reference height above ground of 30 ft. Reading these figures, it may be determined that the basic wind speeds for Edwards Air Force Base, California, are approximately 70, 65, and 50 mph for R values of 100, 50, and 25 years, respectively.

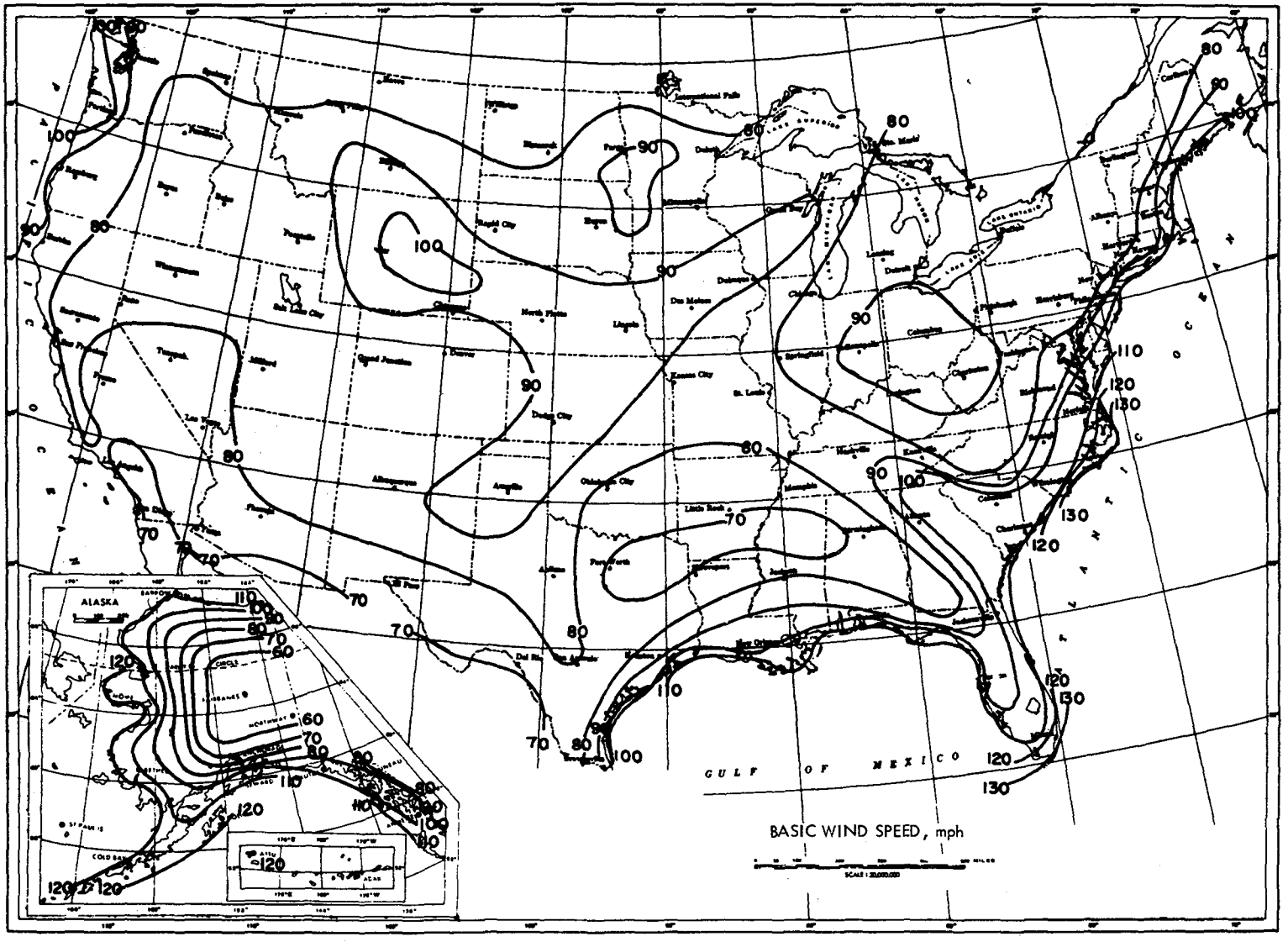

Figure B-1. Annual Extreme Fastest Mile Speed 30 Feet Above Ground, 100-Year Mean Recurrence Interval (Adapted from Ref. 40)

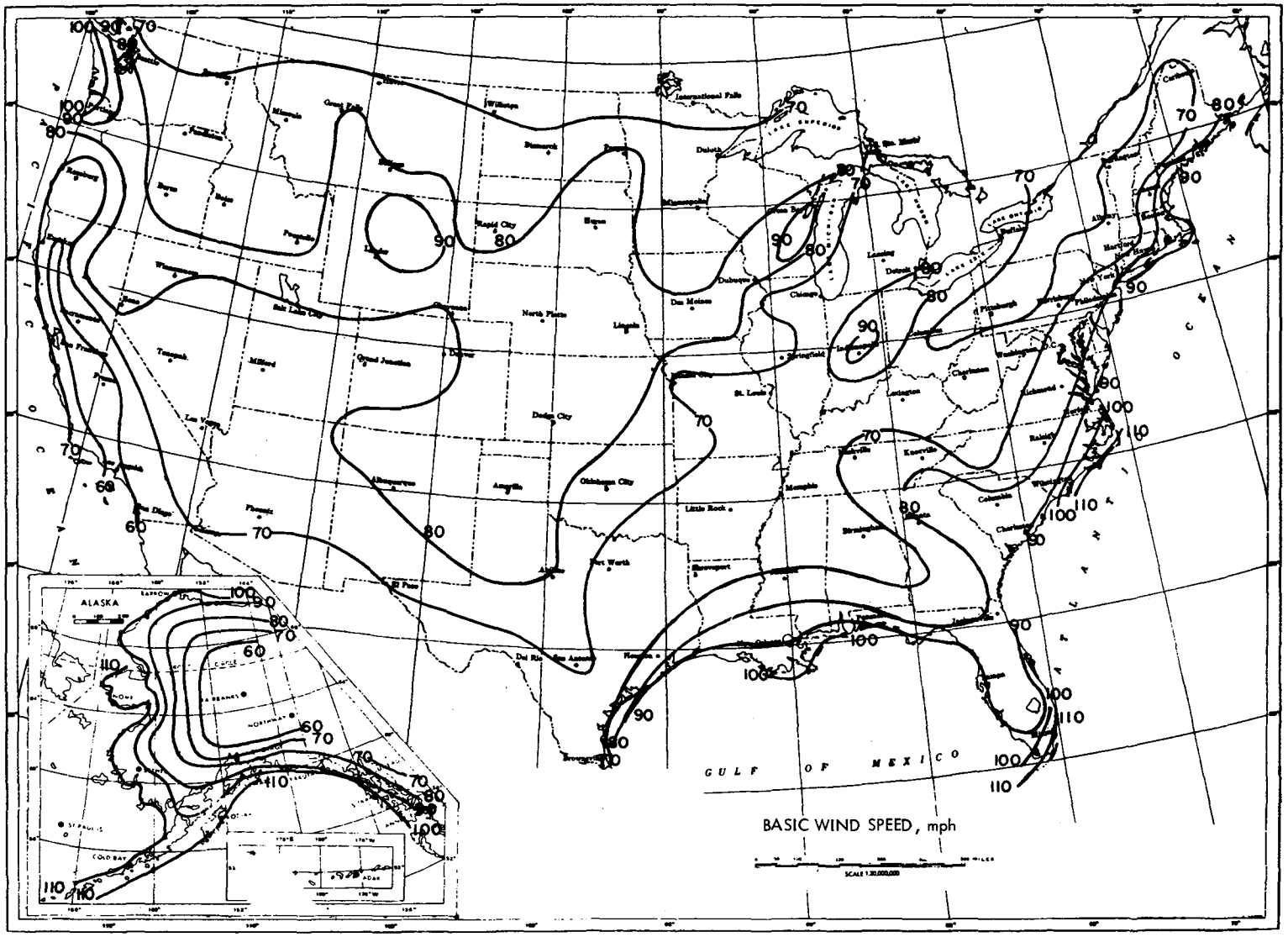

Figure B-2. Annual Extreme Fastest Mile Speed 30 Feet Above Ground, 50-Year Mean Recurrence Interval (Adapted from Ref. 40)

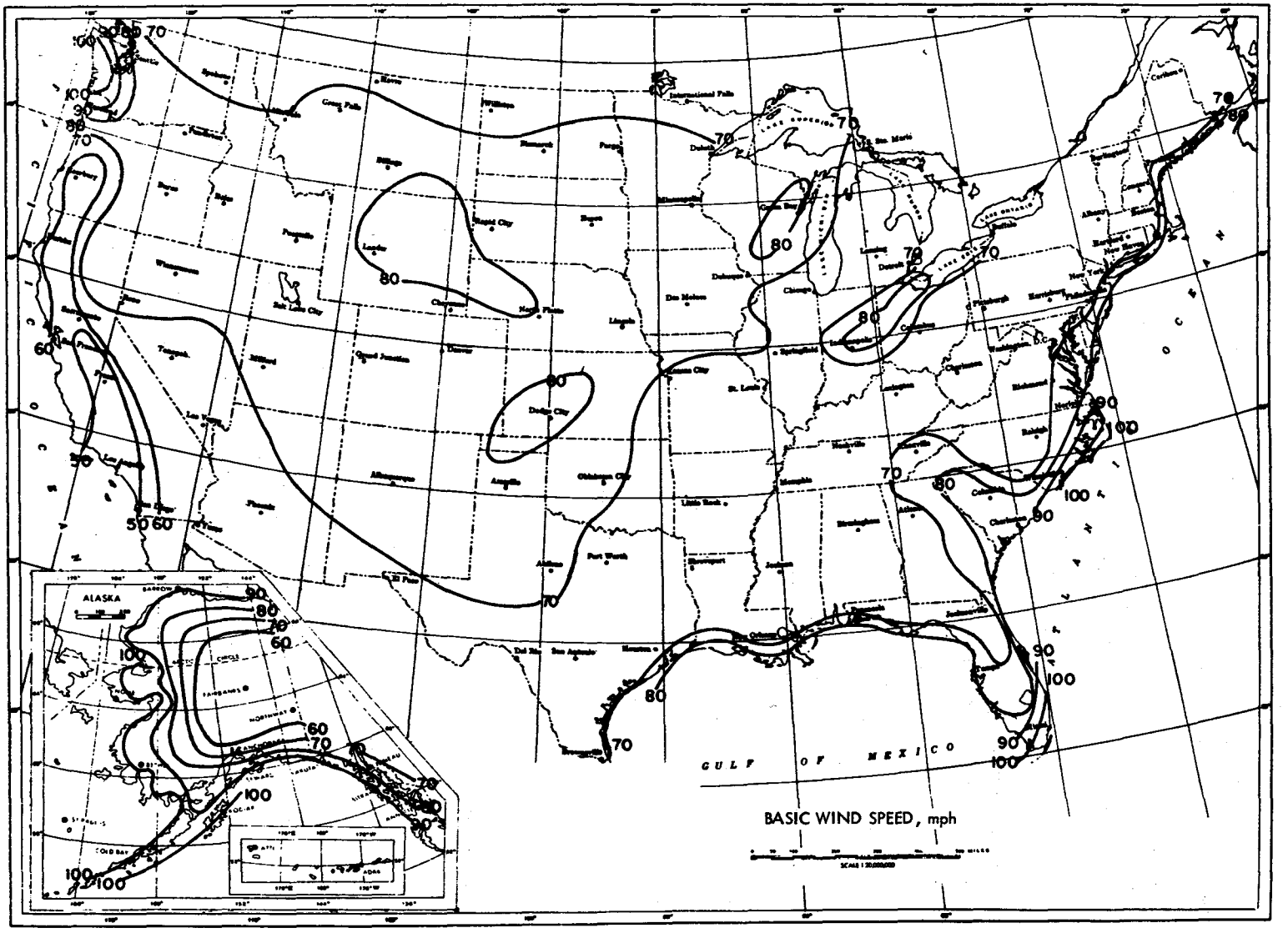

Figure B-3. Annual Extreme Fastest Mile Speed 30 Feet Above Ground, 25-Year Mean Recurrence Interval (Adapted from Ref. 40)

APPENDIX C

APPROXIMATE WIND FORCE RATIOS FOR A SQUARE PLATE

Wind forces are proportional to the dynamic pressure $\rho V^2/2$ where ρ is air density and V is time-averaged wind speed. Consider a square plate with basic dimension L mounted vertically, with a variable ground spacing which is a fraction b of the basic dimension, i.e., $g = bL$. The center of the plate is located at a height $g + L/2$ above ground. Assuming, for a moment, that the force coefficient is unity, the integrated wind force is:

$$\text{Force} = \int (\rho V^2/2)\, dA$$

where the differential area dA is Ldz. For a power-law wind velocity profile $V = Bz^{1/n}$, where B = constant,

$$\text{Force} = (\rho L B^2/2) \int_g^{g+L} (z)^{2/n} dz$$

$$\text{Force} = \frac{n \rho L B^2}{2(n+2)} \left[(bL + L)^{(n+2)/n} - (bL)^{(n+2)/n} \right] \qquad \text{(C-1)}$$

At the centerline $V = V_o$, at $z = g + L/2$, so that the force corresponding to V_o is:

$$\begin{aligned} \text{Force}_{CL} &= (\rho V_o^2/2) L^2 \\ \text{Force}_{CL} &= (\rho B^2 L^2/2)(z_o)^{2/n} \\ \text{Force}_{CL} &= (\rho B^2 L^2/2)(bL + L/2)^{2/n} \end{aligned} \qquad \text{(C-2)}$$

The ratio of Equation (C-1) to Equation (C-2) is

$$\text{Ratio} = \frac{n}{(n+2)} \left\{ \frac{\left[(1+b)^{\left(\frac{n+2}{n}\right)} - (b)^{\left(\frac{n+2}{n}\right)} \right]}{(1/2 + b)^{2/n}} \right\} \qquad \text{(C-3)}$$

which is plotted in Figure 17a of the text.

If the total force is based on V_{max} which occurs at the top of the plate where $z = g + L$, the force is:

$$\text{Force} = (\rho B^2 L^2/2)(bL + L)^{2/n} \qquad \text{(C-4)}$$

and the ratio of Equation (C-4) to Equation (C-2) is:

$$\text{Ratio} = [(1 + b)/(1/2 + b)]^{2/n} \qquad \text{(C-5)}$$

which is plotted in Figure 17b of the text.

APPENDIX D

SELECTED WIND TUNNEL RESULTS OF THE MODEL GOLDSTONE RADIO ANTENNA

Extensive wind tunnel results for a model of the 210-ft-dia Goldstone radio antenna are given in Ref. 13. In addition to investigation of the basic configuration, effects were measured for: (1) alidade contributions, (2) changes in reflector support structure, (3) changes in base configuration, (4) boundary-layer velocity profile, and (5) axial loads on quadripod legs. Most of the data were taken using the normal wind tunnel boundary layer (thin compared to the reflector diameter); some data were taken using an approximate 1/7 power velocity profile. Only results for the basic configuration are presented here.

Model Description

Size: 18-in.-dia dish (paraboloidal)
Scale factor: 1/140
h/D = 0.149, f/D = 0.420
Outer 25% of dish radius had 25% porosity
Dish centerline: located 0.535 dia above tunnel floor
Moment center: located 0.142 dia aft of reflector vertex

Air (Wind) Conditions

Wind speed: 242 mph = 355 ft/sec
Dish Reynolds number: 3.4×10^6
Boundary layer: normal wind tunnel, and 1/7 power-law profile

Data Reduction

Stability-axis system (Figure 21)
Dynamic pressure: at dish centerline
Corrected for wind tunnel blockage

Results for the three force coefficients and the three moment coefficients are shown in Figures D-1 through D-6, for the basic configuration. Peak values for the axial and lateral force coefficients, and the yaw (pitch) moment coefficient occurred at 5-deg elevation angle (probably 0 deg, actually). Peak coefficient values occurred at elevation angles of 50 deg, 60 deg, and 75 deg for lift, pitch-moment, and roll-moment, respectively. Note that, with exception of the lateral force coefficient, all coefficients exhibited both positive and negative values.

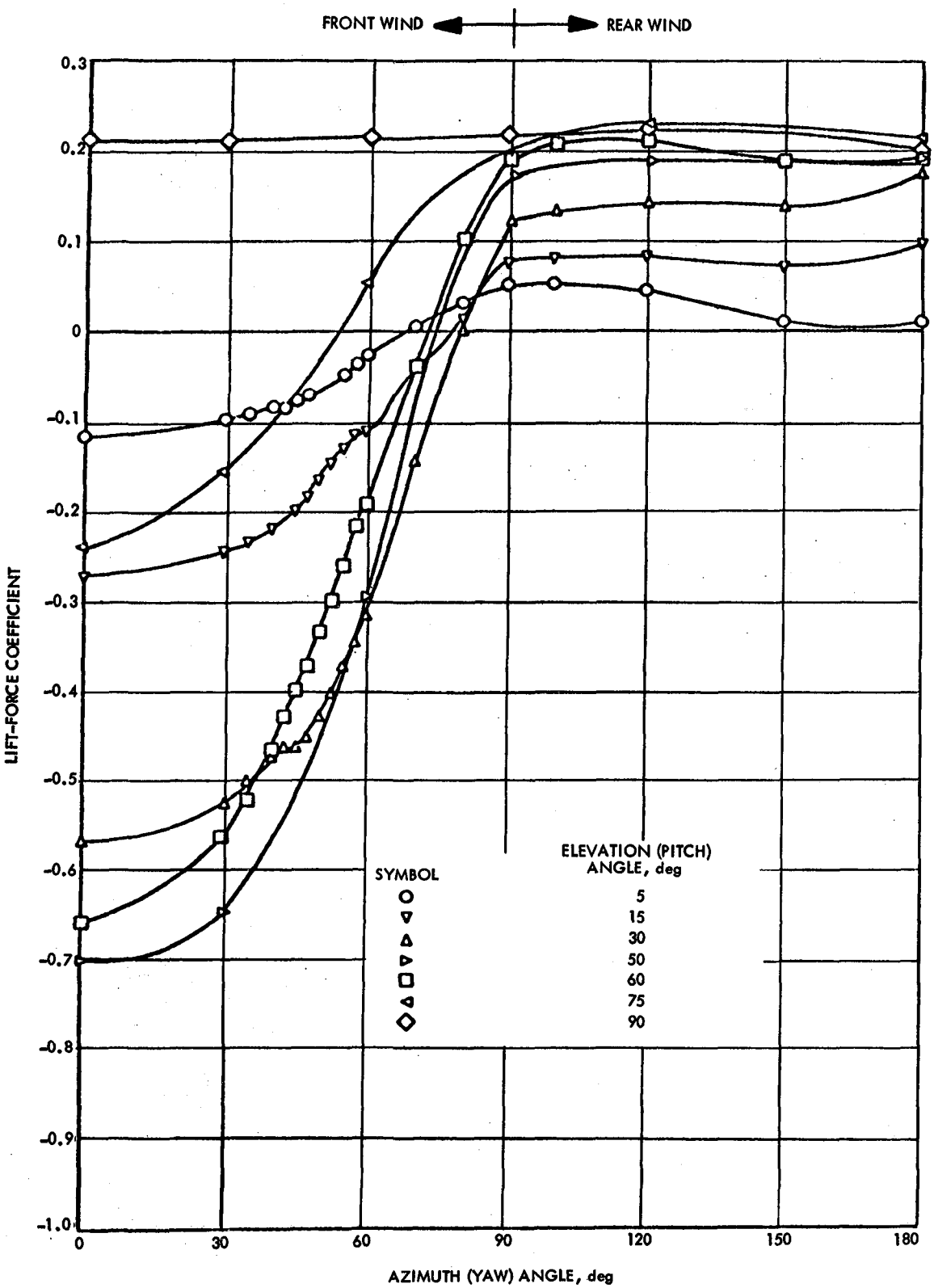

Figure D-1. Effect of Antenna Attitude on Lift-Force Coefficient (From Ref. 13)

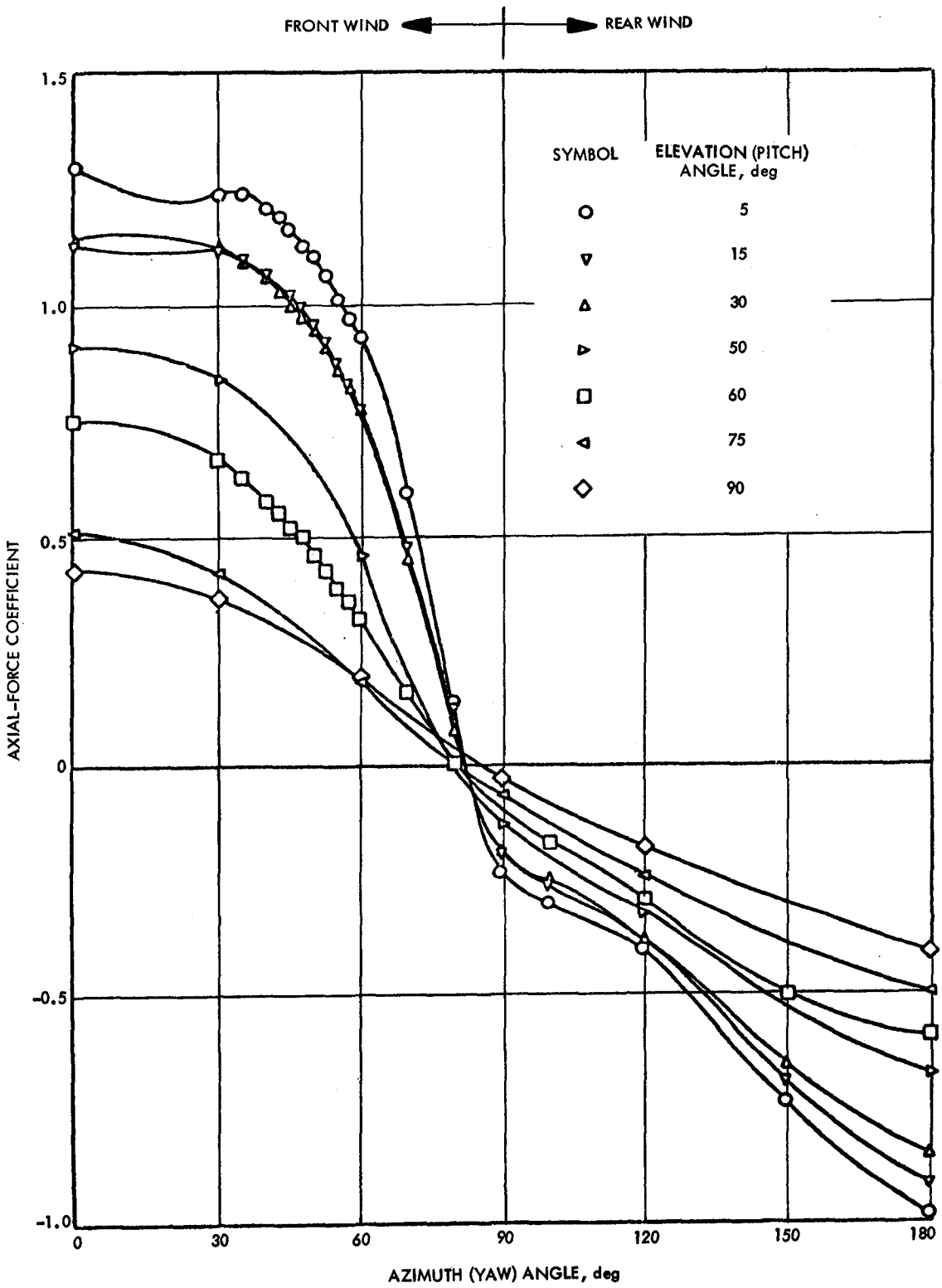

Figure D-2. Effect of Antenna Attitude on Axial-Force Coefficient (From Ref. 13)

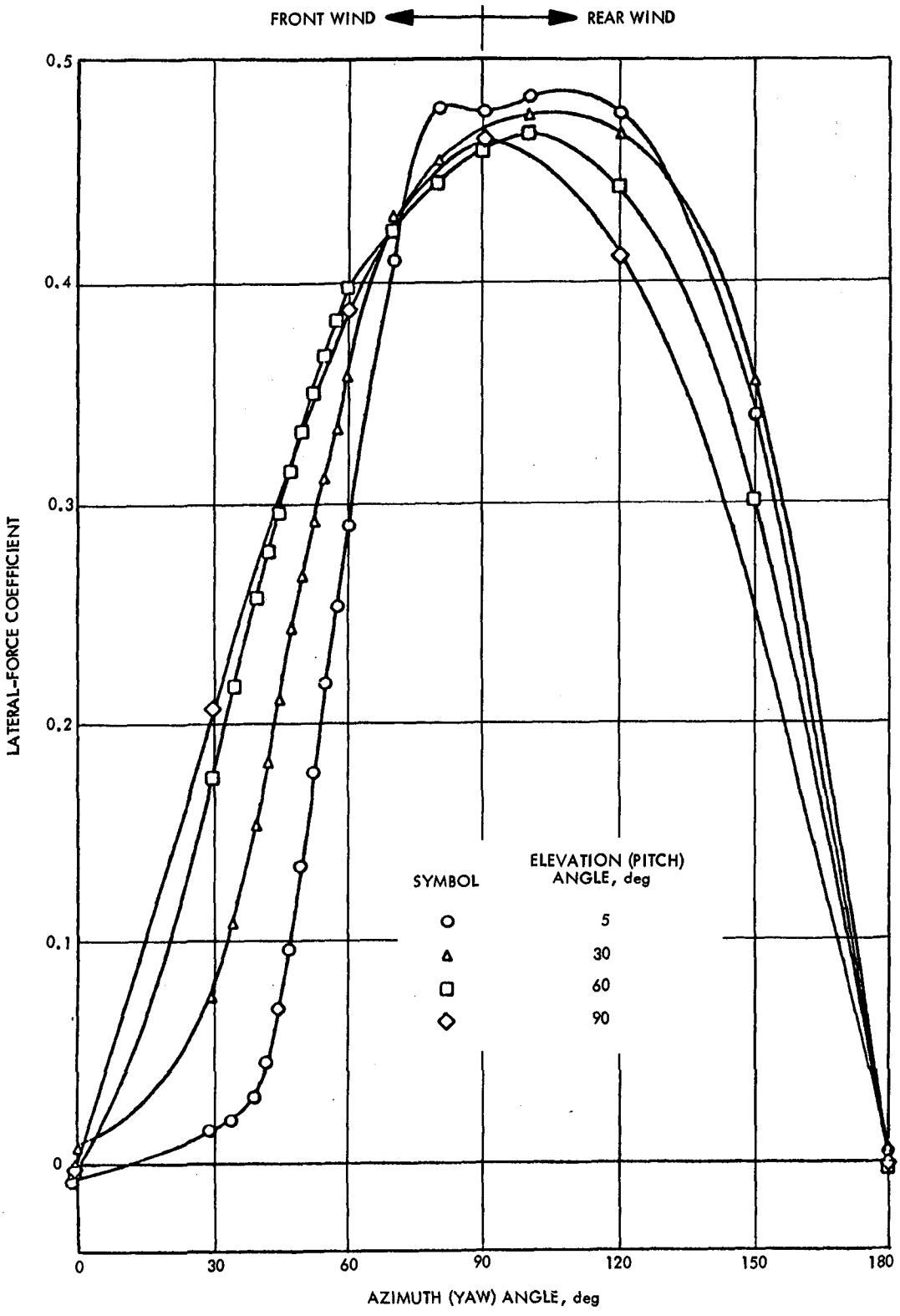

Figure D-3. Effect of Antenna Attitude on Lateral-Force Coefficient (From Ref. 13)

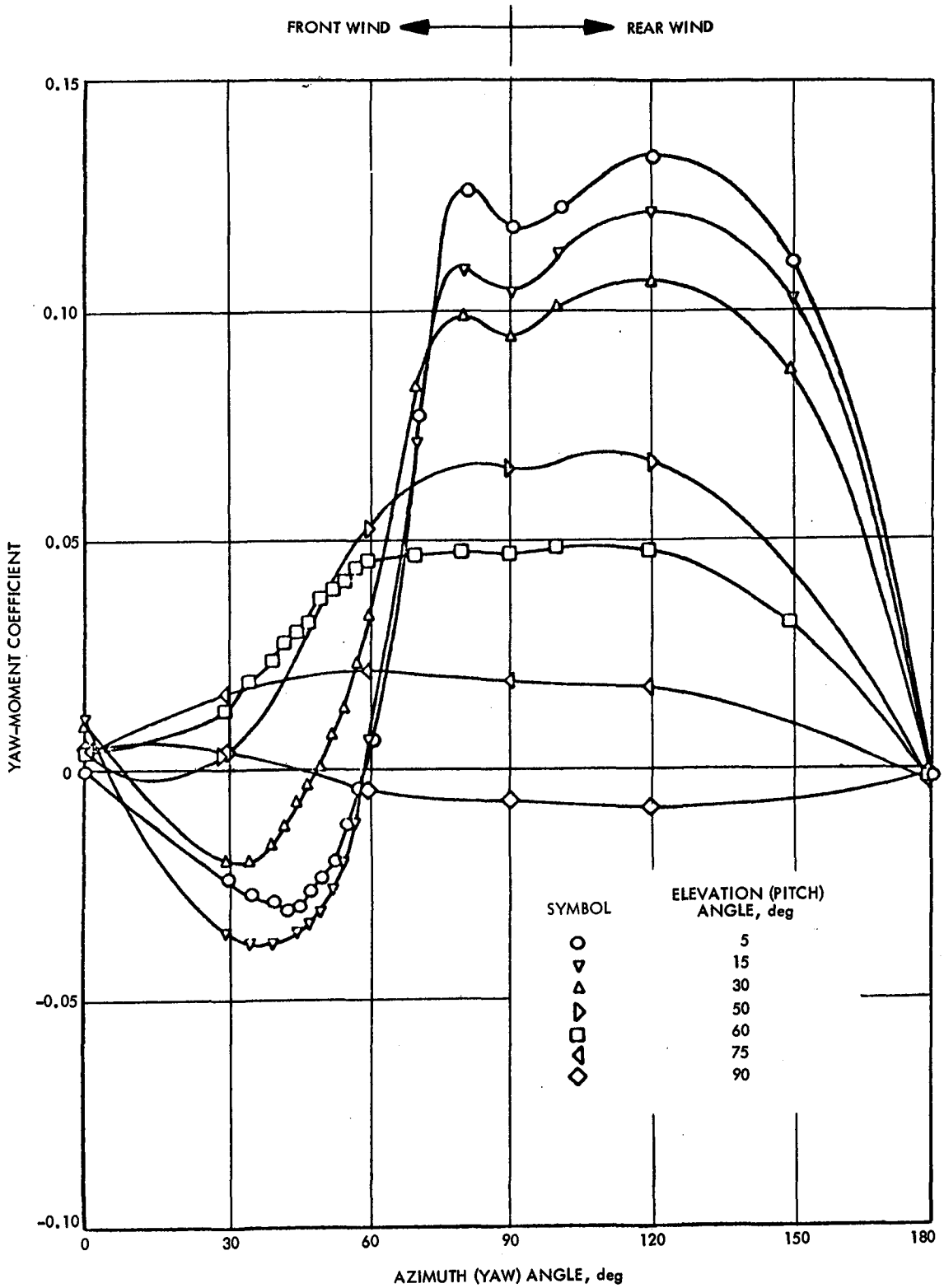

Figure D-4. Effect of Antenna Attitude on Yaw-Moment Coefficient (From Ref. 13)

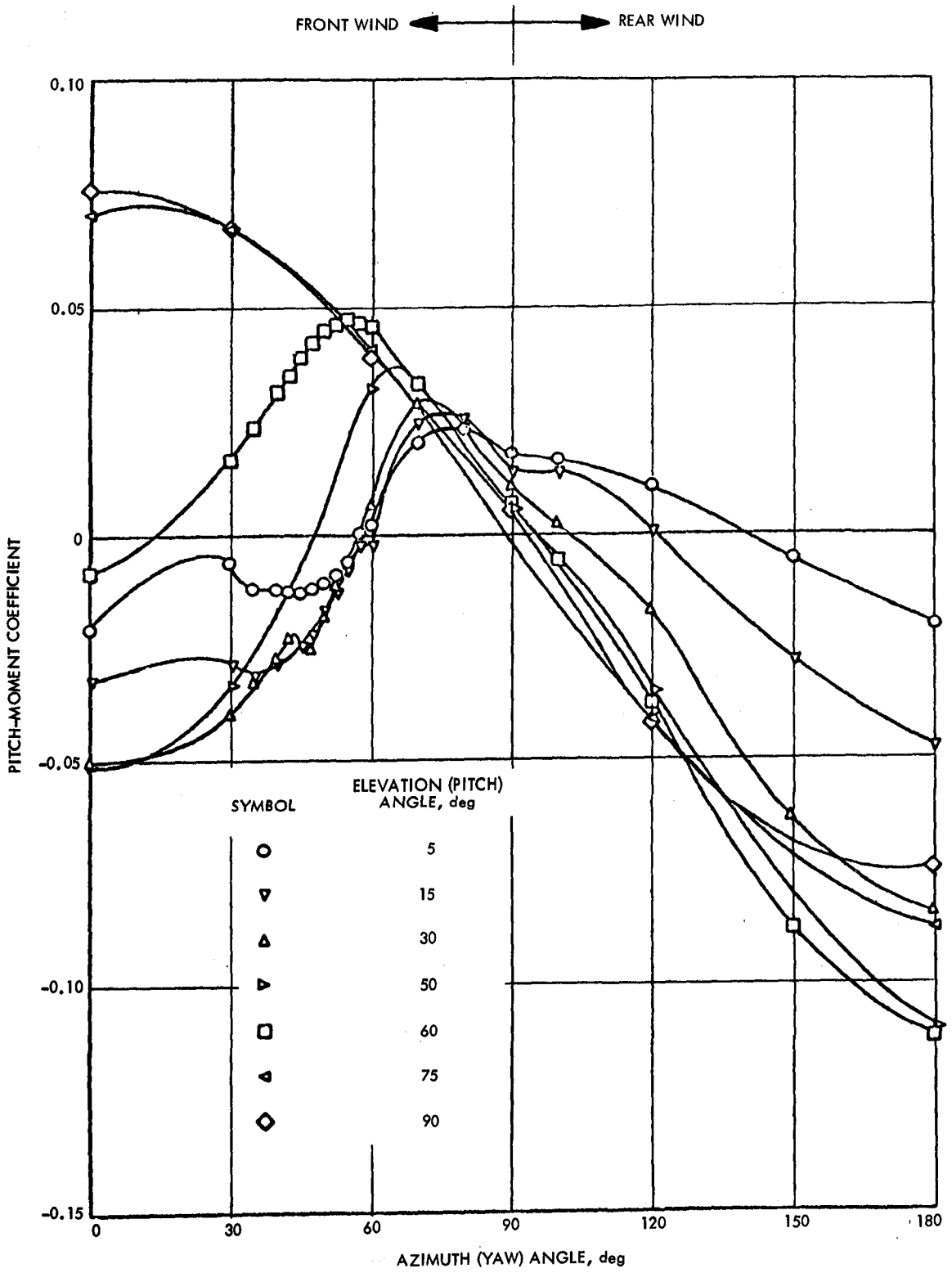

Figure D-5. Effect of Antenna Attitude on Pitch-Moment Coefficient (From Ref. 13)

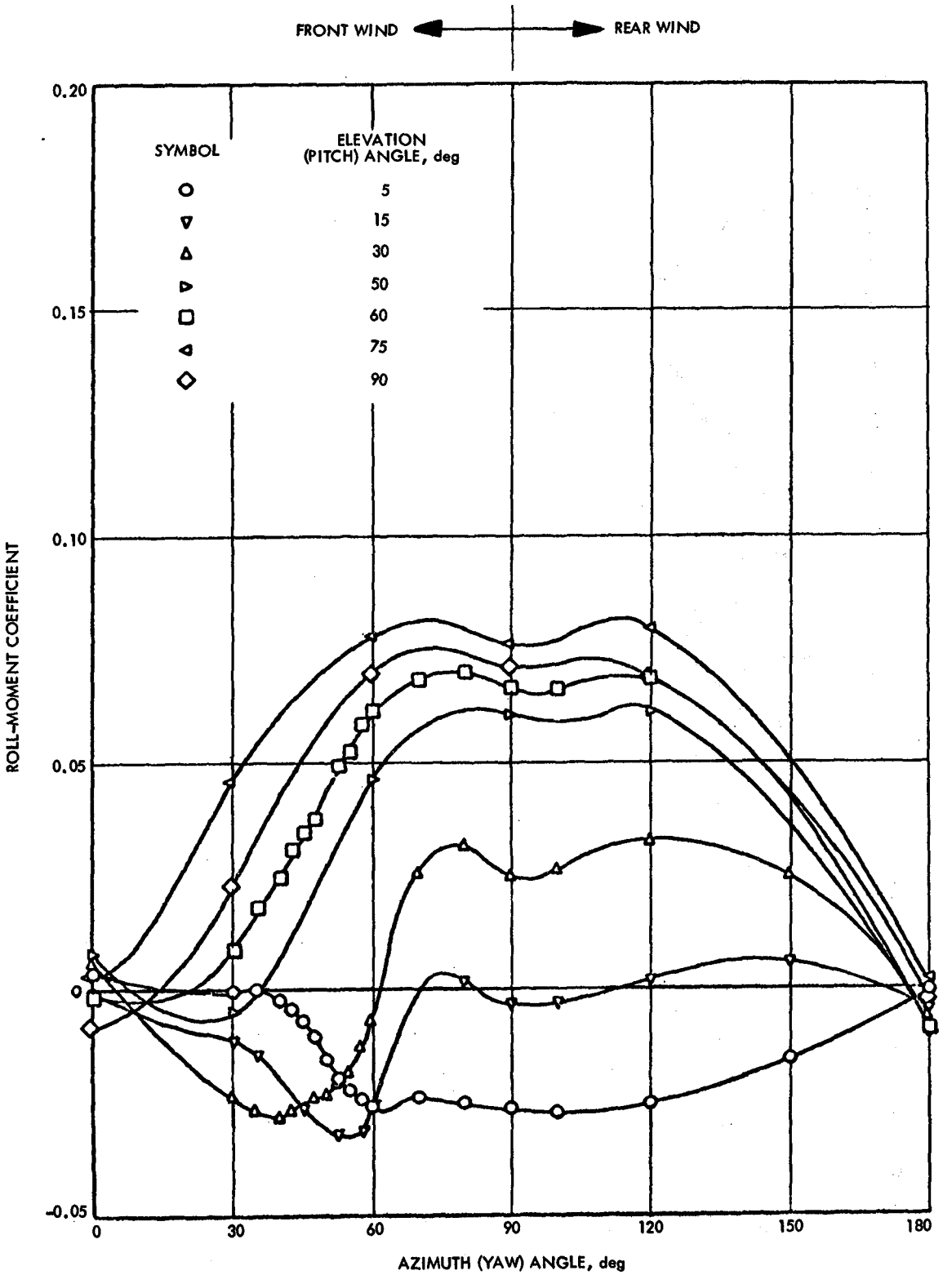

Figure D-6. Effect of Antenna Attitude on Roll-Moment Coefficient (From Ref. 13)

APPENDIX E

WIND TUNNEL RESULTS OF A FULL-SCALE HELIOSTAT

Some force and moment coefficient data are available for a single, full-scale heliostat that was tested in the large NASA Ames wind tunnel (Ref. 61). The prototype McDonnell Douglas/DOE flat-plate heliostat has a wind specification of 50 mph maximum operational velocity (including gusts) and a maximum survival velocity of 90 mph (including gusts), both referenced to a 30-ft height above ground; compare these values with Figure 18.

The force and moment data were taken at the base (see Figure E-1, which shows the coordinate system). The angle of attack α is the elevation angle and β is the azimuth angle; the heliostat is normal to the wind when $\alpha = 90$ deg. Test Reynolds number was about 6.5×10^6. Lift and drag coefficient data are shown in Figures E-2 and E-3, respectively. Reference to calculations based on data from the American Society of Civil Engineers (Ref. 101) is denoted by "ASCE Data," where λ denotes the aspect ratio of a rectangular plate. Positive and negative stall occur when the angle of attack is about 30 deg and 150 deg, respectively. As the angle of attack approaches 90 deg (zero lift), it is seen in Figure E-3 that the mirror drag is best represented by two flat plates with aspect ratio of $\lambda = 3$. (See Figure E-1.)

Base moment coefficients are shown for two azimuth angles in Figures E-4 and E-5. With the mirror side to the flow (Figure E-4), it is seen that the pitch-moment is closely approximated by flat-plate data. Departures are seen, however, when the structural side is toward the wind (Figure E-5), and more turbulence is generated in the range of α from 25 deg to 45 deg where the maximum lift is generated.

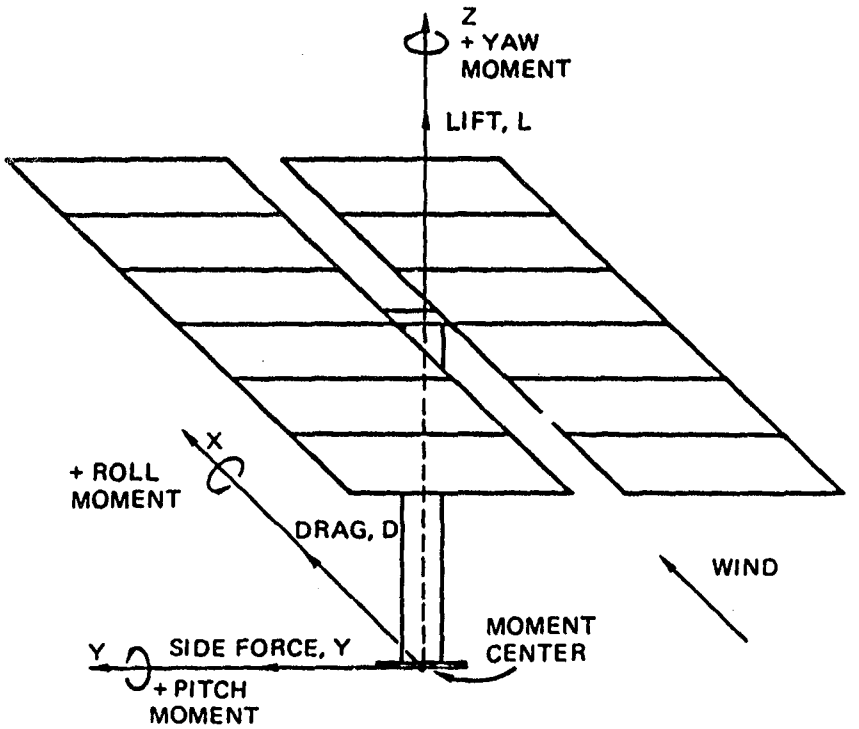

Figure E-1. Coordinate System for Forces and Moments (From Ref. 61)

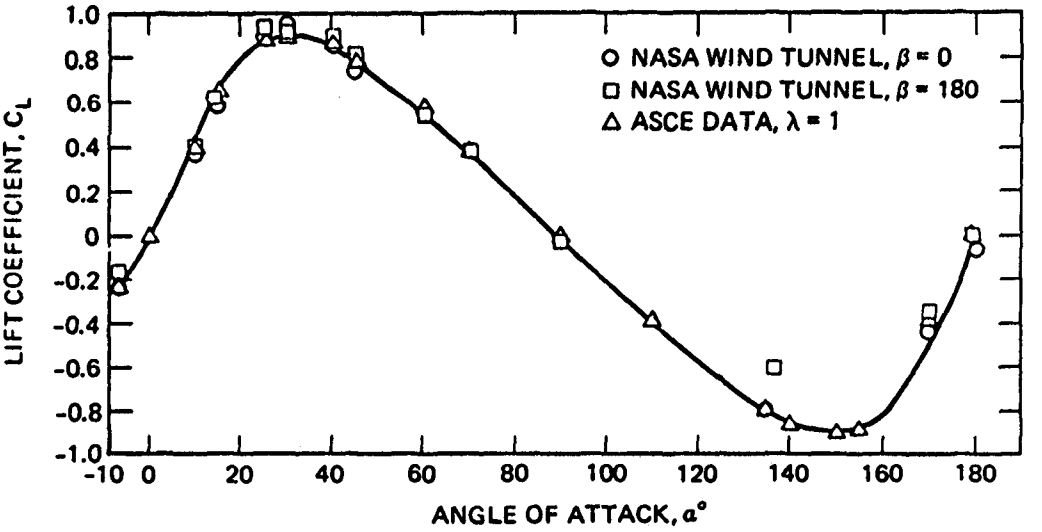

Figure E-2. Lift vs Angle of Attack (From Ref. 61)

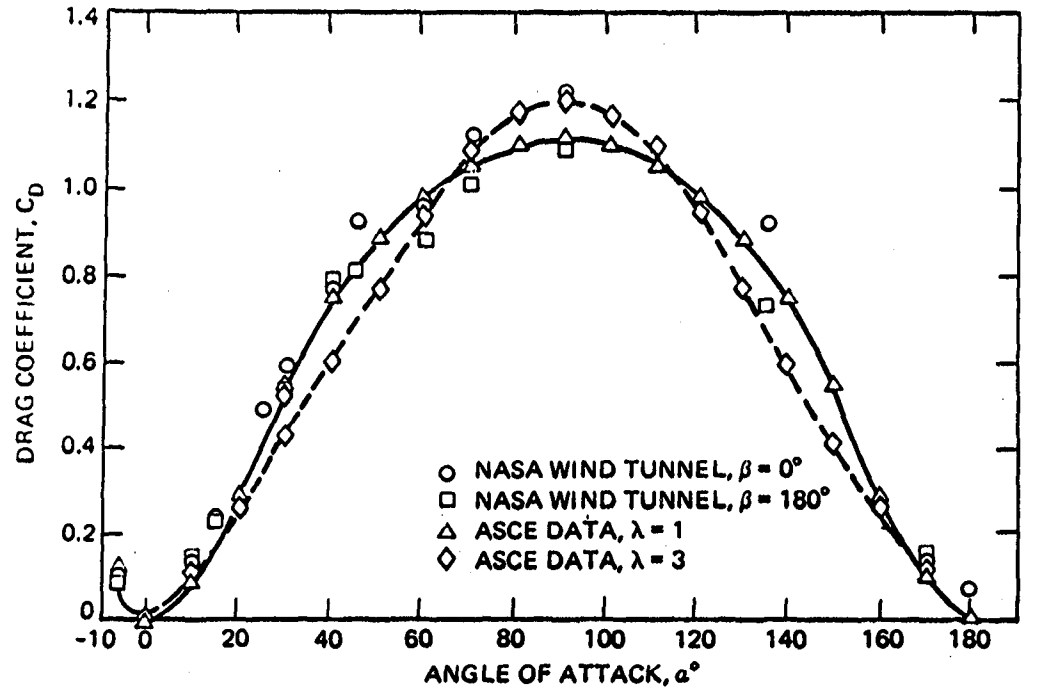

Figure E-3. Drag vs Angle of Attack (From Ref. 61)

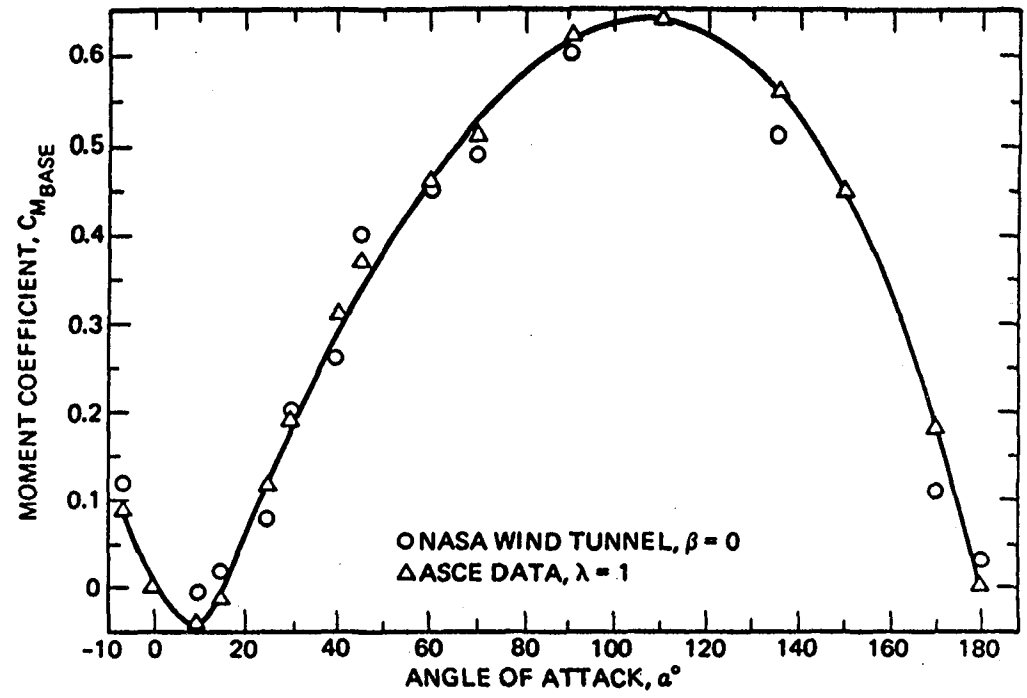

Figure E-4. Base Moment vs Angle of Attack, 0-deg Azimuth (From Ref. 61)

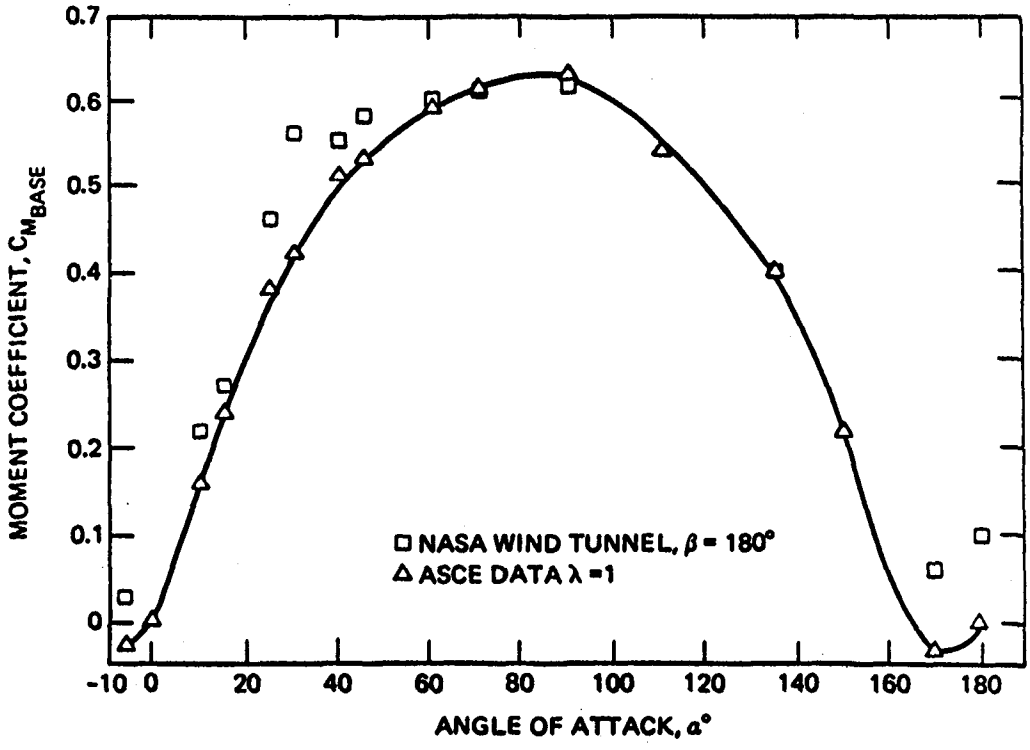

Figure E-5. Base Moment vs Angle of Attack, 180-deg Azimuth (From Ref. 61)

APPENDIX F

ANALYTICAL RESULTS FOR A SECOND-GENERATION HELIOSTAT

Work on second-generation heliostats performed for DOE by Northrup, Inc., is reported in Ref. 65. This later design is different than shown in Figure E-1 (Appendix E); it is not designed to stow facing downward and therefore does not have the vertical gap seen in Figure E-1. The angle of attack used in Ref. 65 is equivalent to 90 deg minus the angle of attack used in Ref. 61. In this Appendix, the same manner of plotting data is used as was employed in Appendix E. Reference 65 reports wind load calculations based on the ASCE methods of Ref. 101; these methods also were used in Ref. 61 (see Figures E-2 through E-5).

Analytical wind force coefficients (Ref. 65) are shown in Figure F-1. The pressure coefficient and the maximum base moment coefficient are shown in Figure F-2. The maximum base moment, in this case, occurs with a rearward wind, i.e., the structure side of the heliostat faces the wind, which is comparable to Figure E-5. The agreement of the data shown in Figure F-1 with the data of Figures E-2 and E-3 is reasonably good. The same is true of the data for moment coefficient, Figure F-2 and Figure E-5.

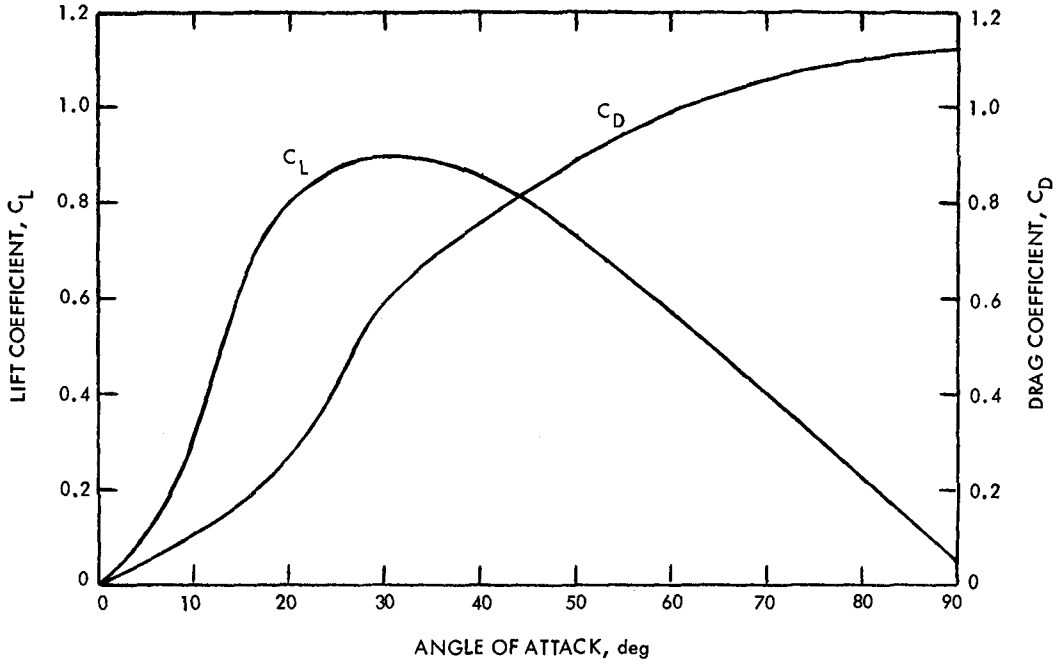

Figure F-1. Lift and Drag vs Angle of Attack
(Based on Data in Ref. 65)

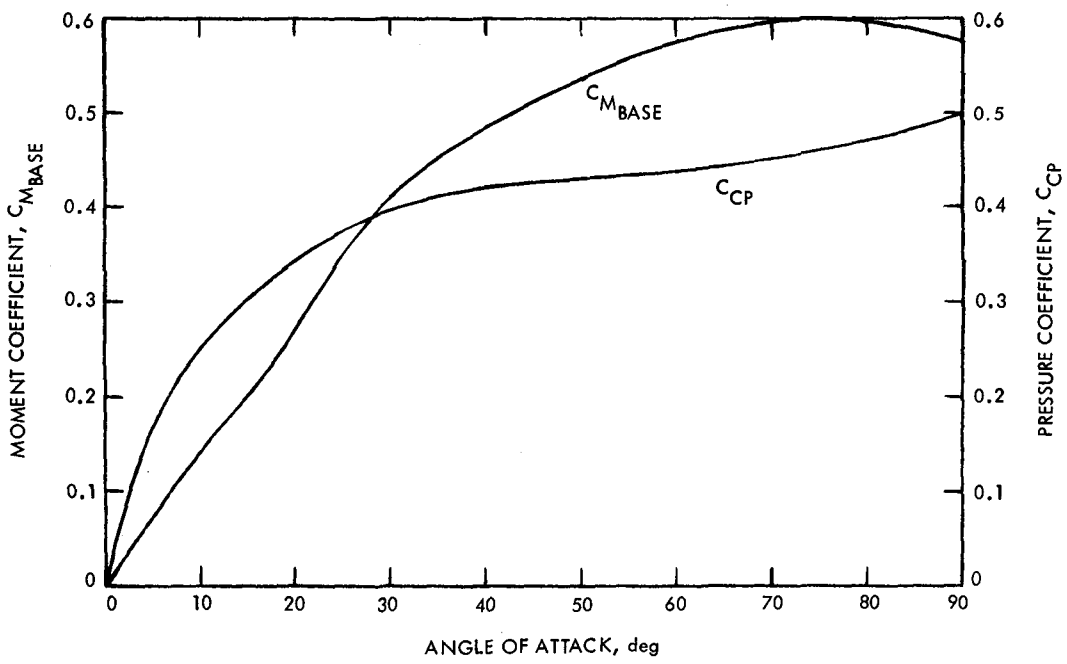

Figure F-2. Maximum Base Moment and Pressure
vs Angle of Attack
(Based on Data in Ref. 65)

★U.S. GOVERNMENT PRINTING OFFICE: 1984 -544 -063/10387 REGION 1

United States Department of Energy
Office of Scientific and Technical Information
Post Office Box 62
Oak Ridge, Tennessee 37831

OFFICIAL BUSINESS
PENALTY FOR PRIVATE USE, $300

POSTAGE AND FEES PAID
DEPARTMENT OF ENERGY
DOE-350

U.S.MAIL

320 FS- 1
NATIONAL AERONAUTICS AND SPACE ADM
ATTN LIBRARY
LANGLEY RESEARCH CENTER
HAMPTON, VA 23665